

---

# **Application of CRISSP-2D Finite Element Modelling in Predicting Ice Formation Processes Upstream of the Jenpeg Generating Station**

---

by

**Milan Bijeljanin**

A thesis submitted to the Faculty of Graduate Studies of  
the University of Manitoba  
in partial fulfillment of the requirements for the degree of

**Master of Science**

Department of Civil Engineering  
University of Manitoba  
Winnipeg, Manitoba, Canada

Copyright © 2013 by Milan Bijeljanin

---

## Abstract

The purpose of this study is to develop, evaluate, and apply a CRISSP-2D river ice model for a highly complex reach of the Nelson River upstream of the Jenpeg Generating Station in northern Manitoba. The calibrated model is applied in a backcasting scenario to evaluate its potential of predicting the river ice regime associated with specific hydraulic and meteorologic conditions. Secondly, a real-time application is conducted in collaboration with Manitoba Hydro to forecast overnight ice conditions as part of the 2011 Ice Stabilization Program.

The model is shown to be fully capable of predicting the onset and type of ice regime that occurs. Spatial variation in ice generation across the study region is accurately captured, including locations of thermal bridging and initial ice front advance. Several modelling limitations associated with parameterization limit model accuracy during the latter stages of freeze-up and are identified as enhancement opportunities.

## Acknowledgements

I would like to acknowledge my advisor, Dr. Shawn Clark, for his support and guidance throughout my university career. You inspired my interest in water resources and had the confidence and patience to see me through this project. You have been a role model for me and have greatly helped my development as an engineer. Thank you.

I would also like to thank the staff from Manitoba Hydro for their support throughout this project. In specific, thank you Jarrod Malenchak for giving me the knowledge and insight needed to successfully complete this project. You were an invaluable resource in helping me over the many speed bumps I experienced. Thank you also to Mike Morris, Brian Giesbrecht, and Scott Herbert for your contributions to this project.

I acknowledge and graciously appreciate the generous funding contributions that made this research possible. Thank you to the Natural Science and Engineering Research Council of Canada, the Government of Manitoba, Manitoba Hydro, the University of Manitoba, and to the private scholarship donors.

Lastly, thank you to my family and friends for your continuing support. Thank you to my mom and dad for your encouragement and for the many sacrifices you have made. I hope I have made you proud.

# Table of Contents

Abstract .....	i
Acknowledgements .....	ii
List of Figures .....	vii
List of Tables .....	xi
Nomenclature .....	xii
<b>CHAPTER 1: Introduction .....</b>	<b>1</b>
1.1 Background .....	1
1.2 Boundary Heat Exchange.....	8
1.2.1 Energy Budget.....	8
1.2.2 Linear Heat Transfer.....	25
1.3 River Ice Processes.....	26
1.3.1 Nucleation .....	27
1.3.2 Frazil Ice.....	29
1.3.3 Border Ice.....	32
1.3.4 Skim Ice.....	39
1.3.5 Ice Regimes .....	43
1.4 River Ice Models.....	46
1.4.1 ICEDYN.....	46
1.4.2 RIVICE .....	47
1.4.3 VARY-ICE .....	48
1.4.4 River1D .....	49
1.4.5 RICEN.....	49
1.4.6 MIKE-ICE .....	50
1.4.7 River2D .....	50
1.4.8 CRISSP-2D .....	51
1.5 Research Objectives .....	52
<b>CHAPTER 2: Numerical Model .....</b>	<b>53</b>
2.1 CRISSP-2D Overview .....	53

---

## Table of Contents

---

2.2	Hydrodynamic Module.....	54
2.3	Water Temperature Module.....	56
2.4	Thermal Ice Module.....	61
2.5	Dynamic Ice Module.....	66
2.6	Input Data.....	67
2.7	Calibration Parameters.....	71
<b>CHAPTER 3: Study Area .....</b>		<b>74</b>
3.1	The Nelson River.....	74
3.2	Lake Winnipeg Regulation.....	79
3.3	Data Availability.....	82
3.3.1	Bathymetric Data.....	82
3.3.2	Imagery Data.....	84
3.3.3	Hydrometric Data.....	86
3.3.4	Meteorological Data.....	90
<b>CHAPTER 4: Model Development .....</b>		<b>91</b>
4.1	Bathymetric Data Analysis.....	91
4.2	Mesh Generation.....	93
4.3	Boundary Conditions.....	98
4.4	Model Assumptions.....	100
<b>CHAPTER 5: Hydrodynamic Simulations.....</b>		<b>102</b>
5.1	Introduction.....	102
5.2	Initial Conditions.....	102
5.3	Hydrodynamic Calibration.....	104
5.4	Hydrodynamic Validation.....	110
5.4.1	Water Surface Profile.....	111
5.4.2	Water Velocity Distribution.....	113
5.4.3	Flow Distribution.....	118
5.5	Boundary Condition Sensitivity.....	120
5.6	Summary.....	122

---

Table of Contents

---

<b>CHAPTER 6: Ice Simulations</b> .....	124
6.1 Introduction.....	124
6.2 Water Temperature Simulation.....	124
6.3 Initial Conditions .....	127
6.4 Thermal Ice Calibration .....	128
6.4.1 Border Ice Formation (tc, vcrskm, vcrbom).....	129
6.4.2 Skim Ice Formation (hi0) .....	136
6.4.3 Frazil Ice Formation (vnu).....	143
6.4.4 Mass Exchange Processes (theta, beta1, vbb, hf0, anmaxfra) .....	148
6.5 Dynamic Ice Calibration.....	155
6.5.1 Ice Boom Representation .....	155
6.5.2 Freeze-up Jam (thi0, anmax) .....	156
6.5.3 Surface Ice Submergence (crifr).....	157
6.6 Comprehensive Ice Validation.....	161
6.6.1 2003 .....	162
6.6.2 2005 .....	166
6.6.3 2006 .....	171
6.6.4 2008 .....	175
6.6.5 2009 .....	181
6.6.6 2010 .....	185
6.7 Summary .....	188
<b>CHAPTER 7: Freeze-up Forecasting</b> .....	195
7.1 Introduction.....	195
7.2 Modelling Process .....	195
7.2.1 Initial Conditions .....	198
7.2.2 Boundary Conditions .....	199
7.3 Model Application .....	200
7.3.1 November 13-14, 2011 Simulation .....	200
7.3.2 November 17, 2011 Forecast .....	201
7.3.3 November 18, 2011 Forecast .....	203
7.4 Summary .....	206

---

Table of Contents

---

<b>CHAPTER 8: Conclusions and Future Work</b> .....	208
8.1 Research Summary .....	208
8.2 Conclusions.....	209
8.3 Future Work and Recommendations .....	213
<b>REFERENCES</b> .....	217
<b>APPENDIX A: Hydrodynamic Validation Results</b> .....	227
<b>APPENDIX B: Linear Heat Transfer Results</b> .....	240

## List of Figures

Figure 1.1. Equilibrium Ice Jam Profile .....	45
Figure 3.1. Map of Manitoba showing Nelson River hydrology.....	75
Figure 3.2. Overview of the Lake Winnipeg Regulation Project.....	80
Figure 3.3. Summary of available cross-sectional data (red).....	83
Figure 3.4. Channel extents pre-construction (red) and post-construction (blue).....	85
Figure 3.5. Overview of hydrometric gauging locations in the study area.....	87
Figure 3.6. Jenpeg calculated outflow performance, 1995-2008 .....	88
Figure 3.7. Statistical analysis of average daily freeze-up flow (Nov-Dec) .....	89
Figure 4.1. Summary of available original (red), proxy (yellow), and estimated flood zone (white) bathymetric data.....	92
Figure 4.2. Outline of CRISSP-2D model and reach boundaries.....	94
Figure 4.3. CRISSP-2D mesh.....	95
Figure 4.4. Mesh approximations within the Metchanais Channel.....	96
Figure 4.5. Final CRISSP-2D mesh bathymetry .....	97
Figure 4.6. 8-Mile Channel flow relative to the Nelson River West Channel.....	99
Figure 5.1. Mesh bathymetry modifications: +1.85 m (red) and -0.5 m (blue) ..	105
Figure 5.2. Hydrodynamic calibration model error for all gauges.....	106
Figure 5.3. 2008 open water season final calibration .....	108
Figure 5.4. Hydrodynamic validation performance .....	112
Figure 5.5. Two-dimensional water velocity distribution – November 18, 2010.....	114
Figure 5.6. Ice formation on the Lower West Channel looking upstream – November 18, 2010 .....	114
Figure 5.7. Ice formation on the Upper West Channel looking downstream - November 18, 2010 .....	115

---

## List of Figures

---

Figure 5.8. Ice formation on the Ominawin Channel looking upstream - November 18, 2010 .....	115
Figure 5.9. Ice formation on Whiskey Jack Narrows looking downstream - November 18, 2010 .....	116
Figure 6.1. Calibrated border ice progression shown in white – 2007 freeze- up period.....	132
Figure 6.2. Border ice validation – November 15, 2004.....	133
Figure 6.3. Ice formation on the Lower West Channel looking upstream – November 15, 2004 .....	133
Figure 6.4. Ice formation on Manitou Rapids looking upstream – November 15, 2004.....	134
Figure 6.5. Ice formation on Whiskey Jack Narrows looking downstream – November 15, 2004 .....	134
Figure 6.6. Ice formation on the Upper Ominawin Channel looking upstream – November 15, 2004 .....	135
Figure 6.7. Effect of initial skim ice thickness on ice front thickness – start of freeze-up.....	138
Figure 6.8. Effect of initial skim ice thickness on ice front thickness – middle of freeze-up.....	139
Figure 6.9. Effect of initial skim ice thickness on ice front thickness – end of freeze-up.....	140
Figure 6.10. Effect of Nusselt number on ice front thickness – start of freeze-up.....	145
Figure 6.11. Effect of Nusselt number on ice front thickness – middle of freeze-up.....	146
Figure 6.12. Effect of Nusselt number on average frazil concentration – 2007 freeze-up.....	147
Figure 6.13. Effect of frazil rising velocity on ice front thickness – start of freeze-up.....	150
Figure 6.14. Effect of frazil rising velocity on ice front thickness – middle of freeze-up.....	151
Figure 6.15. Effect of frazil rise velocity on frazil concentration downstream of Manitou Rapids – 2007 freeze-up .....	152

---

## List of Figures

---

Figure 6.16. Effect of initial frazil ice parcel thickness on ice front thickness – start of freeze-up .....	154
Figure 6.17. Effect of critical Froude number on ice front thickness – start of freeze-up .....	158
Figure 6.18. Effect of critical Froude number on ice front thickness – middle of freeze-up .....	159
Figure 6.19. Froude number distribution pre-cutback (left) and post-cutback (right) .....	160
Figure 6.20. Measured freeze-up flow and air temperature, 2003 .....	163
Figure 6.21. Simulated ice thickness, November 4, 2003 .....	164
Figure 6.22. Skim ice bridging at Manitou Rapids looking upstream, November 4, 2003 .....	165
Figure 6.23. Ice cover on the Upper Ominawin Channel looking upstream, November 4, 2003 .....	165
Figure 6.24. Measured freeze-up flow and air temperature, 2005 .....	167
Figure 6.25. Simulated ice thickness, November 16, 2005 .....	168
Figure 6.26. Location of primary skim ice front looking upstream, November 16, 2005 .....	169
Figure 6.27. Location of secondary skim ice front looking upstream, November 16, 2005 .....	169
Figure 6.28. Local skim ice bridging on the Upper Ominawin Channel, November 17, 2005 .....	170
Figure 6.29. Local skim ice bridging on the Upper Ominawin Channel, November 7, 2006 .....	172
Figure 6.30. Measured freeze-up flow and air temperature, 2006 .....	172
Figure 6.31. Simulated ice thickness, November 7, 2006 .....	174
Figure 6.32. Location of primary skim ice front looking upstream, November 7, 2006 .....	175
Figure 6.33. Measured freeze-up flow and air temperature, 2008 .....	176
Figure 6.34. Simulated ice thickness, November 11, 2008 .....	177

---

## List of Figures

---

Figure 6.35. Simulated ice thickness, November 14, 2008.....	178
Figure 6.36. Location of the primary ice front looking upstream, November 14, 2008 .....	179
Figure 6.37. Location of the secondary ice front looking upstream, November 14, 2008.....	179
Figure 6.38. Measured freeze-up flow and air temperature, 2009.....	182
Figure 6.39. Simulated ice thickness, November 30, 2009.....	184
Figure 6.40. Measured freeze-up flow and air temperature, 2010.....	186
Figure 6.41. Simulated ice thickness, November 18, 2010.....	187
Figure 6.42. Location of the primary front looking upstream, November 18, 2010 .....	187
Figure 6.43. Ice regime correlation to overnight flow and air temperature, 2003 to 2010 .....	190
Figure 7.1. Rolling window sequence schematic for forecast simulations .....	197
Figure 7.2. Measured freeze-up flow and air temperature, 2011 .....	201
Figure 7.3. Freeze-up Regime, November 17, 2011, 7:00 am .....	202
Figure 7.4. Forecast vs. Measured Flow, November 17-18, 2011 .....	204
Figure 7.5. Freeze-up Regime post-cutback, November 18, 2011, 7:00 am ....	205
Figure 7.6. Skim ice floes upstream of the secondary front, November 18, 2011 .....	205

## List of Tables

Table 1.1. Summary of Current Hydroelectric Power Generation in Manitoba .....	5
Table 1.2. Albedos values for different ice and snow conditions .....	17
Table 2.1. CRISSP-2D input file summary .....	68
Table 2.2. CRISSP-2D calibration parameters .....	71
Table 3.1. Statistical flow classification during freeze-up.....	89
Table 5.1. Documented vs. calibrated Manning channel bed roughness .....	109
Table 5.2. Flow distribution comparison of connecting channels.....	119
Table 5.3. Boundary condition sensitivity, lower quartile flow condition.....	121
Table 5.4. Boundary condition sensitivity, upper decile flow condition .....	121
Table 6.1. Comparison of linear heat transfer methods.....	126
Table 6.2. Ice module parameterization .....	189

## Nomenclature

Symbol	Units	Description
$A$	[m <sup>2</sup> ]	Cross-sectional area of a channel
$a_0$	[m <sup>2</sup> ]	Surface area of a frazil ice particle
$B$	[m]	Width of open water sections parallel to the direction of the wind
$B_0$	[m]	Spanwise channel width of open water sections
$C$	[0 to 10]	Degree of cloud cover
$C_0$	[W/m <sup>2</sup> °C]	Bulk linear heat transfer coefficient
$C_p$	[J/kg°C]	Specific heat of water, given as 4,186
$d$	[m]	Ice particle diameter
$d_e$	[m]	Average frazil crystal thickness
$d_f$	[m]	Average frazil crystal length
$d_n$	[-]	Current Julian day assuming 365 days in a year
$E$	[m <sup>3</sup> /m <sup>3</sup> s]	Net volumetric rate of loss of frazil due to mass exchange at top and bottom boundaries
$e_a$	[mb]	Vapour pressure
$e_{an}$	[-]	Porosity of anchor ice
$e_f$	[-]	Porosity of frazil ice
$e_s$	[mb]	Saturation vapour pressure
$F_n$	[m <sup>-3</sup> ]	Number of frazil crystals per unit volume
$g$	[m/s <sup>2</sup> ]	Gravitational constant, given as 9.806
$h_i$	[m]	Total ice thickness
$h_f$	[m]	Surface frazil ice thickness
$h_s$	[m]	Solid ice thickness

---

## Nomenclature

---

<b>Symbol</b>	<b>Units</b>	<b>Description</b>
$H$	[degrees]	Local hour angle of the sun
$H_w$	[m]	Water depth
$K_w$	[W/m°C]	Thermal conductivity of water
$L_0$	[m]	Streamwise channel length of open water sections
$L_i$	[J/kg]	Heat of fusion of ice, given as 333,400
$N$	[m <sup>3</sup> /m <sup>3</sup> ]	Volumetric ice concentration
$N_f$	[0 to 1]	Frazil concentration
$N_s$	[m <sup>2</sup> /m <sup>2</sup> ]	Concentration of surface ice per unit area
$N_u^f$	[-]	Nusselt number
$N_v^g$	[m <sup>3</sup> /m <sup>3</sup> ]	Thermally grown frazil particle concentration
$P_0$	[kPa]	Barometric pressure at sea level
$P_a$	[kPa]	Barometric air pressure at a particular altitude
$Q$	[m <sup>3</sup> /s]	Total channel discharge
$q_t$	[m <sup>2</sup> /s]	Total two-layer unit width discharge
$R$	[m]	Hydraulic radius
$R_L$	[0 to 1]	Long wave surface reflectivity of a water body
$R_S$	[0 to 1]	Short wave albedo of the surface boundary
$S$	[m/m]	Average water surface slope
$s$	[m/m]	Channel bed slope
$t$	[sec]	Time
$T_a$	[°C]	Air temperature measured at an elevation of 2 meters above ground level
$T_{ak}$	[Kelvin]	Absolute temperature of the atmosphere measured at an elevation of 2 meters above ground level
$T_w$	[°C]	Water temperature

---

## Nomenclature

---

<b>Symbol</b>	<b>Units</b>	<b>Description</b>
$T_{wk}$	[Kelvin]	Absolute temperature of the water body
$\Delta T_w$	[°C]	Absolute degree of supercooling in the water body
$T_i$	[°C]	Ice surface temperature
$T_m$	[°C]	Freezing point of water
$T_s$	[°C]	Surface water temperature
$u_v$	[m/s]	Average vertical turbulence intensity
$U_c$	[m/s]	Critical velocity for frazil adhesion at the border ice edge
$U_s$	[m/s]	Open water surface velocity adjacent to the border ice edge
$U_v$	[m/s]	Limiting vertical water velocity beyond which surface ice will not form
$\nu$	[m <sup>2</sup> /s]	Kinematic viscosity of water
$\nu_b$	[m/s]	Buoyant velocity of frazil particles
$V_a$	[m/s]	Wind velocity measured at an elevation of 2 meters above ground level
$V_f$	[m <sup>3</sup> ]	Volumetric production of ice for a given time period
$w$	[m]	Channel width
$\Delta w$	[m]	Incremental border ice growth for a given time period
$\alpha$	[degrees]	Solar altitude
$\beta$	[m/s]	Rate of re-entrainment of surface ice
$\gamma$	[m/s]	Rate of accretion of frazil particles to the bed
$\epsilon_a$	[0 to 1]	Emissivity of the atmosphere
$\epsilon_w$	[0 to 1]	Surface emissivity of the water body
$\theta$	[0 to 1]	Probability of deposition of frazil particles at the surface layer
$\theta_z$	[degrees]	Zenith angle

---

## Nomenclature

---

<b>Symbol</b>	<b>Units</b>	<b>Description</b>
$\rho_i$	[kg/m <sup>3</sup> ]	Density of ice
$\rho_w$	[kg/m <sup>3</sup> ]	Density of water
$\sigma$	[W/m <sup>2</sup> K <sup>4</sup> ]	Stefan-Boltzmann constant, given as $5.670 \times 10^{-8}$
$\varphi_*$	[W/m <sup>2</sup> ]	Net heat flux within the water column
$\varphi_E$	[W/m <sup>2</sup> ]	Latent heat flux at the water surface
$\varphi_{CC}$	[W/m <sup>2</sup> ]	Short wave radiation heat flux reaching the Earth's surface under cloudy skies
$\varphi_{CL}$	[W/m <sup>2</sup> ]	Short wave radiation heat flux reaching the Earth's surface under clear skies
$\varphi_G$	[W/m <sup>2</sup> ]	Channel bed heat flux at the channel bottom
$\varphi_H$	[W/m <sup>2</sup> ]	Sensible heat flux at the water surface
$\varphi_L$	[W/m <sup>2</sup> ]	Long wave radiation heat flux at the water surface
$\varphi_{LA}$	[W/m <sup>2</sup> ]	Long wave radiation heat flux emitted by the atmosphere
$\varphi_{LC}$	[W/m <sup>2</sup> ]	Long wave radiation heat flux emitted by the atmosphere under clear skies
$\varphi_{LR}$	[W/m <sup>2</sup> ]	Long wave radiation heat flux reflected by the water body
$\varphi_{LW}$	[W/m <sup>2</sup> ]	Long wave radiation heat flux emitted by the water body
$\varphi_P$	[W/m <sup>2</sup> ]	Precipitation heat flux at the water surface
$\varphi_S$	[W/m <sup>2</sup> ]	Short wave radiation heat flux at the water surface
$\varphi_{S_0}$	[W/m <sup>2</sup> ]	Solar radiation heat flux incident on a horizontal plane outside of the Earth's atmosphere
$\varphi_{wi}$	[W/m <sup>2</sup> ]	Net heat flux between anchor ice and the water column

---

# CHAPTER 1:

## Introduction

---

### 1.1 Background

The unique hydrology within the Province of Manitoba provides ideal conditions for hydroelectric power generation. The central portion of the province is situated at the heart of an extensive drainage basin, collecting water from an area of roughly one million square kilometres extending west to the Rocky Mountains, south to the United States, and east to Lake Superior. This central depression to which practically all runoff is collected forms Lake Winnipeg, the eleventh largest freshwater lake in the world by surface area.

From the east, water reaching the lake via the Winnipeg River passes through a series of topographical drops separating the prairie steppes from the Laurentian plateau (Denis & Challies, 1916). The resulting sequence of rapids and falls form a set of six natural power generation sites along the river. In the western reaches of the drainage basin exists the Saskatchewan River. At its outlet, flow from the river is routed through Cedar Lake before travelling an additional 6.4 km and discharging into Lake Winnipeg. The reach between the two lakes is dominated

by a series of rapid drops, providing potential for the development of a high-head generating station. The Red and Assiniboine Rivers, whose drainage basins encompass the large part of southern Manitoba, possess minimal hydroelectric potential due to the gradual topography of the prairie lowland. Other relatively minor rivers exist within the remainder of the Lake Winnipeg tributary basins; however, their dependable discharge is inadequate to support large-scale hydropower developments.

All water that exits Lake Winnipeg does so via the Nelson River, which routes the flow through northeastern Manitoba and eventually into Hudson Bay. The river is segregated into two reaches: the Upper Nelson River extending 400 km from Lake Winnipeg to Split Lake, and the Lower Nelson River extending an additional 300 km from Split Lake to the mouth. The upper reach of the river passes through a region of relatively low relief, and is characterized by an alternating series of shallow lakes and rapid drops. Flow is split between islands by narrow channels that typically feature sections of well-defined rapids. These rapids account for the large majority of the head drop that occurs in this reach.

The lower reach of the Nelson River differs greatly from the upper, with the primary difference being a significant increase in average slope from 0.00012 m/m to 0.00058 m/m. The channel straightens to follow a general north-easterly direction to Hudson Bay, with Gull Lake, located approximately 175 km upstream of the outlet, providing the only means of natural storage. The majority of rapids

along the Lower Nelson River are constrained to downstream of this reservoir with each representing a potential power generation site.

Much of the remaining portion of northern Manitoba is within the Churchill River drainage basin. Itself, the Churchill River offers a generation potential similar to that of the Nelson; however, today much of its flow is diverted into the Nelson River system via the Burntwood River. Completed in 1977, the Churchill River Diversion increases the generation potential of the Lower Nelson River by roughly 2,000 megawatts and adds an additional 700 megawatts of generation potential to the Burntwood River (Manitoba Hydro, n.d.).

This potential for hydroelectric development within Manitoba was first documented in detail in 1916 (Denis & Challies, 1916). By this time, developments along the Winnipeg River were already underway with two generating stations – the Pinawa and Pointe du Bois Generating Stations - having been built to serve the populations of Brandon and Winnipeg. Over the next forty years, an additional five power development projects took place on the Winnipeg River at Great Falls (1928), Slave Falls (1948), Seven Sisters Falls (1952), Pine Falls (1952), and McArthur Falls (1955), effectively maximizing the total generation capacity of the river.

By the 1960's, advancements to long distance power transmission made sites on the Saskatchewan and Nelson Rivers feasible options in meeting the Province's

growing energy demand. The first of the stations built on either of these rivers was the Kelsey Generating Station on the Upper Nelson River, whose initial purpose was to provide power for mining operations in northern Manitoba. This was followed by the construction of both the Grand Rapids Generating Station on the Saskatchewan River and the High-Voltage Direct Current (HVDC) infrastructure required for long distance transmission to Winnipeg.

Subsequent hydroelectric developments on the Lower Nelson River were dependent on the establishment of a long term storage reservoir with which to supply each station. This was largely due to the lack of natural storage on this reach, which would have required a significant degree of flooding within the forebay for a conventional dam to function. Alternatively, a run-of-the-river design was employed whereby a primary storage reservoir is located far upstream of each dam. Regulation of this reservoir allowed for a controlled release of flow to correspond with any forecasted long-term energy demands. The result was a significant reduction in the forebay storage necessary to supply the plant over the long term.

The run-of-the-river design has been applied to all current hydroelectric developments on the Lower Nelson River, including the Kettle, Long Spruce, and Limestone Generating Stations. Short term storage, necessary for day-to-day operations, is provided by Stephens Lake: a reservoir formed as a result of the Kettle Generating Station. Long term storage is accomplished through regulation

of Lake Winnipeg, ensuring that a sufficient supply of water is maintained for winter operation and risk mitigation.

The Nelson River represents the single largest source of hydroelectric generation in the Province, as shown in Table 1.1. Facilitating this development is the utilization of Lake Winnipeg as a natural long term storage reservoir, making power generation on the Lower Nelson River both economically and environmentally feasible. The key aspect of this regulation is in the ability to store a portion of the high summer flows in Lake Winnipeg for use during winter months when energy demand is higher. In addition, local water users benefit from an ability to provide a level of drought and flood mitigation. Control of Lake Winnipeg outflow was accomplished in 1976 through the Lake Winnipeg Regulation (LWR) Project.

Table 1.1. Summary of Current Hydroelectric Power Generation in Manitoba

<b>Station</b>	<b>Location</b>	<b>In Service</b>	<b>Generation Capacity (MW)</b>
Kelsey GS	Upper Nelson River	1961	250 (5%)
Grand Rapids GS	Saskatchewan River	1968	479 (9%)
Kettle GS	Lower Nelson River	1974	1,220 (23%)
Jenpeg GS	Upper Nelson River	1976	133 (3%)
Long Spruce GS	Lower Nelson River	1979	1,010 (19%)
Limestone GS	Lower Nelson River	1990	1,340 (26%)
Wuskwatim GS	Burntwood River	2012	200 (4%)
Generation South*	Winnipeg River	<1955	589 (11%)

\* Represents a total of six generating stations located on the Winnipeg River

The extent of the Lake Winnipeg Regulation Project includes the construction of the Jenpeg Generating Station and Control Structure (Jenpeg), excavation of three man-made channels, and numerous other channel improvements. Located approximately 130 km downstream of Lake Winnipeg, Jenpeg controls the outflows from the lake by varying the hydraulic gradient through the outlet channels. To increase flow into the Nelson River, operators lower the forebay level at the station thereby increasing the hydraulic gradient and promoting the release of water from Lake Winnipeg. Alternatively, the forebay elevation is raised to reduce outflows from the lake. This is the inverse of what one would expect on natural streams, where subcritical reaches are characterized by proportional increases in water elevation with increases in flow.

Encompassing a large portion of the Upper Nelson River, the LWR project is situated within an area of very complex hydraulics. It was recognized early in the design process that this system of shallow lakes, steep rapids, and multiple flow splits and merges would provide unique challenges during the winter period (Zbigniewicz, 1997). As such, Jenpeg was strategically placed in a location that allowed for some control over the freeze-up processes taking place upstream. The original design also included a timed flow cutback during the freeze-up period; however, this cutback was deemed too costly in terms of lost generation both at Jenpeg and on the Lower Nelson and was eliminated from the operation strategy in 1977.

In subsequent years, high winter outflows from Lake Winnipeg along with the complexity of the outlet channels combined to produce very dynamic and unfavourable ice processes upstream of the station. In 1977, outflow capacity from the lake was significantly decreased due to the formation of a hanging dam on one of the outlet channels. In addition, 1983 saw the entire powerhouse shut down due to a frazil ice blockage at the intake (Zbigniewicz, 1997). As a result, the original flow cutback was reinstated within the Ice Stabilization Program in 1984.

Today, the Ice Stabilization Program provides a means of monitoring and optimizing the ice formation processes upstream of the station primarily through a strategically timed flow cutback. By reducing the flow, it is expected that the resulting decrease in water velocities will promote the development of a stable and smooth ice cover, and that any problems associated with frazil ice generation will be largely avoided. The benefits of the program are two-fold: 1) the short term risk of frazil blockages at the Jenpeg intakes is minimized, and 2) the conveyance capacity of the Lake Winnipeg outlet channels is increased during winter months. It is estimated that the annual benefit of the program since its initiation is roughly \$2 million (Zbigniewicz, 1997).

Decisions regarding the optimal timing, duration, and degree of cutback made as part of the program are largely based on current conditions and a short-term weather forecast. How well the system functions is dependent solely on operator

experience during freeze-up and their knowledge of the typical ice regime of the upstream channels. There exists no means of evaluating the outcome of a decision or its sensitivity to error prior to its implementation. It is the purpose of this research to provide such a means through the development of a CRISSP-2D river ice model that is to be used as an operational tool within the Ice Stabilization Program. The fundamental theories which form the basis for CRISSP-2D and other river ice models are outlined in the following sections.

## 1.2 Boundary Heat Exchange

The formation of ice in any environment begins with the cooling of the water body through boundary heat exchange. Considering a static column of water in a river or lake, heat is either lost or gained through both the upper (water surface) and lower (channel bed) boundaries. Whenever the net exchange is negative, heat will be lost from the water column and the body will cool. Ice generation commences when the water temperature reaches the freezing point and continues for as long as conditions permit. The rate of cooling is an important parameter in ice studies as it influences both the timing and mechanisms of ice formation.

### 1.2.1 *Energy Budget*

Under natural conditions, a body of water is subjected to numerous means of heat transfer. The net heat gain or loss within a water column may be modelled

by applying the full energy balance at each boundary. This approach is presented in Equation 1.1:

$$\varphi_* = \varphi_S + \varphi_L + \varphi_E + \varphi_H + \varphi_P + \varphi_G \quad [1.1]$$

Where the net heat transfer ( $\varphi_*$ ) is given as a sum of the short-wave radiation ( $\varphi_S$ ), long-wave radiation ( $\varphi_L$ ), latent ( $\varphi_E$ ), sensible ( $\varphi_H$ ), precipitation ( $\varphi_P$ ), and channel bed ( $\varphi_G$ ) heat fluxes at the upper/lower boundaries.

#### *Short-Wave Radiation Heat Flux*

The primary source of short-wave radiation reaching the water surface is the solar radiation emitted by the sun. The intensity of the incoming radiation varies with Earth's distance from the sun, with the solar constant of  $1367 \text{ W/m}^2$  representing the standard value (Frohlich & Brusa, 1981). Annual variations of this value have been measured on the order of 3%, and a constant of  $1380 \text{ W/m}^2$  has been found to give good results for winter conditions (Ashton, 1986). Practical application of the solar constant for calculating the incoming solar radiation incident on a horizontal plane is presented in Equation 1.2 (Iqbal, 1983):

$$\varphi_{S_0} = I_0 E_0 \cos(\theta_z) \quad [1.2]$$

where:  $\varphi_{S_0}$  represents the solar radiation incident on a horizontal plane outside of the Earth's atmosphere [ $\text{W/m}^2$ ]

$I_0$  represents the solar constant [ $\text{W/m}^2$ ]

$E_0$  represents the eccentricity correction factor of Earth's orbit [-]

$\theta_z$  represents the zenith angle [degrees]

The Earth's orbital distance changes with time due to its elliptical orbit about the sun, resulting in a relative increase or decrease in solar radiation intensity throughout the year. The eccentricity correction factor is applied in Equation 1.2 to adjust for this relative change. The factor represents the current deviation of the Earth's orbit from the mean orbital distance, called one astronomical unit, and may be calculated using the relationship presented in Equation 1.3 (Duffie & Beckman, 1980):

$$E_0 = \left(\frac{r_0}{r}\right)^2 = 1 + 0.033\cos\left(\frac{2\pi d_n}{365}\right) \quad [1.3]$$

where:  $r_0$  represents one astronomical unit; given as  $1.496 \times 10^8$  [km]

$d_n$  represents the current Julian day assuming 365 days in a year

The remaining term in Equation 1.2 is the zenith angle, which can be defined as the angular position of the sun relative to the vertical axis directly above an observation point. Varying with latitude, time of year, and time of day, this term accounts for the decrease in incoming solar radiation due to the angle of incidence of the rays on the Earth's curved surface. The decrease will vary from 0% if the zenith angle is  $0^\circ$  to 100% if the zenith angle is  $90^\circ$ . This term may be

calculated by considering each of its individual components, as per Equation 1.4 (Iqbal, 1983):

$$\cos(\theta_z) = \sin(L) \sin(\delta) + \cos(L) \cos(\delta) \cos(H) \quad [1.4]$$

where:  $L$  represents the geographic latitude [degrees]  
 $\delta$  represents the declination angle of the sun [degrees]  
 $H$  represents local hour angle of the sun [degrees]

Within Equation 1.4, two additional terms are introduced. The sun's declination angle can be described as the angular offset between its position and the equator. Over the course of the year, this angle varies between 23°27' north during the summer solstice, 0° during the equinoxes, and 23°27' south during the winter solstice. Assumed to be constant for any given day, the declination can be approximated using Equation 1.5 (Cooper, 1969):

$$\delta = 23.45 \cos \left\{ \frac{360}{365} (d_n + 284) \right\} \quad [1.5]$$

The second term is the local hour angle of the sun, which describes the instantaneous position of the sun in the sky according to the daily rotation of the Earth about its axis. Noon represents an angle of zero, and varies from a positive value in the morning to a negative value in the afternoon. Counting from midday, an angular adjustment of ±15° per hour is applied.

Application of Equation 1.2 is valid under the assumption that the incoming solar radiation is incident on a level, horizontal surface and that losses within the atmosphere are negligible. However, atmospheric losses through adsorption, scattering, or reflection are significant and must be considered when applying the full energy budget. These losses may be classified into two groups – those occurring under clear skies and those occurring under overcast skies. Under clear skies, the solar radiation reaching the ground may be empirically computed using Equation 1.6 (Glover & McCulloch, 1958):

$$\varphi_{CL} = (0.99 - 0.17M)\varphi_{S_0} \quad [1.6]$$

where:  $\varphi_{CL}$  represents the short wave radiation heat flux reaching the Earth's surface under clear skies [ $W/m^2$ ]  
 $M$  represents the optical air mass at a particular altitude [-]

In Equation 1.6, the optical air mass is a measure of the atmospheric thickness through which the solar radiation must travel. This thickness is largely dependent on the incidence angle of the incoming rays, and can be estimated using Equation 1.7 (Klein, 1948):

$$M = \frac{P_a}{P_0} [\sin(\alpha) + 0.15(\alpha + 3.885)^{-1.253}]^{-1} \quad [1.7]$$

where:  $P_a$  represents the local barometric air pressure [kPa]

$P_0$  represents the barometric air pressure at sea level [kPa]

$\alpha$  represents the solar altitude,  $\alpha = 90 - \theta_z$  [degrees]

Utilization of the local and sea level barometric pressures in Equation 1.7 allows for estimation of the local optical air mass at different elevations. In this case, air pressure is used as an analog for quantifying the impedance imposed by the air molecules on the incoming solar radiation. By definition, an increase in air pressure is associated with an increase in air mass above a particular point, and therefore, an increased likelihood of loss for incoming solar rays. If barometric pressure is not available, the optical air mass may also be estimated using the local altitude above sea level through the relationship presented in Equation 1.8 (Lunde, 1980):

$$\frac{P_a}{P_0} = \exp(-0.0001184z) \quad [1.8]$$

where:  $z$  represents the local altitude [m]

With increasing cloud cover, more of the incoming solar radiation will be lost prior to reaching the Earth's surface. This is due primarily to the significant increases in scattering, reflection, and adsorption of solar rays by airborne water droplets. The degree of loss is dependent on the cloud cover that is present, which is usually represented as a number ranging from zero (no cloud cover) to ten (full cloud cover). This parameter may be correlated to the amount of radiation

reaching the ground surface through the empirical approach presented in Equation 1.9 (Wunderlich, 1972):

$$\varphi_{CC} = (1 - 0.0065C^2)\varphi_{CL} \quad [1.9]$$

where:  $\varphi_{CC}$  represents the short wave radiation heat flux reaching the Earth's surface under a cloud cover [W/m<sup>2</sup>]  
 $C$  represents the degree of cloud cover [0 to 10]

Of the radiation that reaches the ground under both clear and overcast conditions, a portion is returned back to the atmosphere due to the natural reflectance of the Earth's surfaces. The portion of reflected radiation to incident radiation characteristic of a particular material is often termed its albedo. Based on this definition and assuming that the remainder of the radiation is adsorbed, it is possible to estimate the net solar radiation available for boundary heat exchange using Equation 1.10:

$$\varphi_S = (1 - R_S)\varphi_{CC} \quad [1.10]$$

where:  $R_S$  represents the short-wave albedo of the surface [0 to 1]

The albedo of a surface will vary depending on the incident wavelength, surface characteristics, latitude, solar altitude, and other environmental factors. In the case of river ice models, the albedo of water, ice, and snow surfaces are

particularly important parameters in controlling both the ice formation and breakup regimes within a channel. The albedo of water has been shown to be highly dependent on the solar altitude, whereby the degree of adsorption is proportional to the incidence angle. Typical values range from 6% to 10%; however, the albedo of the water surface can increase to 30% for low solar altitudes and rough water (Burt, 1954; Cogley, 1979). One method of empirical estimation of the albedo of water based on this relationship is presented in Equation 1.11 (Anderson, 1954):

$$R_S = A\alpha^B \quad [1.11]$$

where:  $A, B$  represent empirical constants for different cloud types [-]

Average values for the empirical constants  $A$  and  $B$  in Equation 1.11 vary from 1.18 and -0.77 for clear skies to 0.20 and -0.30 for overcast, respectively (Anderson, 1954). Each can also be approximated empirically using Equations 1.12 and 1.13 (Brady, Graves, & Geyer, 1969):

$$A = 2.20 + \frac{C_r^{0.7}}{4.0} - \frac{(C_r^{0.7} - 0.4)^2}{0.16} \quad [1.12]$$

and,

$$B = -1.02 + \frac{C_r^{0.7}}{16.0} + \frac{(C_r^{0.7} - 0.4)^2}{0.64} \quad [1.13]$$

where:  $C_r$  represents the cloudiness ratio;  $C_r = 1 - \varphi_{CC}/\varphi_{CL}$  [-]

Generally, the presence of a cloud cover acts to decrease the albedo for most winter conditions in the northern hemisphere (Wiscombe & Warren, 1981). Incoming solar radiation is scattered, or diffused, as it passes through a cloud and its incidence angle is shifted. Since the diffused radiation typically has an incident angle of  $50^\circ$ , this shift often results in a decrease in the effective zenith angle and a corresponding decrease in albedo (Wiscombe & Warren, 1981; Gardner & Sharp, 2010). This relationship applies for the majority of incident surfaces, including water, snow, and ice, given that the solar altitude is less than  $40^\circ$ .

The albedos of snow and ice are typically controlled by the same factors. Surface roughness plays a minor part by acting to decrease the albedos of both, particularly at low solar altitudes (Carrol & Fitch, 1981). In the case for snow, albedo is directly dependent on the snow grain size distribution. As grain size increases, as is often associated with ageing or moist snow, the albedo of the snow surface has been observed to decrease (Wiscombe & Warren, 1981; Meinander et al., 2008; Gardner & Sharp, 2010). The equivalent factor for clear freshwater ice is air entrainment, whereby its albedo increases with increasing bubble distribution, but decreases with relative bubble size (Henneman & Stefan, 1999).

One of the other major factors controlling ice albedo is the type of ice that is present (Bolsenga, 1969). The presence of snow ice in particular, which forms by upwelling and freezing of water through a snow covered ice sheet, acts to significantly increase ice albedo (Bolsenga, 1977; Perovich, Maykut, & Grenfell, 1986). The typical ranges for different ice and snow conditions are presented in Table 1.2 (Bolsenga, 1969; Iqbal, 1983):

Table 1.2. Albedos values for different ice and snow conditions

<b>Type of Surface</b>	<b>Albedo [%]</b>
Clear lake ice	10
Pancake ice	31
Slush ice	41
Snow ice	46
Fresh snow	82
Stable snow	65
Melting snow	25

Both snow and ice undergo a process of albedo decay, whereby changes in their physical properties cause a decrease in solar radiation reflectance over time (Henneman & Stefan, 1999). The albedo of fresh snow may decrease by as much as 40%, driven by grain size increases and the introduction of water to within the snow matrix (Meinander et al, 2008). Ice albedo has also been observed to decrease by over 50% in a response to thinning of the ice cover (Heron & Woo, 1994). Due to the difficulty in modeling these long-term variations,

the albedo of the ice/snow boundary layer is often treated as a calibration parameter in river ice models.

### *Long-Wave Radiation Heat Flux*

The Earth's natural energy emits radiation back into space in the form of long-wave radiation. In terms of magnitude, long-wave radiation is greater than the net solar radiation reaching the ground, and represents the second largest heat flux during winter conditions. At the water surface, the long-wave energy balance can be categorized into three individual fluxes: 1) energy emitted by the water body, 2) energy emitted by the atmosphere, and 3) inbound atmospheric energy reflected by the water body. Combined, the net long-wave radiation can be described through Equation 1.14:

$$\varphi_L = -\varphi_{LW} + (\varphi_{LA} - \varphi_{LR}) \quad [1.14]$$

where:  $\varphi_{LW}$  represents the radiation emitted by the water body [W/m<sup>2</sup>]  
 $\varphi_{LA}$  represents the radiation emitted by the atmosphere [W/m<sup>2</sup>]  
 $\varphi_{LR}$  represents the radiation reflected by the water body [W/m<sup>2</sup>]

Emittance of long-wave radiation from a water body can be represented as a function of the temperature of the body according to the Stefan-Boltzmann law, as shown in Equation 1.15:

$$\varphi_{LW} = \epsilon_w \sigma T_{wk}^4 \quad [1.15]$$

where:  $\epsilon_w$  represents the surface emissivity of the water body [0 to 1]  
 $\sigma$  represents the Stefan-Boltzmann constant; given as  
 $5.670 \times 10^{-8}$  [W/m<sup>2</sup>K<sup>4</sup>]  
 $T_{wk}$  represents the absolute water temperature [Kelvin]

The emissivity is defined as the ratio of net to total blackbody radiation emitted by a body at a particular surface temperature. Typically, the emissivity of most natural surfaces is relatively high, ranging from 0.94 to 0.99. For water and ice, the surface emissivity is given as 0.97 – meaning that 97% of incoming long-wave radiation is adsorbed (Ashton, 1986). By this definition, long-wave surface reflectivity can also be determined, as shown in Equation 1.16:

$$R_L = 1 - \epsilon_w \quad [1.16]$$

where:  $R_L$  represents the long-wave surface reflectivity of a body [0 to 1]

The second component of the long-wave radiation balance at the water surface is the incoming radiation that is emitted by the atmosphere. The rate of emittance is primarily dependent on the meteorological conditions that are present, including air temperature, amount of water vapour in the atmosphere, and cloud cover. Once again, the Stefan-Boltzmann law is applied, as presented in Equation 1.17:

$$\varphi_{LC} = \epsilon_a \sigma T_{ak}^4 \quad [1.17]$$

where:  $\varphi_{LC}$  represents the radiation emitted by the atmosphere under clear skies [ $\text{W}/\text{m}^2$ ]

$\epsilon_a$  represents the emissivity of the atmosphere [0 to 1]

$T_{ak}$  represents the absolute air temperature measured at an elevation of 2 m [Kelvin]

Numerous methods exist for estimating the atmospheric emittance, with each being expressed as a function of air temperature and relative humidity. Two such methods are provided in Equations 1.18 (Brunt, 1932) and 1.19 (Satterlund, 1979), as follows:

$$\epsilon_a = c + d\sqrt{e_a} \quad [1.18]$$

or,

$$\epsilon_a = 1.08 \left[ 1 - \exp\left(-e_a^{T_{ak}/2016}\right) \right] \quad [1.19]$$

where:  $e_a$  represents the vapour pressure [mb]

$c, d$  represent empirical coefficients; given as 0.52 and 0.065, respectively [-]

Estimation of saturated vapour pressure over both water and ice for a particular temperature is possible through application of the Goff-Gratch equation, as outlined in the World Meteorological Organization Standards and Recommended Practices (World Meteorological Organization, 1988). Knowledge of the relative humidity allows for estimation of the actual vapour pressure required in Equations 1.18 and 1.19.

Under cloudy conditions, an additional factor must be applied to account for the increases in atmospheric back radiation emission. The relationship outlined in Equation 1.20 has been widely applied for this purpose:

$$\varphi_{LA} = \varphi_{LC}(1 + kC^2) \quad [1.20]$$

where:  $k$  represents an empirical constant; typically given as 0.0017 [-]

The amount of radiation that is reflected can therefore be estimated by applying Equation 1.16, as outlined in Equation 1.21:

$$\varphi_{LR} = (1 - \epsilon_w)\varphi_{LA} \quad [1.21]$$

Utilizing the relationships presented in Equations 1.15 to 1.21, it is possible to expand and simplify Equation 1.14 to yield the net long-wave radiation flux at the water surface, as shown in Equation 1.22:

$$\varphi_L = \epsilon_w \sigma [-T_{wk}^4 + \epsilon_a (1 + kC^2) T_{ak}^4] \quad [1.22]$$

It is evident from Equation 1.22 that the presence of clouds plays an important factor in the cooling of a water body, particularly at night. Clouds act as an insulator of long-wave radiation, increasing atmospheric reflectance by 10-35% and slowing the cooling process (Ashton, 1986). The net is an insulating effect which slows ice formation during cloudy conditions.

#### *Latent and Sensible Heat Fluxes*

In nature, water readily changes state from liquid to vapor through the process of evaporation. For evaporation to occur, however, water molecules must consume energy in order to free them from their liquid bonds, thereby resulting in a net loss of latent heat energy from the system. The process is driven by relative differences in vapor pressure between the water surface and the air above it, taking place whenever the air is not fully saturated. Turbulent air motion resulting from wind represents the primary transport mechanism, with molecular diffusion and buoyant convection contributing under calm conditions.

The latent heat flux due to evaporation has been studied extensively and numerous relationships exist for estimating its value. The relationship presented in Equation 1.23 has been found to give good results for sub-freezing air temperatures and has been adopted within river ice engineering (Ashton, 1986; Rimsha & Donchenko, 1957):

$$\varphi_E = -[6.04 + 0.263(T_w - T_a) + 2.95V_a](e_s - e_a) \quad [1.23]$$

where:  $T_w$  represents the water temperature [°C]  
 $T_a$  represents the air temperature measured at 2 m [°C]  
 $V_a$  represents the wind velocity measured as 2 m [m/s]  
 $e_s$  represents the saturation vapour pressure [mb]

Relative differences in water and air temperature also produce a two-way conductive heat flux, either cooling or warming the water body. Under winter conditions, air temperatures are typically below freezing and energy is conducted away from the water body, constituting a net loss of sensible heat energy. Typically, this heat loss is proportional to the latent heat flux, and may be estimated using Equation 1.24 and 1.25 (Bowen, 1926):

$$\varphi_H = R_B \varphi_E \quad [1.24]$$

$$R_B = \frac{cP_a}{10000} \frac{(T_w - T_a)}{(e_s - e_a)} \quad [1.25]$$

where:  $R_B$  represents Bowen's Ratio [°C]  
 $c$  represents Bowen's constant; given as 0.6 [-]

These relationships have been shown to be applicable during winter conditions (Dingman, Weeks, & Yen, 1968). Consideration should be given, however, in

situations where air temperature is very low, as the assumption of proportionality between latent and sensible heat fluxes may not hold (Ashton, 1986).

### *Precipitation Heat Flux*

The introduction of rain or snow into a water body brings with it a net heat flux that either cools or warms the water. Of particular importance for river ice modeling is the energy consumption that occurs when snow is warmed and melted upon contact with the water surface. If it is assumed that the snow entering the system is of the same temperature as the air, the net heat flux can be estimated through Equation 1.26:

$$\varphi_p = -(92.5 - 0.611T_a)I_p \quad [1.26]$$

where:  $I_p$  represents the snowfall intensity, given in terms of equivalent rain intensity [mm/hr]

In Equation 1.26, consideration is given to both the warming of snow to its melting point (second term) and its subsequent melting (first term). The relationship assumes a water temperature of 0°C, and would require modification if the precipitation is in the form of rain.

### *Channel Bed Heat Flux*

The heat flux from the channel bed is typically a net gain into the system as a result of the conductive energy from friction with the bed, groundwater seepage,

and geothermal input. Generally, the groundwater and geothermal components of the total flux are fairly constant and relatively small, and therefore are often ignored. The heat flux generated by bed friction can be directly correlated to the channel geometry and the discharge, the relationship for which is outlined in Equation 1.27 (Tsang, 1982):

$$\varphi_G = \frac{9797.5Qs}{w} \quad [1.27]$$

where:       $Q$     represents the channel discharge [ $\text{m}^3/\text{s}$ ]  
                  $s$     represents the channel slope [ $\text{m}/\text{m}$ ]  
                  $w$     represents the channel width [ $\text{m}$ ]

### 1.2.2 *Linear Heat Transfer*

The full energy balance approach, in whole or in part, is seldom applied in river ice engineering practice due to the inherent lack of information within northern regions. The installation and maintenance of data recording equipment in the remote and harsh northern landscapes presents numerous financial and logistic limitations. In northern Manitoba, data collection is sparsely distributed and is often of poor quality. A common alternative to this approach is to simply assume that the net heat loss at the water surface is proportional to the difference in air and water temperatures. A bulk heat transfer term is applied to account for the cumulative heat exchange at the water surface, irrespective to the origin or distribution of the individual fluxes. This approach is outlined in Equation 1.28:

$$\varphi_* = C_0(T_a - T_w) \quad [1.28]$$

where:  $C_0$  represents the bulk heat transfer coefficient [W/m<sup>2</sup>°C]

The heat transfer coefficient varies greatly depending on the properties of each boundary layer, current meteorological conditions, and time of year. Typical values for the heat transfer coefficient between water and air during times of cooling range from 15 to 25 W/m<sup>2</sup>°C, and have been shown to increase proportionally with wind speed (Prowse, 1995).

### 1.3 River Ice Processes

The mechanics through which ice formation on lakes and rivers take place are influenced by a wider variety of meteorological and environmental factors, dictating if, when, and what type of ice will be generated. If weather conditions permit, ice nucleation at the water surface will commence forming microscopic ice particles. Once the particles are formed, they may either remain afloat forming static surface ice, or be entrained within the water body forming frazil ice. The vertical turbulence within the water body governs this process, and it is not uncommon to see both static and frazil ice processes take place on a particular reach with spatially and temporally varying levels of turbulence.

### 1.3.1 Nucleation

Under normal conditions, ice particles cannot be formed unless an initial size has already been attained, leading to the requirement for an initial nucleus upon which the subsequent growth of an individual ice particle can take place (Tsang, 1982). A similar theory governing the condensation of water vapour in the atmosphere is well established, whereby particles referred to as “Cloud Condensation Nuclei” provide the initial source for nucleation. In both instances, the size of the nucleation particle must exceed a temperature-dependent minimum value, which, in the case of ice, can be estimated through Equation 1.29 (Ashton, 1986):

$$r_{crit} = \frac{5.9 \times 10^{-8}}{\Delta T_w} \quad [1.29]$$

where:  $r_{crit}$  represents the critical radius for nucleation [cm]

$\Delta T_w$  represents the absolute degree of supercooling [°C]

The introduction of ice nuclei into a water body may occur through either spontaneous crystallization or artificial means. Primary ice particles are formed through these processes, termed homogeneous and heterogeneous nucleation.

#### *Homogeneous Nucleation*

Under some statistical chance, the random movement of water molecules within a water body may produce a structure that is identical in shape and orientation to

ice crystals. If the size of this embryo exceeds the critical size, growth is made possible and an ice particle is formed in the water. As per Equation 1.29, the statistical chance of developing an embryo of sufficient size increases with the degree of cooling, and only becomes a significant source of nucleation in waters supercooled to  $-40^{\circ}\text{C}$  (Tsang, 1982). Such a high degree of supercooling is not observed in nature, and as a result, homogeneous nucleation does not contribute to ice formation outside of carefully controlled laboratory environments.

### *Heterogeneous Nucleation*

Heterogeneous nucleation occurs when a foreign object serves as the nucleation center for ice formation. Because of the increased surface tension present at the liquid/solid interface, the statistical chance of the water molecules around the foreign particle obtaining the orientation of ice crystals increases. Similar to homogeneous nucleation, a higher degree of supercooling will work to promote ice formation; however, the threshold temperature is significantly higher. For inorganic compounds, this temperature may range from  $-30^{\circ}\text{C}$  to  $-3.5^{\circ}\text{C}$ , whereas for organic compounds, it can reach as high as  $-0.9^{\circ}\text{C}$  (Robert, 1979).

Heterogeneous nucleation is of particular interest when considering the development of border ice on a river. Due to fluctuations in water level, the river bank may be subjected to periodic cooling by the air. If the temperature of the bank material is cooled to below its threshold and the water elevation is raised such that its surface contacts the supercooled zone, ice formation will occur. This

is often the first ice phenomena that is observed on the water surface and is the main source of border ice growth in low turbulence zones.

### *Secondary Nucleation*

Nucleation through both homogeneous and heterogeneous means is classified as primary due to the fact that both initiate ice crystallization. In a process referred to as secondary nucleation, primary ice particles may collide and shear, thereby forming secondary ice nuclei and multiplying the total number of ice growth surfaces. As these new particles grow, they too experience shear and produce a chain reaction capable of generating significant volumes of ice.

### *1.3.2 Frazil Ice*

The formation of frazil ice in a river or lake is a dynamic process by which ice crystals are entrained within turbulent water. The presence of frazil is always associated with supercooled water; however a distinct discrepancy exists between the degrees of supercooling observed at the time of frazil production ( $\sim 0.03^{\circ}\text{C}$ ) and that specified by the theories governing heterogeneous nucleation ( $> 0.9^{\circ}\text{C}$ ) (Clark, 2006). As a result, the origin of frazil is still somewhat misunderstood. One viable theory suggests that a molecular sub-layer exists at the water surface which is capable of experiencing a degree of supercooling sufficient for heterogeneous nucleation. Any ice particles that are created within this layer are subsequently submerged and distributed throughout the depth by turbulence forming frazil ice (Michel, 1967). While it does comply with accepted nucleation principles, this theory has been subject to dispute given that

measurements of water surface temperatures during frazil ice production have not reached nucleation thresholds (Osterkamp & Gilfilian, 1975).

A second theory suggests that frazil ice is formed as a result of sprays crystallizing in the air and falling back into the water body (Gilfilian, Kline, Osterkamp, & Benson, 1972; Osterkamp, 1977). Formed as a result of wave breaking, splashing, and bubble bursting, airborne droplets are easily cooled to their heterogeneous nucleation threshold temperature. Once ice is initiated, growth will continue in water only several hundredths of a degree below freezing. While the theory has been questioned due to the droplets only being subject to cooling within the intermediate boundary layer whose temperature is close to 0°C, airborne ice crystals have been observed to occur above a supercooled water surface during cold temperatures (Osterkamp, Ohtake, & Warntment, 1974).

Airborne dust particles cooled to below their threshold temperature contacting the water boundary can also cause instantaneous heterogeneous nucleation and subsequent frazil formation in supercooled water (Tsang, 1982). However, it is hypothesized that the molecular boundary layer does not reach a sufficient degree of supercooling and that heterogeneous nucleation from particles other than ice is unlikely (Clark, 2006). Nonetheless, the airborne ice and dust particle theories are the most widely accepted sources for ice nucleation and frazil initiation.

One of the primary requirements for frazil production is the presence of supercooled water, which occurs when the water is cooled to below its freezing temperature. The latent heat of fusion released through frazil generation acts to offset the continued heat loss from the water body and return the system to thermal equilibrium. The total volume of ice generation required to balance the net heat deficit for a given duration of time may therefore be estimated using the physical relationship outlined in Equation 1.30:

$$V_f = -\frac{L_0 B_0}{\rho_i L_i} \int_{t=t_1}^{t=t_2} \phi_* dt \quad [1.30]$$

where:  $V_f$  represents the volumetric production of ice over a specified time period [ $m^3$ ]  
 $L_0$  represents the streamwise length of open water sections [m]  
 $B_0$  represents the spanwise width of open water sections [m]  
 $\rho_i$  represents the density of ice [ $kg/m^3$ ]  
 $L_i$  represents the heat of fusion of ice; given as 333,400 [J/kg]

The frazil is considered to be active throughout the supercooled generation process. During this time, the small ice particles will adhere to one another forming frazil flocs, which in turn stick together and float to produce frazil pans and rafts. Alternatively, the particles may adhere to the channel bed to form anchor ice. Suspended flocs may also shear and act as secondary nuclei for further frazil production. The presence of active frazil in a channel or lake has

significant risk implications to engineering infrastructure as it tends to accumulate on most underwater objects and may potentially clog trash racks or intake gates (Zbigniewicz, 1997; Dale & Ettema, 2006).

### 1.3.3 *Border Ice*

Border ice forms through heterogeneous nucleation of riverbank material in calm and quiescent water. It is typically the first surface ice to be observed on rivers, occurring after as little as 25 cumulative degree-days of freezing and in areas where the depth averaged water temperature is well above the freezing point (Michel, Mascotte, Fonseca, & Rivard, 1982). Once initiation occurs, the border ice will advance as long as environmental conditions support continual heat loss from the water body and the water level remains relatively stable as to not cause the ice to break or release from the bank. Specific mechanisms governing border ice growth vary from reach to reach, however the principle relationships remain the same. It is generally accepted that all border ice forms through two means: thermal growth and frazil accretion. In many instances, both mechanisms will take place on a specific river reach; however, one will dominate depending on hydraulic conditions.

Thermally grown border ice is controlled by heat loss at the water surface and not by mass exchange processes. Thermal growth is often of secondary importance on larger rivers; however, it plays a major part in the development of a surface ice cover on small rivers and brooks. Typically, this process is most dominant during the initial stages of border ice development, with decreasing

importance as the water body becomes supercooled and the border ice edges advance into the more turbulent waters near the center of the channel. In certain situations, border ice growth also dominates the final stages of freeze-up, when the concentration of surface ice floes is minimal and any open water sections must close thermally.

The formation of static surface ice is dependent on the presence of a stratified surface layer of supercooled water. Given that surface ice may form while the average water temperature is above the freezing point, it is often beneficial to estimate ice growth based on the surface water temperature. It is generally accepted that surface water temperatures between 0°C and -1.1°C produce surface ice formation (Matousek, 1984a). The exact level of supercooling required, however, is difficult to quantify due in part to a lack of measurements during freeze-up. As a result, this value is often determined through calibration by comparing the timing of the first thermal ice observation to the estimated surface water temperature given by Equation 1.31 (Matousek, 1984a):

$$T_s = T_w + \frac{\varphi_*}{1130u + bV_a} \quad [1.31]$$

where:  $T_s$  represents the surface water temperature [°C]  
 $u$  represents the average water velocity in the cross-section [m/s]  
 $b$  represents a channel width factor [-]

The channel width factor can be calculated using Equation 1.32 (Matousek, 1992):

$$b = \begin{cases} 15 & ; \quad B \leq 15 \\ -0.9 - 5.8 \ln(B) & ; \quad 15 < B \leq 3800 \\ 47 & ; \quad B > 3800 \end{cases} \quad [1.32]$$

where:  $B$  represents the width of open water in the wind direction [m]

Vertical mixing must be at a minimum to facilitate the formation of a supercooled layer at the water surface. Therefore, this process is only observed on the quiescent regions along the bank or in deep, slow moving sections. In a laboratory environment, static surface ice was found to form for all water velocities less than 0.24 m/s (Hanley & Michel, 1977). The rate of growth was independent of water velocity and was found to increase with decreasing air temperatures. In natural environments, however, this threshold is typically suppressed to between 0.06 and 0.15 m/s by the inclusion of countless environmental and hydraulic variables such as wind-induced turbulence or secondary currents (Michel et al., 1982; Matousek, 1984b; Santeford, 1990).

Estimation of thermal surface ice formation in natural environments is a complicated exercise that must consider, either directly or indirectly, the numerous variables governing its growth. The most significant of these include the rate of heat loss, the surface turbulence due to wind, and the degree of vertical mixing present. One of the only methods for quantifying this process is

presented in Equation 1.33, which correlates thermal surface ice growth to a limiting vertical velocity (Matousek, 1984b):

$$U_v = \frac{\varphi_*}{1130(-1.1 - T_w)} - \frac{bV_a}{1130} \quad [1.33]$$

where:  $U_v$  represents the limiting vertical velocity beyond which surface ice will not form [m/s]  
 $b$  represents a channel width factor [-]

The relationship outlined in Equations 1.33 does not allow for computation of growth rate, and only estimates the overall extent of thermal border ice growth. It can be assumed that this process occurs relatively quickly on most fast-flowing rivers and that the full extent of thermal border ice is formed over the course of one to two days. The largest difficulty in applying this method lies in the correlation of the calculated limiting vertical velocity to either measured or estimated values. Measurement can be accomplished directly utilizing acoustic Doppler profiling, however, this becomes difficult during freeze-up and only yields point data. Alternatively, the vertical velocity distribution can be estimated using three-dimensional computational models, but this too quickly becomes unfeasible for large reaches. Nonetheless, this method has been widely accepted for border ice growth prediction in non-supercooled water and has been shown to provide good results at the onset of freezing (Miles, 1993).

Where water velocities exceed the 0.06 to 0.15 m/s threshold, any new ice needles that form on the longitudinal ice edge are sheared off and thermal growth of border ice ceases either in whole or in part. An increase in turbulence within these zones also prevents thermal stratification at the water surface and acts to simultaneously cool the entire water column. Should the column become supercooled, frazil particles will form throughout its depth and those near the surface will contribute to frazil accretion at the border ice edge. Within these higher velocity and turbulence zones, frazil accretion is the only mechanism supporting continued border ice advancement.

On larger or steep rivers, the presence of active frazil within the water body can act to quickly expand the border ice extent. This mechanism can be expanded to include accretion from other frazil ice phenomena, including frazil pans and frazil slush. The ice cover that results is generally characterized by a successive series of thin layers of frazil particles accumulating towards the center of the channel. The presence of frazil near the water surface also acts to increase the net heat loss from the water body and reduce the effect of turbulence (Newbury, 1968). As a result, one commonly observed phenomenon is that of banded ice, where thermal growth intercepts layers of frazil accretion.

Two methods exist for estimating border ice growth in supercooled water where active frazil is present. The first was developed for the Nelson River in northern Manitoba and applies an empirical approach in estimating border ice growth with

time based on the cumulative net heat loss, as per Equation 1.34 (Newbury, 1968):

$$\Delta w = \frac{mn}{2} \int_{t=t_1}^{t=t_2} \varphi_* dt \quad [1.34]$$

where:  $\Delta w$  represents the growth of border ice for a given time period [m]  
 $m$  represents the adhesion parameter for slush ice [-]  
 $n$  represents the number of boundaries on which border ice can grow [-]

The adhesion parameter relates the portion of slush ice that is retained at the ice edge, and can be estimated using the relationship presented in Equation 1.35 (Newbury, 1968):

$$m = \frac{a}{(AS)^b} \quad [1.35]$$

where:  $A$  represents the cross-sectional area of the reach [m<sup>2</sup>]  
 $S$  represents the average water surface slope [m/m]  
 $a, b$  represent empirical calibration coefficients [-]

While the relationship presented in Equations 1.34 and 1.35 is simplistic and requires only easily attainable information, it does have several shortcomings. Due to its assumption of equal border ice growth at both banks and a constant growth rate, the effect of reach geometry and other causes of differential growth

are not considered. In addition, its empirical approach fails to include numerous pertinent parameters, including hydrometric and frazil ice conditions. The second approach considers both of these parameters directly, as outlined in Equation 1.36 (Michel et al., 1982):

$$\Delta w = \frac{R}{\rho_w L_i} \int_{t=t_1}^{t=t_2} \varphi_* dt \quad [1.36]$$

where:  $R$  represents a dimensionless growth parameter [-]

$\rho_w$  represents the density of water [kg/m<sup>3</sup>]

The dimensionless growth parameter relates the border ice growth rate to a given heat loss, and can be approximated using Equation 1.37 (Michel et al., 1982):

$$R = \frac{14.1 N_f^{1.08}}{(U_s/U_c)^{0.93}} \quad [1.37]$$

where:  $N_f$  represents the frazil concentration [%]

$U_s$  represents the open water surface velocity adjacent to the ice edge [m/s]

$U_c$  represents the critical velocity for frazil adhesion at the ice edge [m/s]

It should be noted that the critical velocity for frazil adhesion varies from reach to reach and is often treated as a calibration parameter in border ice models, typically ranging from 0.4 to 0.6 m/s (Tsang, 1982; Matousek, 1984b; Santeford, 1990). Where surface water velocities exceed this limit, the shearing action at the ice edge inhibits frazil accretion, negating or even reversing subsequent border ice advance. A relationship that is based on the physical limits of this definition is often applied in determining the border ice growth regime of a channel, as given in Equation 1.38 (Michel et al., 1982):

$$\left\{ \begin{array}{ll} U_s/U_c \leq 0.167 & ; \text{ thermal growth} \\ 0.167 < U_s/U_c \leq 0.167, & ; \text{ frazil accretion} \\ 1.0 < U_s/U_c & ; \text{ negligible growth} \end{array} \right. \quad [1.38]$$

During supercooled conditions, the relationships given in Equations 1.36 and 1.37 have been shown to provide the most accurate prediction to border ice growth. Equations 1.34 and 1.35 can be used to provide a reasonable approximation of total ice growth, however, its assumption of constant growth rate may lead to overestimation during the latter parts of the freeze-up season (Miles, 1993).

#### 1.3.4 Skim Ice

The formation of skim ice shares many similarities with that of both border and frazil ice. Similar to the formation of thermal border ice, a supercooled water surface layer may form in areas of low water velocity and provide conditions suitable for small particles of ice to form at the water surface. If the vertical

turbulence is sufficiently high, these particles will become entrained within the water column forming frazil ice. Alternatively, if the vertical turbulence is low, the particles will remain at the water surface and will quickly grow laterally to form skim ice. Given that this ice is not attached to the channel bank, it is free to travel downstream with the flow and eventually bridge to form an initial ice cover.

The formation of skim ice is an extremely rapid process and may act to form an ice cover over a significant portion of the reach in as little as one day. As with thermal border ice, the rate of growth is difficult to determine and typically only the extent and timing of skim ice formation can be predicted. One of the requirements that must be considered is the presence of a supercooled layer at the water surface, which can be estimated using Equations 1.31 and 1.32 and compared to a critical value through calibration. If this condition is satisfied and surface ice particles are generated, the distinction between skim and frazil formation can be made through comparison of particle buoyant velocity to the vertical turbulence in the channel. If each particle is assumed to take the shape of a thin circular disk, its buoyancy can most accurately be estimated using Equation 1.39 (Morse & Richard, 2009):

$$v_b = av^{1-2b}d^{2b-1}\left(\frac{Xv^2}{d^2}\right)^b \quad [1.39]$$

where:  $v_b$  represents the ice particle buoyant velocity [m/s]  
 $v$  represents the kinematic viscosity of the water [m<sup>2</sup>/s]

$d$  represents the particle diameter [m]

$X$  represents the Best number [-]

$a, b$  represent empirical coefficients [-]

The Best number defines particle and fluid characteristics and can be determined through Equation 1.40 (Morse & Richard, 2009):

$$X = \frac{2\rho_i h_p g (\rho_w / \rho_i - 1) d^2}{\rho_w v^2} \quad [1.40]$$

where:  $h_p$  represents the particle thickness [m]

$g$  represents the gravitational constant, given as 9.806 [m/s<sup>2</sup>]

Values for the empirical coefficients in Equation 1.39 can be estimated using the relationships in Equations 1.41 and 1.42 (Morse & Richard, 2009):

$$a = \frac{\delta_0^2 [(1 + cX^{0.5})^{0.5} - 1]^2}{4 X^b} \quad [1.41]$$

and,

$$b = \frac{1}{2} cX^{0.5} [(1 + cX^{0.5})^{0.5} - 1]^{-1} (1 + cX^{0.5})^{-0.5} \quad [1.42]$$

where:  $c$  represents an empirical constant;  $c = 4\delta_0^{-2} C^{-1/2}$  [-]

$\delta_0$  represents an empirical constant, given as 5.827 [-]

$C$  represents an empirical constant, given as 0.6 [-]

The result obtained through Equation 1.39 yields an approximate threshold of vertical mixing required to entrain ice particles of a particular size. A means of estimating the vertical turbulence is not well established, however, one method is presented in Equation 1.43 (Matousek, 1992):

$$u_v = \frac{0.0121u}{(M_z C_z)^{0.305} R^{0.5}} \quad [1.43]$$

where:  $u_v$  represents the average vertical turbulence intensity [m/s]

$C_z$  represents the Chezy coefficient [ $m^{0.5}s$ ]

$M_z$  represents a Chezy adjustment;  $M_z = 0.7C_z + 6$  [-]

$R$  represents the hydraulic radius [m]

The relationships presented in Equations 1.39 and 1.43 provide one method for distinguishing between frazil and skim ice formation on a channel. Where the vertical turbulence exceeds the rise velocity of ice particles, frazil ice will form. The opposite holds true for skim ice. Due to the stochastic nature of Equation 1.43 and a distribution in particle size, however, it should be understood that where the two values are near equal, frazil and skim ice generation are both present and neither process is dominant.

### 1.3.5 *Ice Regimes*

The level of turbulence in a river or lake typically defines the type of ice process, or the ice regime, that occurs. Given changes to the flow or meteorological conditions present, it is not uncommon for multiple ice regimes to take place on the same body of water. This change may be tied to long-term (year to year) variations, such as drought or flood years, or more dynamic short-term (day to day) variability through flow regulation or unstable weather. In any case, the overall ice formation mechanism that dominates at any particular time can be defined by one of three ice regimes (Santeford, 1990).

#### *Slow Regime*

The slow regime is limited to areas of extremely quiescent water where the vertical turbulence is minimal. Thermal stratification occurs at the water surface easily developing a layer of supercooled water. Starting at the banks, a network of ice needles forms at the surface and spreads quickly towards the center until an initial surface bridge is formed. If conditions persist, the ice will expand both upstream and downstream and the entire sheet will thicken until a permanent cover is developed. The slow regime is the primary mechanism for ice formation on lakes, and is only observed on extremely low flowing or wide rivers whose surface velocities are negligible.

#### *Transitional Regime*

The transitional regime represents a balance in the ice cover formation between wholly static and dynamic natures. Thermal border ice growth still takes place

along the banks of the channel; however, the higher velocity zones near the center of the channel limit its growth. The remaining open water sections are allowed to supercool and the vertical turbulence dictates whether skim or frazil ice is formed. Under the transitional regime, the vertical turbulence does not entrain surface particles resulting in large sheets of skim ice being formed at the water surface and transported downstream with the flow in what is commonly referred to as a skim ice run.

Once the individual skim ice sheets are large enough, frequent enough, or reach a narrowing in the channel, they will press against the border ice and eventually jam to bridge the channel. Bridging is also commonly observed at locations of bridge piers or other obstructions in the river. Subsequent sheets accumulate on the upstream leading edge and progressively build up until a stable ice cover is developed. The slow regime is often characteristic of medium and large rivers with a mild slope.

### *Fast Regime*

The fast regime is dependent primarily on dynamic ice processes for the development of an ice cover and therefore requires vertical mixing strong enough to entrain surface ice particles. Similar to the transitional regime, thermal border ice growth ceases when the edge reaches the higher velocity zones at the center of the channel. As the remaining open water becomes supercooled, surface ice particles are entrained throughout the water column forming frazil ice. While the frazil is active, particles near the surface will adhere to the border ice edge and

contribute to its growth through frazil accretion. Alternatively, particles near the bed may adhere to rocks and other features to form anchor ice. Those particles in suspension will adhere together to form frazil flocs, which, when large enough, will float to the surface as slush.

Eventually, the slush freezes to form small frazil pans on the water surface. Given enough time in close proximity to one another, these small pans freeze together and continue to agglomerate, reaching several meters in size. Rubbing and grinding against both one another and border ice tends to give them a round shape, from which they get the name pancake ice. Initial bridging occurs through juxtaposition of these surface ice floes at a channel narrowing or obstruction and the ice cover expands upstream. The ice front progression under the fast regime is relatively slow due to some of the pans being submerged under the leading edge and typically adheres to the characteristics of an equilibrium jam, as shown in Figure 1.1. The jam in this case is much thicker than that of a skim ice run and may result in a local thick deposit of frazil under an ice cover, known as a hanging dam.

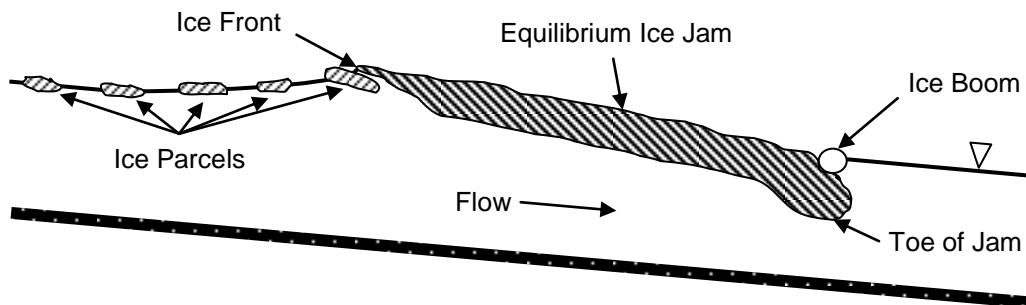


Figure 1.1. Equilibrium Ice Jam Profile

The fast regime is characteristic of steep rivers, especially where a series of rapids are involved. High bed roughness may also increase vertical turbulence in a channel such that frazil is formed on mild rivers (Matousek, 1992). A similar process of frazil formation has also been observed on lakes given sufficient vertical mixing due to wind (Daly & Ettema, 2006). The fast regime presents the largest risk to engineering infrastructure and is often avoided or mitigated through design or operation.

## 1.4 River Ice Models

Since the 1970's, significant effort has been applied towards developing a means of estimating and predicting river ice formation. Based on the physical and empirical relationships governing ice formation, numerous one- and two-dimensional models have since been developed for solving river ice problems throughout the world. These models are formulated and solved numerically for the primary reason that this approach allows for direct consideration of the various hydraulic, thermal, and ice processes that contribute to the formation of an ice cover. An overview of the most widely applied models is provided in the following subsections.

### 1.4.1 *ICEDYN*

The ICEDYN model is the latest version in the series of river ice models developed by Acres International Limited since 1973. At its core, ICEDYN is a

one-dimensional finite difference model that employs a four-point implicit scheme to solve the St. Venant equations for conservation of mass and momentum (Carson & Groeneveld, 1997). The model has recently expanded on its predecessor ICESIM to allow for simulation of time-varying flows through coupling of separate hydrodynamic and ice mechanic modules at discrete time steps.

The primary use of the model is towards simulation of fragmented ice cover formation during both freeze-up and break-up periods. The volume of ice supply is either provided (break-up) or computed using heat transfer theory (freeze-up). Subsequent transport and deposition of surface ice is governed primarily by critical velocity criteria (Judge, Lavender, Carson, & Ismail., 1997). The model also includes calculations for border ice growth, mechanical thickening by shoving, and ice erosion due to hydro peaking. ICESIM and ICEDYN have had numerous successful applications in northern Manitoba and other northern regions of Canada (Carson & Groeneveld, 1997).

#### *1.4.2 RIVICE*

The RIVICE model was initiated in 1988 by a consortium of five major consulting firms in an effort to develop a model capable of simulating unsteady ice regimes. Time-varying flows are solved through application of the one-dimensional finite difference solution to the St. Venant equations using the Galerkan technique of weighted residuals (Martinson, Sydor, Marcotte, & Beltaos, 1993). The

hydrodynamic solution is then coupled with that of 11 other modules to provide a comprehensive output of hydraulic and ice conditions.

The model is capable of simulating most river ice formation mechanisms, including border, skim, frazil, and anchor ice. Border ice width may either be specified by the user or computed using one of two methods. Skim, frazil, and anchor ice are then estimated based on the net heat balance and several empirical relationships (Holder & Saade, 1991). Once a surface bridge is formed, ice cover evolution follows the same algorithms as that of the ICEDYN model, including those for accumulation of surface ice at the leading edge, mechanical thickening due to shoving, and deposition and erosion of ice under a cover (Martinson et al., 1993).

#### 1.4.3 VARY-ICE

The VARY-ICE model has been developed and used by KGS Group since the early 1970's to solve one-dimensional river ice problems. Its predecessor, ICE-PRO, is closely related to the RIVICE model, employing the same algorithms in solving the relationships controlling ice generation, transportation, deposition, and erosion (Curi, Carson, & Gee, 2001). Improvements to the ICE-PRO algorithms have been made and incorporated into VARY-ICE, with the most notable being the addition of an unsteady-state solution for time-varying flows.

#### 1.4.4 *River1D*

The River1D hydraulic routing model developed at the University of Alberta has recently been updated to include routines for simulating the heat balance at the water surface and some thermally driven ice-water mass exchange processes (Andrishak & Hicks, 2008). The hydraulic routing component applies the characteristic-dissipative-Galerkin finite element scheme in solving the one dimensional St. Venant equations. The model approximates the channel geometry using rectangular cross-sections and allows for unsteady-state solutions. Water heating and cooling, frazil ice formation and transport, thermal ice growth, and ice front progression are all solved using a purely Eulerian frame of reference. Border, skim, and anchor ice formation has not yet been incorporated into the model framework.

#### 1.4.5 *RICEN*

The RICEN model was developed in the 1990's at Clarkson University to address river ice problems in a comprehensive manner. River hydraulics are represented through the one-dimensional St. Venant equations and solved using a four-point implicit finite difference scheme. The solution is coupled with a thermal and ice condition sub-model to yield estimates of water temperature, frazil ice concentration, border and skim ice growth, anchor ice growth, ice transport, ice cover progression, under-ice transport and deposition, and thermal growth and decay of static ice (Shen, Wang, & Lal, 1995). The model also applies a unique

two-layer ice transport module where both suspended and surface ice transport is considered.

#### 1.4.6 *MIKE-ICE*

The MIKE-ICE model is an add-on to the Danish Hydraulic Institute's MIKE11 suite of hydraulic modelling software that enables it to consider thermal ice processes taking place on a reach during cooling periods. The model applies the six-point Abbott-Ionescu scheme in solving the one-dimensional St. Venant equations through finite difference discretization. The full energy balance is then applied to calculate the change in water temperature and frazil generation. The model also considers surface ice formation, ice cover progression through juxtaposition, under-ice transport and deposition, border ice growth, and thermal growth and decay of static ice (Theriault, Saucet, & Taha, 2010). Border ice is calculated using a limiting velocity criteria, which is compared to a two-dimensional approximation of local water velocity based on flow depth.

#### 1.4.7 *River2D*

Initially developed as a hydraulic model for fish habitat at the University of Alberta, the River2D model is currently undergoing an update to include river ice processes. The model's framework is based on the two-dimensional solution of the depth-averaged Navier-Stokes equations using the characteristic-dissipative-Galerkin finite element scheme (Blackburn & Steffler, 2002). Through a purely Eulerian frame of reference, the model considers the energy balance at the water surface, supercooling and frazil generation, rise and transport of surface ice,

bridging and frontal progression, and border ice formation (Wojtowicz, 2010). To date, application of the model has been limited to either open water or winter ice cover conditions as the river ice components are still in a state of testing and validation.

#### 1.4.8 *CRISSP-2D*

CRISSP-2D is a comprehensive two-dimensional river ice model developed at Clarkson University as an extension to the DynaRICE model, expanding on it to include both ice dynamics and thermal ice processes. The current model is capable of simulating most river ice processes, including water cooling, frazil formation, skim and border ice growth, suspended and surface ice transport, ice cover progression, under-ice transport and deposition, mass exchange processes, and thermal growth and decay of static ice (Shen et al., 1995). The model has also been recently updated to include anchor ice growth, decay, and release, as well as aufeis processes (Malenchak, Doering, & Shen, 2011). River hydraulics are represented using the two-dimensional depth-averaged Navier-Stokes equations and solved in finite element form using the streamline upwind Petrov-Galerkin approach. A Lagrangian discrete parcel method is utilized to simulate ice dynamics and transport. A full description of model components is provided in Chapter 2.

## 1.5 Research Objectives

The application of the various river ice prediction models is often hindered by their various assumptions and limited applicability to large-scale studies. Many river ice problems are highly dynamic and, as a result, are often simplified to a certain degree to make representation in a one-dimensional modelling environment feasible. Two-dimensional models, while generally providing a more comprehensive output, require significantly higher computation power and are therefore limited to use on smaller reaches. Secondly, few have advanced beyond the developmental stage for use as an engineering tool. To this end, the research objectives of this study are two-fold: 1) develop a predictive tool for use in the Jenpeg Ice Stabilization Program that is capable of providing a quantifiable estimate of frazil, skim, and border ice growth on the short term, and 2) validate the use of two-dimensional numerical modelling for use in regional scale river ice studies.

This study applies measured and observed data towards meeting the research objectives. A total of ten years (2001 to 2010) serves as the basis for model calibration and validation. Each year is analyzed independently for both open water and freeze-up to assess the overall model performance. Simulations stemming from measured history are validated against first- and second-hand observations of the ice regime. In specific, this research focuses on border ice formation, skim and frazil ice generation and transport, and ice front progression.

---

# CHAPTER 2:

## Numerical Model

---

### 2.1 CRISSP-2D Overview

At the time of writing, CRISSP-2D is the only publically available two-dimensional river ice model and often represents the only means of simulating river ice conditions in reaches with complex geometry, flow characteristics, or ice regimes. Development of the model began in 2000 at Clarkson University by Dr. Hung Tao Shen as an extension to the DynaRICE model, primarily expanding on it to include thermal ice calculations. In its current state, the model consists of six individual modules that, when coupled, provide a comprehensive simulation of both hydrodynamics and ice dynamics. Each module is outlined as follows and is discussed in more detail in the following sections:

- Hydrodynamic Module;
- Water Temperature Module;
- Thermal Ice Module;
- Dynamic Ice Module;
- Undercover Ice Transport and Accumulation Module; and,
- Ice Cover Breakup Module.

CRISSP-2D relies on both the hydrodynamic and ice modules to form a comprehensive prediction of river ice conditions. At specific intervals in model time, the hydrodynamic solution is paused and its output at this time is used to update the ice dynamic solution in increments. Applying the newly generated river ice conditions, the hydrodynamic solution starts again and continues until the next interval. In this way the model is coupled, with each interval being referred to as the coupling time step.

Within the model framework, river hydrodynamics, energy transfer, and border ice are defined using an Eulerian frame of reference, whereas skim ice and river ice dynamics are defined in Lagrangian form. The primary difference between the two methods is in the way movement of water, energy, and ice parcels (discrete groups of ice particles) are tracked. In the Eulerian approach, a static location is chosen over which the movement of parcels are tracked. In the Lagrangian approach, the individual parcels themselves are tracked with both space and time. The Lagrangian approach for modelling river ice dynamics was chosen primarily because of its flexibility in modelling complex river ice problems with high deformity, typical to occur at ice boundaries or booms.

## 2.2 Hydrodynamic Module

The hydrodynamics of a reach are represented by CRISSP-2D through an Eulerian implementation of the finite element method, which ultimately solves the

two-dimensional depth-averaged Navier-Stokes equations using a streamline upwind Petrov-Galerkin approach. The relationship representing the conservation of mass in both the streamwise ( $x$ ) and spanwise ( $y$ ) direction is summarized in Equation 2.1 (Liu & Shen, 2005):

$$\frac{\partial H_w}{\partial t} + \frac{\partial(q_{tx})}{\partial x} + \frac{\partial(q_{ty})}{\partial y} = \frac{\partial}{\partial t}(Nh'_i) \quad [2.1]$$

where:  $H_w$  represents the total water depth [m]  
 $q_t$  represents the total two-layer unit width water discharge [ $m^2/s$ ]  
 $N$  represents the volumetric ice concentration [ $m^3/m^3$ ]  
 $h'_i$  represents the submerged ice thickness [m]

Similarly, the conservation of momentum can also be determined through application of Equations 2.2 and 2.3, respectively:

$$\begin{aligned} \frac{\partial q_{tx}}{\partial t} + \frac{\partial}{\partial x} \left( \frac{q_{tx}^2}{H_t} \right) + \frac{\partial}{\partial y} \left( \frac{q_{tx}q_{ty}}{H_t} \right) \\ = f q_{ty} + \frac{1}{\rho_w} (\tau_{sx} - \tau_{bx}) + \frac{1}{\rho_w} \left( \frac{\delta T_{xx}}{\delta x} + \frac{\delta T_{yx}}{\delta y} \right) - g H_t \frac{\delta \eta}{\delta x} \end{aligned} \quad [2.2]$$

$$\begin{aligned} \frac{\partial q_{ty}}{\partial t} + \frac{\partial}{\partial x} \left( \frac{q_{tx}q_{ty}}{H_t} \right) + \frac{\partial}{\partial y} \left( \frac{q_{ty}^2}{H_t} \right) \\ = -f q_{tx} + \frac{1}{\rho_w} (\tau_{sy} - \tau_{by}) + \frac{1}{\rho_w} \left( \frac{\delta T_{xy}}{\delta x} + \frac{\delta T_{yy}}{\delta y} \right) - g H_t \frac{\delta \eta}{\delta y} \end{aligned} \quad [2.3]$$

where:  $H_t$  represents an equivalent water depth for the total two-layer discharge [m]

$f$  represents the Coriolis coefficient [-]

$\tau$  represents the bed ( $b$ ) and surface ( $s$ ) shear stresses [ $\text{N/m}^2$ ]

$T$  represents eddy viscosity parameters [-]

$\eta$  represents the water surface elevation [m]

The relationships outlined in Equations 2.1 to 2.3 are modified forms of the Navier-Stokes shallow water equations to account for two-layer flow. Water is allowed to pass through both the lower layer beneath the ice cover, as well as the upper ice layer as either seepage or moving ice. Using the model, these equations are calibrated to observed values by adjusting the Manning channel bed roughness parameter for individual reaches during open water conditions. A global Manning roughness for ice is also available for simulations during ice cover conditions.

### 2.3 Water Temperature Module

The simulation of water temperature and suspended frazil ice concentration are both carried out within the water temperature module of CRISSP-2D, relying heavily on the net energy balance at the water surface. This balance is quantified using either the full energy budget if sufficient data is available, or through a linear heat transfer approximation where only air temperature is required. The net

energy transfer from the water column can then be quantified using the relationship presented in Equation 2.4:

$$\frac{\delta H_w e_T}{\delta t} = \varphi_* + \rho_i L_i H E \quad [2.4]$$

where:  $e_t$  represents the thermal energy of the ice-water mixture in the water column [J/m<sup>3</sup>]  
 $E$  represents the net volumetric rate of loss of frazil due to mass exchanges at the surface and bed [m<sup>3</sup>/m<sup>3</sup>s]

Changes in thermal energy over a set time period are used to estimate changes to both water temperature and suspended frazil concentration on a nodal basis, as outlined in Equation 2.5:

$$e_t = \rho_w C_p (1 - N) T_w - \rho_i N L_i \quad [2.5]$$

where:  $C_p$  represents the specific heat of water; given as 4,186 [J/kg°C]

Using Equations 2.4 and 2.5, both water temperature and suspended frazil concentration are formulated in conservative form and solved using finite element approximations. An example showing the conservative form of the water temperature approximation is provided in Equation 2.6:

$$\begin{aligned} \frac{\delta T_w H_w}{\delta t} + \frac{\delta q_{tx} T_w}{\delta x} + \frac{\delta q_{ty} T_w}{\delta y} \\ = \frac{\delta}{\delta x} \left( v_T \frac{\delta T_w H_w}{\delta x} \right) + \frac{\delta}{\delta y} \left( v_T \frac{\delta T_w H_w}{\delta y} \right) - \frac{\varphi_*}{H_w \rho_w C_p} \end{aligned} \quad [2.6]$$

where:  $v_T$  represents a horizontal exchange coefficient [-]

The relationship provided in Equation 2.6 and the equivalent one for suspended frazil ice concentration consider both advective and diffusive transport mechanisms, as well as the various heat fluxes that occur along the channel bed, water surface, and within suspension. The two equations do not consider, however, the influence of thermal frazil ice growth or mass exchange processes on water temperature and suspended frazil ice concentration. These processes are considered separately and coupled with the result of the advection and diffusion relationships to provide a comprehensive output. In CRISSP-2D, the change in suspended ice concentration is calculated by first considering the thermal growth of frazil particles, as given in Equation 2.7:

$$\frac{\delta N_v^g}{\delta t} = - \frac{1}{\rho_i L_i} \frac{N_u^f K_w}{d_e} a_0 T_w F_n \quad [2.7]$$

where:  $N_v^g$  represents the volumetric thermally grown frazil particle concentration [ $m^3/m^3$ ]

$N_u^f$  represents the Nusselt number [-]

$K_w$  represents the thermal conductivity of water [ $W/m^\circ C$ ]

$d_e$  represents the average frazil crystal thickness [m]

$a_0$  represents the surface area of a frazil particle;  $a_0 = \pi d_f d_e$  [m<sup>2</sup>]

$d_f$  represents the average frazil crystal length [m]

$F_n$  represents the number of frazil crystals per unit volume,

$$F_n = N/V_p \text{ [crystals/m}^3\text{]}$$

$V_p$  represents the mean crystal volume;  $V_p = \pi d_f^2 d_e / 4$  [m<sup>3</sup>]

The overall suspended ice concentration at the end of each time step is then calculated by combining the output from Equation 2.7 with that of the advection and diffusion relationship, as outlined in Equations 2.8 to 2.11:

$$N_f^{n+1} = \frac{q_v^n}{p_v^n} + \left( N_f^n - \frac{q_v^n}{p_v^n} \right) \exp(-p_v^n \Delta t) \quad [2.8]$$

where:

$$p_v^n = \frac{\theta V_b^n + \gamma}{H^n} \quad [2.9]$$

$$V_b^n = \left[ \left( v_b N_f^n - \varepsilon_y \frac{\delta N_f^n}{\delta y} \right) / N_f^n \right] \quad [2.10]$$

and,

$$q_v^n = \frac{\beta h_i^n N_s^n}{H^n} + \frac{\delta N_v^g}{\delta t} \quad [2.11]$$

- where:
- $N_f$  represents the overall volumetric frazil particle concentration in the current ( $n$ ) and next ( $n + 1$ ) time step [ $\text{m}^3/\text{m}^3$ ]
  - $\theta$  represents the probability of deposition of frazil particles at the surface layer [0 to 1]
  - $\gamma$  represents the rate of accretion of frazil particles to the bed per unit area [ $\text{m}/\text{s}$ ]
  - $\varepsilon_y$  represents the a vertical mixing coefficient [ $\text{m}^2/\text{s}$ ]
  - $\beta$  represents the rate of re-entrainment of surface ice per unit area [ $\text{m}/\text{s}$ ]
  - $h_i$  represents the total ice thickness;  $h_i = h_s + (1 - e_f)h_f$  [m]
  - $h_s$  represents the solid ice thickness [m]
  - $e_f$  represents the porosity of frazil ice at the surface [-]
  - $h_f$  represents the surface frazil ice thickness [m]
  - $N_s$  represents the concentration of surface ice per unit area [ $\text{m}^2/\text{m}^2$ ]

Water temperature at the end of each time step is calculated in a similar manner, considering both advection and diffusion transport as given by Equation 2.6, as well as the additional change due to the thermal growth of frazil ice. This relationship is provided in Equation 2.12:

$$T_w^{n+1} = T_w^n \exp\left(-\frac{N_u^f K_w a_0 F_n}{d_e \rho_w C_p (1 - N_f^{n+1})} \Delta t\right) \quad [2.12]$$

where:  $T_w$  represents the water temperature in the current ( $n$ ) and next ( $n + 1$ ) time step [ $^{\circ}\text{C}$ ]

$a_0$  represents the surface area of a frazil particle;  $a_0 = \pi d_f d_e$  [ $\text{m}^2$ ]

Overall, the calculation of both water temperature and suspended frazil concentration is based on the concept of thermal equilibrium, whereby the heat deficit present in a supercooled water column is offset by the latent heat released in the formation of frazil ice. The total volume of frazil generated is such that the water column returns to a state of equilibrium, in this case the freezing point.

## 2.4 Thermal Ice Module

All remaining ice formation processes are simulated within the thermal ice module, including border ice, skim ice, mass exchange with the bed and surface, and static ice growth and decay. In particular for border and skim ice, the prediction routines are relatively simple, relying solely on a check of the physical criteria governing each process, which, if satisfied, instantaneously generates the full volume of ice in each coupling time step. More specifically, the static border ice routine checks the following criteria at each node:

- Water surface temperature is less than a user specified critical value required for nucleation;
- Frazil buoyant velocity exceeds the vertical turbulence intensity;
- Depth-averaged velocity is less than a user defined critical value; and,
- The node is adjacent either to a land boundary or existing border ice.

Similarly, the skim ice routine checks for the following:

- Water surface temperature is less than 0°C;
- Frazil buoyant velocity exceeds the vertical turbulence intensity; and,
- The water surface is not covered by a stationary ice cover

If all conditions are satisfied, an initial border ice cover or skim ice parcel is generated in each element using a user defined thickness and a concentration of 1.0. In both cases, the nodal water surface temperature is calculated using the relationship outlined in Equation 1.31. This criterion is particularly useful in calibrating the timing of border ice formation through adjusting the critical water surface temperature parameter. It may also be used to calibrate the border ice extent; however, this process has been shown to be highly dependent on local water velocity and should be calibrated accordingly using the critical velocity for border ice parameter. Frazil buoyant velocity and the magnitude of vertical turbulence are estimated using methods similar to those described in Equations 1.39 and 1.43, and require little calibration beyond defining the frazil particle size. Dynamic border ice prediction is not incorporated into CRISSP-2D; however

potential exists for doing so utilizing the frazil accretion relationship outlined in Equation 1.36.

Frazil ice that is generated in the water column undergoes several mass exchange processes as the particles flocculate, rise to the surface, and contribute to the surface ice run by forming frazil pans or attaching to the underside of existing surface ice. This process may also be reversed, whereby surface particles are re-entrained into the flow in areas of high turbulence. In CRISSP-2D, this bi-directional process is modeled using a two-layer mass exchange between the suspended and surface layers. The net mass exchange between the two layers during a given time interval is calculated using the relationship defined in Equation 2.13:

$$\frac{\delta M_{if}}{\delta t} = [\theta v_b N_f N_s - \beta h_i N_s + \theta v_b N_f (1 - N_s)] \rho_i \quad [2.13]$$

where:  $M_{if}$  represents the net mass exchange between the suspended and surface layers per unit area [ $\text{kg}/\text{m}^2$ ]

The first two terms on the right hand side of Equation 2.13 define the volume of ice exchanged with ice covered areas, whereas the third term deals with open water. As a result, it is possible to distribute these volumes accordingly, between that which goes towards forming new parcels (open water condition) and that which contributes to the thickening of existing parcels or static ice (ice covered

condition). Calibration of these processes is dependent on user defined frazil particle rise velocity, deposition probability, and re-entrainment rate parameters.

Whenever a new frazil ice parcel is formed, its properties are defined using a user specified initial condition. Each parcel is assumed to be square with an area equivalent to the element in which it was formed. Similar to skim ice, the initial thickness is defined by the user. The concentration of each parcel is then calculated knowing the volume of ice reaching open water and the initial parcel dimensions. In subsequent time steps, addition of frazil ice to the undersurface of existing parcels acts to only increase their concentration and not their thickness. When a maximum is reached, further additions of frazil ice contributes to parcel thickening.

A second mass exchange process may also occur if the suspended frazil is in an active state, with the individual particles sticking to bed material to form anchor ice. This process may also include anchor ice thickening by thermal means and both should be considered when modelling. In CRISSP-2D, the rate of anchor ice growth or decay is solved using a similar approach to that of surface ice mass exchange, whereby a frazil ice accretion rate parameter is applied as shown in Equation 2.14:

$$\frac{\delta h_{an}}{\delta t} = \frac{1}{1 - e_{an}} \left( \gamma N_f + \frac{\varphi_{wi}}{\rho_i L_i} \right) \quad [2.14]$$

where:  $h_{an}$  represents the net thickness of anchor ice [m]  
 $e_{an}$  represents the porosity of anchor ice [0 to 1]  
 $\varphi_{wi}$  represents the heat flux between the anchor ice and channel flow [W/m<sup>2</sup>]

Once again, calibration of the anchor ice routines is largely dependent on the frazil accretion rate parameter. The model also includes an ability to simulate both thermal and mechanical anchor ice release. It should be noted that the anchor and aufeis sub-routines have recently been updated, but the changes have yet to be incorporated into a production version of the model.

The last major component of the thermal ice module simulates the thermal growth and decay of a static ice cover. In the absence of frazil ice, the solid ice cover will freeze in a downward direction thermally, producing what is known as black ice. The rate of thickening can be related to the heat loss from the water column, an example of which is provided in Equation 2.15 and used within the CRISSP-2D model:

$$\frac{\delta h_i}{\delta t} = \frac{1}{\rho_i L_i} [-\varphi_s + C_{ia} + C_{ib}(T_i - T_a) - C_{wi}(T_w - T_m)] \quad [2.15]$$

where:  $C_{ia}$  represents a linear heat transfer coefficient between ice and air [W/m<sup>2</sup>]

$C_{ib}$  represents a linear heat transfer coefficient between ice and air [ $\text{W}/\text{m}^2\text{°C}$ ]

$T_i$  represents the ice surface temperature [ $\text{°C}$ ]

$C_{wi}$  represents a linear heat transfer coefficient between water and ice [ $\text{W}/\text{m}^2\text{°C}$ ]

$T_m$  represents the freezing point of water [ $\text{°C}$ ]

Thermal decay of a solid ice cover is solved using the same relationship. A modification is also included to account for surface ice thickening due to the deposition of frazil particles on the under-surface of the ice.

## 2.5 Dynamic Ice Module

The dynamic ice module applies the Lagrangian Discrete Parcel Method to simulate the transport of surface ice parcels and their interaction with each other, static surface ice, the channel bed, or any booms that are present. The moving surface ice is considered as a two-dimensional continuum, with each particle conserving mass, energy, and momentum. In addition to the physical characteristics of each parcel, the module also considers the action of both internal and external forces, which are factored into the momentum equation as shown in Equation 2.16:

$$M_i \frac{\delta \vec{V}_i}{\delta t} = \vec{R}_i + \vec{F}_a + \vec{F}_w + \vec{G} \quad [2.16]$$

where:

- $\vec{V}_i$  represents the two-dimensional parcel velocity [m/s]
- $M_i$  represents the parcel mass;  $M_i = \rho_i N_s h_i$  [kg/m<sup>2</sup>]
- $\vec{R}_i$  represents the two-dimensional internal resistive forces [N]
- $\vec{F}_a$  represents the two-dimensional wind drag force [N]
- $\vec{F}_w$  represents the two-dimensional water drag force [N]
- $\vec{G}$  represents the two-dimensional gravitational force [N]

Internal resistance is calculated using a viscoelastic-plastic model based on the Mohr-Coulomb yield criteria. The remaining non-advective terms are solved for using kernel interpolation with neighbouring particles. The model also allows for a simplified “free drift” ice dynamic calculation, where particle interaction with each other, solid ice, the channel bed, or booms is not calculated.

## 2.6 Input Data

The data required to operate the CRISSP-2D model is organized in a series of up to 21 files that explicitly define the physical properties of the model domain, boundary and initial conditions, meteorological information, parameter values, active and inactive model components, and output options. A full summary of each file is provided in Table 2.1:

Table 2.1. CRISSP-2D input file summary

<b>Filename</b>	<b>Description</b>
*.brk	Defines the ice breakup properties
*.dsc	Defines locations along which output data is to be provided
*.elv	Time series of elevation data along each elevation boundary
*.flx	Time series of discharge data along each discharge boundary
*.geo	Defines the physical properties of the model domain, including node, element, reach, and boundary information
*.hdw	Optional hydrodynamic hot start information
*.hot	Optional ice parcel hot start information
*.iqb	Defines the ice discharge from the upstream boundary and some ice parameters
*.nbm	Defines the properties of booms, if present
*.par	Global parameter definitions
*.pfl	Defines longitudinal profiles along which output data is to be provided
*.plt	Graphical geometry file for use in plotting
*.prt	Printout of the most recent model results
*.ptm	Defines the time interval for model output
*.str	Optional parcel stress hot start information
*.swi	Defines active and inactive model components
*.tbc	Time series of water temperature data along each upstream boundary
*.tim	Defines the model time controls, including simulation date, duration, time steps, and hot starts
*.wea	Time series of global meteorological conditions
*.wnd	Time series of global wind conditions
linke.dat	Geometry files used to speed up calculations

---

Only the most basic data is required for the model to simulate the hydrodynamics in a reach, with additional information being required as more sophisticated simulations are performed. The required data for any type of simulation is summarized as follows:

- Hydrodynamics
  - Location of study area (latitude, longitude);
  - Reach boundary information (northing, easting);
  - Distributed reach bathymetry (elevation);
  - Reach geomorphological characteristics (channel roughness);
  - Boundary discharge (cms); and,
  - Boundary water surface elevation (m)
- Thermal calculations
  - Water temperature at upstream boundary (°C); and,
  - Either air temperature (°C) or full meteorological information
- Dynamic ice simulations
  - Wind speed (m/s) and direction (degrees);
  - Ice discharge at upstream boundary ( $\text{m}^3/\text{m}^3$ ); and,
  - Number and location of ice booms

As is often the case, not all of the required data is available for the specific location and time period studied. One or more model inputs may have to be assumed and the model domain adjusted such that these assumptions are valid. For instance, the upstream model boundary may be relocated to lie near the

outlet of a lake such that the incoming surface ice concentration can be assumed to be negligible and the water temperature to be near freezing. Supplementary information is also required for the purposes of calibrating the model. This data usually consists of some first- or second-hand observations of ice conditions in the area during the time or freeze-up. Key items to document would include:

- Water level measurements (m);
- Discharge measurements, particular at flow splits (cms);
- Water temperature measurements (°C);
- Date of first ice observed;
- Timing and extent of border ice growth;
- Presence of skim or frazil ice;
- Surface ice concentration ( $\text{m}^3/\text{m}^3$ );
- Suspended ice concentration ( $\text{m}^3/\text{m}^3$ );
- Ice front location;
- Ice thickness (m); and,
- The locations of any ice jams, hanging dams, or other ice phenomena

Ideally, the data required for calibration should originate primarily through first hand observations and be supplemented using remote measurements and sensing. Satellite photography is shown to be particularly useful in spatially observing the extent and presence of different ice types, as well as the areal surface ice concentration (Lindenschmidt, van der Sande, Demski, & Geldsetzer, 2011).

## 2.7 Calibration Parameters

The use of most computer models as engineering tools is dependent on the successful calibration of their parameters. Due to the physical basis for the CRISSP-2D model, the parameter set is limited to logical and well-established variables. The most important of these variables and their use in the freeze-up calibration procedure are summarized in Table 2.2:

Table 2.2. CRISSP-2D calibration parameters

Parameter	File	Description	Equation
cnn	*.geo	Manning's roughness for the channel bed	2.1, 2.2, 2.3
cnisld	*.iqb	Manning's roughness for solid ice	2.1, 2.2, 2.3
cni	*.iqb	Manning's roughness for single layer surface ice	2.1, 2.2, 2.3
cnimax	*.iqb	Manning roughness for ice jams	2.1, 2.2, 2.3
htmin	*.par	Minimum water depth	2.1, 2.2, 2.3
albedo	*.par	Albedo of ice	2.6
hwa	*.par	Linear heat transfer coefficient between water and air	2.6, 2.15
hia, alp	*.par	Linear heat transfer coefficients between ice and air	2.15
cwi	*.par	Linear heat transfer coefficient between water and ice	2.15
tc	*.par	Minimum water surface temperature for border ice growth	N/A
vcrskm	*.par	Maximum velocity for border ice growth	N/A
vcrbom	*.par	Maximum velocity for frazil accretion	N/A

<b>Parameter</b>	<b>File</b>	<b>Description</b>	<b>Equation</b>
hi0	*.par	Initial skim ice thickness	N/A
theta	*.par	Probability of deposition of frazil particles reaching the surface	2.9, 2.13
beta1	*.par	Rate of re-entrainment of surface frazil particles per unit area	2.11, 2.13
vbb	*.par	Rising velocity of frazil particles	2.10, 2.13
hf0	*.par	Initial thickness of frazil surface floes	N/A
anmaxfra	*.par	Maximum concentration for frazil ice floes	N/A
anmax	*.iqb	Maximum concentration of ice parcels	N/A
thi0	*.iqb	Surface ice thickness of each parcel	N/A
ef	*.par	Porosity of frazil ice	2.11, 2.13
vnu	*.par	Nusselt number	2.7, 2.12
df	*.par	Frazil crystal length	2.7, 2.12
de	*.par	Frazil crystal thickness	2.7, 2.12
xkwp	*.par	Thermal conductivity between water and suspended frazil	2.7, 2.12
poran	*.par	Porosity of anchor ice	2.14
gama	*.par	Rate of accretion of frazil particles to anchor ice	2.9, 2.14
crifr	*.par	Critical Froude number for surface ice submergence	N/A

---

In some situations, not all of the parameters listed in Table 2.2 are used by the model and therefore do not require calibration. For instance, if the full energy budget method is selected to model heat transfer, many of the linear heat transfer coefficients are not used. Alternatively, certain simulations or conditions require calibration of parameters not listed in Table 2.2. Given that the objective

of this research centers on freeze-up modelling, only those parameters pertinent to the ice regime will be calibrated. More specifically, the calibration of the model will focus on: *cnn*, *hwa*, *tc*, *vcrskm*, *vcrbom*, *hi0*, *theta*, *beta1*, *vbb*, *hf0*, *anmaxfra*, *anmax*, *thi0*, *vnu*, *xkwp*, and *crifr*. The remaining parameters do not significantly influence the freeze-up regime and will be defined using typical or assumed values.

---

# CHAPTER 3:

## Study Area

---

### 3.1 The Nelson River

The Nelson River Valley lies in an area of heavy glaciation, as evidenced throughout the region in the presence of till, moraines, eskers, and glacial scouring. In addition, the surficial geology is largely dominated by lacustrine soils, which had been deposited during the post-glaciation period when much of northern Manitoba and the surrounding areas were covered by glacial Lake Agassiz. It was the Nelson River Valley that provided the final drain for this massive lake during its retreat into Tyrrell Sea, present day Hudson Bay.

From its source at Lake Winnipeg to its mouth at Hudson Bay, the valley can be characterized into three distinct geological regions, all formed as a result of glaciation. The lower 150 km of the river downstream of Stephen's Lake traverses the Hudson Bay Lowlands, a low-lying wetland area that had once been inundated by Tyrrell Sea. Isostatic rebound has since exposed the ground surface revealing thick deposits of poorly drained organic soils of marine origin. The far upstream extent of this region is characterized by a series of low

escarpments that form many of the natural hydroelectric generation sites on the Nelson River, as shown in Figure 3.1 (Newbury, 1968).

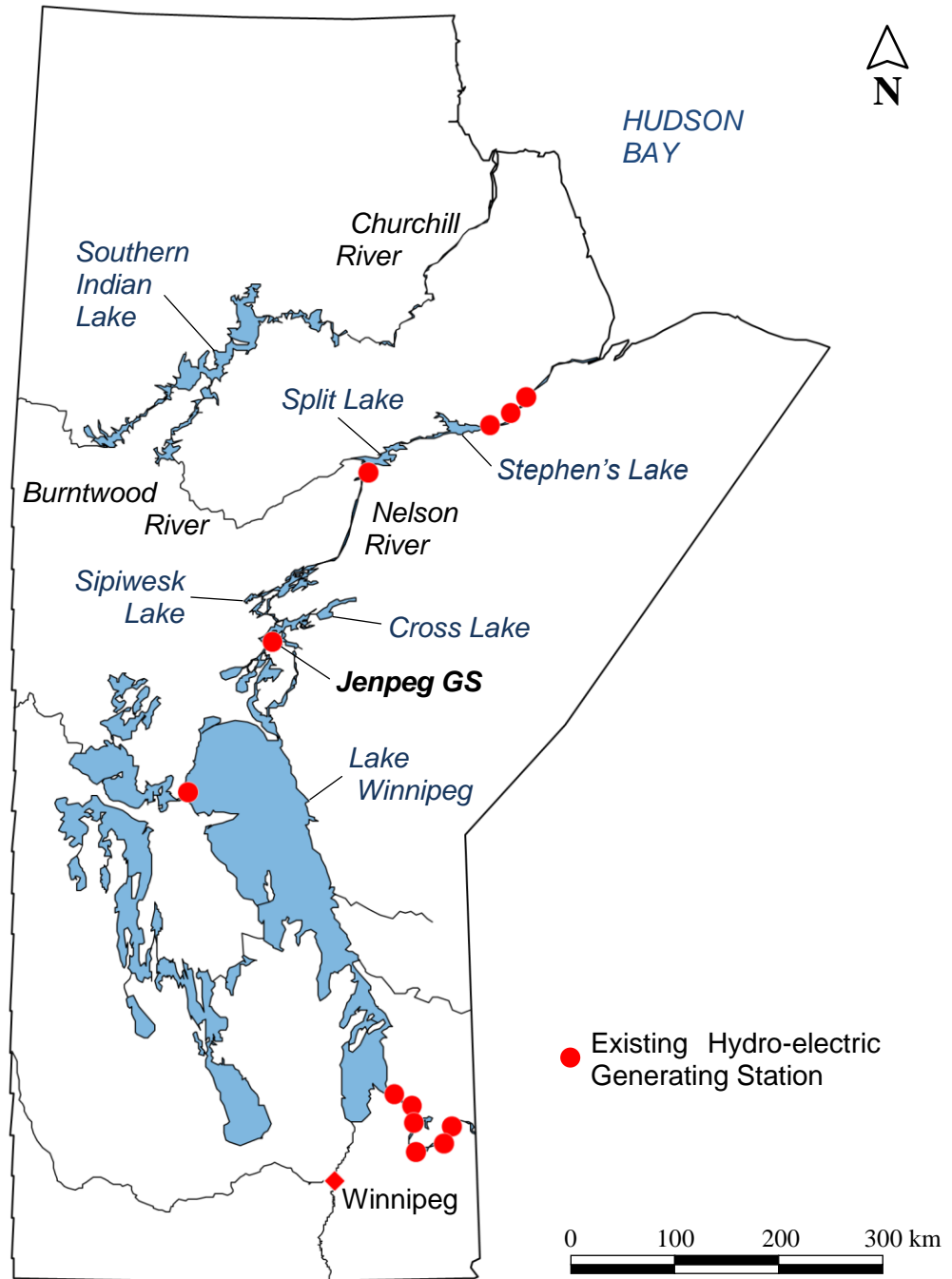


Figure 3.1. Map of Manitoba showing Nelson River hydrology

The second region extends an additional 150 km upstream to Split Lake, covering an area of thick igneous rock deposits that are littered with discontinuous eskers, moraines, drainage channels, and outwash deposits (Newbury, 1968). At Split Lake, a distinct shift in local geology marks the transition between the Lower and Upper portions of Nelson River. The third region encompasses the Upper Nelson River, extending nearly 400 km from Split Lake to Lake Winnipeg. A series of depressions in the bedrock form three major basins: Lake Winnipeg, Cross Lake, and Sipiwesk Lake. The depressions are overlain by as much as 30 meters of lacustrine clays, with the exposed bedrock protrusions at the lip of each boundary forming a series of rapids and falls in the steep and irregular interconnecting channels (Newbury, 1968).

The hydraulics of the Nelson River are extremely complex, particularly within the upper portion between Lake Winnipeg and Sipiwesk Lake. The lone natural outlet of Lake Winnipeg occurs along its northeast shore at Warren Landing, where the outflow is immediately split into two channels around Ross Island. To the east, roughly 15% of the flow is routed through Little Playgreen Lake and a series of narrow channels before eventually draining into Cross Lake. The larger West Channel, which carries the remaining 85% of the flow, first enters Playgreen Lake, passes through Whiskey Jack Narrows, and into Kiskittogisu Lake. Three narrow outlets leave Kiskittogisu Lake through a series of rapids: Kisipachewuk Rapids to the south, Ominawin Rapids to the north, and Metchanais Rapids in the center. The three outlets merge to form a single unified Lower West Channel,

which crosses Manitou and Saskatchewan Rapids before discharging into Cross Lake and merging with the East Channel flow.

Downstream of Cross Lake, a similar pattern of narrow rock-controlled channels is observed. Merged flow from the east and west outlet channels passes over Eves Rapids and Ebb and Flow Rapids, respectively, before merging and dropping an additional 10 meters over Whitemud Falls. Downstream of the falls, the channel follows the general northwest trend of jointing and glaciation in the area over another series of rapids before entering into Sipiwesk Lake.

The remaining portion of the Upper Nelson River spanning Sipiwesk Lake and Split Lake flows in a singular straight channel, trending to the east for 30 km before turning north for an additional 115 km. The direction and geometry of the reach can be directly correlated to the local lithology of the area, which trends east and north parallel to the respective sections of the channel (Newbury, 1968). Fault zones form two sets of rapids on the northern reach: Devil Rapids and Grand Rapid. The six-meter granite ledge forming Grand Rapid is the present day location of the Kelsey Generating Station.

At Split Lake, the hydroelectric potential of the Nelson River effectively doubles due to its confluence with the Burntwood River and the Churchill River Diversion (Manitoba Hydro, n.d.). It is the resulting increase in flow combined with a series of rapids in the downstream reach that provide such favourable conditions for

hydroelectric development. Flow is controlled by a series of gneiss-pegmatite rock bands that protrude above the bedrock, each of which forms a set of rapids in the channel (Newbury, 1968). Downstream of Split Lake, the channel flows uninterrupted in a northwest direction across Birthday Rapids, Gull Rapids, Wapicho Rapids, Upper and Lower Kettle Rapids, and Long Spruce Rapids. Both Kettle and Long Spruce Rapids have been developed for their hydroelectric potential, with Gull Rapids representing the next development site on the Nelson River with the proposed Keeyask Generating Station. Stephens Lake, the only significant reservoir on the Lower Nelson River located roughly 90 km downstream of Split Lake, was formed as a result of the construction of the Kettle Generating Station.

The remaining portion of the Lower Nelson River flows through the Hudson Bay Lowlands. The upper 50 km of the reach passes through a series of limestone ledges forming Upper, Middle, and Lower Limestone Rapids. Upper Limestone Rapids is the location of the Limestone Generating Station, while the Lower Limestone Rapids, located 28 km downstream, lie near the location of the proposed Conawapa Generating Station. Downstream, the overall channel slope flattens, opening to a large estuary nearly 30 km long. The flow depth along the lower portion of the reach is controlled largely by tidal variations in Hudson Bay.

The design of the Kettle, Long Spruce, and Limestone Generating Stations each employ a run-of-the-river approach, whereby minimal storage is available for

energy storage. Stephens Lake provides all of the short-term storage along the Lower Nelson River. Long-term storage is provided far upstream at Lake Winnipeg, whose hydraulic regime is controlled such that flow arrives at the downstream stations to coincide with increases in energy demand. The Jenpeg Generating Station, located just upstream of Cross Lake along the Nelson River West Channel, provides this primary control. As such, the study area for this research is limited to the reach of the Nelson River between Lake Winnipeg and Cross Lake. For modelling purposes, the domain has been further constrained to the reach downstream of Playgreen Lake, as shown in Figure 3.2.

### 3.2 Lake Winnipeg Regulation

Control of inflows into the Nelson River was achieved in 1976 with the completion of the Lake Winnipeg Regulation Project. The project utilizes a comprehensive approach designed to mitigate many of the natural obstructions to channel conveyance, particularly during low flow and winter conditions. In addition to the Jenpeg Generating Station, the project includes the construction of three bypass channels: the 2-Mile Channel, the 8-Mile Channel, and the Ominawin Bypass Channel. The 2-Mile Channel, located on Big Nossy Point near the natural outlet at Warren Landing, alleviates the restrictions imposed by sand and gravel deposits at the southern extent of Playgreen Lake and ultimately increases conveyance of the outlet channels by as much as 50%. The 8-Mile Channel, located roughly 30 km downstream of the East/West Channel split, bypasses the

relatively flat gradient through Playgreen Lake and routes a portion of the water directly into Kiskittogisu Lake. The Ominawin Bypass Channel, located downstream of Kiskittogisu Lake, is designed to bypass the natural rock constrictions in the Kisipachewuk, Metchanais, and Ominawin Channels. A map outlining the location and extent of the LWR project is provided in Figure 3.2.

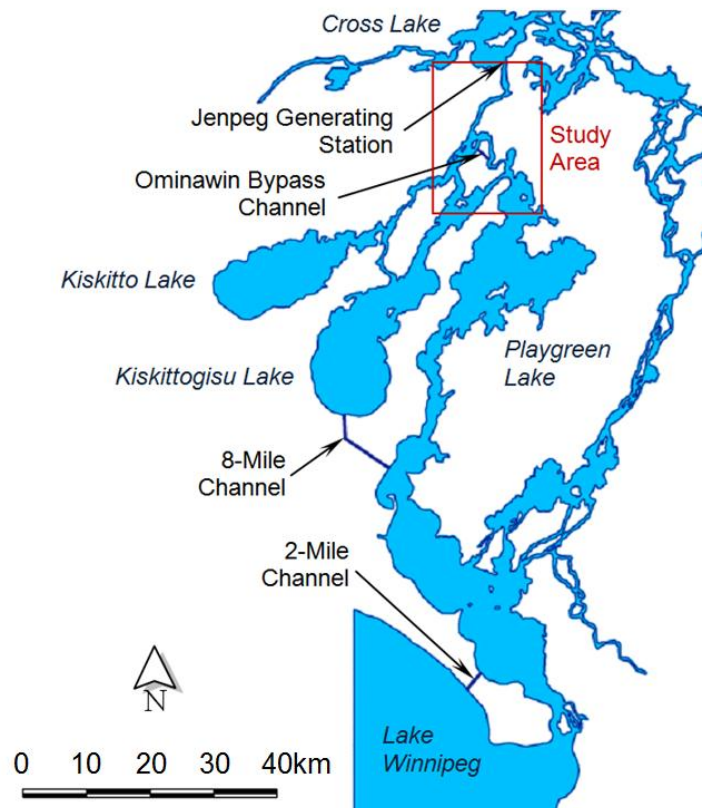


Figure 3.2. Overview of the Lake Winnipeg Regulation Project

As previously outlined, the project also includes a river ice component called the Ice Stabilization Program, which was implemented in an effort to control the ice regime in the channels between Lake Winnipeg and Cross Lake. The typical ice

regime in this area consists of static border ice formation in the lakes and larger bays commencing typically in late November or early December. The individual connecting channels experience some border ice growth in low-velocity areas; however, the bulk of the channel icing occurs through surface ice bridging and juxtaposition. The dominance of a particular surface ice run – whether frazil or skim ice – is largely dependent on the flow characteristics at the time of freezing. It is estimated that a flow rate of  $1650 \text{ m}^3/\text{s}$  (cms) defines this threshold, whereby a lower flow rate results in skim ice formation and a higher flow rate results in frazil ice formation (Tuthill, 1999).

As a part of the licensing associated with the LWR project, Manitoba Hydro has a mandate to perform the following:

- Maintain the elevation of Lake Winnipeg to between 216.7 meters (711 ft) and 217.9 meters (715 ft) above sea level (ASL).
- Maintain the elevation of the Jenpeg Generating Station forebay to between 213.97 meters (702 ft) and 217.93 meters (715 ft) ASL.
- Maintain a minimum outflow from Lake Winnipeg of 708 cms (25,000 cfs).
- Limit any change in outflow to less than 425 cms (15,000 cfs) in any 24 hour period.

Of these, the most pertinent to this research and the operation of Jenpeg during freeze-up is the flow change restriction. On average, a flow reduction of 990 cms

is required to achieve the desired rate of 1650 cms, meaning that the cutback may take two or more days to achieve in full at a rate of 425 cms.

### 3.3 Data Availability

As a part of the LWR Project, the channels between Lake Winnipeg and Cross Lake were heavily gauged and mapped. The resulting data has been disseminated through internal databases, models, and reports, many of which have been made available for this study. A majority of the temporary hydrometric gauges installed for design and construction purposes have since been removed. Those that remain, the data they provide, and the various other sources of information utilized as part of this research are outlined in Sections 3.3.1 to 3.3.4.

#### 3.3.1 *Bathymetric Data*

Available bathymetric data was provided by Manitoba Hydro in the form of a one-dimensional HEC-RAS model of the Upper Nelson River. The source data for this model originates from a series of pre-construction cross-sectional soundings conducted between 1957 and 1971 by Manitoba Hydro and the Lakes Board, which focused on mapping the channel bed between Lake Winnipeg and Cross Lake. Not included in the model are any measurements of the overbank areas short of the occasional floodplain elevation necessary for design purposes. As such, little is currently known regarding these overbank areas, many of which were flooded post-construction.

A GIS map showing the layout of cross sections in the area was also provided; however, the information contained therein is shown to be highly inaccurate. A second hand-drawn map, Manitoba Hydro Drawing 7001-R-6 dated September 1970, proved to be a much better representation of the general location and orientation of each cross-section. This map was digitized and georeferenced, and ultimately used to locate and orient each cross-section. The distribution and location of the 209 provided cross-sections is outlined in Figure 3.3.

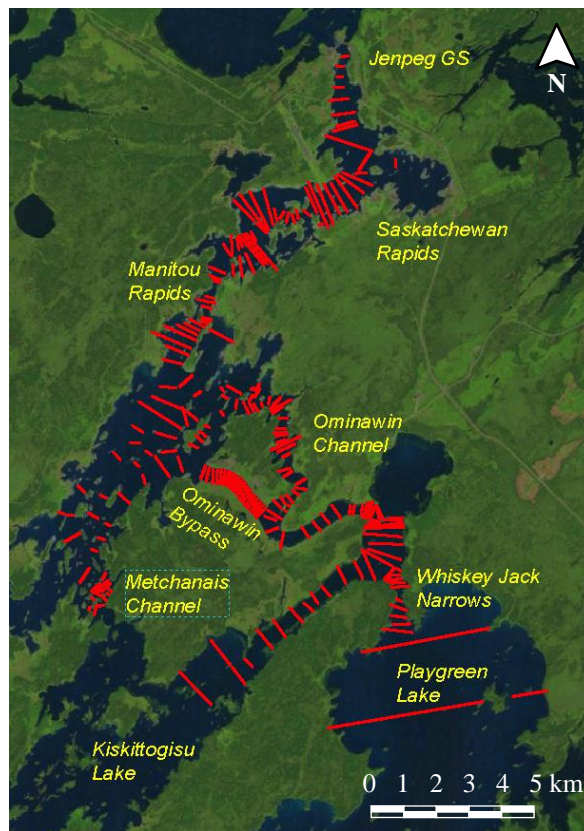


Figure 3.3. Summary of available cross-sectional data (red)

Very few cross-sections were available within the localized forebay region of the study area. The bathymetry in this area was determined using a contour map originally developed for the ice boom study conducted by LaSalle Hydraulics Laboratory. Extending 3,750 meters upstream from the station, a distributed 3-dimensional scatter set was produced from this map and the bed elevations were mapped accordingly.

### *3.3.2 Imagery Data*

The process of outlining the model domain as well as locating and orienting each cross-section required an original georeferenced image on which to ground truth the data. A high resolution (10 meter) SPOT 4 satellite image taken in 2006 was used for this purpose, namely to locate the left and right bank of each cross-section along the observed shoreline. Given that the image was taken post-construction, however, it was difficult to define some of the original cross-section extents in the now flooded lower reach of the domain. A second satellite image was used in these instances. Taken in 1972 by the Landsat 7 satellite, this low resolution (60 meter) image made it possible to estimate the original channel thalweg, and subsequently locate the deepest station within each cross-section. As shown on Figure 3.4, the original channel and the post-construction flooded areas are evident through a comparison of the satellite images.

A series of aerial photographs were also made available by Manitoba Hydro documenting the ice regime upstream of Jenpeg during the years 2003 to 2011.

The low-altitude photographs taken during helicopter observations provided a

qualitative look at the various ice processes taking place on a sub-daily basis throughout the entire freeze-up period. These photographs were used primarily in calibrating the river ice component of the CRISSP-2D model; however, by comparing the location, distribution, and timing of ice floes, it may also be possible to extrapolate approximations of water surface velocity or the presence of any preferential paths.

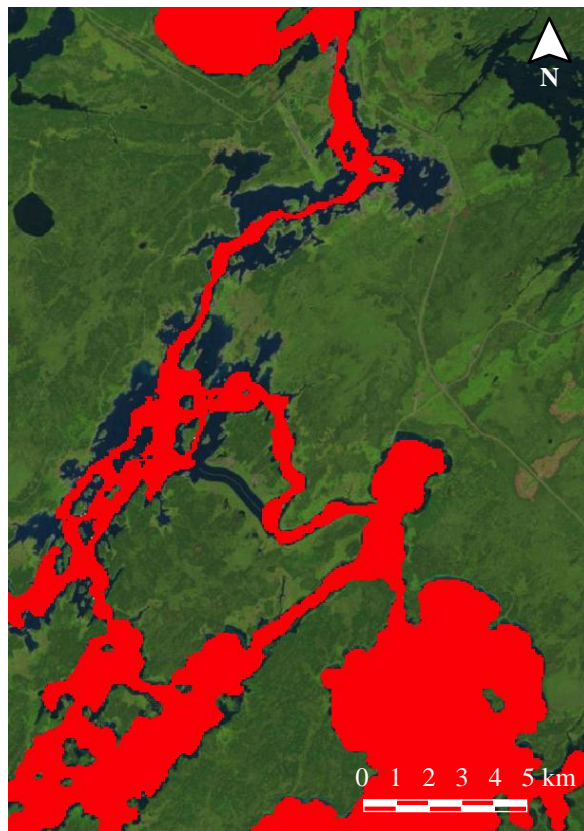


Figure 3.4. Channel extents pre-construction (red) and post-construction (blue)

### 3.3.3 *Hydrometric Data*

Hydrometric data within the study reach consists of water surface elevation and water temperature measurements taken at each of the five Manitoba Hydro gauging locations shown on Figure 3.5, as well as a rated flow at Jenpeg. The hourly water surface elevation data for each gauge, provided between the years 2000 to 2011, was checked and corrected for errors using a uniform offset from the measurements taken at one of the other four gauges. The station forebay elevation during this time period was also provided; however, it was discovered that the vertical datum referenced differed from that of the remaining gauges. In addition, the forebay datum adjustment of -0.116 meters was found to not be applicable under all conditions. For this reason, the forebay elevation data was omitted from this study. Alternatively, the data from gauge 05UB701, located approximately 700 meters upstream of Jenpeg, was used as a direct analog.

Hourly water temperature data at each gauge was also provided for the same time period. Due to a high degree of error observed in all of the measurements, the data was corrected using a combination of uniform offsets, averaging, and linear interpolation. In cases where a gauge seemed to function normally but stabilized to a winter water temperature either above or below 0°C, an equivalent offset was applied to correct the data. If more than one gauge was functioning during the same time period, the corrected measurements from each gauge were averaged. If no gauges were functioning, a linear interpolation between the previous and subsequent corrected measurements was applied. Lastly, an over-

winter temperature of 0.01°C was assumed. The result is a global time series of water temperature data across the entire study domain.

The flow data calculated at Jenpeg is supplemented with Acoustic Doppler Current Profiler (ADCP) measurements taken in the various upstream channels. This data provides an estimation of the various flow splits between channels and lakes and serves to validate the rating curves used for translating the forebay water surface elevation into a station flow. A total of 106 measurements taken within the station forebay between 1995 and 2008 were compared to the rated values and are outlined in Figure 3.6.



Figure 3.5. Overview of hydrometric gauging locations in the study area

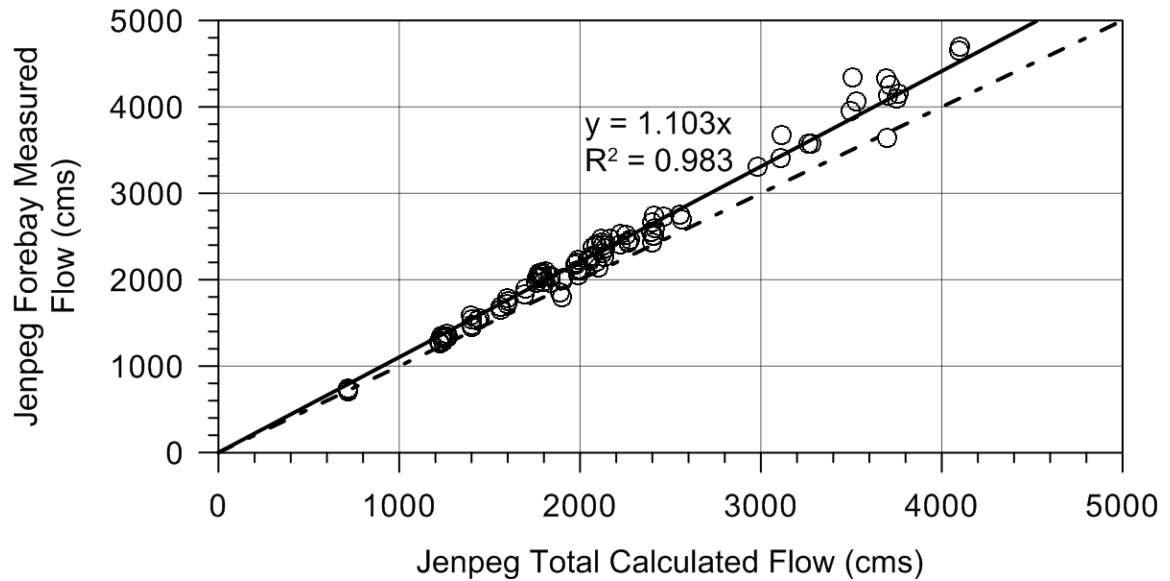


Figure 3.6. Jenpeg calculated outflow performance, 1995-2008

As evidenced by Figure 3.6, the station flow is underestimated by roughly 10% when calculated based on the station rating curve. This is attributed to two factors: 1) the Jenpeg Powerhouse has not been performance tested and the calculated discharge is based on the design curve for each unit, and 2) noted inconsistencies within the design spillway discharge rating curves. It is estimated that powerhouse flows are under-reported by 7% and the spillway by 15% (Manitoba Hydro, 2010). Future use of rated flow at Jenpeg for the purposes of this research applies a uniform 10% increase over reported values.

The flow at Jenpeg ranges historically between a low of 280 cms to a high of 5405 cms. During freeze-up (November 1 to December 31), the variability is reduced by operational and physical limitations to between 700 cms and 4330 cms. A large majority (90%) of flow during freeze-up lies within the 1500 to 3000

cms range. The analysis provided in Figure 3.7 and Table 3.1 provides a quantifiable classification of average daily flow during this time.

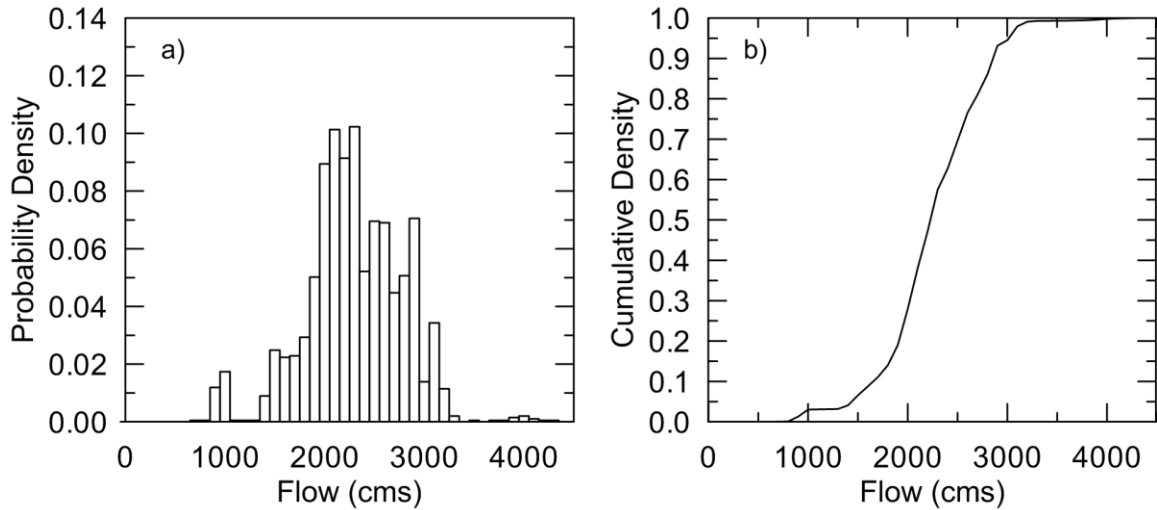


Figure 3.7. Statistical analysis of average daily freeze-up flow (Nov-Dec)

Table 3.1. Statistical flow classification during freeze-up

Classification	Flow [cms]
Lower decile (10%)	1745
Lower quartile (25%)	2048
Median (50%)	2317
Upper quartile (75%)	2656
Upper decile (90%)	2955

This analysis is performed on the histogram of measured flow between 1979 and 2011. Of note is the influence of the annual flow cutback on the flow distribution. At 1650 cms, the cutback represents a lower decile flow and its presence in the data sample acts to shift the entire distribution to the left.

#### 3.3.4 *Meteorological Data*

Historical meteorological information for use in this research was retrieved online from the Environment Canada Weather Office using the closest weather station located at the Norway House Airport (YNE/71410). A complete history of hourly air temperature, dew point temperature, barometric pressure, visibility, cloud cover, wind speed, and wind direction exists for this station dating back to 1973. There exists potential to supplement this data with measurements taken at nearby Manitoba Hydro weather stations, particularly to account for local air temperature or cloud cover variations. For forecasting purposes, the overnight low temperature provided by Environment Canada for Norway House may be used. Alternatively, The Weather Network publishes a 36-hour forecast of air temperature, cloud conditions, wind speed, and wind directions at Norway House, which provides a more comprehensive outlook on expected conditions. For the purposes of this research, the hourly forecast provided by The Weather Network has been utilized.

---

# CHAPTER 4:

## Model Development

---

### 4.1 Bathymetric Data Analysis

The distribution, density, and quality of bathymetric data within the model domain varies considerably on a reach by reach basis. This is partly evident by the cross-section layout presented on Figure 3.3. Downstream of Manitou Rapids, the channel bathymetry is well defined and of good quality. Upstream of Manitou Rapids, particularly within the Upper West Channel, Metchanais Rapids, and Kiskittogisu Lake, the quality and availability of bathymetric data is very limited or completely lacking. In these situations, a process of estimating the bathymetry using either nearby cross-sections or knowledge of the flow characteristics in the area was employed.

Where possible, measured cross-sections were assumed to be characteristic of the channels in which they were taken and were copied in both the upstream and downstream directions as required. Areas where no original data was available, most notably in the Kiskittogisu Lake region, bathymetry was estimated using that of similar channels and was adjusted as needed during the hydrodynamic

calibration. In total, 143 (41%) proxy cross-sections were used to map areas of limited knowledge, as shown in Figure 4.1.

In the lower reaches of the model, much of the overbank elevations areas were not measured during the original pre-construction mapping exercise. The elevation of these flood zones was estimated using either measurements where available, constant bank elevations specified by Manitoba Hydro in HEC-RAS, or knowledge of the channel. Each of these flood zones and the data points used to estimate them are also outlined in Figure 4.1.



Figure 4.1. Summary of available original (red), proxy (yellow), and estimated flood zone (white) bathymetric data

## 4.2 Mesh Generation

CRISSP-2D employs a dynamic finite element mesh consisting of linear triangles. The Surface-water Modelling System (SMS), developed by Aquaveo™, is used to develop the mesh, define node and element properties, and specify any open and closed boundaries. Typically, CRISSP-2D is limited to 6,000 nodes or 10,000 elements, however, these limitations were increased to 20,000 nodes and 30,000 elements on account of the large model domain.

Discretization of the model domain began with defining the model boundaries, including any large islands or other significant hydraulic features. In an effort to decrease the total number of elements, small bays and other insignificant features were ignored when outlining the mesh. Doing so allowed adjacent nodes to follow the natural streamlines expected within the channels and thereby decrease overall numerical error. The upstream boundaries were extended to include portions of both Playgreen and Kiskittogisu Lakes, primarily to eliminate the need for defining an incoming ice concentration.

Subsequently, the entire domain was categorized into individual reaches sharing similar hydraulic properties. Care was taken to segregate the original channel from the overbank flood zones, facilitating the ability to define these areas as regions of shallow depth and increased roughness. The 24 reaches comprising the model domain are presented on Figure 4.2, with reaches 4, 6, 8, 10, 12, and 23 representing flood zones.

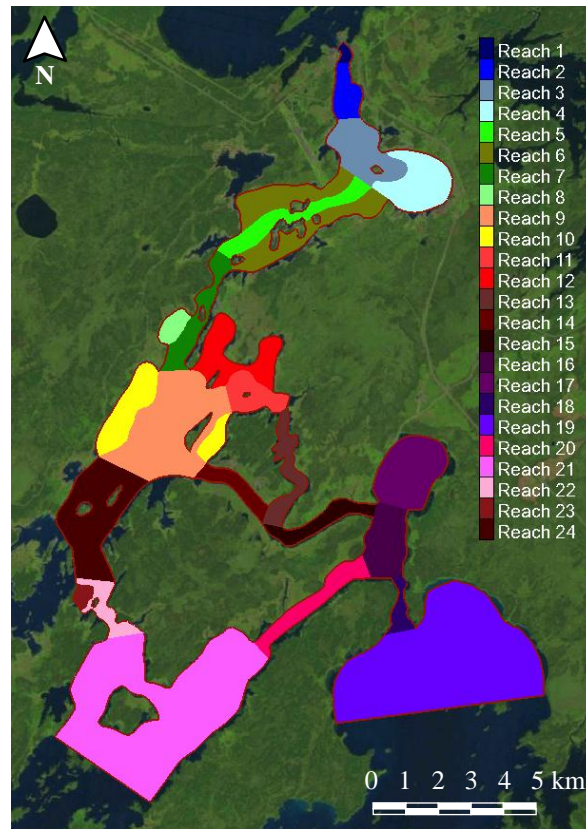


Figure 4.2. Outline of CRISSP-2D model and reach boundaries

The mesh was constructed independently for each reach by specifying the perimeter node spacing and allowing SMS to populate the remaining interior nodes. Once again, care was taken to vary the element size from reach to reach as dictated largely by channel width. Larger elements were used in lakes and bays, and smaller elements were used in narrow reaches. The initial mesh, consisting of 6,584 nodes and 11,962 elements, provided fast computation time but was found to produce significant errors (~40%) in flow conservation during steady-state test conditions. As a result, the mesh was refined, increasing the total number of nodes and elements to 13,250 and 24,313, respectively. A minimum of nine nodes were used to map all channel cross-sections as

recommended in literature (Steffler & Blackburn, 2002). Subsequent testing shows a model accuracy of approximately 1% during steady-state conditions. The final mesh geometry with elements ranging from 10 meters to 500 meters in size is shown in Figure 4.3.



Figure 4.3. CRISSP-2D mesh

In order to limit the number of elements and thereby reduce computation time, many of the smaller islands were omitted from the mesh. In most cases, including them requires significant increases to the mesh density and computation time, which are typically not warranted due to limited improvements in accuracy. The most notable instance of this is the Metchanais Channel, shown

in Figure 4.4, which is characterized by a series of small islands and shallow channels. In this instance, only the large Harvey Island is included in the mesh, with the remaining small islands being represented as sections of elevated bed.

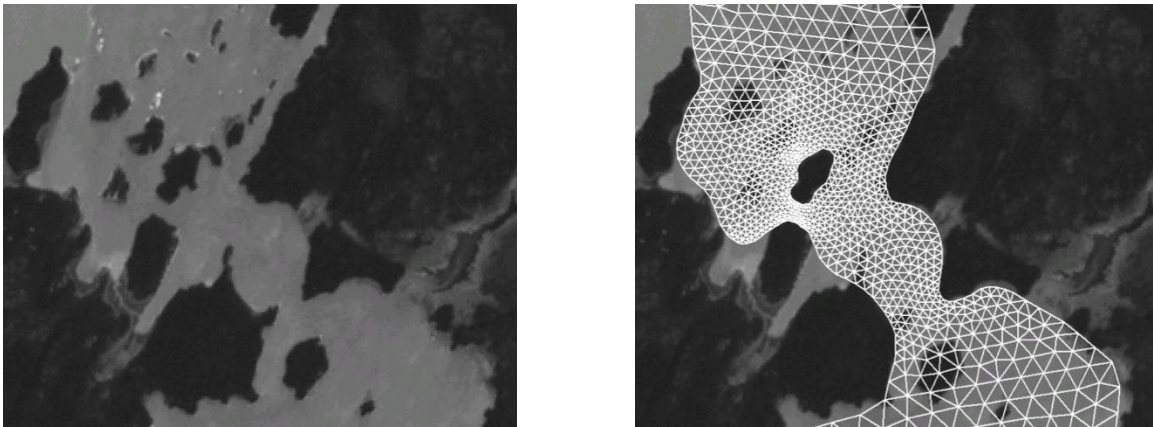


Figure 4.4. Mesh approximations within the Metchanais Channel

To account for the constriction head losses not modelled as a result of the omissions of small islands, the roughness of each affected reach was artificially increased during the hydrodynamic calibration. In all cases, the effect on the river ice regime in the lower reaches of the model is negligible. Locally, the ice regime within Metchanais Channel did change, however its effect is typically not recognized downstream due to the presence of a solid ice cover in the Upper West Channel. In all other cases, the omitted islands made up only a small portion of the total channel width and their omissions has little to no effect on river hydraulics.

Bathymetric data was mapped onto each finite element node using an Inverse Distance Weighted (IDW) scheme. To aid in this process, each cross-section was linearly interpolated every 7.5 meters such that data points existed near each mesh node. The node elevations were then calculated using the corresponding elevations from the four closest bathymetric scatter points. Minor adjustments were made where the interpolation scheme failed to accurately capture the channel bed, yielding the final mesh bathymetry shown in Figure 4.5.

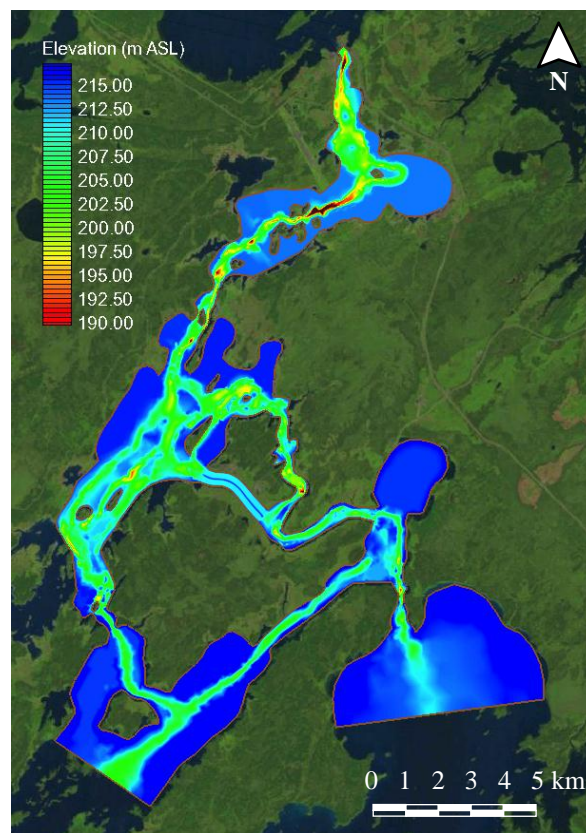


Figure 4.5. Final CRISSP-2D mesh bathymetry

### 4.3 Boundary Conditions

For hydrodynamic simulations of subcritical flow regimes, CRISSP-2D requires that either discharge, water surface elevation, or both be specified at each open boundary. In regards to this study, the presence of a control structure makes defining the downstream boundary condition simple. At the upstream extent, either the elevation of both Playgreen and Kiskittogisu Lakes or a time series of lake inflows is required.

Given the presence of gauge 05UB704 on Playgreen Lake, the first boundary conditions that were tested included a downstream discharge boundary at Jenpeg and an upstream water surface elevation boundary along both lakes. The gauge measurement was used directly to specify the elevation of Playgreen Lake. A uniform negative offset was estimated using the head drop through Whiskey Jack Narrows as measured by gauge 05UB017 and applied to approximate the elevation of Kiskittogisu Lake. Lastly, the calculated flow at Jenpeg was applied at the downstream boundary.

A series of test cases determined that these boundary conditions did not function properly, particularly during conditions of rapidly varying flow. Since discharge was allowed to cross the upstream boundaries in either direction, situations where the flow through Jenpeg was quickly reduced caused negative flow through Whiskey Jack Narrows and out of Playgreen Lake. This condition is

never observed in nature, thereby warranting a change to the hydrodynamic boundary conditions.

Reversing the boundary conditions by specifying a water surface elevation at the downstream boundary and an inflow at each upstream boundary provides the easiest fix to this problem. By specifying an inflow into each lake, water is forced to flow downstream and exit through Jenpeg. The water surface elevation as measured by gauge 05UB701 is then be used to specify the downstream elevation boundary. The flow distribution between Playgreen and Kiskittogisu Lakes was estimated using ADCP discharge measurements through 8-Mile Channel. It was assumed that the flow through 8-Mile Channel constitutes the entire inflow into Kiskittogisu Lake, with the remainder entering Playgreen Lake. An estimate of this flow is provided in Figure 4.6.

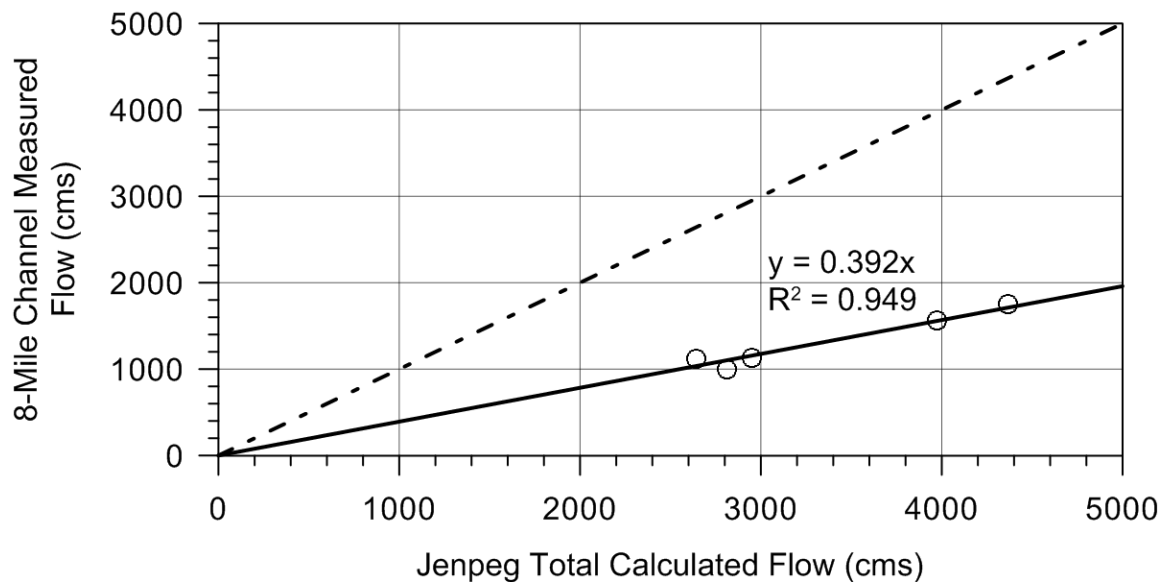


Figure 4.6. 8-Mile Channel flow relative to the Nelson River West Channel

Using the five available measurements, it is possible to estimate that the 8-Mile Channel carries approximately 39% of the total Nelson River West Channel flow. Based on this assessment, the flow split between Playgreen and Kiskittogisu Lakes is assumed to be 60/40%, respectively. It should be noted, however, that none of the five measurements referenced in Figure 4.6 were taken during low flow conditions typical during the flow cutback (Jenpeg total flow of 1,650 cms or less) and that errors may be introduced as a result.

Ice simulations require the definition of two additional boundary conditions: upstream incoming water temperature, and upstream incoming ice concentration. As previously discussed, the upstream boundaries were extended into both Playgreen and Kiskittogisu Lakes to simplify estimating these values. As each of the lakes become ice covered early in the freeze-up season, the incoming ice concentration during freeze-up is assumed to be negligible. At the same time, the water temperature in the lake stabilizes near the freezing point, providing the ability to specify a constant value for extended simulations. For the case of this study, a water temperature of 0.01°C is assumed for ice-on conditions.

#### 4.4 Model Assumptions

Several assumptions are made when developing the model and defining the boundary conditions in an effort to limit the domain. The most significant of these is the exclusion of the Kisipachewuk Channel from the model domain. It is

assumed that the effect of the Kisipachewuk Channel on the overall ice regime of the study area is negligible and its inclusion would primarily act to increase computation time. The flow from Kisipachewuk Channel is instead routed through Metchanais Channel, effectively increasing its conveyance by 65%. The net effect of this shift in flow is localized to within this reach as the flow from both channels naturally merges just downstream of Metchanais Channel.

The second omission from the model domain is an outflow boundary representing the discharge loss into Kiskitto Lake. As part of the LWR Project, Kiskitto Lake was dammed to segregate its ecosystem from the effects of water level changes associated with the construction and operation of Jenpeg. A control structure regulates flow into the lake to mimic the natural variation in water level for the benefit of fish, wildlife, and recreational users. The total outflow constitutes a very small portion of the total Nelson River West Channel flow and did not warrant inclusion in the model.

Lastly, it has been observed that high north winds across Lake Winnipeg can cause wind setdown on the north basin of the lake and reverse the flow through 8-Mile Channel, 2-Mile Channel, and Warren Landing. The frequency and intensity of this local phenomenon is not well understood, as are its effects on the channels downstream of Playgreen and Kiskittogisu Lakes. As such, flow reversal at each upstream boundary has not been considered in this study.

---

# CHAPTER 5:

## Hydrodynamic Simulations

---

### 5.1 Introduction

Due to the sensitivity of river ice processes to water velocity and vertical turbulence intensity, an integral step in developing an accurate model is ensuring that the hydraulics of the study domain are being modelled accurately. Given the physical basis for the CRISSP-2D model, this exercise primarily involves calibrating the Manning channel bed roughness ( $cn$ ) in each reach such that the simulated water surface profiles and flow distributions for different flow conditions match the observations during the same time period. The methods employed in calibrating the model hydrodynamics are discussed in the following sections.

### 5.2 Initial Conditions

An initial estimate for the Manning roughness in each reach was provided through a series of internal Manitoba Hydro memorandums discussing the progress of various backwater studies carried out by the Hydraulic Engineering Department (Coley, 1971; Carson, 1972; Phelps, 1973). The studies

independently determined the Manning bed roughness in each reach by calibrating to a measured head drop between two gauges. Since the same process is used in calibrating the CRISSP-2D model; it is reasonable to assume that these studies provide at the very least an initial estimation of approximate range of expected bed roughness values. A constant overbank roughness of 0.050 is assumed in accordance with these studies.

Each hydrodynamic simulation was initialized using a steady-state solution of the first time step. Beginning with zero flow and a horizontal water surface profile, the model was spun up through a gradual increase in total flow (55 cms/hour) and decrease to the downstream water surface elevation boundary (-0.05 m/hour). Once both the flow and elevation boundaries reached the necessary levels, the model was allowed to stabilize. The steady-state solution was then applied within the primary simulation to serve as a hot start. Doing so accomplishes three things: 1) it minimizes errors associated with model spin up, 2) reduces the amount of time required to perform subsequent simulations of the same time period, and 3) allows for easier processing of results.

An optimal time step of 0.85 seconds was determined based on both Courant's criteria and manual testing, and was therefore employed in all hydrodynamic simulations. Reducing the time step was found to produce minimal accuracy gains and was not warranted. Increasing the time-step produced model errors during periods of dynamic flow, particularly at model boundaries.

### 5.3 Hydrodynamic Calibration

Due to its highly dynamic nature, the open water season of 2008 was chosen as the calibration time period. The water surface elevation as measured at gauge 05UB701 varied considerably (between 213.78 meters to 217.25 meters ASL), encompassing a large portion of the station's operating range. The flow rate was equally as dynamic, covering a range from 1640 cms to 3800 cms. Due to the nature of the operating strategy at Jenpeg, particularly during the flow cutback, it is also important for the model to be able to accurately capture rapid changes in flow. The open water year 2008 also provided ideal conditions for testing this scenario, with flow changes ranging as high as  $\pm 280$  cms/hour.

Given subcritical flow, calibration of the model began at the downstream boundary and progressed upstream. The Manning channel bed roughness was iteratively adjusted on a reach by reach basis until the simulated water surface elevation at the closest upstream gauge matched what was measured. The focus then shifted onto the next upstream gauge and the process was repeated until the entire model domain was calibrated.

In two situations, adjustment of the Manning bed roughness alone did not yield satisfactory results. In calibrating the reach between gauges 05UB701 and 05UB703 in the Lower West Channel, it was evident that periods of low water surface elevation were being underestimated whereas periods of medium to high elevation were correctly simulated. Adjusting the Manning roughness in this

scenario worked to correct the underestimation of low elevations, but caused medium to high elevations to be overestimated. The solution was to raise the channel bed in a short reach close to the upstream station, effectively creating a broad weir that would maintain the proper stage during periods of low elevation. A similar exercise was necessary in the Ominawin Channel where the channel bed was lowered; the extents of both changes are outlined in Figure 5.1.

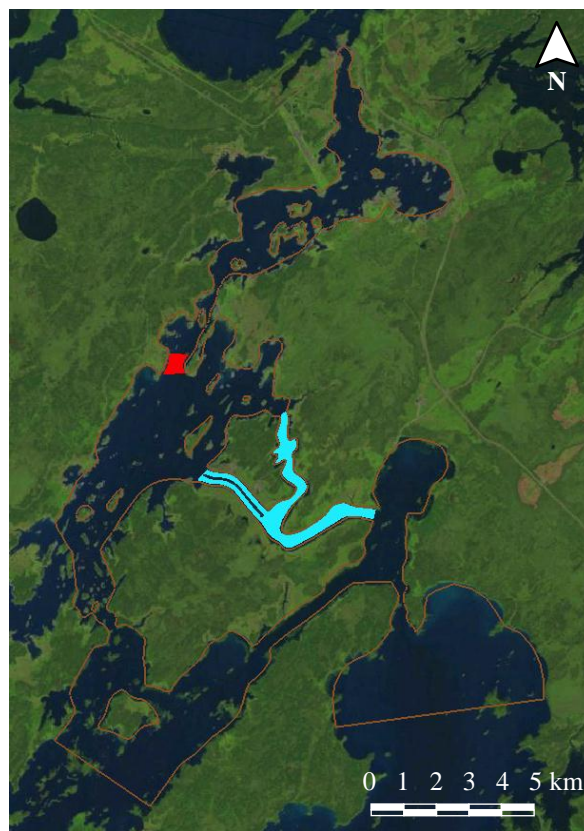


Figure 5.1. Mesh bathymetry modifications: +1.85 m (red) and -0.5 m (blue)

The 1.85 meter raising of the bed near Manitou Rapids and the 0.5 meter lowering of the bed in the Ominawin Channels represents 13% and 6% of the average flow depth, respectively. Each is justified on the basis of: 1) the limited

bathymetric data available to map each region, 2) accuracy of the initial measurements, and 3) the sum of the many erosion and depositional processes that have taken place across the entire study domain in the decades since the original channel bed mapping.

Calibration of the hydrodynamic module yields excellent results. The model error across the entire study domain is minimal and well within an acceptable range of  $\pm 20$  cm for the majority of the simulation, as shown in Figure 5.2.

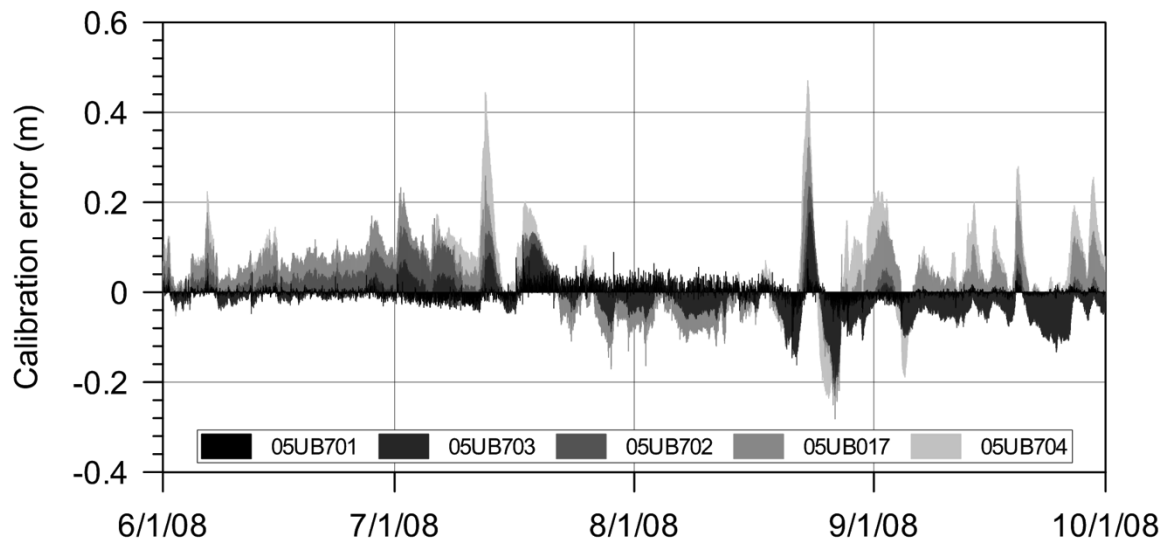


Figure 5.2. Hydrodynamic calibration model error for all gauges

As expected, the closest gauge to the downstream boundary shows the least error, ranging from -0.15 to + 0.13 m. Progressing upstream, errors in the model increase, ranging between -0.20 to 0.18 m for gauge 05UB703, -0.23 to 0.23 m for gauge 05UB702, -0.28 to 0.34 m for gauge 05UB017, and -0.24 to 0.47 m for

gauge 05UB704. A large degree of error is explained by the inherent lag introduced into the model by utilizing the measured flow at Jenpeg to define the upstream boundary condition. Increasing with distance upstream from Jenpeg, this lag is clearly evident in the calibration results shown in Figure 5.3.

The lag delays the model's response to flow change by approximately one to two days, effectively shifting the simulated results at each gauge later in time. This, in turn, produces the largest source of error in the results. A second source of error, particularly for gauge 05UB704 on Playgreen Lake, stems from the exclusion of wind effects on Lake Winnipeg. During extreme north wind events, the elevation of the Lake Winnipeg North Basin may decrease in excess of 1 meter due to wind set-down. Given that the average head drop between Lake Winnipeg and Playgreen Lake is only 0.2 to 0.5 m, the effect may extend downstream as far as Whiskey Jack Narrows and thereby cause the model results to seem inaccurate.

The final calibration yields Manning bed roughness values ranging from 0.015 to 0.123. The latter, as previously discussed, is assigned to Metchanais Channel and is attributed to the omission of islands and other constrictions from the mesh. All but one of the remaining open water reaches are found to lie within a roughness range of 0.020 to 0.045, typical of large, clean, and straight rivers (Chow, 1959). A summary of the Manning roughness values used in the model is provided in Table 5.1.

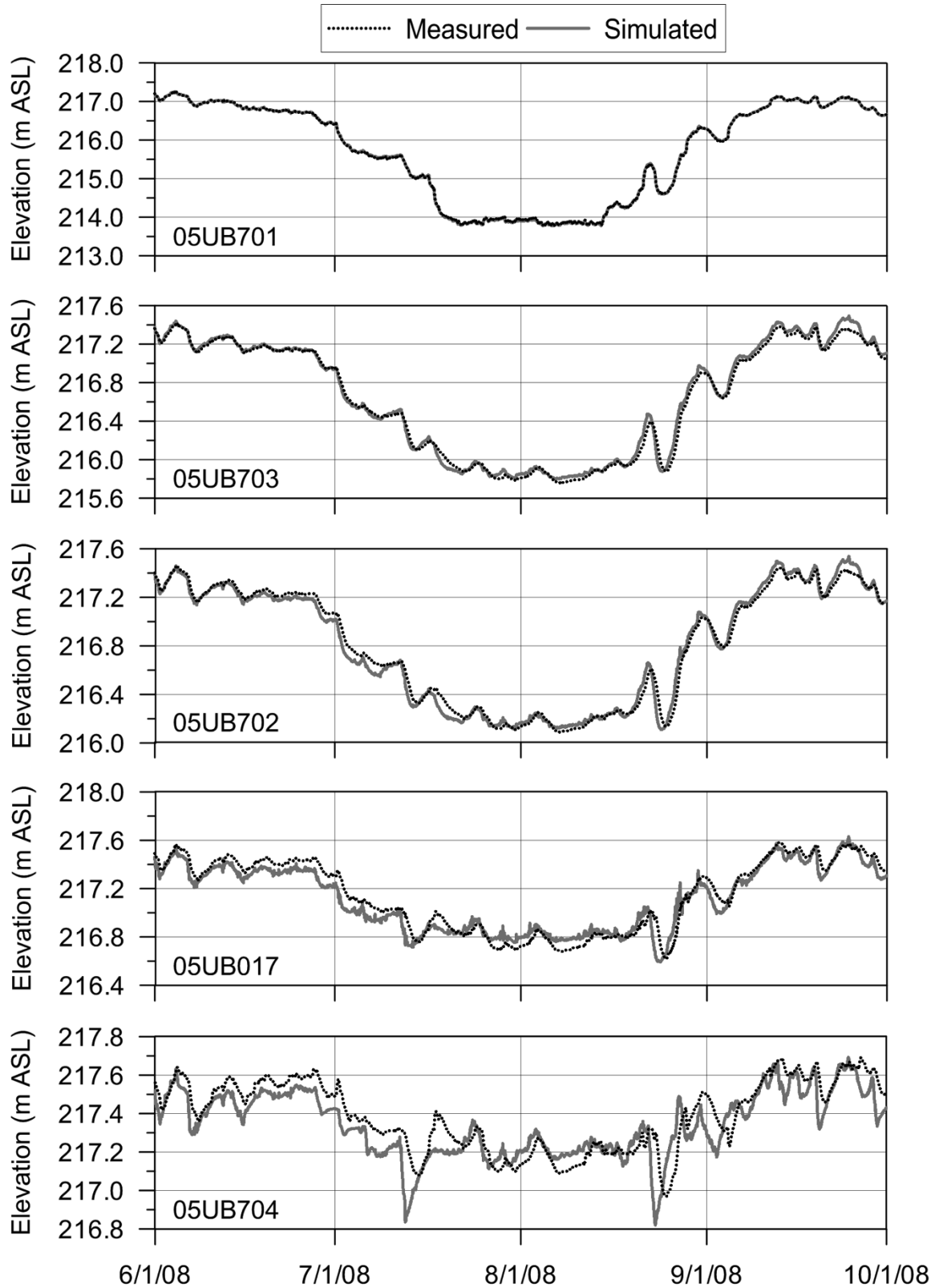


Figure 5.3. 2008 open water season final calibration

Table 5.1. Documented vs. calibrated Manning channel bed roughness

Reach	Documented Manning Roughness	Calibrated Manning Roughness
1	N/A	0.015
2	0.035	0.022
3	0.045	0.027
4	0.050	0.050
5	0.042	0.025
6	0.050	0.050
7	0.042	0.027
8	0.050	0.050
9	0.050	0.040
10	0.050	0.050
11	0.042	0.042
12	0.050	0.050
13	0.056 to 0.060	0.040
14	N/A	0.030
15	0.044	0.045
16	0.038	0.025
17	N/A	0.045
18	N/A	0.025
19	0.023 to 0.037	0.030
20	0.047	0.040
21	0.048	0.030
22	0.045	0.123*
23	0.050	0.123*
24	0.050	0.040

\* Artificially increased to account for constriction head losses

In all but two cases, the calibrated Manning roughness is lower in this calibration than what was documented in pre-construction studies. One basis for this may be the utilization of different modelling approaches. The difference between the one-dimensional direct integration method utilized in the former studies and the two-dimensional Navier Stokes equations utilized by CRISSP-2D carries with it a different set of assumptions, considerations, and level of detail that leads to a variation in modelled channel roughness. A second explanation for this difference is the physical changes that have taken place in the channel since the original studies were performed. A decrease in roughness is expected to occur under both erosion and deposition, which undoubtedly constitutes some of the difference. In addition, since the Manning roughness is inversely proportional to depth, the flooding associated with the construction of Jenpeg may have also acted to increase depth and lower the bed roughness.

#### 5.4 Hydrodynamic Validation

The hydrodynamic parameterization of the model was validated using both a split sample approach and by examining secondary processes. The open water seasons from 2001 to 2007 and 2009 to 2010 inclusive provided the data set for validation, which included both years of low flow (2004) and extreme high flow (2005). The entire operating range of the station was modelled within the nine-year data set, including the low flows typical of the freeze-up flow cutback. The results from the model validation are provided in the following sections.

#### 5.4.1 *Water Surface Profile*

The primary method of validating the model was the utilization of a split sample approach to simulate the water surface profile in the study region. Doing so ensured that the model functions as intended not only for the time period for which it was calibrated, but also for the majority of other potential hydraulic conditions that can be expected to occur. The model was validated under these conditions without changing any of the calibrated model parameters or functions. Each open water season was analysed independently to observe any local errors.

The full validation results for each of the nine years are presented in Appendix A. Overall, the model's performance is excellent, accurately simulating the wide range of conditions within the validation study periods. Local errors are observed in two simulations: 2001 and 2005. In the 2001 case, the second upstream gauge 05UB703 is underestimated during a one month portion of the simulation. Given that this underestimation is not observed on subsequent upstream gauges and that similar flow conditions in 2006 and 2009 are accurately modelled, this error is most likely attributed to measurement error. In 2005, the only flood year modelled, the error is higher overall due to the more extreme flow condition. Secondly, a distinct shift from underestimation to overestimation is observed at each gauge. This may be attributed to the effect of Lake Winnipeg on regulating the water elevation in the outlet channels, a process that is not captured using the current boundary conditions.

The performance of the model for the entirety of the validation simulations is presented on Figure 5.4. Gauge 05UB701 is not shown due to its high correlation to the downstream elevation boundary which it defines. The coefficient of determination for this gauge is 0.9997. As expected, the model exhibits an increasing degree of error in relation to upstream extent.

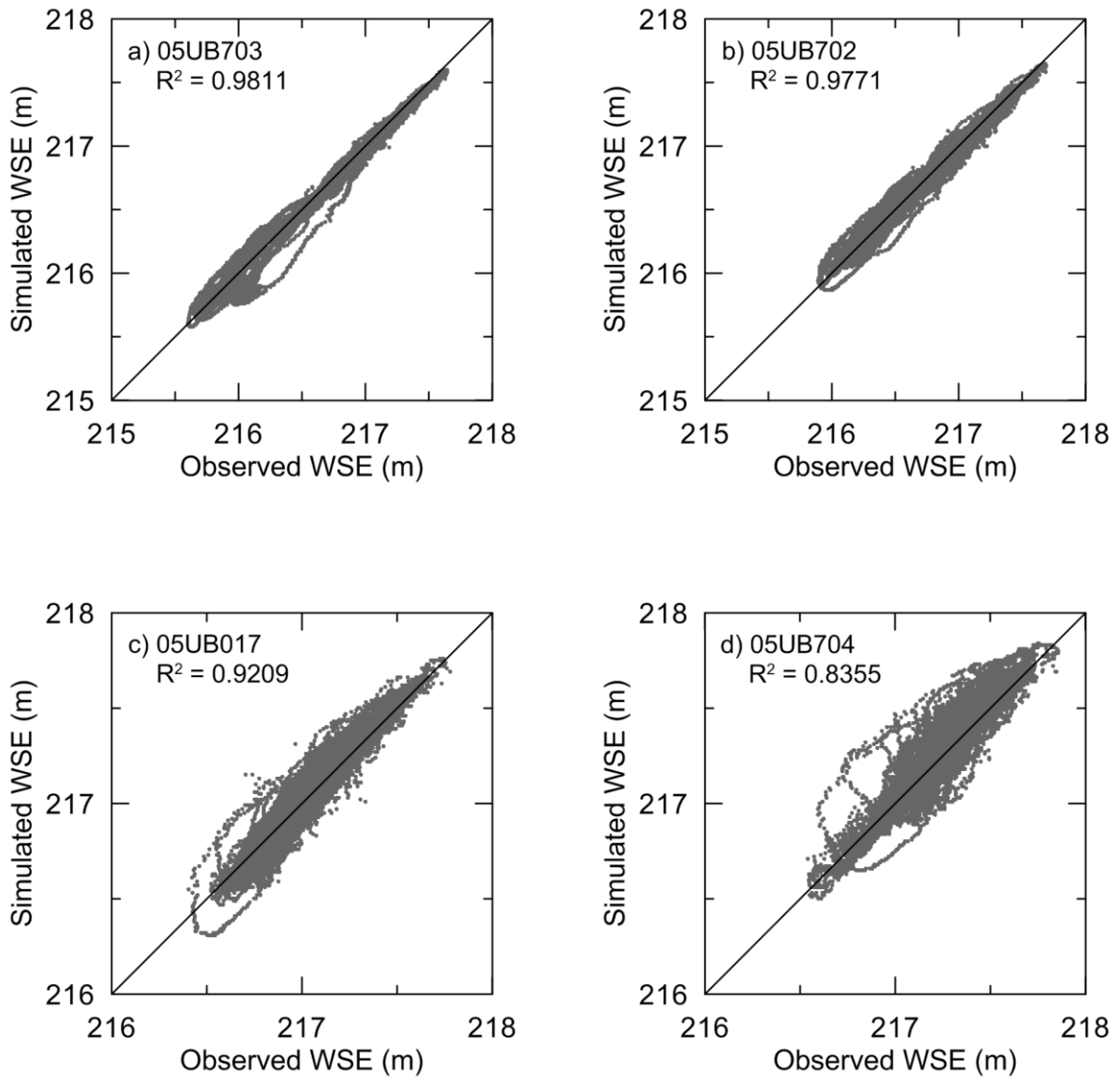


Figure 5.4. Hydrodynamic validation performance

With the exception of a few local errors in either the simulated or measured data, the performance of the model is well within an acceptable range. The largest absolute error for any one gauge does not exceed 0.50 meters with a large majority (98.5%) lying within the  $\pm 0.20$  meter range. Errors in the model tend to increase with lower water surface elevation, coinciding with periods of increased flow. Periods of low flow typical of the flow cutback featured relatively smaller errors, and are largely attributed to the model lag previously discussed.

#### *5.4.2 Water Velocity Distribution*

A second means of validating the model hydrodynamics involved analysing the simulated two-dimensional water velocity distribution. Given that water velocity plays an integral part in the formation of border and skim ice, this validation also served to assess the model's potential in simulating the static ice components of the freeze-up regime. By recalling that static border ice formation takes place wherever water velocity does not exceed 0.06 to 0.15 m/s, it should be reasonable to correlate its observed presence with the simulated water velocity distribution map of the same time period.

The distribution presented in Figure 5.5 outlines the expected range of border ice extent based on the typical range of limiting water velocities. The subsequent series of photographs presented in Figure 5.6 through Figure 5.9 outline the observed ice formation that had taken place in select channels during the same time period, November 18, 2010. This represents the full pre-cutback border ice extent for the 2010 freeze-up year during an upper decile flow of 3,250 cms.

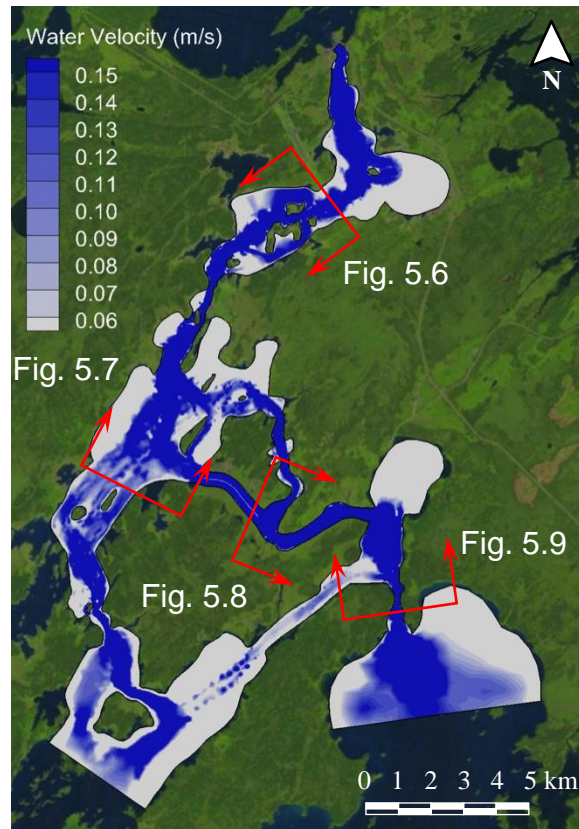


Figure 5.5. Two-dimensional water velocity distribution – November 18, 2010



Figure 5.6. Ice formation on the Lower West Channel looking upstream – November 18, 2010



Figure 5.7. Ice formation on the Upper West Channel looking downstream - November 18, 2010



Figure 5.8. Ice formation on the Ominawin Channel looking upstream - November 18, 2010



Figure 5.9. Ice formation on Whiskey Jack Narrows looking downstream - November 18, 2010

Beginning in the Lower West Channel as shown in Figure 5.6, it is evident that the zones of border ice formation are well represented in the simulated water velocity distribution. The high water velocities in the main channel ensure that it remains free of border ice at all times. In addition, the model accurately captures the localized zones of increased water velocity along both the north and south banks as flow is routed past a series of islands. Typically, these localized zones remain open well into the freeze-up season, gradually freezing over post-cutback.

The Upper West Channel, shown in Figure 5.7, is an area of concern due to the limited bathymetric data available; however, it too is accurately modelled. Looking downstream of the Ominawin Bypass Channel, the flow splits around a long island creating a main channel to the west and secondary channel to the

east. Both channels remain free of border ice up until the flow cutback, at which time they bridge by either thermal ice growth or surface ice floes. The simulated water velocities in these channels seem to support this formation regime.

The Upper Ominawin Channel and the Ominawin Bypass Channel are shown in Figure 5.8. Due to the high flow rate and relatively narrow channels in this reach, border ice is seldom observed. This is also represented in the model results, which predicts negligible border ice growth. Where the model is not in agreement, however, is in the Lower Ominawin Channel, a portion of which is shown to be ice covered in Figure 5.8. It seems that too much flow is routed through this lower reach producing relatively higher water velocities and inhibiting border ice growth. The full effect of this error on the ice regime of the region is expected to be relatively insignificant due to the likely presence of a static ice cover downstream of the channel. Any surface ice floes that form will bridge at this location and quickly juxtapose to produce a full ice cover.

The ice formation within the area of Whiskey Jack Narrows, shown in Figure 5.9, is once again accurately described, with both the model and observations supporting the presence of a preferential flow path along the east bank. The low water velocity predicted within the shallow Kiskittogisu Channel extending west downstream of Whiskey Jack Narrows also supports the static ice cover that is observed to form early in the freeze-up season. Not shown in the series of photographs is the Metchanais Channel, in which the border ice growth is under

predicted. This is attributed to the exclusion of the Kisipachewuk Channel from the mesh and the resulting net increase in Metchanais Channel flow. As a result, this region of the model was excluded from the detailed hydrodynamic validation.

Overall, with the exception of a few localized errors, the water velocity distribution predicted by the model is in good agreement with observed static ice conditions for the high flow condition. Based on this assessment, it is also evident that border ice growth is closely tied to water velocity. Furthermore, it is expected based on these results that the critical velocity governing border ice growth will lie near the top of the expected range.

#### *5.4.3 Flow Distribution*

The last method of validating the model hydrodynamics involved a comparison of the measured and simulated flow distribution between the Ominawin, Metchanais, Kisipachewuk, and Kiskittogisu Channels. The data set for this consisted of four flow measurements in each channel taken between the months of June and October, 1979. The measurements were correlated to the corresponding calculated Jenpeg flow from the same time, producing an estimate of the percent flow distribution in each channel. For comparison, the flow distribution data from each of the hydrodynamic validation simulations was combined and the average percent flow distribution was estimated. The results of this analysis are presented in Appendix A and are summarized in Table 5.2.

Table 5.2. Flow distribution comparison of connecting channels

Channel	Measured Flow Distribution [% Total Flow]	Simulated Flow Distribution [%Total Flow]
Lower Ominawin Channel	12.4	28.7
Ominawin Bypass Channel	49.6	35.5
<b>Total Ominawin Channel</b>	<b>62.0</b>	<b>64.2</b>
Metchanais Channel	22.9	34.0
Kisipachewuk Channel	15.7	N/A
<b>Total Metchanais and Kisipachewuk</b>	<b>38.6</b>	<b>34.0</b>
Kiskittogisu Channel	9.7	5.5

Overall, the flow distribution comparison clearly outlines the model's inaccuracy in simulating the flow distribution between the Lower Ominawin and the Ominawin Bypass Channels. Roughly twice as much flow is routed through the Lower Ominawin Channel as was measured, which supports the observations made in the water velocity distribution analysis. An effort was made to correct this by adjusting the channel bed roughness in both the Lower Ominawin Channel and the Ominawin Bypass Channel; however this method was not shown to be successful, requiring excessive and unrealistic changes to achieve the desired results. The subsequent step was to re-examine and adjust the model bathymetry to better reflect the series of rapids present in the channel; however, given the channels relative insignificance in the overall ice regime this exercise was not warranted.

Comparison of the flow distribution between the Lake Kiskittogisu outlet channels demonstrates that the model performs well. The total Ominawin Channel flow is in close agreement between the measured and simulated results, as is the total flow through the Metchanais and Kisipachewuk Channels. The flow rate through Kiskittogisu Channel is relatively minor and any disparity can be overlooked. The channel is thought to flow bi-directionally, with the few available measurements showing a southwesterly flow into Kiskittogisu Lake. Conversely, the model predicts a northeastern flow, attributed primarily to the routing of Kisipachewuk Channel flow through Metchanais Channel. Given that the contribution of Kiskittogisu Channel to the overall flow regime is minimal and the corresponding water velocities are small, this error should have no impact on the ice regime.

## 5.5 Boundary Condition Sensitivity

The limited availability of data used to determine the upstream boundary discharge made it necessary to analyse the model's sensitivity to variations in this distribution. This became particularly important when considering that the flow distribution was determined without the use of any low-flow condition data. A series of steady-state simulations were established utilizing both a lower quartile flow condition of 1905 cms and an upper decile flow condition of 3965 cms. In each series of simulations, the flow distribution between Playgreen and Kiskittogisu Lakes was varied between the range of 45/65 to 75/25. The net effect on the model was then determined by analyzing the corresponding change

to Ominawin, Metchanais, and Kiskittogisu Channel flows. The results of this are presented in Table 5.3 and Table 5.4 for the lower quartile and upper decile flow conditions, respectively. Also included is the percent increase or decrease in each channel's conveyance relative to the total shift in flow.

Table 5.3. Boundary condition sensitivity, lower quartile flow condition

Upstream Flow Distribution	Playgreen Lake [cms]	Kiskittogisu Lake [cms]	Ominawin Channel [cms]	Metchanais Channel [cms]	Kiskittogisu Channel [cms]
45/55	-286	+286	-36 (-13%)	+38 (+13%)	+249 (+87%)
50/40	-190	+190	-21 (-11%)	+23 (+12%)	+168 (+88%)
55/45	-95	+95	-9 (-9%)	+10 (+11%)	+85 (+90%)
<b>Baseline</b>	<b>1,143</b>	<b>762</b>	<b>1,226</b>	<b>640</b>	<b>117</b>
65/35	+95	-95	+9 (+9%)	-7 (-8%)	-88 (-93%)
70/30	+190	-190	+13 (+7%)	-12 (-6%)	-179 (-94%)
75/25	+286	-286	+22 (+8%)	-20 (-7%)	-266 (-93%)

Table 5.4. Boundary condition sensitivity, upper decile flow condition

Upstream Flow Distribution	Playgreen Lake [cms]	Kiskittogisu Lake [cms]	Ominawin Channel [cms]	Metchanais Channel [cms]	Kiskittogisu Channel [cms]
45/55	-595	+595	-68 (-11%)	+71 (+12%)	+525 (+88%)
50/40	-396	+397	-40 (-10%)	+43 (+11%)	+355 (+90%)
55/45	-198	+198	-16 (-8%)	+19 (+10%)	+180 (+91%)
<b>Baseline</b>	<b>2,379</b>	<b>1,586</b>	<b>2,542</b>	<b>1,365</b>	<b>196</b>
65/35	+199	-198	+16 (+8%)	-11 (-6%)	-188 (-94%)
70/30	+397	-396	+27 (+7%)	-21 (-5%)	-376 (-95%)
75/25	+595	-595	+45 (+7%)	-40 (-7%)	-556 (-94%)

It is evident from the results of the boundary condition sensitivity analysis that, by far, the largest effect of shifting flow between the two upstream boundaries is observed on the Kiskittogisu Channel. Both the Ominawin and Metchanais Channel are minimally impacted, either increasing or decreasing their conveyance by only  $\pm 13\%$  of the total flow shift. As such, this analysis shows that the overall ice regime of the modelled region is not largely dependent on the upstream boundary flow distribution and that errors in its estimation will cause only local changes to the ice formation on Whiskey Jack Narrows and within the Kiskittogisu Channel.

## 5.6 Summary

The calibration and validation of the CRISSP-2D hydrodynamic parameters is proven to be successful. In most instances, both the water surface profile and the water velocity distribution are in agreement with either measured values of observed conditions. An inherent lag is introduced into the model by shifting the flow boundary to the upstream extents of the model, thereby constituting much of the error observed in the calibrated water surface profile. The effect of this error on ice simulations is not expected to be great, at least within the lower reaches of the model downstream of Manitou Rapids. Here, the shift is less apparent and should not impact the ice regime significantly.

The flow distribution also presents errors in the total simulated flow through two channels. The Lower Ominawin Channel is simulated to convey twice as much flow as was measured, resulting in a high velocity flow that most likely inhibits border ice growth. Given that border ice is typically observed in this channel, this is clearly a model weakness. The error, however, is expected to be very localized: any surface ice floes that are generated are expected to form a front when they arrive at the static ice just downstream of the channel and quickly act to form a cover. Secondly, the Kiskittogisu Channel is found to convey too little flow and flow in the wrong direction. The ice regime for this channel will not change, however, based on its minimal flow and low water velocities. This error can be fixed in the future by altering the upstream boundary flow distribution or by raising and lowering the Manning bed roughness through the Metchanais and Ominawin Channels, respectively.

As a result of the hydrodynamic validation, many of the assumptions made in an effort to limit the model extent or mesh detail are validated. Overall, the model shows good potential in simulating the river ice regime of the study area, particularly the formation of static border and skim ice. Where errors are observed hydrodynamically, they are either minor or locally limited, and are expected to have little to no impact on the overall ice regime.

---

# CHAPTER 6:

## Ice Simulations

---

### 6.1 Introduction

Simulation of ice processes in CRISSP-2D requires the calibration and validation of a number of parameters controlling the water cooling rate, border ice growth, skim and frazil ice production, rate of transportation and deposition, and thermal and mechanical thickening. The most efficient method for doing so is to analyze each parameter independently and merge the results to form a comprehensive model. Each of the parameters examined and the procedures used in their calibration and validation are discussed in the following sections.

### 6.2 Water Temperature Simulation

The simulation of water cooling within CRISSP-2D is reliant on an estimation of the net energy balance at the water surface. Either the full energy budget or the linear heat transfer methods can be used within the model. For this project, the linear heat transfer method is applied primarily due to the limited availability of comprehensive forecast weather data for use in predicting over-night ice

conditions. As such, the entire cooling process within the water body is dependent on a bulk heat transfer parameter as outlined in Equation 1.28.

Calibration of the water-to-air heat transfer coefficient ( $h_{wa}$ ) was performed independent of CRISSP-2D utilizing the annual cooling trend in the average measured water temperature between the years of 2001 and 2010. This was necessary given the lack of spatially varying water temperature data in the study domain. Three analyses were conducted: a short-term average linear approach, a long-term average linear approach, and a global linear approach. The cooling curve, beginning on September 1 of each year and ending when the water temperature reaches 2.0°C, was modelled using the relationship in Equation 2.4. An average water depth of roughly five meters was used in the relationship as determined by a CRISSP-2D hydrodynamic simulation of the same time period.

In the short-term average linear approach, the heat transfer coefficient for each year was optimized using a least squares regression between the measured and simulated water temperature on an hourly resolution. Subsequently, an average of all years was taken to serve as the bulk parameter. The long-term average linear approach performed the same operation; however the simulations were optimized using only the final temperature and not the full cooling curve. Doing so sacrifices accuracy when modelling local short-term variability in water temperature but ensures that the overall rate of cooling matches. Again, an average value provided the bulk parameter.

The short- and long-term average linear methods both provide a good estimate of the cooling curve, with bulk heat transfer coefficients of 23.99 and 27.09 W/m<sup>2</sup>°C, respectively. Both values are near the top of the expected range of 15 to 25 W/m<sup>2</sup>°C. This is primarily due to the year 2004 where the heat transfer coefficient was found to be exceedingly high, ranging between 35.45 and 43.47 W/m<sup>2</sup>°C. As a result, its inclusion in both averaging approaches raises the bulk heat transfer coefficient by over ten percent.

A way of compensating for this is to utilize the global linear approach in which the cooling trends from all years were optimized simultaneously using a global parameter, thereby placing less weight on any outlier years. The bulk heat transfer coefficient for this method was determined to be 22.38 W/m<sup>2</sup>°C, which is more in agreement with the expected range and better describes average years. The accuracy of all three approaches is very similar, with the full performance curves for each outlined in Appendix B and summarized in Table 6.1.

Table 6.1. Comparison of linear heat transfer methods

<b>Method</b>	<b>Bulk Heat Transfer Coefficient [W/m<sup>2</sup>°C]</b>	<b>Slope</b>	<b>R<sup>2</sup></b>
Short-term Linear Average	23.99	0.980	0.958
Long-term Linear Average	27.09	0.964	0.951
Global Linear	22.38	0.990	0.957

The similarity in the statistics of each method suggests that selection of either of the parameter choices does not significantly affect the model results. This is further supported by the inherent and sometimes significant natural variability in the bulk heat transfer coefficient and the relatively short duration of freeze-up simulations. The parameter value of  $22.38 \text{ W/m}^2\text{°C}$  is recommended for use in the model, primarily due to its better representation of average conditions.

### 6.3 Initial Conditions

Each ice simulation was initialized using a hot start, which represents a steady-state solution of the first time-step. Both hydrodynamics and thermodynamics were considered such that subsequent ice simulations were initialized using a steady-state water depth, water velocity, and water temperature at each node. Whenever possible, the time period for dynamic ice simulation was extended to provide enough lead-time such that ice formation commenced one or two days after the simulated start date. As a result, any ice that existed prior to the simulation start date was considered to be minimal and was neglected from the majority of ice simulations. In certain cases where an ice simulation was extended or restarted mid freeze-up, the corresponding output files describing the location and characteristics of the ice cover from the original simulation were used to initialize the subsequent one.

Due to the presence of thermal advection and diffusion in the model, the original hydrodynamic time step of 0.85 seconds was found to be too coarse for thermodynamic and ice simulations. Numerical instability was found to occur in high-velocity reaches in direct coincidence with the advance of a temperature gradient through that reach. It was determined that the cause of this instability stemmed from the addition of diffusion as a transport mechanism, which caused the temperature gradient to bypass certain nodes as it advanced through the high velocity reaches. To correct this, the hydrodynamic time step was lowered to 0.70 seconds. The ice dynamic time step was found to have minimal impact and was set at 1.40 seconds. Lastly, the coupling time step was kept at its default value of 900 seconds.

#### 6.4 Thermal Ice Calibration

The calibration of the thermal ice components of the CRISSP-2D model consisted of defining the parameters that control border and skim ice growth, frazil ice generation, and mass exchange processes with the water surface. Each component of the model was isolated and analyzed independently using various flow conditions. Calibration was conducted qualitatively by comparing modelled results with photographs of the study region taken during the same date and time. Where neither measurements nor observations existed for comparison, a sensitivity analysis was conducted and the parameter value was chosen accordingly. These included the parameters governing skim and frazil ice

formation, and certain mass exchange processes. The calibration procedure for each of the thermal ice parameters is outlined in the following sections.

#### 6.4.1 *Border Ice Formation ( $t_c$ , $v_{crskm}$ , $v_{crbom}$ )*

The first observance of ice in the study area is limited to static ice growth in the lakes and bays, followed by border ice growth in the wider, slow moving channels. Modelling of these processes in CRISSP-2D is performed based on critical value criteria defining: 1) the minimum surface water temperature required for border ice growth ( $t_c$ ), 2) the maximum water velocity above which static border ice will not form ( $v_{crskm}$ ), and 3) the maximum water velocity above which frazil accretion will not occur ( $v_{crbom}$ ). The parameters are each intended to control a well-defined process in the generation of border ice and can therefore be calibrated independently of one another.

The minimum water surface temperature required for border ice growth is typically used to adjust the onset of border ice formation in the model, postponing it later into the freeze-up season with decreases to the parameter value. When calculated over a two-dimensional domain, the surface water temperature varies spatially with water velocity and temporally with changes to air temperature (Equation 1.31). As a result, it can also be used to define the extent of the ice edge in certain situations; however, errors may be introduced in the results during exceedingly cold or warm conditions. For the purposes of this model, only the timing of border ice formation is used to calibrate this parameter.

The maximum velocity limiting static border ice formation can only be used to calibrate the extent of the ice edge from each shore, and is directly correlated to the physical limitations previously discussed. As such, it provides a consistent estimate of border ice growth dependent only on flow magnitude and not on meteorological conditions. An increase to this parameter value extends the border ice extent further towards the channel thalweg. By pairing the limiting velocity parameters with the minimum water surface temperature parameter, it is possible to control the border ice prediction routine and limit its application only to shallow, slow moving sections of the reach. The remaining parameter defining the maximum velocity for frazil accretion at the border ice edge is not active in the current version of CRISSP-2D and will therefore not be discussed; however its intended function is similar to that of *vcrrskm*.

The year 2007 is one of the only years where the initial border ice formation was photographed, and therefore it was chosen as the calibration dataset for all of the border ice parameters. The flow condition during this period was upper decile, with an average pre-cutback flow of between 3100 and 3200 cms. Beginning with the minimum water surface temperature required for border ice growth, the model was calibrated over a range of parameter values and the value best representing the onset of border ice formation was chosen. Subsequently, the limiting velocity for static border ice formation was calibrated by, once again, simulating over a range of parameter values and choosing that which produced the most accurate border ice extent results.

The final border ice parameter values determined through calibration are both well within their expected ranges and in good agreement with prior model results. The initial onset of border ice formation was observed to occur on November 15, 2007 and is accurately captured with a minimum surface water temperature of  $-0.15^{\circ}\text{C}$ . Likewise, a critical water velocity of  $0.13\text{m/s}$  best simulates the overall extent of the border ice cover. The effect of the flow cutback, which occurred between November 18 and 19, 2007, is also reflected in the simulation. Following the cutback of flow to roughly 2350 cms (median flow condition), the border ice extends further into the main channel and a large portion of the Upper West Channel downstream of the Ominawin Bypass Channel develops a cover. The simulated progression of the border ice is presented in Figure 6.1.

The border ice routine was validated using the 2004 freeze-up period, which represented the upper quartile flow condition with an average pre-cutback flow of 2500 cms. The first border ice was observed on November 9, 2004 with the bulk of the growth taking place between November 10 and 11, 2004. Subsequent border ice growth was minimal due to the channel quickly becoming ice covered by the bridging of skim ice floes. The full extent of the simulated border ice is presented in Figure 6.2, with the corresponding observed conditions shown in Figure 6.3 through Figure 6.5.

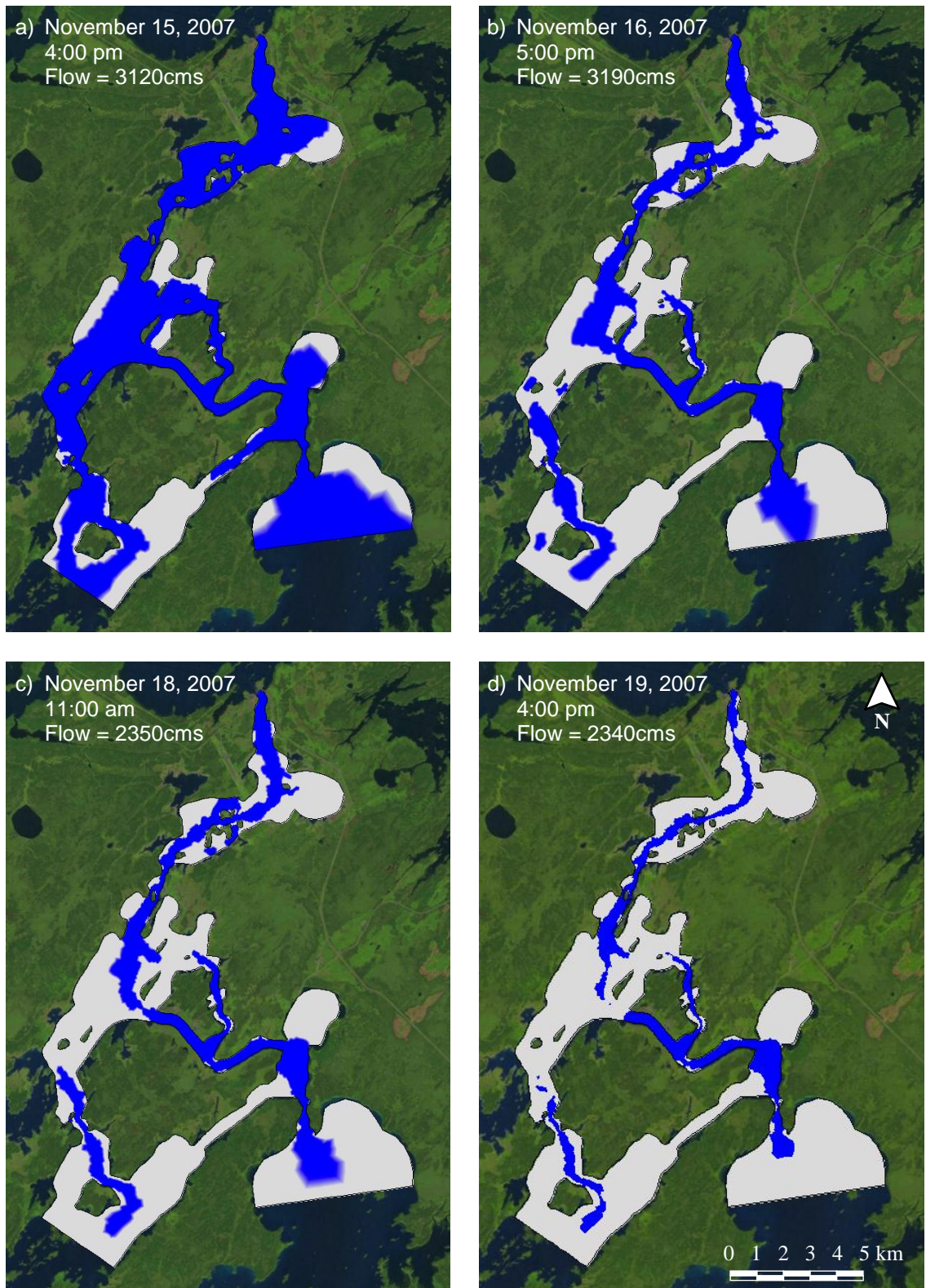


Figure 6.1. Calibrated border ice progression shown in white – 2007 freeze-up period

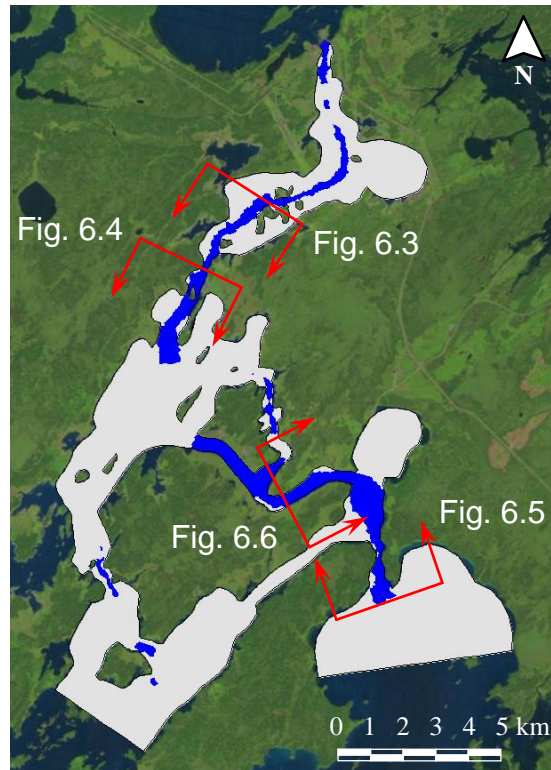


Figure 6.2. Border ice validation – November 15, 2004



Figure 6.3. Ice formation on the Lower West Channel looking upstream – November 15, 2004



Figure 6.4. Ice formation on Manitou Rapids looking upstream – November 15, 2004



Figure 6.5. Ice formation on Whiskey Jack Narrows looking downstream – November 15, 2004



Figure 6.6. Ice formation on the Upper Ominawin Channel looking upstream – November 15, 2004

Comparing the simulated and observed border ice extents over a series of reaches displays the model's ability to accurately simulate this process. The Lower West Channel, shown on Figure 6.3, and the area of Manitou Rapids, shown on Figure 6.4, are both accurately represented in the model results. Travelling downstream from Whiskey Jack Narrows, shown in Figure 6.5, the observed border ice suggests the presence of a preferential path along the right bank followed by a high velocity reach in the Upper Ominawin Channel, shown in Figure 6.6. Once again, the modeled border ice results support both of these observations.

Where the validation fails to match the observed progression of the border ice is in the timing of its initial onset. The model predicts a large portion of the border ice formation to take place on November 9, 2004, whereas the bulk of its growth

was observed to take place between November 10 and 11, 2004. The early onset is attributed to two factors: 1) a likely error in the incoming water temperature, and 2) the instantaneous nature of border ice formation in the model. This suggests that the border ice routine is sensitive to the incoming water temperature. Errors cause the surface water temperature to be either over or underestimated, thereby delaying or advancing the onset of border ice formation. The importance of this sensitivity to the overall ice regime is minimal, however, provided that the dynamic ice processes commence well after the border ice is at its full extent, as is the case during most years.

#### *6.4.2 Skim Ice Formation ( $hi0$ )*

The typical ice regime in the study area during conditions of low flow consists of skim ice formation, transport, and bridging. In CRISSP-2D, skim ice is simulated through a series of large, thin, and solid surface parcels that are transported downstream with the flow. An ice cover is created when the parcels bridge at a boom, channel constriction, or other obstruction to produce an ice front, which quickly progresses upstream with the continued addition of parcels. Given the inherent lack of field data measuring the thickness, concentration, or composition of the relatively weak ice cover, the location of the ice front with time provides the only means of calibrating the skim ice routine during the early freeze-up period.

Each parcel is initialized as a square with area equal to its origin element and a user defined initial skim ice thickness ( $hi0$ ). With time, the parcel thickness increases due to both thermal thickening and frazil deposition; however, neither

of these processes significantly affect the propagation of a skim ice cover during the early freeze-up period. As such, the only user-adjustable parameter controlling the formation of skim ice is the initial parcel thickness. The sensitivity of the ice front progression with time relative to this parameter is presented in Figure 6.7 through Figure 6.9. The observed location of the ice front at the same time is also denoted in red for each figure. A relationship between a simulated ice jam thickness equivalent to 20 times the initial skim ice thickness and the observed ice front location at the same time was found to correlate well across the entire range of parameter values and has been used in this analysis.

At the start of freeze-up for the year 2004, as shown in Figure 6.7, the distribution of skim ice throughout the model remains consistent irrespective of the relative initial skim ice thickness. The location of the forebay ice front is slightly under predicted by the model for values of 0.5 and 1 mm, as denoted by surface ice thicknesses greater than 0.01 m and 0.02 m, respectively. Alternatively, the same ice front is slightly over predicted when applying a higher initial skim ice thickness of either 5 or 10 mm. A second ice front is also present in the Ominawin Bypass Channel where incoming skim ice floes jam against the static ice cover. Of the four parameter values tested, only the thickness of 5 mm accurately represented this process, with the remaining simulations all under predicting the locations of the ice front.

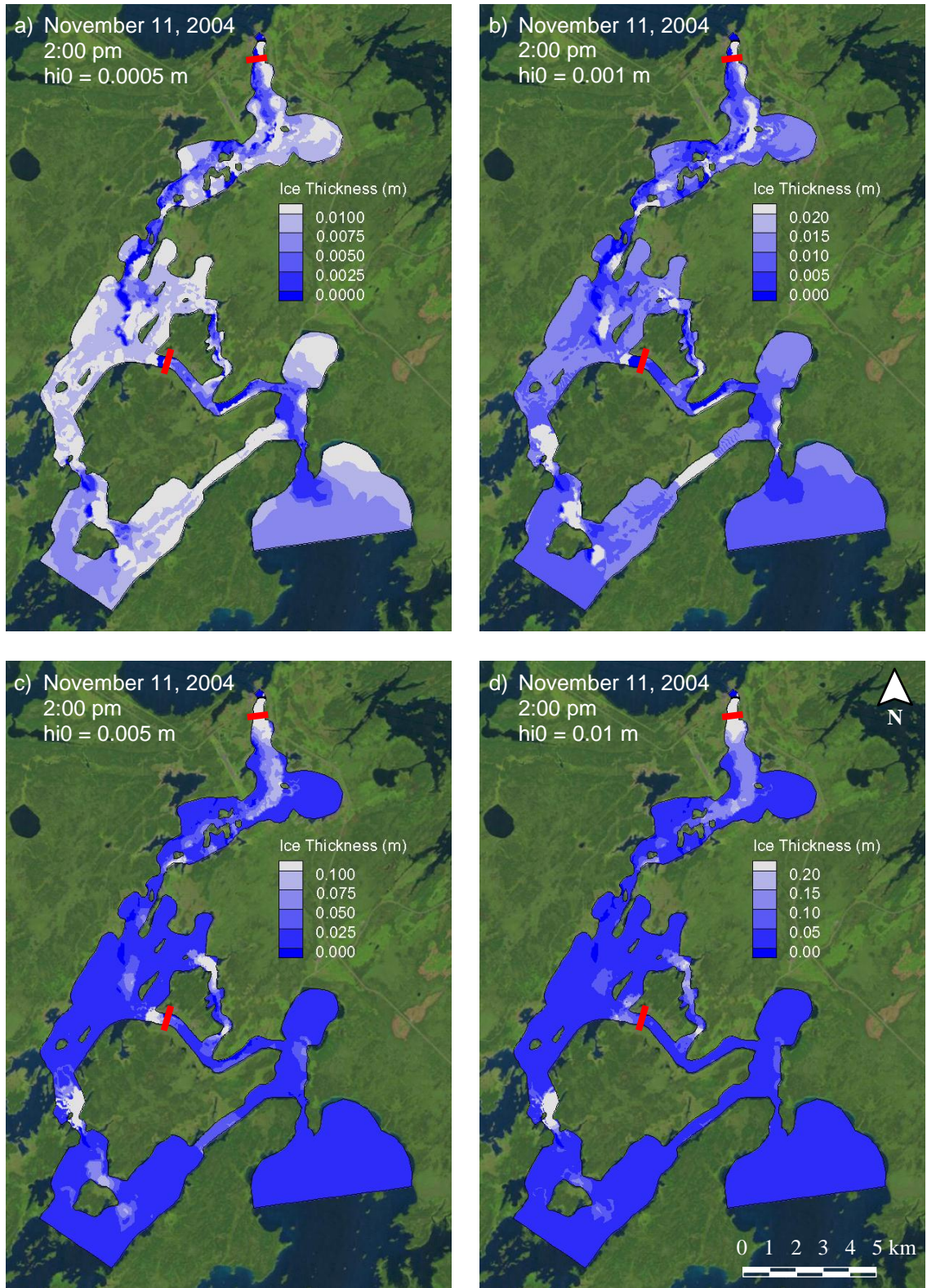


Figure 6.7. Effect of initial skim ice thickness on ice front thickness – start of freeze-up

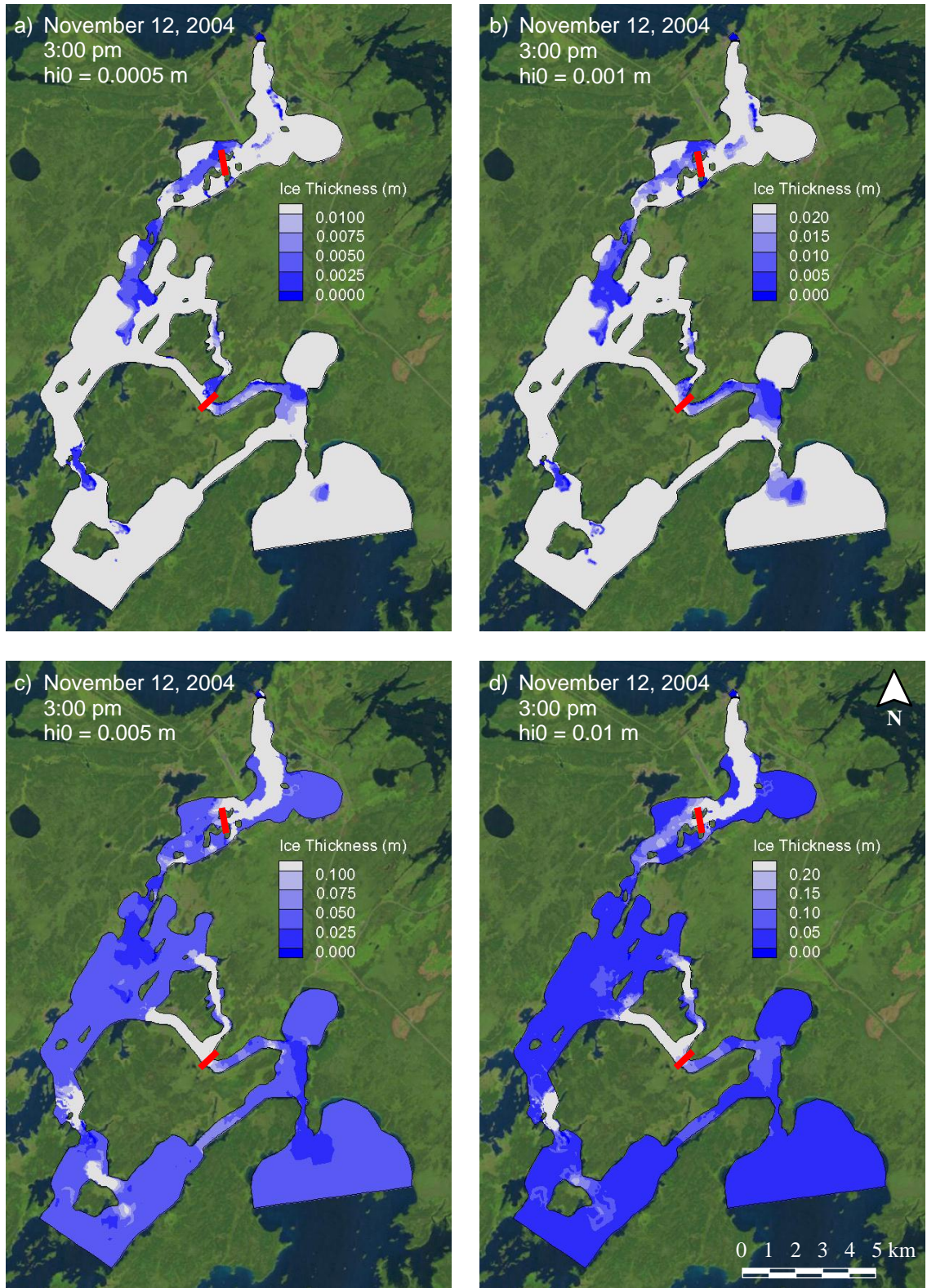


Figure 6.8. Effect of initial skim ice thickness on ice front thickness – middle of freeze-up

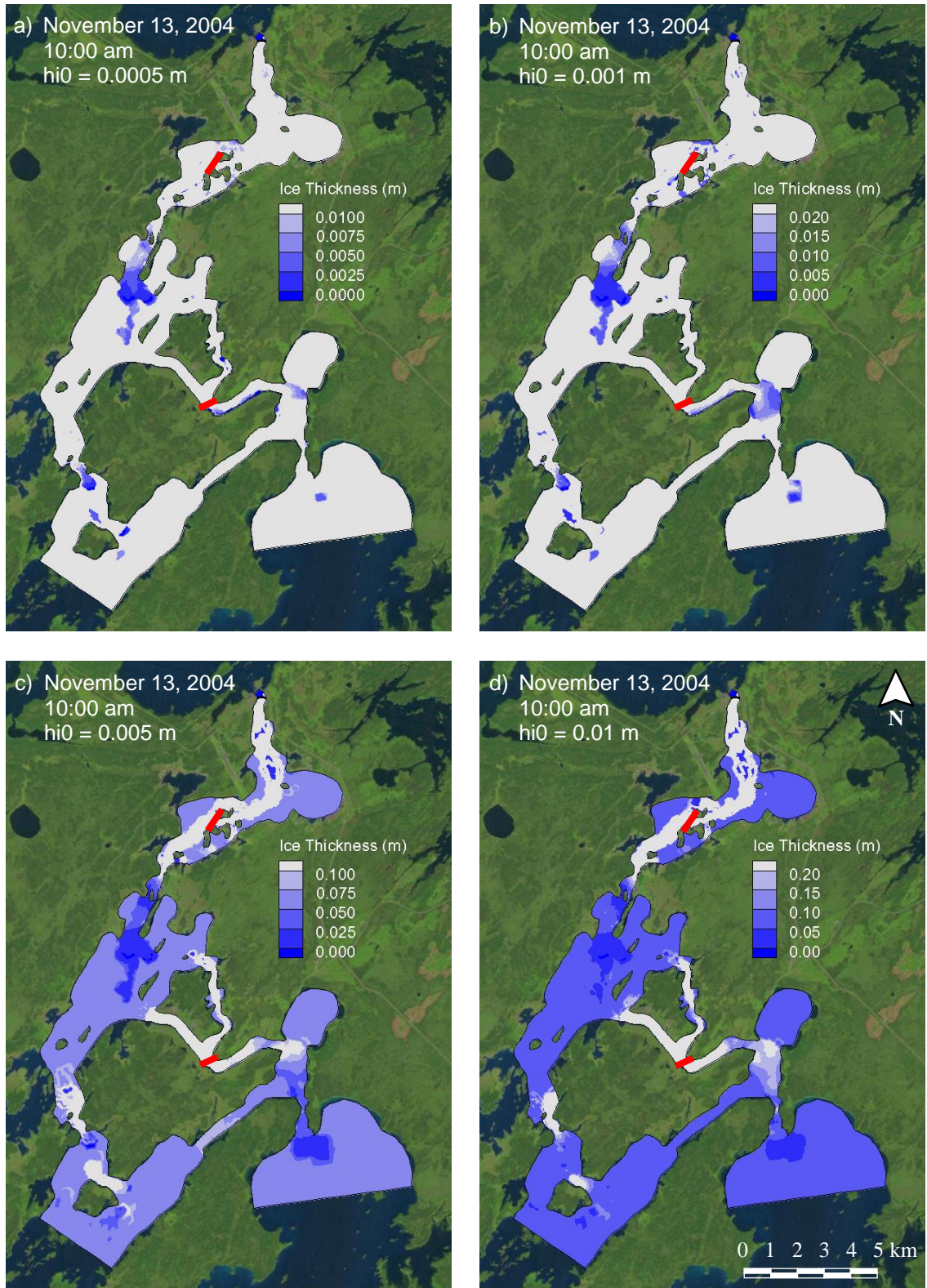


Figure 6.9. Effect of initial skim ice thickness on ice front thickness – end of freeze-up

The simulated ice thickness on November 12, roughly midway through the 2004 freeze-up, is in good agreement with observed ice front location for each parameter value tested, as shown in Figure 6.8. The only slight exception to this is the large volume of ice that is observed upstream of the ice front for the 10 mm simulation, likely suggesting an accelerated advance in subsequent time steps.

The model predicts a majority of the remaining freeze-up to occur over the course of the following day, as shown in Figure 6.9. This process occurs primarily through the continued addition of skim ice at the ice front. Under natural conditions, however, the production and transport of skim ice is largely limited at this stage in the freeze-up regime. This exposes two limitations to model performance under skim ice conditions: 1) the continued formation of skim ice upstream of Manitou Rapids, and 2) the free transport of skim ice upstream of the Upper Ominawin Channel.

The first limitation is a property of the model, whereby the estimation of the vertical turbulence intensity, frazil buoyant velocity, or re-entrainment parameters is simulated in a limited capacity. Under natural conditions, any ice particles that form on the water surface upstream of Manitou Rapids are entrained into the flow within the high turbulence reach and transported downstream in suspension. A majority of these suspended particles deposit on the underside of the ice cover, and very few actually contribute to its advance. Conversely, the model suggests that the vertical turbulence is insufficient to entrain particles and continues

producing skim ice parcels that sustain the growth of the ice front. Unfortunately, the current version of CRISSP-2D computes frazil buoyant velocity using an empirical relationship that does not consider particle size or any user-adjustable parameter, and as such provides no means of calibrating this process.

The second limitation is a property of the mesh discretization, whereby two small islands were omitted from the mesh in the area downstream of Whiskey Jack Narrows. Under natural conditions, these islands restrict the free movement of large skim ice sheets, preventing their contribution, as well any subsequent sheets, to the advancement of the ice front on the Ominawin Channel. Given sufficiently cold conditions, the channel does become ice covered; however this process is delayed considerably relative to the predicted response of the model.

Combined, these two limitations significantly affect the simulated ice regime during the latter stages of a skim ice freeze-up period, and must be considered when analyzing and applying model results for operations decision making purposes. The more significant error relates to the misrepresentation of mass exchange processes within the Manitou Channel and should be reconsidered pending the potential for future versions of CRISSP-2D that allow for the definition of reach-specific parameters. The second limitation may be resolved provided more detailed mesh discretization; however, further analysis should be conducted to investigate the accuracy of the surface ice stoppage criteria in CRISSP-2D and understand its application to skim ice floes.

Based on the results from the beginning and middle of the 2004 freeze-up period, an initial skim ice value of 0.005 m is deemed most appropriate for this study area. It is shown to most accurately capture the observed location of the skim ice front in both the forebay and Ominawin Channel regions. In addition, this value is in good agreement with observed skim ice thicknesses within the study area, which ranged from 0.002 to 0.005 m. Future consideration should be given, however, to the model limitations with respect to end of freeze-up simulations. During these conditions, model results should be interpreted qualitatively where observations and best judgment is used for planning and decision making purposes.

#### *6.4.3 Frazil Ice Formation (vnu)*

During medium to high flow conditions, the ice regime is dominated by frazil ice formation. The limited spatial extent of the dynamic freeze-up regime restricts the full progression of the frazil ice cover primarily to frazil slush floes and periodic frazil pan formation. The frazil that is in suspension typically does not have sufficient time to completely flocculate and rise to the surface, a portion of which may reach the powerhouse and pose a risk of blockage to the station. That which does rise forms weak pockets of frazil slush that are easily submerged on contact with the ice front. Following a flow cutback, the progression of the ice front accelerates through the juxtaposition of poorly defined frazil pans. Under typical conditions, however, only the small portion of the frazil slush that accretes to the leading edge contributes to the advancement of the ice front. As a result, this process is considerably slower than that of the skim ice regime.

CRISSP-2D models the formation of frazil utilizing a concept of thermal equilibrium, whereby any heat deficit that exists due to supercooling is offset by the release of latent heat during the generation of ice crystals. Equation 2.7 outlines the relationship used in CRISSP-2D to calculate the suspended ice concentration with time based on the water temperature, crystal properties, and the Nusselt number ( $vn_u$ ). By definition, the Nusselt number relates the ratio of convective to conductive heat transfer between ice and water. In a turbulent river, the Nusselt number is expected to be greater than unity, with convection representing the dominant form of heat transfer. A value of between two and six is typically applied in ice simulations; its effect within CRISSP-2D between a range of one to seven is shown in Figure 6.10 and Figure 6.11 for the beginning and middle of the 2007 freeze-up period, respectively.

Increasing the Nusselt number has a positive impact on frazil ice generation; however this effect is minimal when translated to ice front progression. Very little difference was observed between all four simulations, with perhaps only the last ( $vn_u = 7$ ) having a discernible impact on the ice front characteristics. A time-series comparison of frazil concentration averaged over the model domain shown in Figure 6.12.

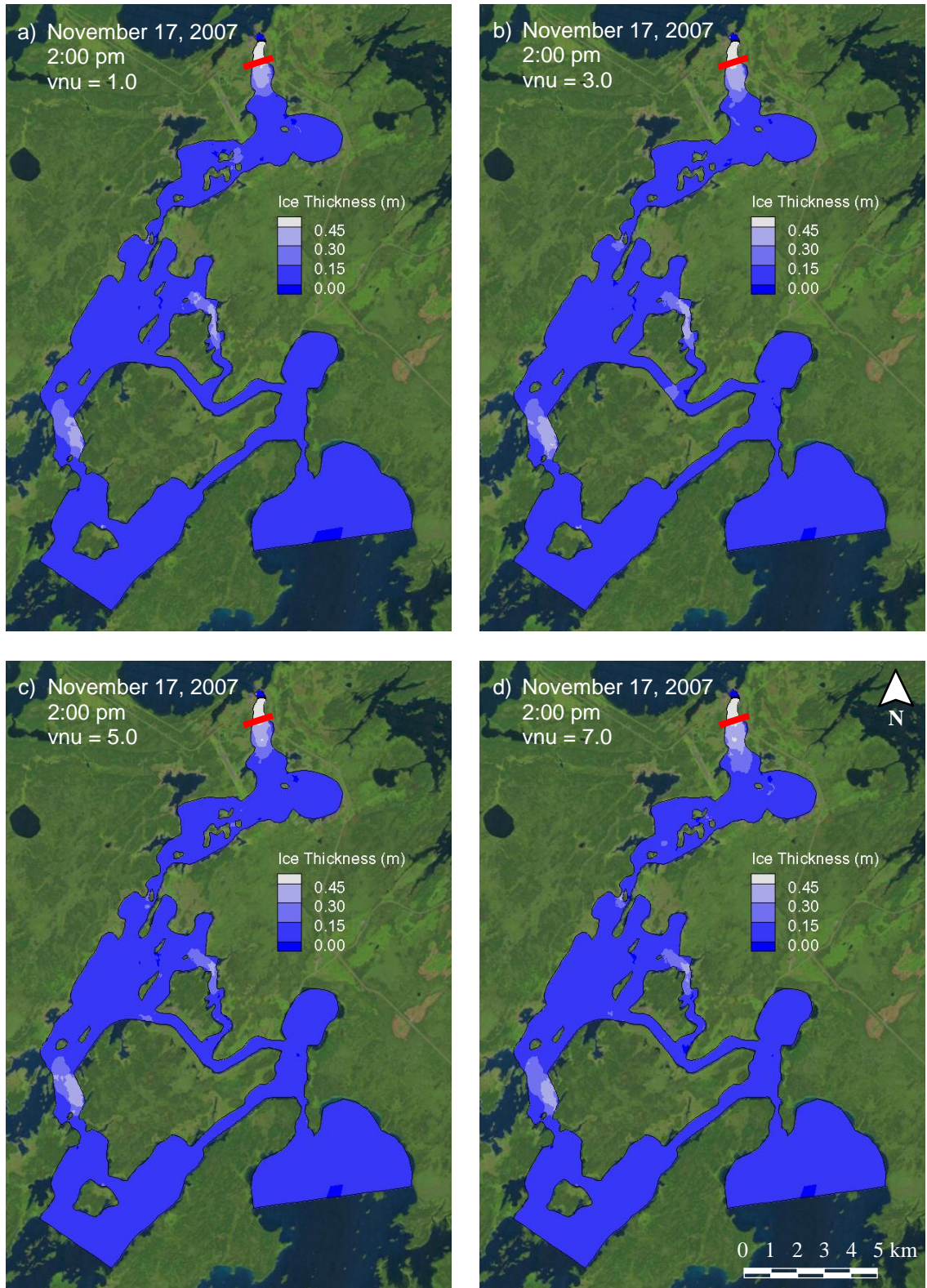


Figure 6.10. Effect of Nusselt number on ice front thickness – start of freeze-up

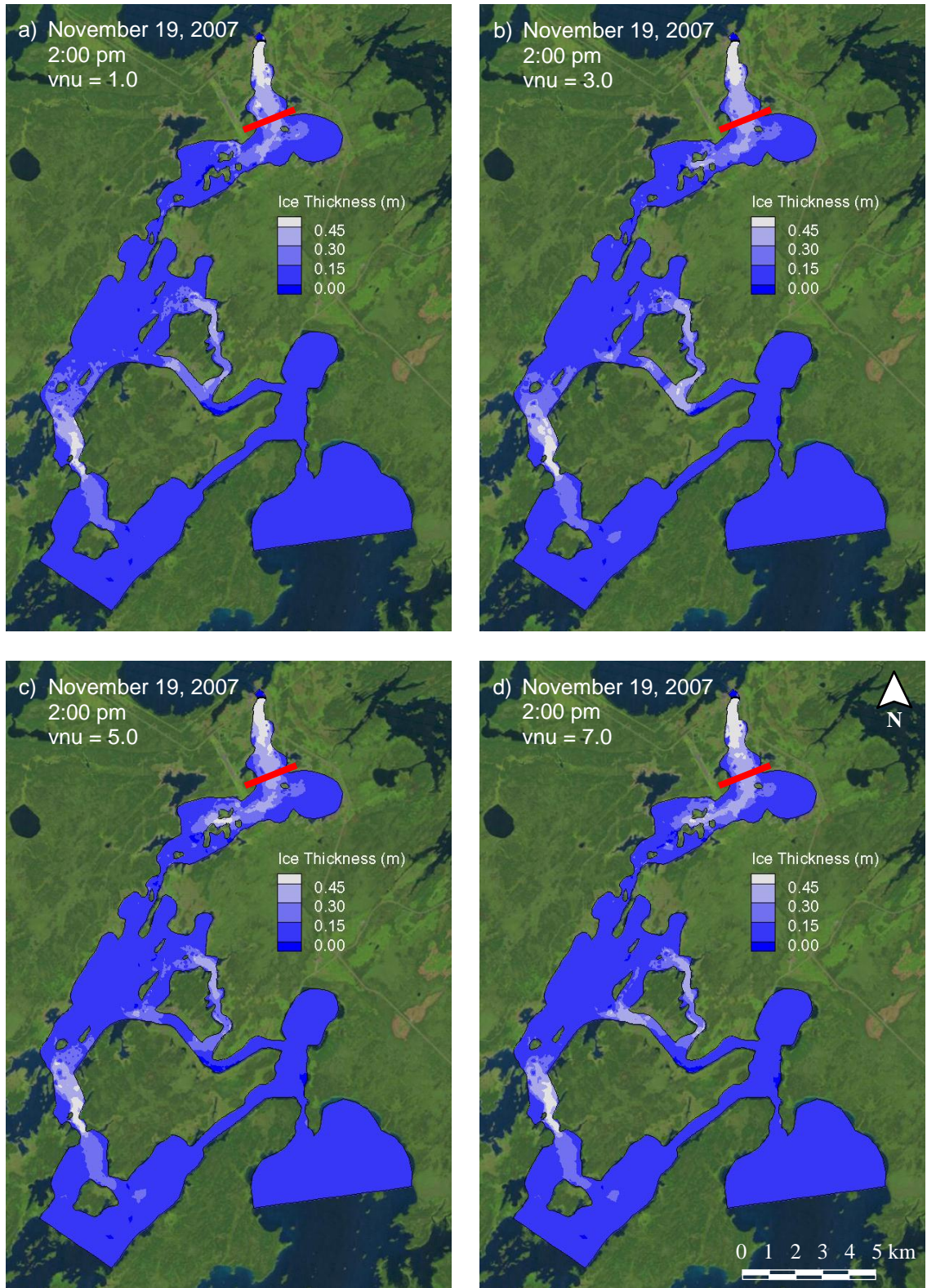


Figure 6.11. Effect of Nusselt number on ice front thickness – middle of freeze-up

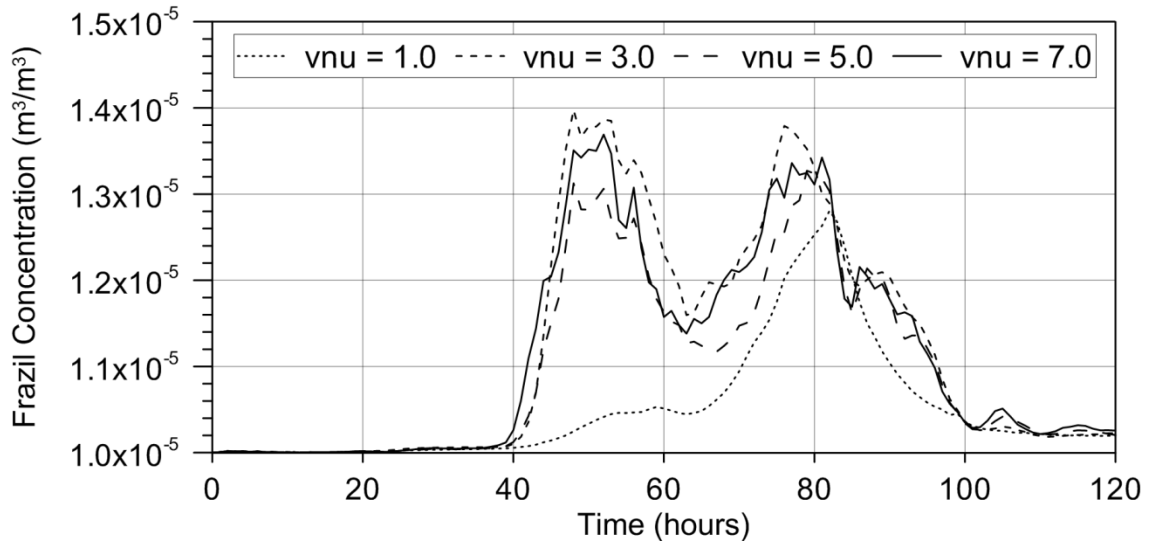


Figure 6.12. Effect of Nusselt number on average frazil concentration – 2007 freeze-up

The time series analysis in Figure 6.12 shows evidence that the total volume of frazil produced does not change considerably. In this regard, it is difficult to predict the significance of the Nusselt number given its effect on both frazil concentration and water temperature (Equations 2.7 and 2.12). The results suggest that there exists a balance whereby the mutual dependence on the Nusselt number causes the relative changes in frazil concentration and water temperature to offset one another and produce similar results for  $vnu \geq 3$ .

A median value of four is most appropriate given the results and is recommended. This is consistent with other ice engineering studies conducted in Northern Manitoba (Malenchak, 2012). It is apparent, however, from the comparisons shown in Figure 6.10 and Figure 6.11 that there exists considerable difficulty in calibrating dynamic ice processes based only on an observed ice

front location. Typically, the observed ice front location matches well with a simulated ice thickness of between 0.30 and 0.45 meters. Based on the equilibrium jam theory, this value varies both spatially and temporally with water velocity and is therefore difficult to determine and apply in a forecasting scenario.

#### 6.4.4 Mass Exchange Processes ( $\theta$ , $\beta_1$ , $v_{bb}$ , $hf_0$ , $an_{maxfra}$ )

Likely due to the very limited spatial scale of the study area, minor changes in the volume of frazil ice generation do not have a significant impact within the model. An alternative is to adjust the parameters governing mass exchange processes that take place within the suspended and surface layers, as modelled using Equations 2.8 and 2.13. These include the probability of frazil ice deposition on the surface ( $\theta_1$ ) and onto existing ice parcels ( $\theta_2$ ), probability of re-entrainment of surface ice ( $\beta_1$ ), frazil rise velocity ( $v_{bb}$ ), initial frazil parcel thickness ( $hf_0$ ), and maximum concentration of frazil within a parcel ( $an_{maxfra}$ ).

Each of the mass exchange parameters is defined globally within the model. As such, it is not possible to isolate and independently calibrate characteristic reaches. Conversely, it is unreasonable to account for the significant variability in mass exchange processes between rapid or quiescent reaches by averaging the global parameter. In this regard, two simplifying assumptions are made. First, it is assumed that all frazil that rises to the surface is deposited onto either an existing or new parcel (i.e.  $\theta_1 = \theta_2 = 1.0$ ). Secondly, ice which exists on the surface as parcels is not re-entrained into the flow as a result of turbulence (i.e.  $\beta_1 = 0.0$ ). A more explicit approach of including these processes includes

either 1) the ability to define reach-specific mass exchange parameters, or 2) explicit calculation of frazil rise velocity based on water velocity as previously identified.

Both deposition and re-entrainment are considered implicitly in the frazil buoyant velocity parameter, which can be suppressed slightly to account for losses due to these phenomena. Based on a theoretical range of between 0.001 and 0.022 m/s, 0.008 m/s represents a suitable average for use in field and laboratory studies (Morse & Richard, 2009). Furthermore, 0.005 m/s is the most commonly observed frazil rise velocity, with the values becoming more depressed with increased turbulence. The model's response over this range is provided in Figure 6.13 and Figure 6.14 for the start and middle of the freeze-up period, respectively.

As with the Nusselt number, the model is not sensitive to changes in frazil rise velocity. Analysis shows that the frazil rise velocity across the entire range tested is sufficient to remove the particles from suspension and produce surface ice parcels. As such, this parameter has little effect during the start of freeze-up, and increases in significance with the upstream progression of the ice front. A time series comparison of frazil concentration immediately downstream of Manitou Rapids is presented in Figure 6.15.

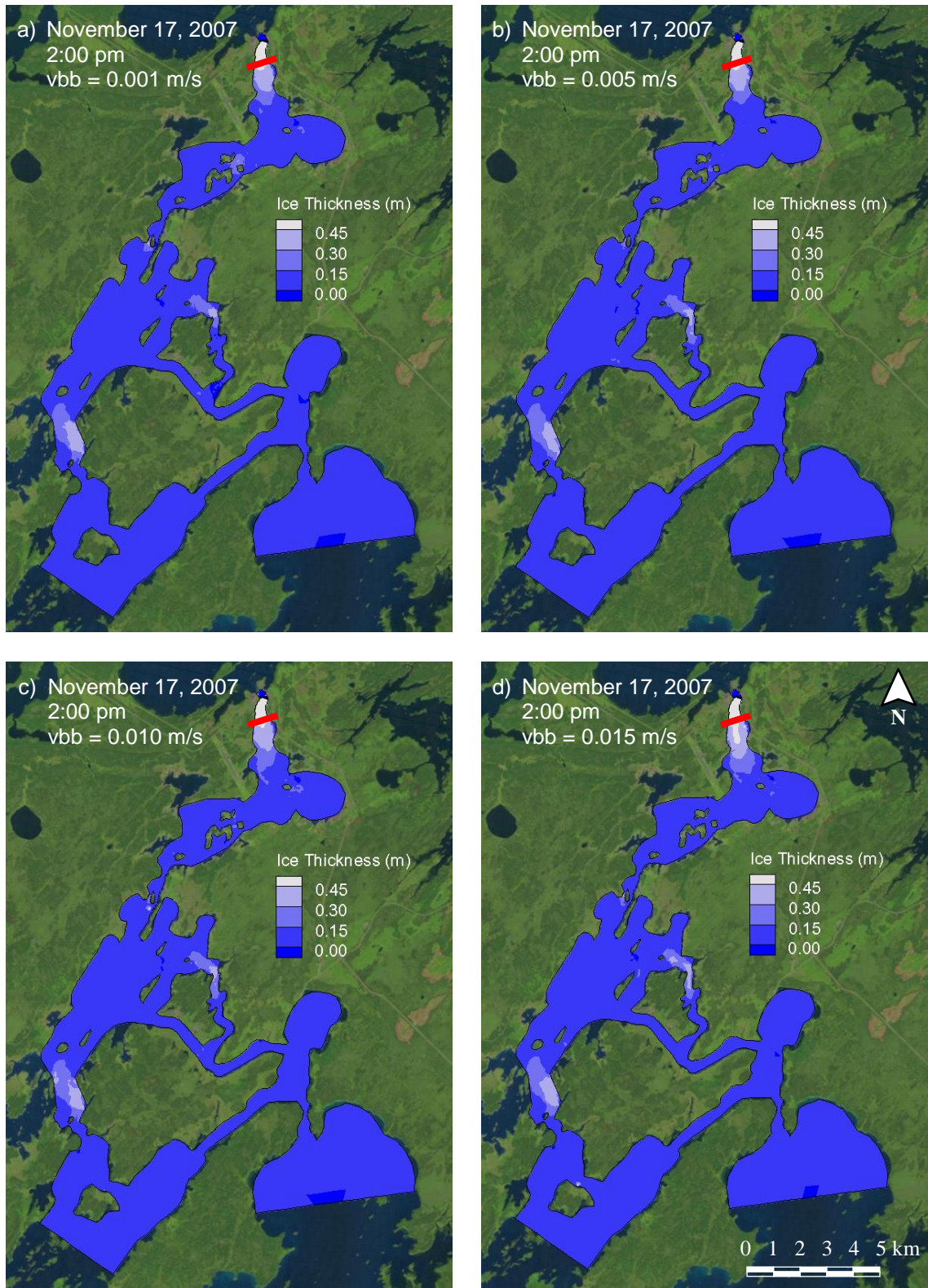


Figure 6.13. Effect of frazil rising velocity on ice front thickness – start of freeze-up

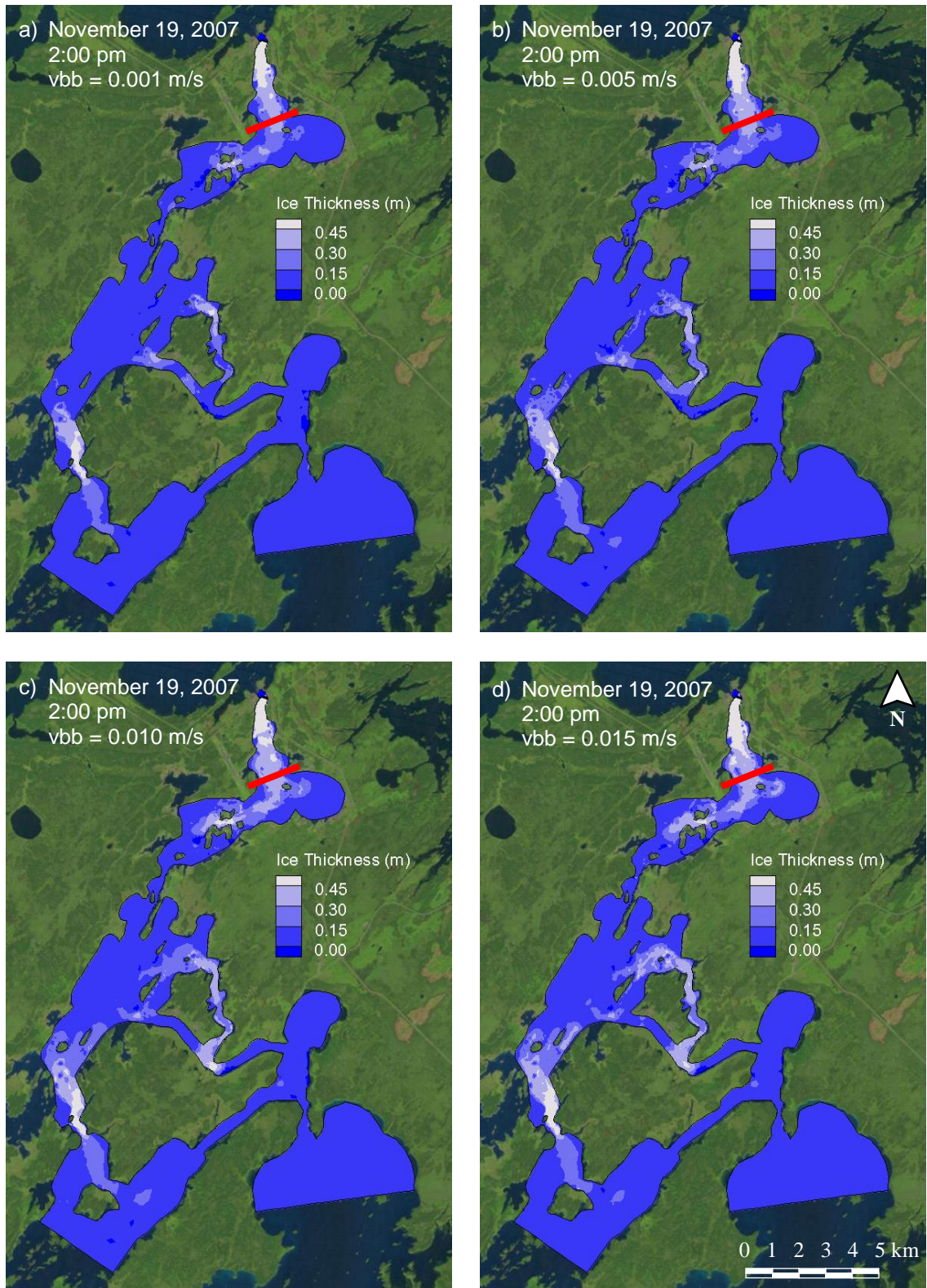


Figure 6.14. Effect of frazil rising velocity on ice front thickness – middle of freeze-up

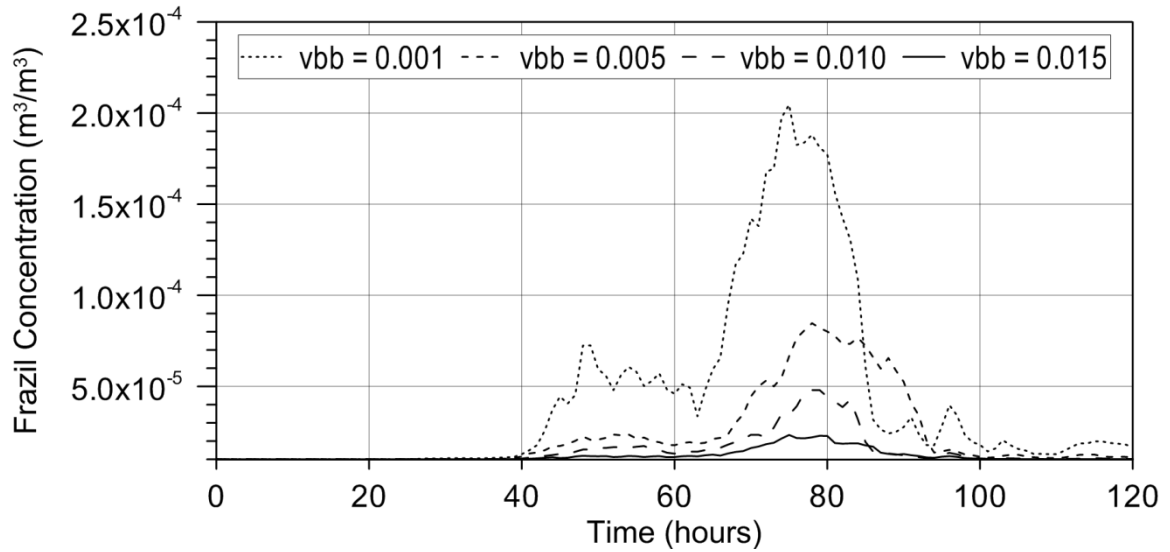


Figure 6.15. Effect of frazil rise velocity on frazil concentration downstream of Manitou Rapids – 2007 freeze-up

The effect of the frazil rise velocity parameter on the simulated concentration downstream of the generation zone is clearly visible in Figure 6.15 and follows the expected response. Essentially this parameter controls the rate at which frazil ice is deposited through buoyancy from the suspension layer to the surface layer. It is logical, therefore, that increasing the rate of removal acts to decrease the volume of entrained ice, and therefore more quickly return the system to a state of minimum concentration ( $1 \times 10^{-5} \text{ m}^3/\text{m}^3$ ). Increasing frazil rise velocity also acts to limit the peak frazil concentration during both the rising and falling legs of the formation process. Ultimately, given the lack of calibration data and the model's insensitivity to this parameter, a frazil rise velocity of 0.005 m/s is recommended for use in this model in accordance with published values.

A new frazil ice parcel is initiated to house all suspended frazil ice that reaches the surface under open water conditions. The physical properties of this parcel are initiated using: 1) a thickness equal to a user defined parameter ( $hf0$ ), 2) an area estimated based on the element in which the parcel originates, and 3) an ice concentration that is calculated based on the ratio between the volume of contributing ice to that of the parcel. Continued addition of frazil ice to existing parcels works to increase their concentration up to a user defined maximum ( $anmaxfra$ ), after which time the concentration remains constant and the parcel thickness increases.

For the purposes of this study, the maximum ice concentration within a frazil ice parcel is set at the default value of  $0.90 \text{ m}^3/\text{m}^3$ . Increasing or decreasing this parameter will inversely affect determining parcel thickness, but should not impact simulated freeze-up processes significantly. In addition, the model is found to be insensitive to changes in the initial frazil ice parcel thickness parameter for both years tested (2007 and 2010). Results from the 2010 freeze-up period are presented in Figure 6.16. The likely cause of this was determined following an analysis of ice parcels during a frazil ice regime. Many of the ice parcels are initiated as skim ice in the slower moving upstream sections, and subsequently thicken through frazil accretion as they travel downstream. As such, true frazil parcels are seldom initiated within the model and the initial frazil ice thickness parameter is rarely applied. This represents a slight limitation of the model; however its effect on the ice regime is minimal.

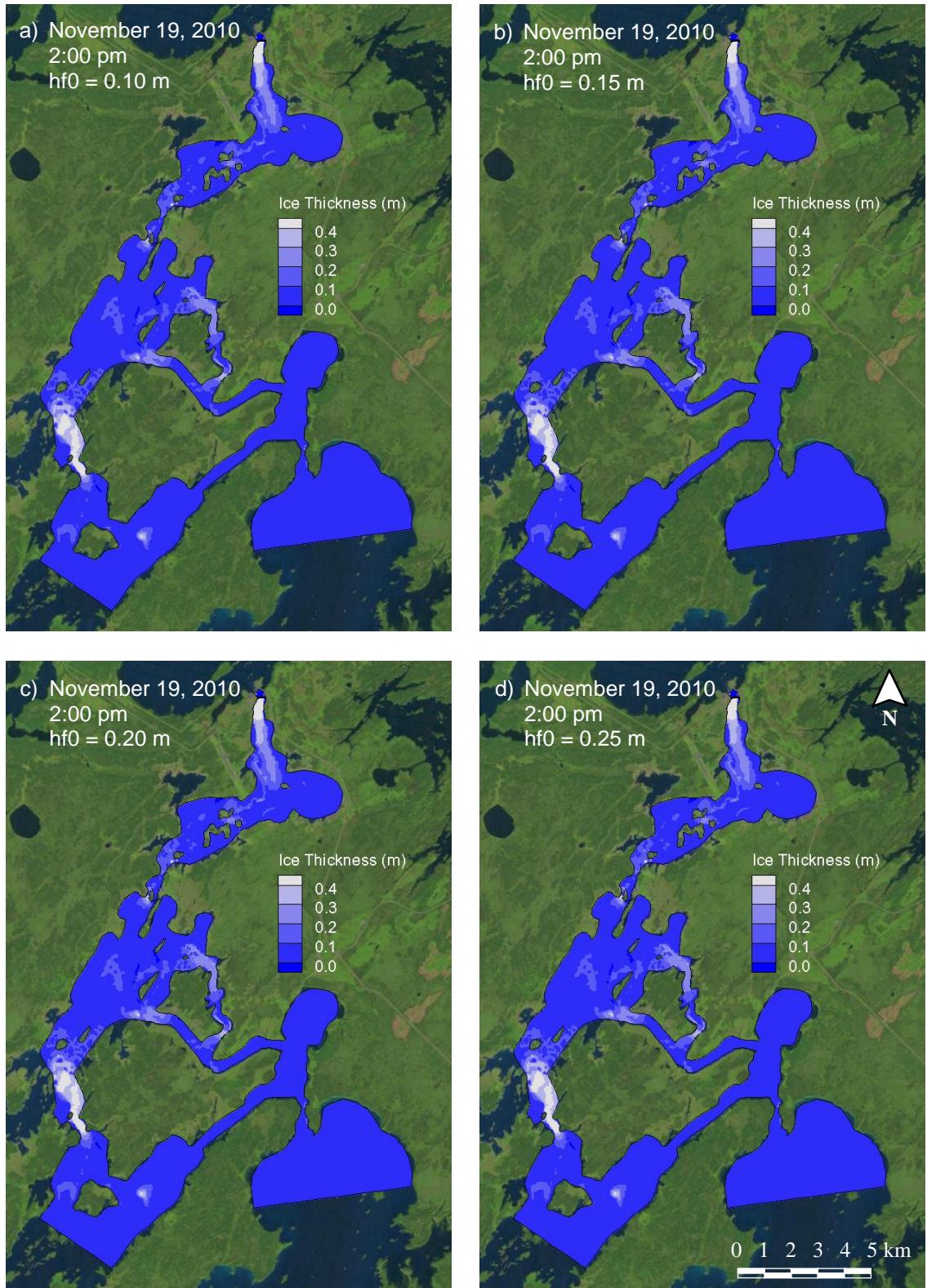


Figure 6.16. Effect of initial frazil ice parcel thickness on ice front thickness – start of freeze-up

A value of 0.15 m is recommended as the initial frazil ice parcel thickness based primarily on a default parameter range. Overall, the thermal ice module within CRISSP-2D is not of significant impact on ice front formation in this study. Internal parameterization controlling mass exchange of frazil react as expected within the model; however the total volume of ice generated and the ice front characteristics do not change significantly.

## 6.5 Dynamic Ice Calibration

The dynamic ice module within CRISSP-2D simulates all of the processes that occur at the water surface in regards to the transport and modification of existing ice parcels. In particular, this includes the interaction of individual parcels with each other, model boundaries, and ice booms. For the purposes of this study, the focus is limited to freeze-up jam formation. As such, undercover ice transport and anchor ice formation are not included in the analysis. The calibration procedures for the remaining parameters controlling the dynamics of ice jam formation are discussed in the following sections.

### 6.5.1 *Ice Boom Representation*

A five-span ice boom was implemented in the model as a means of replicating typical ice front formation characteristics in the Jenpeg forebay, utilizing the location and shape of the first generation boom design circa 1988. The characteristics of each span were adjusted such that boom submergence or

under-boom ice transport does not occur. As such, all ice that comes into contact with the ice boom is retained in an effort to initiate an ice front. Future implementation can be revised to include the updated boom design, as well as dynamic boom loading and failure criteria.

### 6.5.2 Freeze-up Jam ( $thi0$ , $anmax$ )

As parcels are transported downstream, their velocity, concentration, thickness, and internal and external stresses are calculated within CRISSP-2D using the momentum relationship defined in Equation 2.16. An equilibrium jam begins to form when parcels juxtapose against the ice boom or thermal bridge to initiate and subsequently thicken the dynamic ice cover. Thickening continues until externally applied driving forces are balanced by the internal resistive stresses within each parcel. In CRISSP-2D, a maximum single layer ice thickness ( $thi0$ ) criterion is used to approximate the presence of an ice jam. If this criterion is satisfied, that is to say the calculated ice thickness exceeds the maximum for a single layer, an ice jam is assumed to exist. At this time, ice jam dynamics govern and the concentration of each parcel decreases to the maximum for ice jams ( $anmax$ ) through a corresponding change in parcel thickness.

The ice jam formation process within CRISSP-2D is perhaps more applicable to break-up scenarios where the maximum ice jam concentration is generally given as  $0.60 \text{ m}^3/\text{m}^3$ . It can also be applied, however, for freeze-up jams assuming a maximum ice jam concentration equal to or slightly less than that of the incoming ice parcels. For the purposes of this study, the maximum ice jam concentration is

assumed to be  $0.90 \text{ m}^3/\text{m}^3$ , in line with that of frazil ice parcels ( $0.90 \text{ m}^3/\text{m}^3$ ) and slightly less than skim ice parcels ( $1.00 \text{ m}^3/\text{m}^3$ ). In addition, a value of 0.50 m is applied as the maximum single layer ice thickness. Given the relatively simplistic nature of the ice jam routine in CRISSP-2D and its implementation for this study, it is expected that small uncertainties in each of the parameters will not significantly impact ice jam formation.

### 6.5.3 *Surface Ice Submergence (crifr)*

Juxtaposition of surface ice pans is limited by the flow condition present at the leading edge of an ice cover. Surface ice is expected to submerge under the leading edge whenever the forward driving force exceeds the buoyant stability of the parcel. This relationship is modelled empirically in CRISSP-2D through a critical Froude number parameter (*crifr*), which defines the maximum flow condition under which juxtaposition takes place. A value of 0.07 is typically used within the Jenpeg Ice Stabilization Program, however a soft range of 0.05 to 0.10 is widely accepted (Tuthill, 1999). The range is predominantly dependent on the type of ice that is present and is inversely proportional to the porosity of incoming ice floes. Competent ice floes require large driving forces to submerge and are therefore associated within the peak of the critical range of Froude numbers. Conversely, less porous ice floes such as frazil slush are more easily submerged and are typically defined lower within the range. The model's response to the typical parameter range is provided in Figure 6.17 and Figure 6.18 for the start and middle of the freeze-up period, respectively. Once again, the sensitivity with respect to ice front thickness is shown.

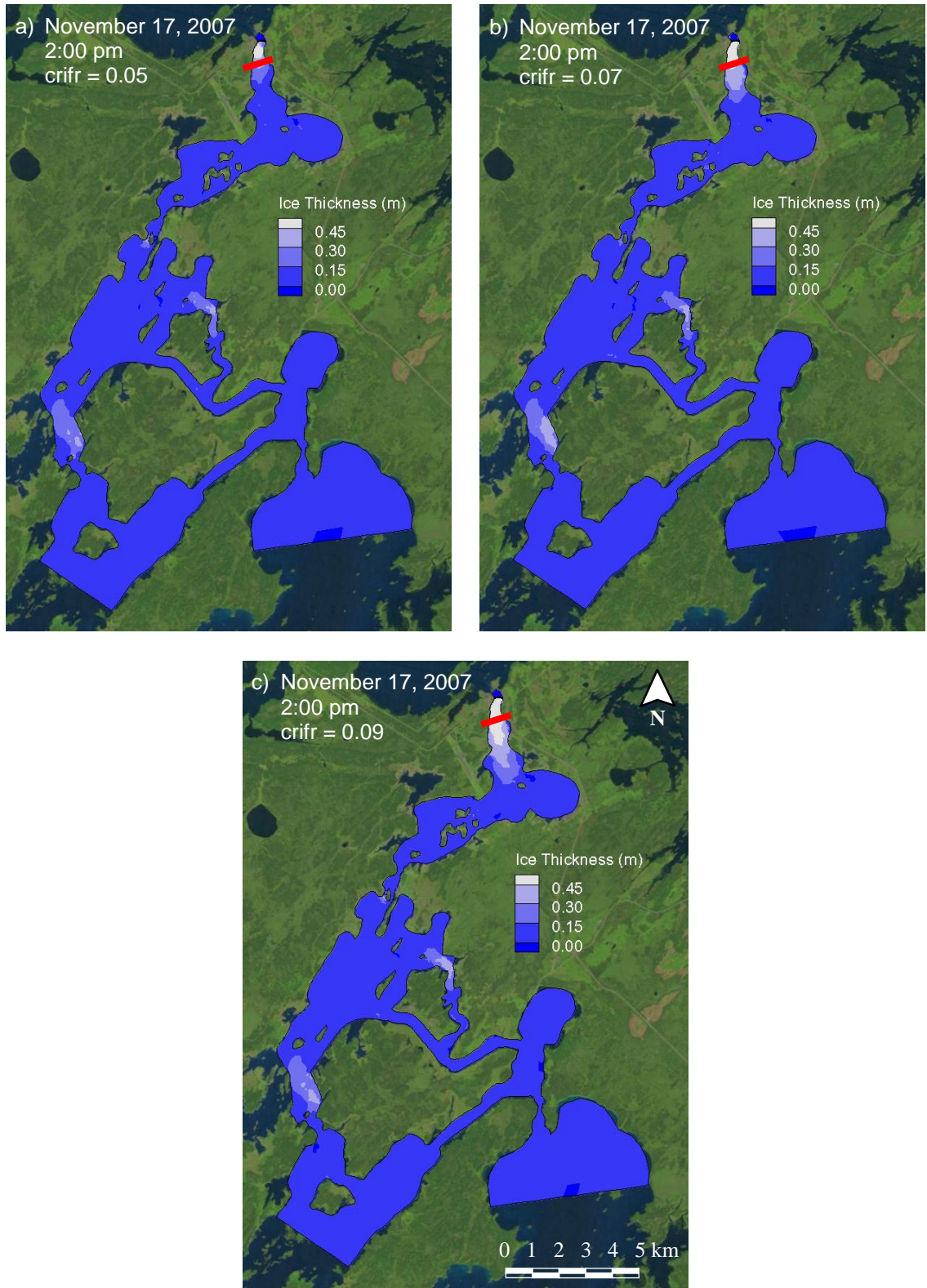


Figure 6.17. Effect of critical Froude number on ice front thickness – start of freeze-up

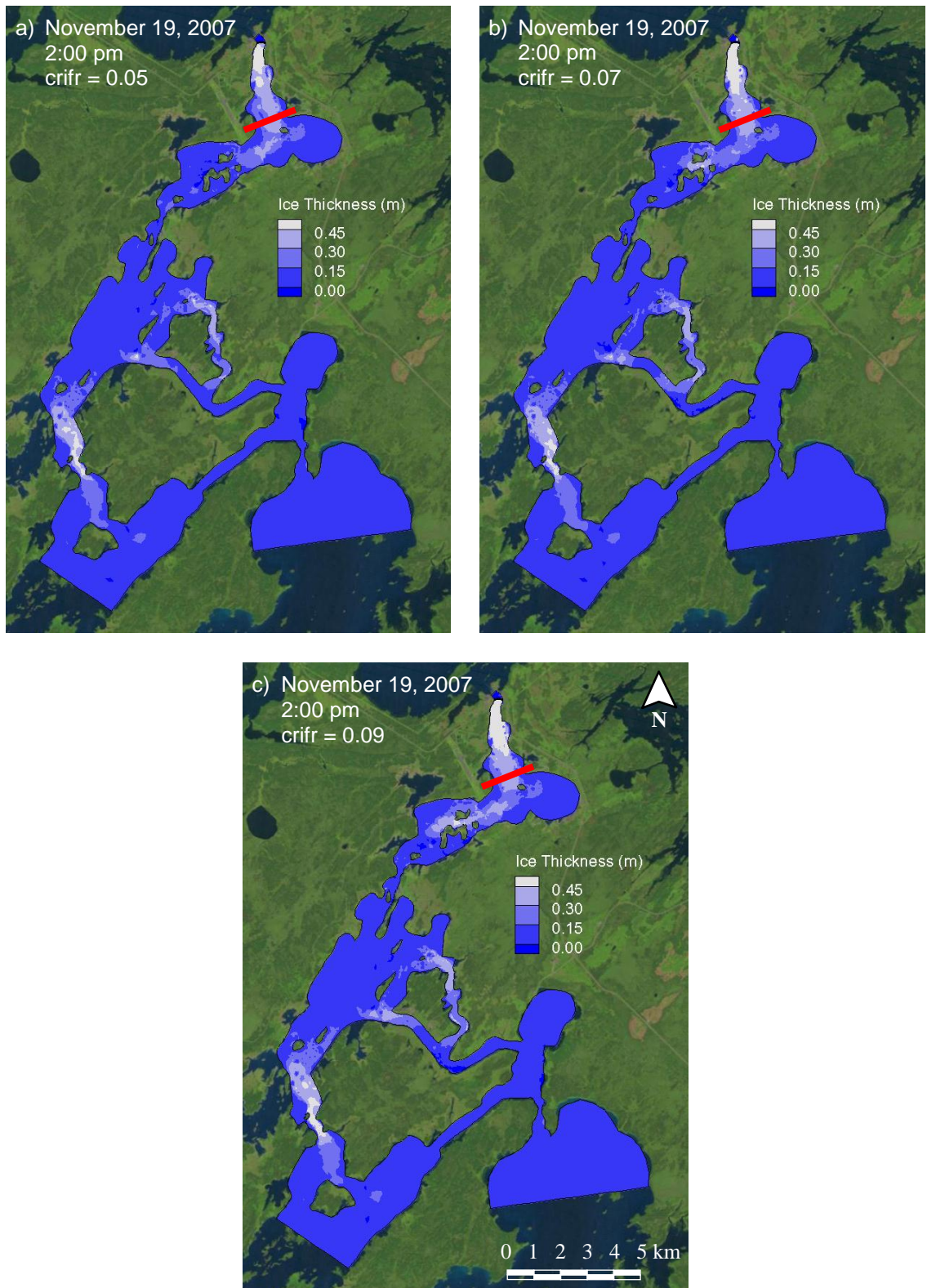


Figure 6.18. Effect of critical Froude number on ice front thickness – middle of freeze-up

The critical Froude number criterion is shown to have a significant impact on the extent and rate of ice front progression. At the minimum value modelled ( $crifr = 0.05$ ), the initial rate of progression is limited by relatively high water velocities within the forebay region. As the critical value is increased, this limitation is relaxed and more ice is able to contribute at the leading edge. The significance of this modelling process is evident in the Froude number distribution presented in Figure 6.19.

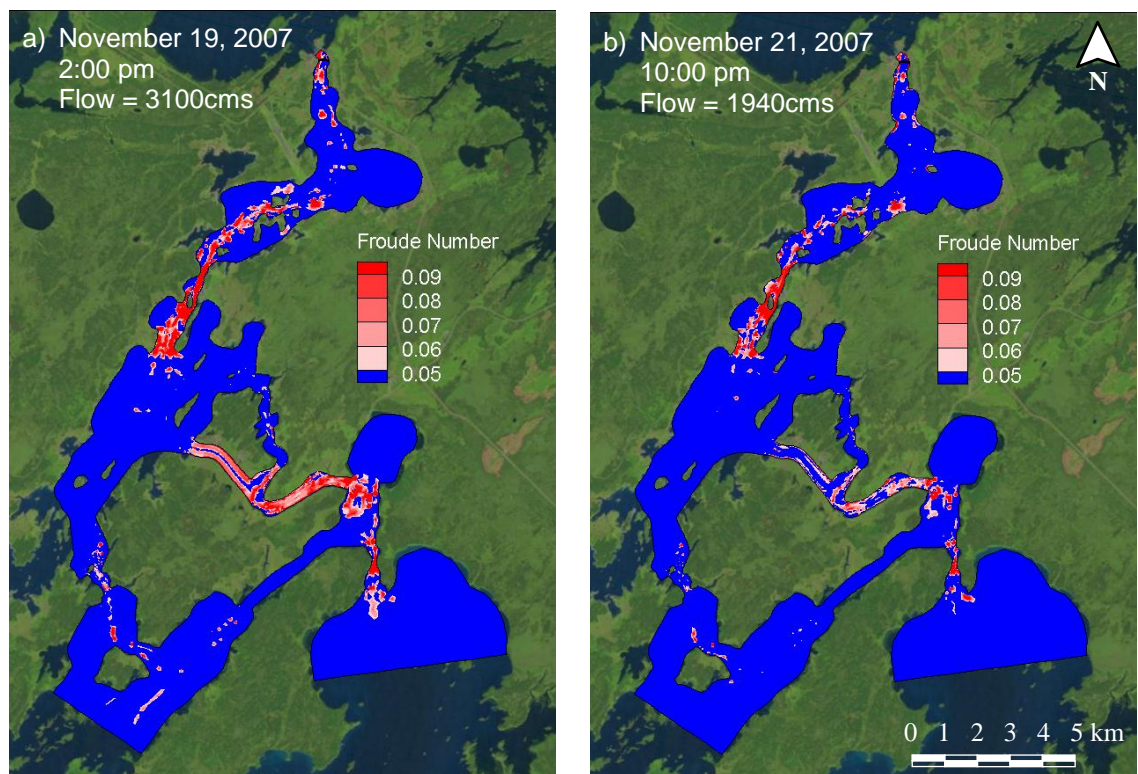


Figure 6.19. Froude number distribution pre-cutback (left) and post-cutback (right)

As evident in Figure 6.19, the highest Froude numbers ( $>0.09$ ) are evident near the area of Manitou Rapids. Velocity in this region stays sufficiently high both

pre- and post-cutback inhibiting juxtaposition of surface ice. This is consistent with the observed ice regime through Manitou Rapids. Downstream of Manitou Rapids and within the forebay region, juxtaposition is dependent largely on the flow rate. During upper decile flows (3100 cms), many areas are simulated to exhibit sufficiently high velocities to limit or inhibit surface ice transport. As flows decrease post-cutback, these limitations are relaxed and an ice front is allowed to develop and progress. This is particularly true for the Ominawin Channels.

The most consistent findings between observed and simulated freeze-up conditions correspond to a critical Froude number of 0.05, for which a modelled ice thickness threshold of 0.30 m correlates to observed conditions with good accuracy. As described in Section 6.4.3, the typical frazil ice regime is limited spatially to the formation of frazil slush or poorly defined frazil pans, for which the critical Froude number required for submergence is also expected to be within the lower portion of the accepted range. As such, a value of 0.05 is recommended for use in this region and deemed appropriate given first hand observations made during the Jenpeg Ice Stabilization Program.

## 6.6 Comprehensive Ice Validation

The ice module parameterization conducted for this study was validated using the observed conditions during six independent time horizons, namely the 2003, 2005, 2006, 2008, 2009, and 2010 freeze-up periods. Skim ice, frazil ice, and

mixed freeze-up regimes are all captured in this dataset to varying degree. Depending on the commencement date of the Ice Stabilization Program, the freeze-up process may have been documented minimally, partially, or fully. A full description of each simulation, including the information available for validation and the model accuracy is provided in the following subsections. Recall that the location of the ice front is approximated by an ice thickness of 0.10 meters for a skim ice regime, and 0.30 to 0.45 meters for frazil ice regimes.

### *6.6.1 2003*

The 2003 freeze-up period was characterized by extremely low flows (lower decile), ranging from under 600 cms to slightly over 1000 cms, as shown in Figure 6.20. Due to this low flow condition prior to freeze-up and the subsequent rapid progression of both primary and secondary fronts, the majority of the ice run was undocumented. A large majority of the surface ice formation was complete prior to the commencement of the Ice Stabilization Program on November 4, 2003. Photographic evidence shows that the freeze-up regime consisted of thermal border and skim ice formation. The only sections that remained ice free were the region of Manitou Rapids and isolated local open leads within the skim ice front. These conditions were shown to persist throughout the freeze-up period, with the only deviation being limited to thermal decay and re-freeze of less competent regions in the skim ice front in response to daily variations in air temperature.

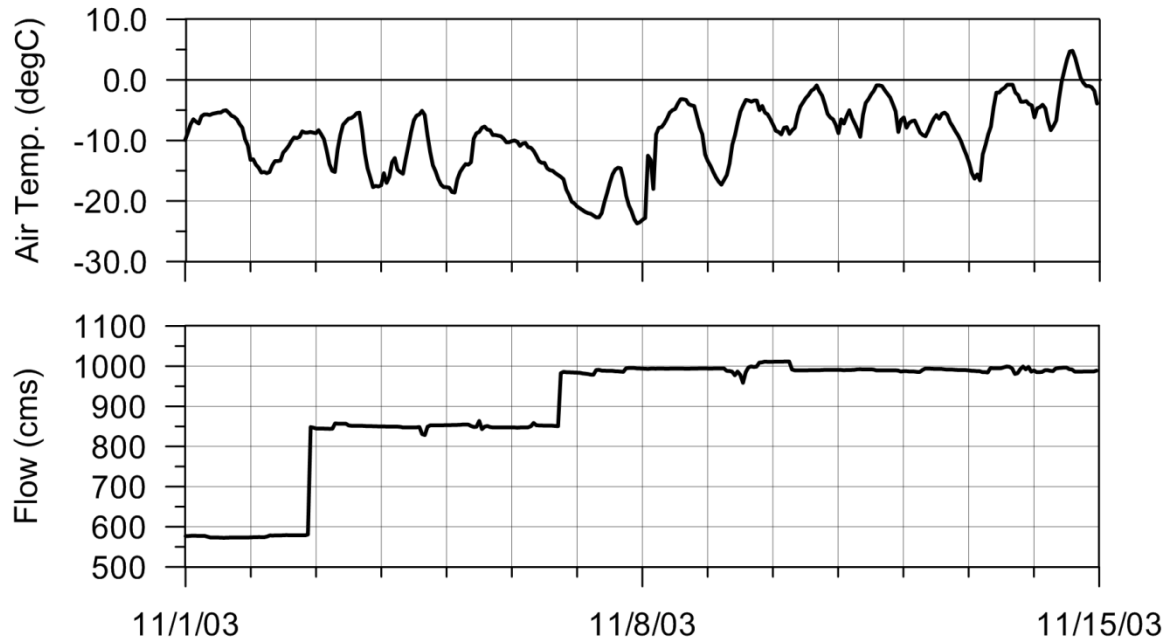


Figure 6.20. Measured freeze-up flow and air temperature, 2003

The freeze-up simulation for the 2003 period spans the time period from November 1, 2003 to November 15, 2003. This period begins with the day on which the incoming water temperature was 2°C and extends for 2 weeks. Border ice is predicted to occur almost immediately (hour 4), with the full extent in place by the end of the first day. Given the extreme low flows, the model predicts a wholly border ice regime with minimal skim ice formation. By November 4, the static ice is well established with ice thicknesses reaching 0.05 m in the main channel and as high at 0.08 m in bays. The model output at this time is shown in Figure 6.21, with comparative observed conditions shown in Figure 6.22 and Figure 6.23. The remainder of the simulation consists primarily of thermal ice thickening, with Manitou Rapids remaining free of an ice cover indefinitely.

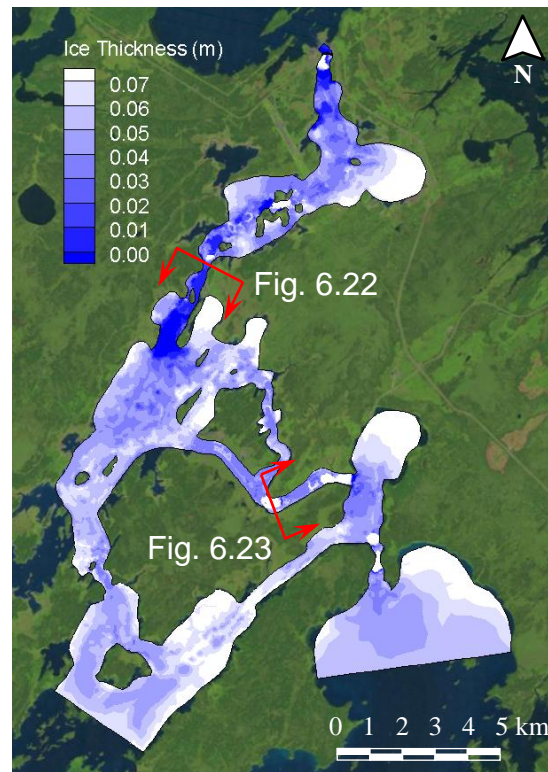


Figure 6.21. Simulated ice thickness, November 4, 2003

For the 2003 freeze-up period, the model correctly predicts the ice regime observed, as well as the rapid proliferation of surface ice. The extent of both the primary and secondary front is accurately captured in the model results. Given the relative lack of photographic evidence prior to formation and the wholly static nature of the ice cover, this freeze-up period does not provide much value in regards to model validation. What can be extracted, however, is that the model does perform as expected during periods of extremely low flow (<1000 cms).



Figure 6.22. Skim ice bridging at Manitou Rapids looking upstream, November 4, 2003



Figure 6.23. Ice cover on the Upper Ominawin Channel looking upstream, November 4, 2003

**6.6.2 2005**

The 2005 freeze-up period was very dynamic, consisting of a mixed skim and frazil ice regime that was driven by dynamic changes to both air temperature and flow rate. When the Ice Stabilization Program commenced on November 16, 2005, the majority of the border ice had formed and the primary front extended through intermittent skim ice bridging to roughly halfway between Saskatchewan and Manitou Rapids. A secondary skim ice front was observed in the Ominawin Bypass Channel, completely bridging the south channel and extending partway into the north channel. The warming trend spanning November 17, 2005 through November 21, 2005 limited further ice propagation and caused the primary front to recede slightly towards Saskatchewan Rapids. The remainder of the ice cover formed between November 22, 2005 and November 24, 2005 first by frazil, and then skim ice following the flow cutback on November 23, 2005. The measured flow and air temperature conditions that drove this freeze-up regime are shown in Figure 6.24.

The freeze-up simulation for the 2005 period spans from November 14, 2005 to November 27, 2005. Initial border ice formation is predicted to occur starting November 14, 2005, with a large majority of the extent in place by November 15<sup>th</sup>, including a secondary bridging downstream of the Ominawin Bypass Channel. Skim ice is predicted to start on November 16<sup>th</sup>, initiating both a primary and secondary front. By 2 pm, the primary front is predicted to extend to halfway between Saskatchewan and Manitou Rapids, and the secondary front to the start

of the Upper Ominawin Channel. The model results at this time are presented in Figure 6.25, with a comparison to observed conditions shown on Figure 6.26 and Figure 6.27.

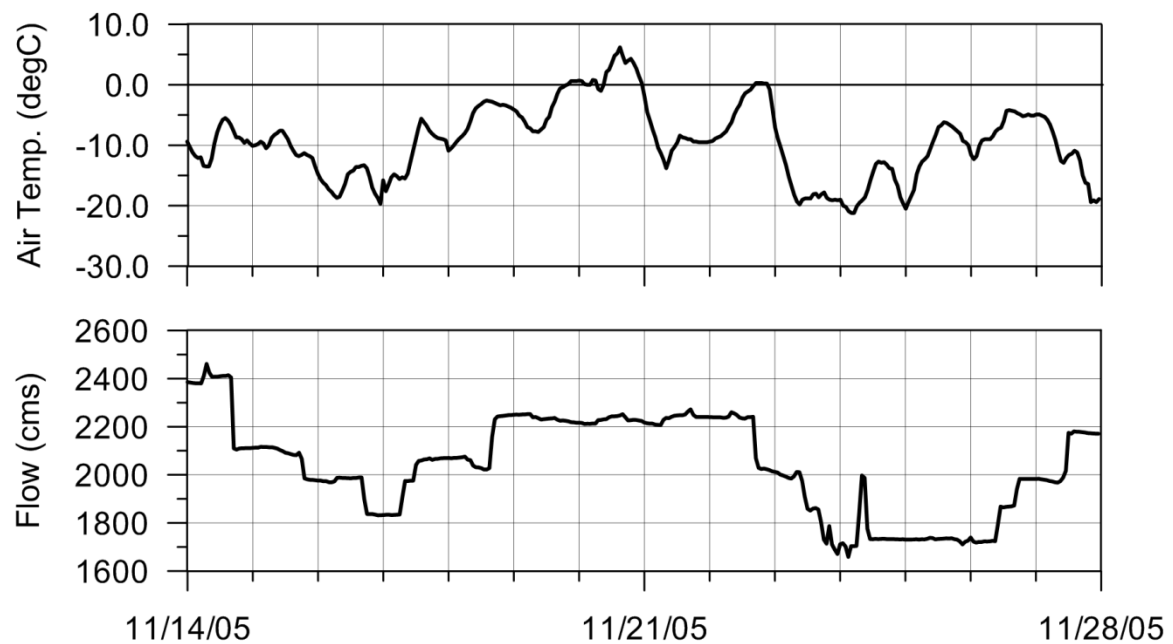


Figure 6.24. Measured freeze-up flow and air temperature, 2005

The model's prediction of the ice regime during the initial stages of frontal progression is accurate for both the primary and secondary front. In addition, the model correctly predicts skim ice as the primary mode of ice formation. Where the simulation fails is in the prediction of continued ice front advance beyond November 16<sup>th</sup>. Ice is predicted to form and accumulate until November 18, 2005 driven by consistently low air temperatures ( $<-10^{\circ}\text{C}$ ). The observed advance, however, ceases on November 16 and does not resume until cooler temperatures return on November 23<sup>rd</sup>.

This suggests that a second phenomenon other than air temperature is driving the ice front progression beyond the initial formation mechanism. These findings are consistent with those of the skim ice calibration where it is speculated that limitations in the model's ability to simulate vertical turbulence intensity, frazil rise velocity, or re-entrainment processes is incorrect. This allows skim ice to continue forming in high velocity zones and contribute to the ice front. In reality, much of this ice remains entrained in the flow and does not contribute to the leading edge of the ice front. Instead the ice cover thickens through deposition of ice particles on its underside.

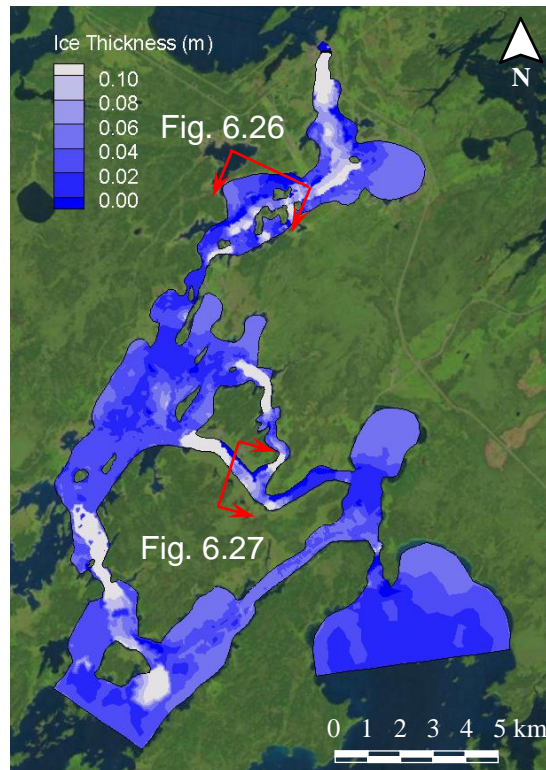


Figure 6.25. Simulated ice thickness, November 16, 2005



Figure 6.26. Location of primary skim ice front looking upstream, November 16, 2005



Figure 6.27. Location of secondary skim ice front looking upstream, November 16, 2005

A second limitation of the model in regards to the skim ice module is in its limited ability to predict local bridging of large skim ice floes in areas of constricted channel width. One such event occurred on November 17<sup>th</sup>, 2005 where a large skim ice floe bridged at the outlet of the Upper Ominawin Channel. This event is shown in Figure 49. The presence of a local bridge generally restricts further downstream travel of surface ice floes, and introduces errors in the model results. These events are generally isolated to Kiskittogisu Lake downstream of Whiskey Jack Narrows, and within the Upper Ominawin Channel.



Figure 6.28. Local skim ice bridging on the Upper Ominawin Channel, November 17, 2005

The remainder of the simulation extending from November 18, 2005 to November 27, 2005 is in agreement with observed conditions. Ice production ceases in response to the increasing temperature trends. Melt is predicted within

the border ice, however the model does not show any retreat in the primary front. As colder temperatures return on November 23<sup>rd</sup>, the model responds with predominantly skim ice generation in the remaining open water sections. This shifts to a predominantly frazil regime on November 26, 2005, following the flow increase to roughly 2000 cms on that date.

### 6.6.3 2006

The 2006 freeze-up was difficult to assess due to the very late start of the Ice Stabilization Program. By the start date of November 7, 2006, roughly 75% of both the primary and 50% of the secondary ice fronts were in place. Both formed through intermittent juxtaposition of skim ice floes. Local bridging was also observed on the upstream portion of the Upper Ominawin Channel, as shown in Figure 6.29. A second local bridge occurred within Kiskittogisu Lake downstream of Whiskey Jack Narrows. These bridges limited the potential for large skim ice flows and significantly inhibited frontal progression in downstream reaches.

The freeze-up regime was further complicated by the initial cooling trend in air temperatures between November 1, 2006 and November 4, 2006, and the subsequent warming period that lasted until November 6, 2006. A full summary of these trends is provided in Figure 6.30. Experience from a similar freeze-up regime that occurred in 2005 suggests that there exists potential for ice cover development and retreat during this period.



Figure 6.29. Local skim ice bridging on the Upper Ominawin Channel, November 7, 2006

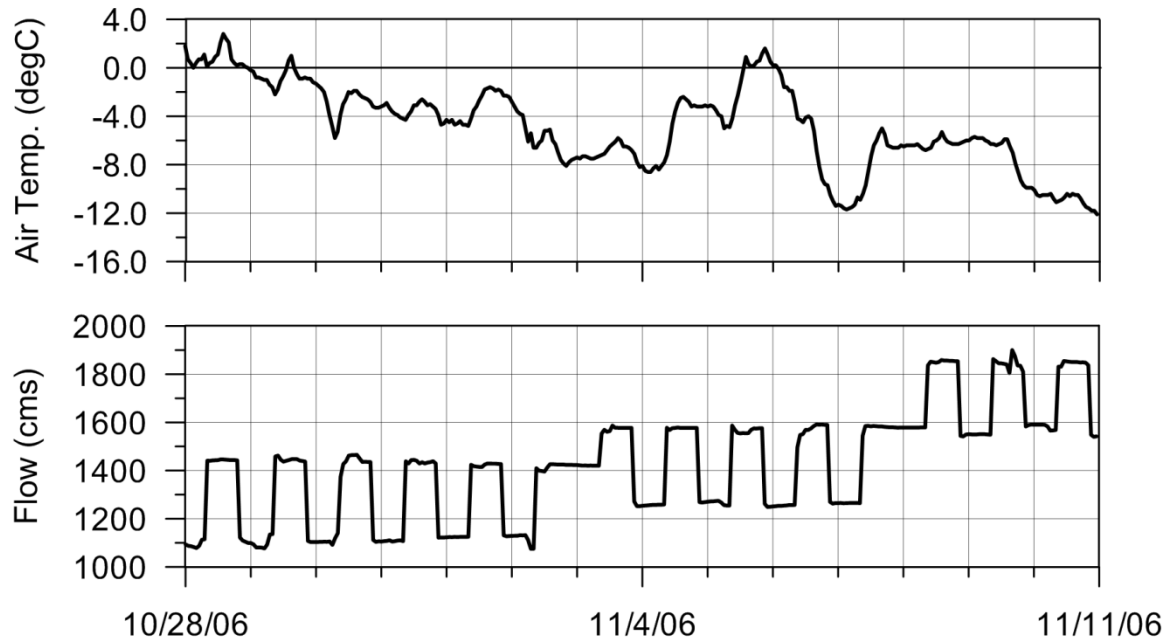


Figure 6.30. Measured freeze-up flow and air temperature, 2006

Following the initial assessment on November 7, 2006, the remainder of the ice regime was limited to isolated frazil ice events and slow thermal advance of border ice. Both processes occurred very slowly; the ice cover was not fully established by the end of the Ice Stabilization Program on November 15, 2006.

The freeze-up simulation for the 2006 period spans from October 28, 2006 to November 10, 2006. Border ice formation is predicted to start on October 30, 2006, but does not get permanently established until November 1, 2006. This is likely due to the generally high air temperatures experienced during the first few days of the simulation. Skim ice formation is predicted to begin on November 2, 2006, with both the primary and secondary ice fronts being initiated at the same time. Both fronts are predicted to advance upstream, forming a complete cover by November 5, 2006. Some melt to the border ice is expected on November 6<sup>th</sup>, however the channel refreezes the next day and the ice cover remains in place for the remainder of the simulation. The model prediction for November 7, 2006 is provided in Figure 6.31, with an observed comparison in Figure 6.32.

The comparison for November 7, 2006 shows that the model results over predict the advance of the primary front. The reasons for this are likely identical to those discussed in the 2005 validation and are shown to be limited to the final stages of freeze-up. The degree of over-prediction is difficult to assess without observations of the ice regime during the initial freeze-up process. A second reason may stem from the presence of a border ice bridge, as shown on Figure

6.31. This bridge forms early on in the simulation during the overnight flow cycling where the flow rates are reduced to roughly 1100 cms. It essentially acts as a second ice boom, initiating the primary front upstream of its typical location.

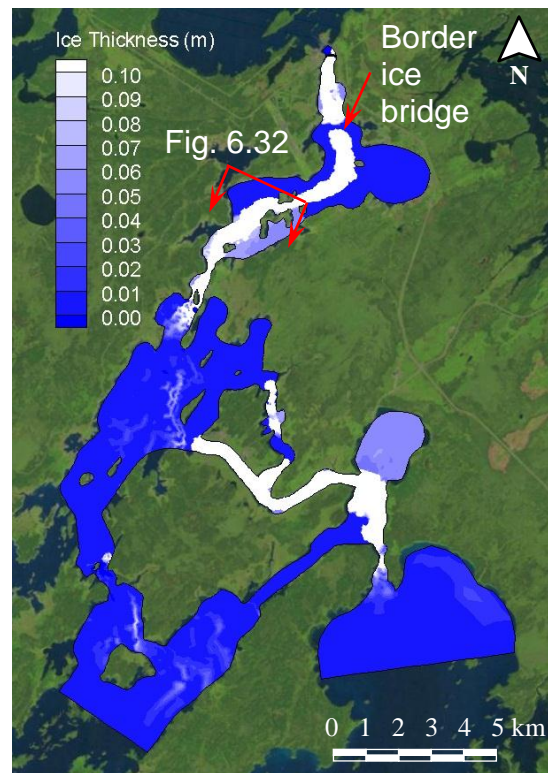


Figure 6.31. Simulated ice thickness, November 7, 2006

Referring to Figure 6.29, the model also cannot predict the local bridging that occurs on the Upper Ominawin Channel, thereby causing the secondary ice front to be over predicted as well. In reality, the effect of this local bridge is two-fold: 1) it limits the potential for large skim ice sheets to form by shortening the development time, and 2) it prevents the skim ice floe from proceeding downstream and contributing to the ice front.



Figure 6.32. Location of primary skim ice front looking upstream, November 7, 2006

The seemingly random phenomena of local bridging is not fully captured by the model, and as such its effect on the ice front cannot be predicted. This leads to an over prediction in the amount of surface ice contributing to the ice front, and may lead to an over-prediction of ice front advance during static ice regimes.

#### 6.6.4 2008

The 2008 freeze-up year provided the opportunity to validate the model against a mixed ice regime beginning with predominantly frazil ice generation and ending with predominantly skim ice generation. The Ice Stabilization Program commenced on November 14, 2008, and once again did not capture the initial cooling trend, shown in Figure 6.33 to extend back beyond November 6<sup>th</sup>. On November 14<sup>th</sup>, the initial observations showed a heavy frazil ice regime forming a primary front that extended upstream to the region of Saskatchewan Rapids.

The secondary front was in its initial stages at this point, extending to the outlet of the Ominawin Bypass Channel through juxtaposition of frazil pans.

By November 15, 2008, a series of flow cutbacks reducing the flow to 1750 cms had initiated heavy skim ice formation in the upstream channels and advanced the primary ice front halfway towards Manitou Rapids. Likewise, the secondary ice front had fully covered the Ominawin Bypass Channel. Warmer temperatures and an increase in flow maintain these conditions until November 17<sup>th</sup>, at which time the majority of the remaining primary and secondary frontal progression was complete by a mixture of skim and surface ice floes.

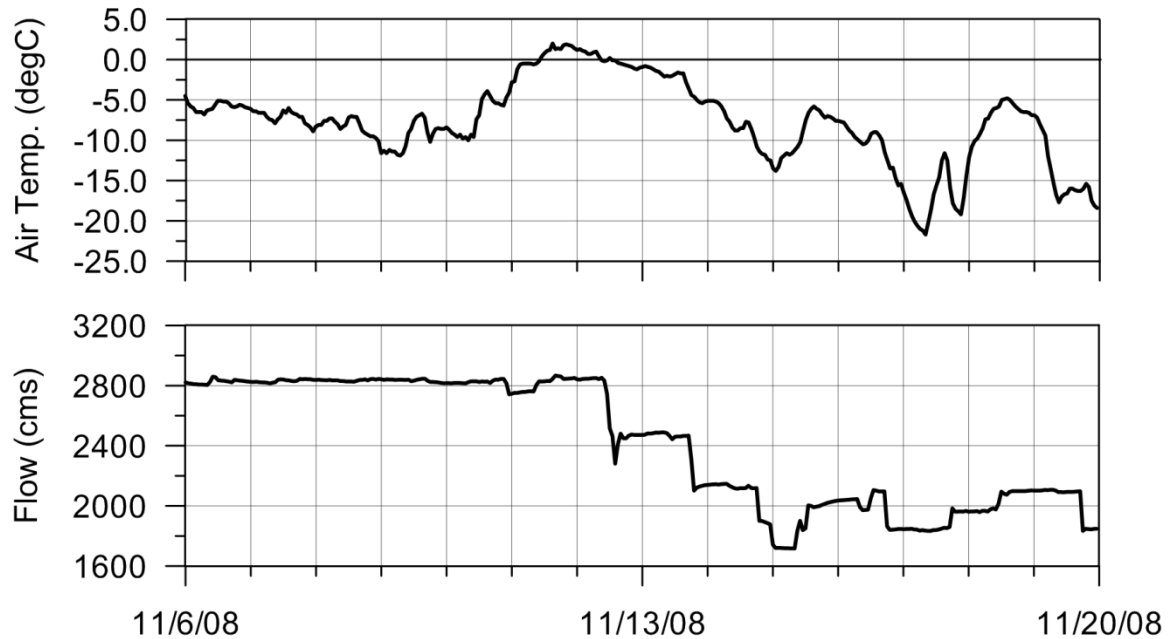


Figure 6.33. Measured freeze-up flow and air temperature, 2008

The freeze-up simulation for the 2008 period spans from November 6, 2008 to November 20, 2008. The majority of border ice is predicted to be in place by November 8<sup>th</sup>; however, the high flows inhibit the formation of a secondary bridge downstream of the Ominawin Bypass Channel. By November 9, 2008, frazil ice generation is predicted throughout the Lower West Channel, largely in response to the incoming water temperature having reached the nucleation point. A primary ice front is initiated and builds up over the next three days to cover the Lower West Channel to just downstream of Manitou Rapids. Similarly, a secondary frazil ice front has developed and extends partway into the Upper Ominawin Channel. The model results following these processes are presented in Figure 6.34. Comparative observations are not available for this period in time.



Figure 6.34. Simulated ice thickness, November 11, 2008

Between November 11, 2008 and November 13, 2008, positive air temperatures are predicted by the model to cause decay of the ice cover; however this is limited to the relatively thin border ice cover only. Very minimal change to either the primary or secondary front is predicted. As cooler temperatures return on November 14<sup>th</sup>, frazil ice is predicted to resume and advance both primary and secondary fronts towards a full cover. A comparison is made between the modeled and observed ice front conditions at this time, with Figure 6.35 showing the simulated ice front thickness, and Figure 6.36 and Figure 6.37 showing the location of the primary and secondary fronts.

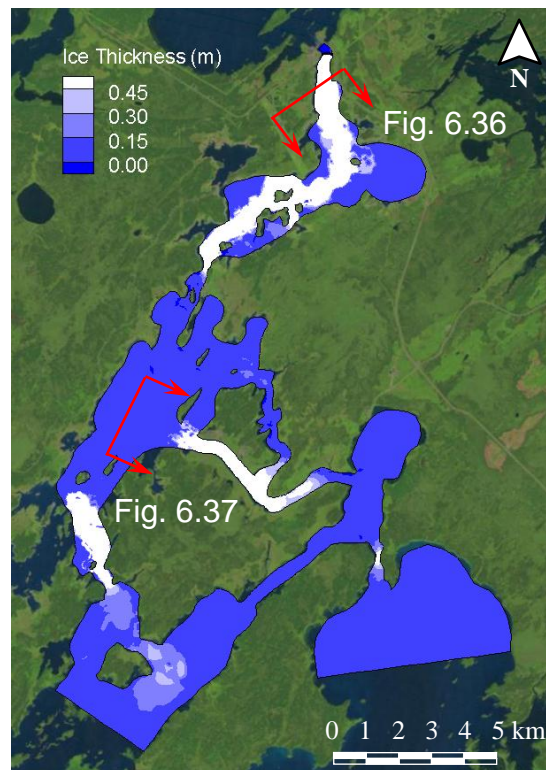


Figure 6.35. Simulated ice thickness, November 14, 2008



Figure 6.36. Location of the primary ice front looking upstream, November 14, 2008



Figure 6.37. Location of the secondary ice front looking upstream, November 14, 2008

It is clear to see that the location of both fronts is overestimated on November 14, 2008. This is likely attributed to the negligible decay predicted during the relatively warm period between November 11, 2008 and November 13, 2008. While it is difficult to assess the extent of the ice cover prior to November 11 or the degree of decay that took place, it is reasonable to assume that some ice cover did exist. This assumption is made on the basis that almost identical conditions experienced prior to November 11 had also occurred between November 14 and November 16. Water temperature during both periods was near the nucleation point, and air temperatures stayed within a range of -5°C and -10°C. Given that moderate frazil and skim ice was observed during the latter period, it can be assumed that similar conditions would have been present during the earlier period.

Subsequent to this initial comparison, the model correctly predicts the shift from frazil to skim ice production following the flow cutback on November 15, 2008. A small frazil generation zone is predicted through Manitou Rapids, and this too is observed to occur during the latter stages of the 2008 freeze-up. Generally speaking, the model does a good job of capturing the freeze-up process for this year; however the location of the ice front seems to predate the observed condition by two to three days. This may or may not be attributed to the warming period of similar duration, as discussed previously.

6.6.5 2009

The 2009 freeze-up period followed a typical skim ice regime, however a unique condition existed that complicated the initial bridging and formation of the primary ice front. The ice boom that typically provides the initial bridging was removed prior to the freeze-up. As a result, any minor ice events that occurred prior to the permanent bridge being established were passed downstream and did not contribute to the primary ice cover.

The Ice Stabilization Program commenced on November 26, 2009 prior to any significant surface ice processes taking place. Evidence of skim ice floes was observed at the powerhouse; however a primary front had not been established. By November 27<sup>th</sup>, the border ice extent was almost complete, including a secondary bridge downstream of the Ominawin Bypass Channel. In response to cooler overnight temperatures and high flows, as shown in Figure 6.38, frazil ice floes were observed in both the Lower West Channel and the Ominawin Bypass Channel. The short development time caused the volume of ice to be minimal, however.

The bulk of ice development commenced on December 1<sup>st</sup> with heavy skim ice floes upstream of both primary and secondary fronts. It is difficult to ascertain whether a primary bridge had formed upstream of the station. The Lower West Channel was experiencing very heavy skim ice floes, however. Skim ice was also observed upstream of the secondary front originating in Kiskittogisu Lake and

travelling downstream through the Upper Ominawin Channel. The secondary front progressed partway through the Ominawin Bypass North Channel. The skim ice regime continues through December 2<sup>nd</sup>, at which time a permanent primary front had formed, extending roughly halfway between Saskatchewan Rapids and Manitou Rapids. The secondary front had advanced to the upstream portion of the Upper Ominawin Channel.

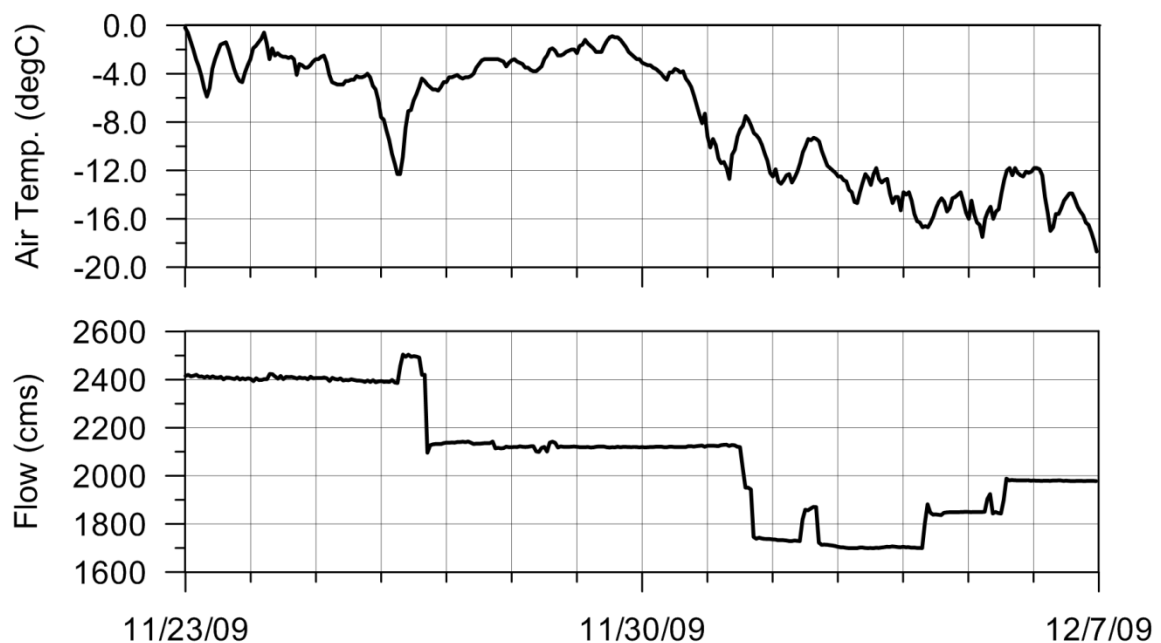


Figure 6.38. Measured freeze-up flow and air temperature, 2009

The formation shifted to a predominantly frazil ice regime starting on December 3, 2009, with the primary front advancing close to the region of Manitou Rapids through frazil accretion at the leading edge. At this point, any further upstream progression was slowed by the short open water reach upstream of the front that

limited the volume of frazil ice generated. By December 5<sup>th</sup>, the ice regime was considered complete with the primary front having advanced to Manitou Rapids.

The freeze-up simulation for the 2009 period spans from November 23, 2009 to December 6, 2009. The formation of border ice is predicted to start on November 24<sup>th</sup> and be complete by November 26<sup>th</sup>. This includes the formation of a secondary thermal bridge downstream of the Ominawin Bypass Channel. Skim ice is predicted to start on the 26<sup>th</sup> but the overall volume is insufficient to initiate either the primary or secondary fronts. Both fronts are initiated on the next day and are predicted to advance minimally.

Over the course of the next three days spanning November 28, 2009 and November 30, 2009, very little surface ice is observed. The model, however, predicts continued skim and frazil production resulting in significant advance of both primary and secondary fronts. The simulated conditions at the end of this time period are shown in Figure 6.39, showing a clear overestimation of surface ice generation due to the premature onset to the ice regime. This error is attributed to the method used in calculating the heat deficit in the model. Using only the air temperature to calculate heat loss is simplistic and neglects the individual components that produce the global deficit. Of particular interest in this case is the long-wave radiation that is re-emitted by the atmosphere. Throughout this three-day period, a low and heavy cloud cover existed that surely acted as an insulating layer to inhibit any significant ice generation.

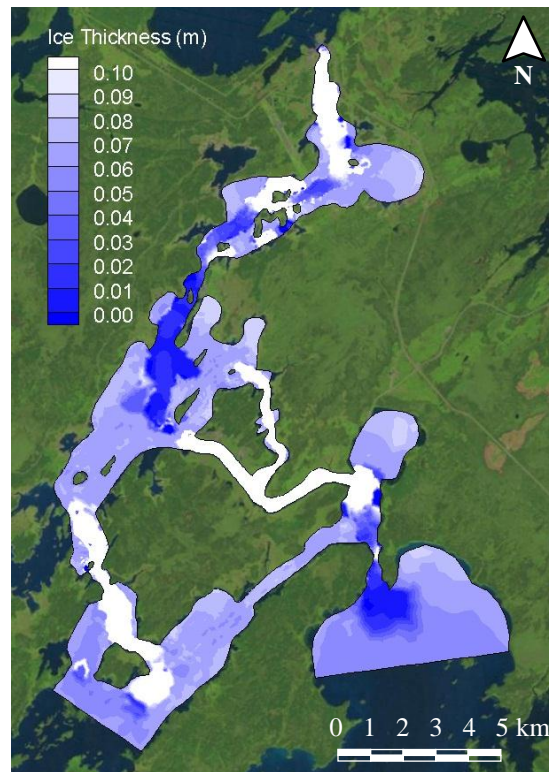


Figure 6.39. Simulated ice thickness, November 30, 2009

For the remainder of the simulation, the model does a good job in predicting the type of ice regime that is present. Skim ice is predicted to remain through December 2<sup>nd</sup> going forward, with isolated frazil generation in Manitou Rapids. This matches observed conditions in that heavy skim ice is predicted to advance the primary front to the region of Manitou Rapids. After this point, turbulence and a short development time inhibit further skim ice generation and the remainder of the ice front develops through frazil ice accretion.

**6.6.6 2010**

The 2010 freeze-up regime was characterized by heavy frazil generation and a very rapid frontal progression for both primary and secondary fronts. When the Ice Stabilization Program commenced on November 18, 2010, a very heavy frazil ice regime was underway with secondary thermal bridging downstream of the Ominawin Bypass Channel having not yet occurred. Frazil ice generated in the Upper Ominawin Channel was observed to form pans as it passed through the Ominawin Bypass Channel and entered the Upper West Channel. Downstream, clear evidence of re-entrainment was visible with a majority of these pans disappearing as they travel through Manitou Rapids. Downstream of Manitou Rapids, a heavy frazil ice regime was evident forming an initial primary front extending just upstream of the ice boom.

By November 19, 2010, an initial flow cutback had resulted in a secondary front forming through thermal bridging downstream of the Ominawin Bypass Channel. This cutback is evident in Figure 6.40. A frazil ice regime was still underway, with the primary front covering roughly 60% of the Lower West Channel. The frazil pans had advanced the secondary front to completely cover the Ominawin Bypass South Channel and had started to spill into the North Channel. This process persisted through November 20<sup>th</sup>, at which time both primary and secondary fronts had been fully established.

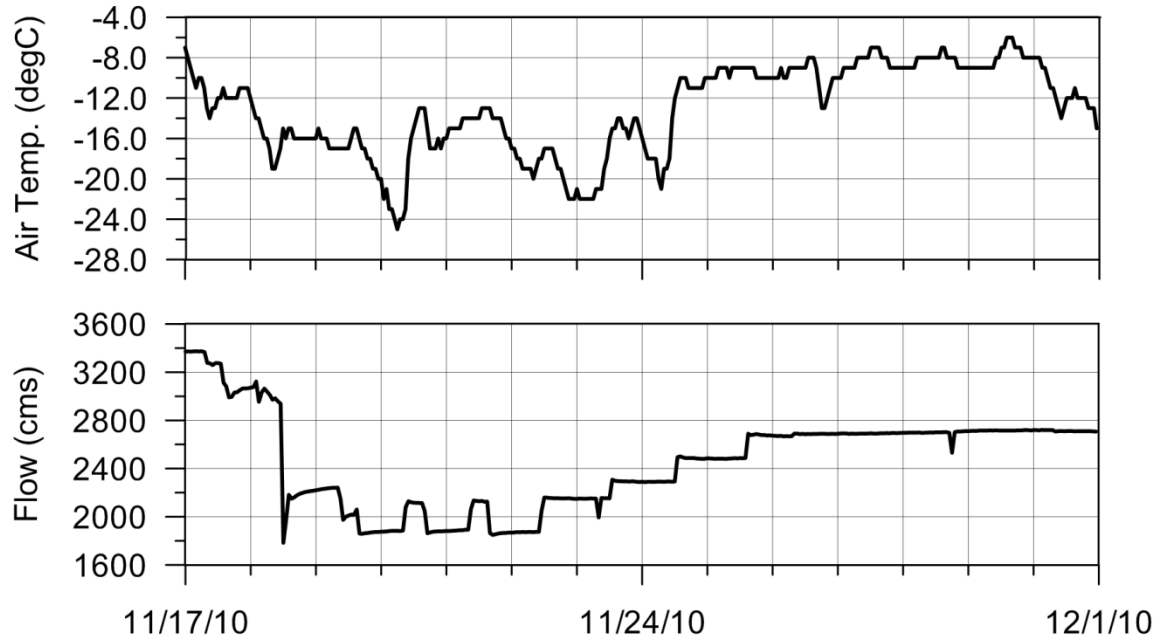


Figure 6.40. Measured freeze-up flow and air temperature, 2010

The freeze-up simulation for the 2010 period spans from November 17, 2010 to December 1, 2010. The full border ice extent is established almost immediately; however no surface ice accumulation is predicted on the first day. By November 18<sup>th</sup>, frazil ice generation is predicted throughout the main channel with the primary front extending just upstream of the boom. In addition, secondary bridging downstream of the Ominawin Bypass Channel has not yet been established. A comparison between the simulated and observed conditions at this time is provided in Figure 6.41 and Figure 6.42.

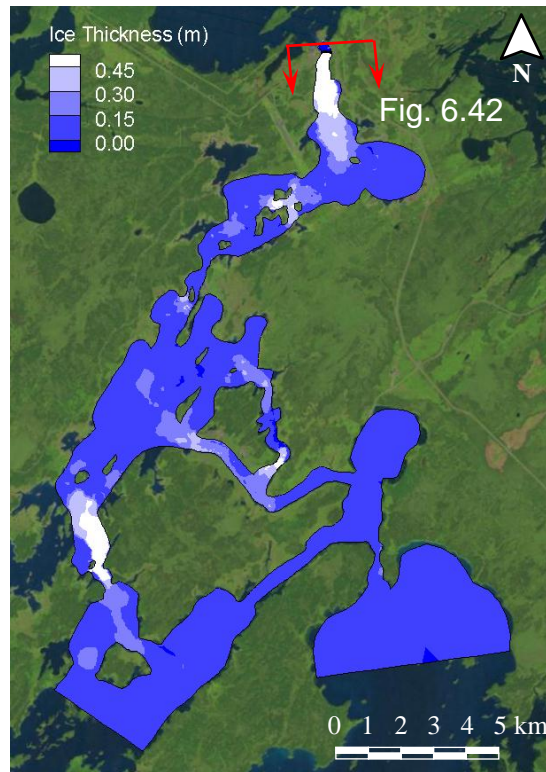


Figure 6.41. Simulated ice thickness, November 18, 2010



Figure 6.42. Location of the primary front looking upstream, November 18, 2010

Overnight, the model correctly predicts the formation of the secondary thermal bridge followed by secondary frontal progression. The nature of the border ice routine in the model causes this bridge to form instantaneously following the flow cutback, unlike the gradual thermal growth that would typically be expected. This produces an overestimation of the secondary front in the model due to its severely premature formation. The primary front location during the final stages of freeze-up is overestimated as well. This is attributed to the simplifying assumptions made in simulating the mass exchange processes, as well as model limitations in defining reach-specific parameters.

## 6.7 Summary

The effort to calibrate and validate the static and dynamic ice modules is successful in identifying both the model's strengths and weaknesses. Six independent freeze-up periods are used to validate the models parameterization in regards to heat exchange, border ice formation, skim ice formation, frazil ice formation, mass exchange processes, and dynamic transport mechanisms. This dataset covers a wide range of meteorological and hydraulic conditions possible in the area and included fully static, dynamic, and mixed ice regimes. The results from this validation showing the final parameterization of both ice modules is provided in Table 6.2.

Table 6.2. Ice module parameterization

Parameter	Description	Value
hwa	Linear heat transfer coefficient between water and air	22.38 W/m <sup>2</sup> °C
tc	Minimum water surface temperature for border ice growth	-0.15°C
vcrskm	Maximum velocity for border ice growth	0.13 m/s
hi0	Initial skim ice thickness	0.005 m
vnu	Nusselt number	4.0
theta	Probability of deposition of frazil particles reaching the surface	1.00
beta1	Rate of re-entrainment of surface frazil particles per unit area	0.00
vbb	Rising velocity of frazil particles	0.005 m/s
hf0	Initial thickness of frazil surface floes	0.15 m
anmaxfra	Maximum concentration for frazil ice floes	0.90 m <sup>3</sup> /m <sup>3</sup>
thi0	Surface ice thickness of each parcel	0.50 m
anmax	Maximum concentration of ice parcels	0.90 m <sup>3</sup> /m <sup>3</sup>
crifr	Critical Froude number for surface ice submergence	0.05

Based on a review of the 2003 to 2010 freeze-up seasons, some predictable patterns are identified with the freeze-up regime. Border ice is observed to start early in the freeze-up and become fully established prior to any surface ice floes being present. Depending on the flow rate, a surface ice run commences as water temperatures reach the nucleation point. The previous rule of thumb used by Manitoba Hydro staff had been that skim ice was predicted to occur if the flow rate was less than 1650 cms, and frazil was predicted if the flow rate was more

than 1650 cms. This assumption is tested by comparing observed ice regimes with their associated flow and air temperature conditions. The results of this analysis are presented in Figure 6.43, which suggests that the 1650 cms estimation is somewhat conservative. A clear divide between frazil and skim ice regimes exists at roughly 2000 cms which may provide a more realistic threshold. Note that this analysis is conducted using the modelled flow (as opposed to rated flow), which applies a 10% increase to account for errors in the reported values.

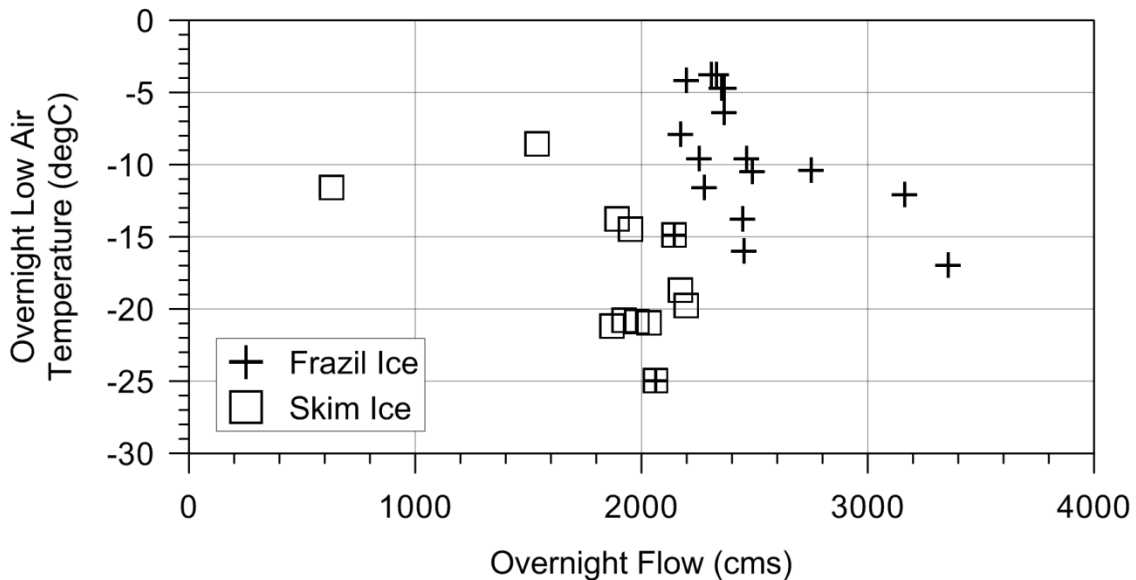


Figure 6.43. Ice regime correlation to overnight flow and air temperature, 2003 to 2010

The results shown on Figure 6.43 are only accurate for the start of freeze-up as the ice regime in this study area is very much specific to local reaches. Frazil ice is present during a skim ice regime; however its contribution to the ice front is negligible. As the skim ice front approaches sections of increased turbulence,

such as Manitou Rapids, skim ice production will cease and the remainder of the ice front forms through frazil accretion.

This somewhat deterministic pattern of events that constitutes a freeze-up regime is relatively easy to foresee. The difficulty comes with trying to predict the timing and volume of ice generated. Using historical conditions, the calibrated model is shown to accurately and consistently predict the onset of both border ice and surface ice formation. Furthermore, the simulation accurately replicates the freeze-up regime associated with a specific flow condition. In a mixed regime consisting of concurrent skim and frazil generation, the generation zones of each are accurately captured. The volume of ice generated is harder to validate, however, the model is shown, in a limited capacity, to be capable of estimating the location of both primary and secondary ice fronts. This is limited to the initial formation period and should not be extended into the latter stages of freeze-up due to several weaknesses in the simulation.

The most significant error in the model simulation involves a clear over prediction of the volume of skim and frazil ice generated during the latter stages of freeze-up. During both regimes, ice that is generated upstream of Manitou Rapids is assumed to pass as surface ice through this zone of high turbulence and thereby allowed to contribute to an advancing ice front. Conversely, the 2010 freeze-up shows a clear example where this surface ice is re-entrained into the flow as it passes through Manitou Rapids. Re-entrainment is defined globally in the model

and this error could not have been corrected without introducing other errors elsewhere in the results. Allowing the user to define reach-specific re-entrainment parameters would allow more control in calibrating this process.

A second model limitation is related to the mass exchange of suspended frazil with surface parcels. A global parameter is defined specifying the rate of rise of suspended frazil, which tends to overestimate the volume of ice that reaches the surface in turbulent sections such as Manitou Rapids and the Upper Ominawin Channels. This overestimation again becomes important during the latter stages of freeze-up as the front approached the frazil generation zone. Particles that should have been in suspension are instead assumed to rise to the surface and contribute to the ice front. A method of defining a local frazil rise velocity would mitigate this problem. A second approach would be to specify a lower deposition probability in turbulent sections; however, this too is globally defined.

A third limitation exists in the model's estimation of heat transfer at the water/air interface. Using a linear heat transfer approach to estimate this flux is a reasonable approximation where more detailed data is not available. However this method is shown to over predict heat loss during periods where the air temperature is only slightly negative (between 0°C and -5°C) and particularly if a cloud cover is present. Positive fluxes such as long wave radiation re-emittance from a cloud cover are not fully captured, and therefore the net heat loss is exaggerated. This causes the model to over predict the volume of ice needed to

balance the heat deficit, and introduces errors in the model such as those discussed in the 2009 validation. The analysis shown in Figure 6.43 suggests that limited ice is to be expected within this temperature range, and what ice did exist was of limited volume.

The model also does not react well to periods where a heat surplus exists, initiating decay in an existing ice cover. Such conditions are common, having occurred to some degree in each of the validation years. The presence of a heat surplus causes errors in the model results whereby the total decay of an ice cover was underestimated.

The last limitation of the model is associated with the presence of a local bridge during a skim-ice regime. These bridges occur typically in Kiskittogisu Lake and the Upper Ominawin Channel and introduce a clear discrepancy in the modelled results. Given that this seemingly random occurrence is very difficult to predict, its presence should be used to augment model results with the understanding that differences are to be expected.

Understanding the model's strengths and limitations is an important part in interpreting the results and gathering the information necessary to make operational decisions. The validation effort conducted for this study identifies opportunities for model application within the Ice Stabilization Program, which add significant value to the forecasting of ice conditions and the optimization of

flow control. In addition, several enhancement opportunities are identified to mitigate or reduce the error associated with either simplifying assumptions or model limitations.

---

# CHAPTER 7:

## Freeze-up Forecasting

---

### 7.1 Introduction

The operational goal of this research is to provide a means of forecasting river ice conditions upstream of the Jenpeg Generation Station operating under a specified flow regime. The work performed to date suggests that good potential exists for applying the model for freeze-up studies. At minimum, it may be used to provide an accurate prediction of the onset of ice formation, as well as the ice regime that is expected to occur. For this study, the 2011 freeze-up period is modelled in real-time in an effort to establish and test the freeze-up forecasting modelling process, and assess the accuracy of the model in this capacity.

### 7.2 Modelling Process

As part of the Jenpeg Ice Stabilization Program, staff from Manitoba Hydro combine experience, first hand observation of ice conditions, and meteorological forecasts to make an informed operating decision in regards to overnight flows during a freeze-up regime. This decision must balance the need to reduce flows

to promote static ice formation with the need to maintain an adequate water supply for downstream generation. A premature flow cutback limits the generation capacity during the freeze-up formation. Secondly, it also poses a drought risk to the generation system downstream. A delayed cutback also carries risk associated with frazil development; unexpectedly low air temperatures may initiate frazil ice generation, which carries with it risks of intake blockages or decreased channel conveyance.

Observations of ice conditions are taken via helicopter twice daily, and are generally limited to the main channel between Jenpeg and Playgreen Lake. This includes Manitou Rapids, the Ominawin Bypass and Upper Ominawin Channel, and Whiskey Jack Narrows. Minimal observations are taken within Kiskittogisu Lake or Metchanais Channel. Flights are scheduled to occur once in the morning, and once in the late afternoon. If conditions deem it favourable to do so, a flow cutback is performed subsequent to the afternoon flight in an attempt to control the overnight ice regime and promote static ice formation. The morning flight typically serves to assess any overnight change.

The schedule of flights typically leaves a six to eight hour window following the morning flight in which to set up, perform, and interpret any forecasting simulations. This includes gathering up-to-date information, setting up the run configuration for different operating scenarios, and processing the model output. The modelling process is designed to work within this time frame by limiting the

duration of each simulation and simplifying the set-up of each run. It is based on a rolling window sequence that breaks down the full freeze-up period into a series of sequential windows. Each window represents a subset of time within the freeze-up period with a discrete beginning and end. The general structure of this is provided in schematic form in Figure 7.1.

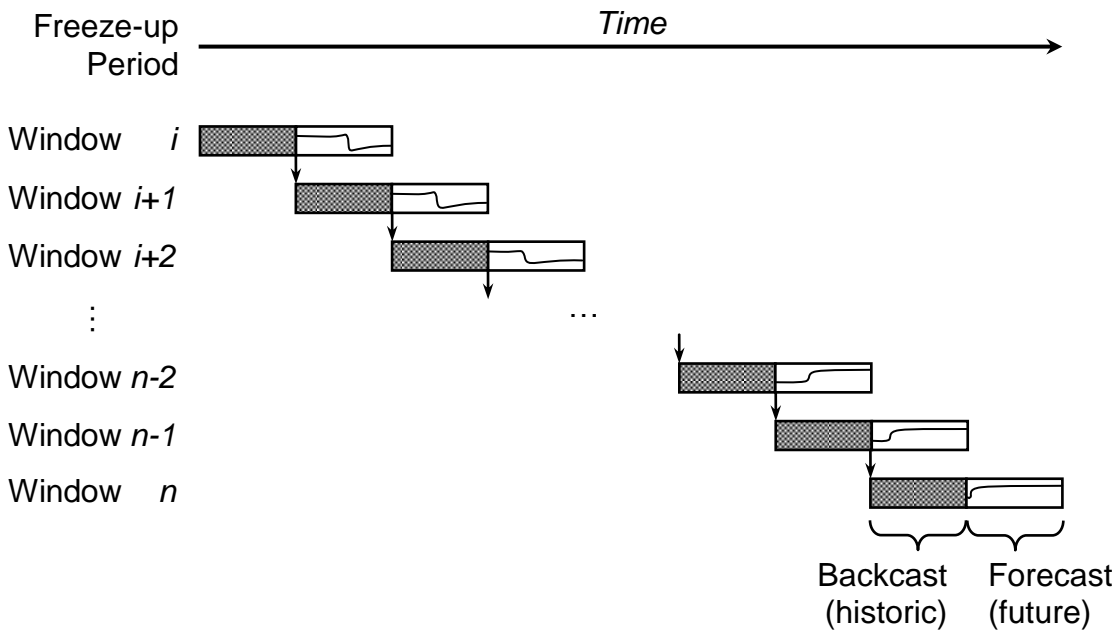


Figure 7.1. Rolling window sequence schematic for forecast simulations

The windows are arranged in chronological order and solved sequentially to form the full solution spanning the entire freeze-up period. Doing so significantly reduces model run times and allows for the simulation to be carried out successively in accordance with the Ice Stabilization Program. A second component of this structure allows for a prediction of the ice regime based on expected future flow and meteorological conditions. Each window can be

extended to include both a backcasting component using measured data, as well as a forecasting component using forecast flow and meteorological conditions. The forecast from one window may then be used to influence the short-term operating strategy.

The modelling process requires each window to be solved successively. Ideally, the first window would commence well before the presence of any ice generation, allowing the entire freeze-up period to be modelled. The window length can be increased or decreased in accordance with data availability or forecast length. A two day window, consisting of one day of measured data and one day of forecast data, was found to work well given the Ice Stabilization Program daily schedule.

### *7.2.1 Initial Conditions*

The rolling window schedule simplifies the process of defining the initial conditions for each simulation. The first window is initialized using a steady-state simulation representative of the first time step. This would generally not include any ice development in the channel, requiring that the first window extend far enough historically to a period of open water. Each successive window is overlapped such that the beginning of the backcasting period in the subsequent window carries forwards the backcasting simulation from the prior. Doing so allows the ending condition of one backcasting simulation to form the initial condition of the following.

If ice is present in the simulation of one window, it may be carried forward to the next as an additional initial condition. This would be dependent on how well the ice simulation matches the observed condition, and whether the carry-forward from one simulation would add value to the subsequent one. One scenario where the ice condition may not be carried over is in the case where the initial onset of ice is predicted to occur prematurely. The subsequent simulation can be started assuming open water conditions and the error associated with the previous run can be eliminated.

### *7.2.2 Boundary Conditions*

The definition of boundary conditions is a significant part of the freeze-up forecast modelling process in that it defines if, when, and to what magnitude the flow cutback is to occur. During the backcasting period, boundary conditions are defined in a manner consistent with prior ice simulations. Forecast conditions may be defined hourly, however, steady-state conditions are assumed in this study. If a flow cutback is planned, it is carried forward at the appropriate time and duration in the simulation as a steady flow. For simplicity, elevation at the downstream boundary is not expected to change. Air temperature, wind speed, and wind direction are estimated throughout the forecasting period using the Weather Network's hourly forecast for Nelson House.

### 7.3 Model Application

Real time modelling of the 2011 freeze-up period began on November 13, 2011, with the Ice Stabilization Program commencing shortly thereafter on November 17, 2011. A limitation with the model was discovered in regards to the forecasting simulations in that a fully dynamic simulation spanning 24 hours could not be completed in the time allotted between flights. Simulation run times increased in proportion to the number of ice parcels present, reaching as high as 45 minutes of real time to simulate 1 hour of model time. As such, all freeze-up forecasting simulations were conducted using free-drift ice mechanics, meaning that only the type, volume, and transport of ice parcels generated could be estimated. Any interaction of ice parcels with one another, the model boundaries, or ice booms was not modelled.

#### *7.3.1 November 13-14, 2011 Simulation*

The first simulation, spanning November 13, 2011 to November 14, 2011, predicts an almost immediate onset of frazil ice generation. Analyzing the data prior to November 13<sup>th</sup> shows some potential for ice generation prior to this date, as shown in Figure 7.2. Beginning on November 6<sup>th</sup>, air temperatures consistently below the freezing point drive the water body to undergo consistent cooling towards the nucleation temperature. By November 11<sup>th</sup>, the incoming water is at the nucleation point with air temperatures staying between 0°C and -5°C. Combined with the high flow rate of roughly 2600 cms suggests that some

degree of frazil ice generation would likely be present. This may account for up to two days of ice generation that is unaccounted for by either the model or the Ice Stabilization Program due to the delayed start for both.

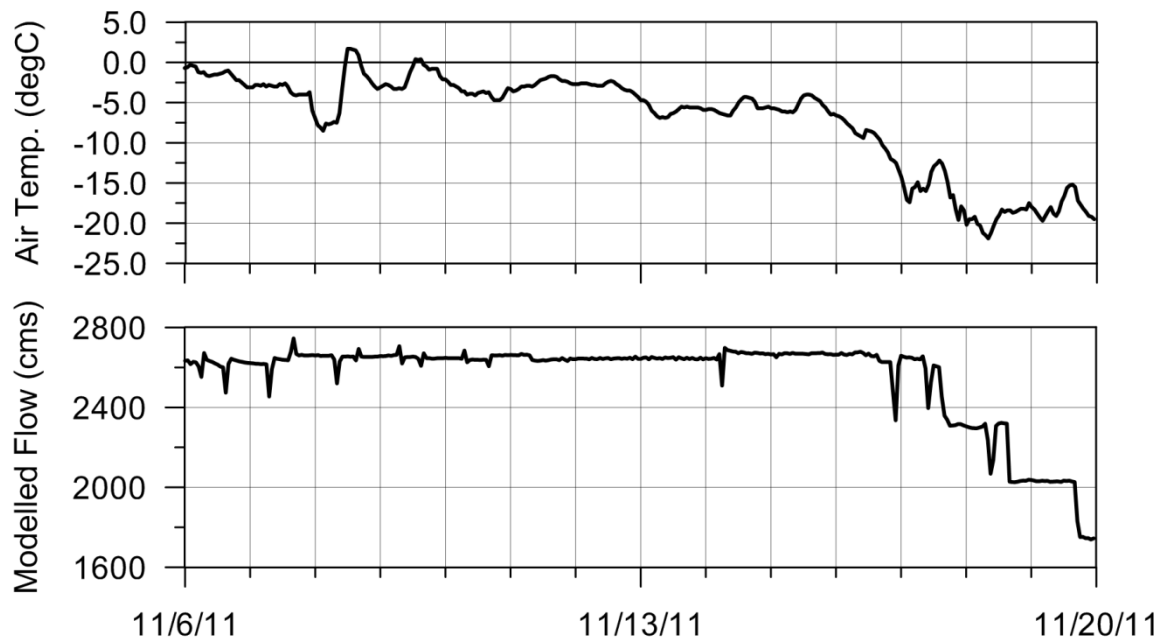


Figure 7.2. Measured freeze-up flow and air temperature, 2011

### 7.3.2 November 17, 2011 Forecast

The first ice forecasting simulation spans a three day period extending from November 14, 2011 to November 17, 2011. Of this, the first two days represent a backcasting simulation, and the last day is meant to provide a forecast of ice conditions expected during the overnight between November 16<sup>th</sup> and 17<sup>th</sup>. A flow cutback was not planned, and flow is assumed to remain steady at 2670 cms. Frazil generation is predicted to continue throughout this simulation,

peaking during the early morning hours of November 17<sup>th</sup>, 2011. The forecast ice regime predicted at this time is shown on Figure 7.3.

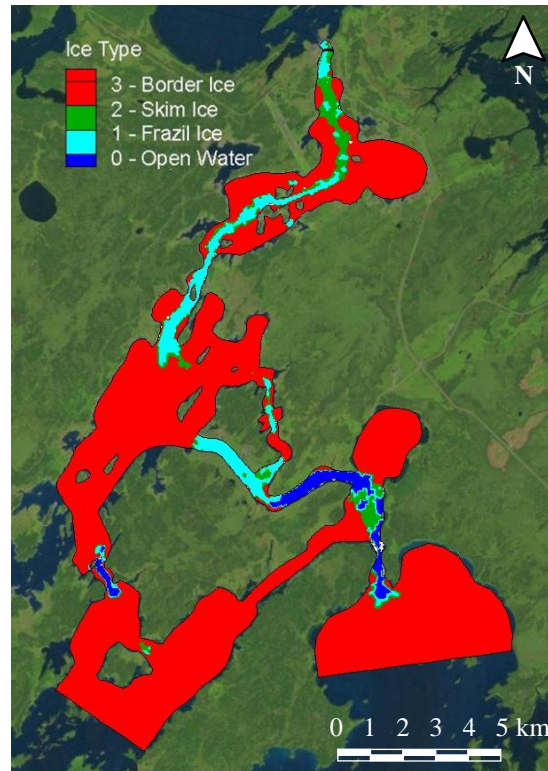


Figure 7.3. Freeze-up Regime, November 17, 2011, 7:00 am

Initial observations made on the morning of November 17, 2011 are in agreement with the model predictions to date. Moderate frazil ice floes were observed in the main channel, with a primary front extending to a point just upstream of Saskatchewan Rapids. A smaller secondary front was also observed within the south portion of the Ominawin Bypass Channel, extending to just downstream of the groin. This evidence shows that the Ice Stabilization Program

commenced late, and supports the model's prediction of an earlier onset of frazil ice generation.

The accuracy in defining the incoming water temperature is shown in this simulation to be an important consideration in ice forecasting. In backcasting simulations, the historic water temperature record was corrected by applying an offset to adjust the stabilized over-winter water temperature to the nucleation point. In forecasting simulations, the stabilized temperature is not known and any correction applied is approximate. Some degree of error is therefore carried forward to each simulation. This error is evident in Figure 7.3, where the secondary frazil ice zone is predicted to be isolated to within the Ominawin Bypass Channel. Frazil ice was observed upstream of this point, suggesting that the incoming water temperature estimate was too high. Future forecasting exercises can mitigate this problem by calibrating water temperature gauges as part of the Ice Stabilization Program.

### *7.3.3 November 18, 2011 Forecast*

The second forecasting simulation carries forward from the previous simulation to predict the freeze-up regime during the overnight period spanning November 17 to 18, 2011. A flow cutback of roughly 300 cms is incorporated as part of this run, reducing the flow rate to 2300 cms at 7:00 pm on November 17. Figure 7.4 shows that the flow forecast incorporating this cutback matches the measured condition quite well.



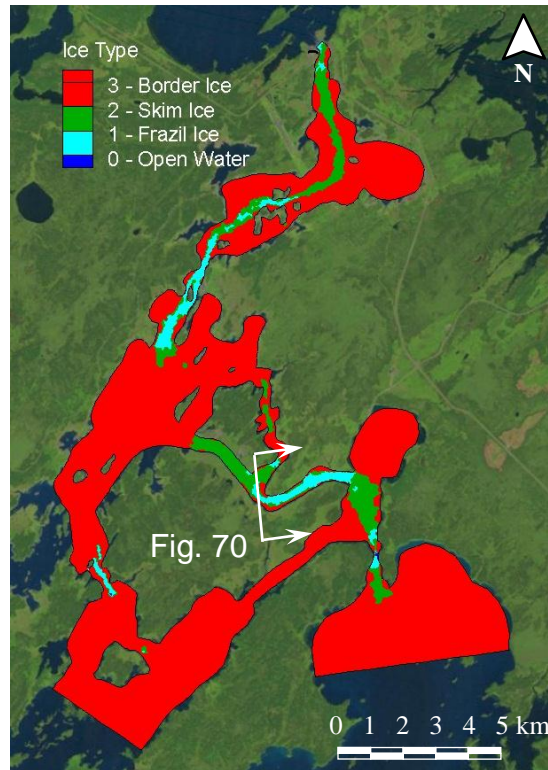


Figure 7.5. Freeze-up Regime post-cutback, November 18, 2011, 7:00 am



Figure 7.6. Skim ice floes upstream of the secondary front, November 18, 2011

Due to data limitations and time constraints, the remainder of the freeze-up season was not forecast in real-time. Through a backcast simulation, the model correctly predicts an increase in static ice generation in response to successive flow cutbacks on November 19 (2000 cms) and November 20 (1750 cms). Further modeling beyond this date is not required as both primary and secondary fronts have completely formed on November 20<sup>th</sup>.

#### 7.4 Summary

The freeze-up forecasting modeling process outlined in this section is applied in a limited capacity for the 2011 freeze-up period and shows good potential for use in future forecasting scenarios. Run-time requirements stemming from the very large scale of the study area and the dynamic ice conditions present limit the model's applicability to simulation of free-drift ice mechanics only. As such, results are limited to the prediction of thermal and dynamic ice generation, mass exchange, and ice transport mechanisms only.

Using a rolling window schedule, the model is shown to be applicable within the requirements of the Ice Stabilization Program. Two real-time forecasting simulations were conducted, providing an accurate and valuable estimate of overnight ice conditions. Several other backcasting simulations augment these findings to confirm the accuracy of modeled results. The model is immediately applicable in forecasting studies towards providing an estimate of the onset of ice

generation, the progression of the static (border) ice cover, and a prediction of the expected system response to a specific scenario.

Enhancement opportunities exist in both model development and the modeling process. Computational efficiency or computing power should be increased to allow for a fully dynamic simulation that is capable of providing an estimate of ice front advance. In addition, the modeling process should be expanded to include real-time monitoring and calibration of input data. An accurate measurement of incoming water temperature is required to properly capture ice generation through the Ominawin Channels. This may be accomplished through a monitoring exercise in which the water temperature reading at gauge 05UB704 on Playgreen Lake is tested and calibrated prior to the commencement of the Ice Stabilization Program.

---

# **CHAPTER 8:**

## Conclusions and Future Work

---

### 8.1 Research Summary

The Jenpeg Generating Station is the most significant component of the Lake Winnipeg Regulation Project and an integral part of the Manitoba Hydro system. It serves the purpose of providing the primary flow control at the upstream reach of the Nelson River and is necessary to ensure an adequate long-term water supply for hydro-electric generation downstream. Lake Winnipeg is used as a long-term storage reservoir and is operated strategically to release flow in preparation for periods of increased demand. This operation also provides secondary benefits in the form of flood and drought mitigation.

Early on in the design process, it was recognized that the Lake Winnipeg outlet channels are susceptible to highly dynamic ice problems. In response, an Ice Stabilization Program was implemented to monitor and optimize the ice formation process within this region. This program combines regular observations of ice conditions with overnight meteorological forecasts towards strategically controlling the flow to promote a static ice regime. The benefits of this program

are two-fold: 1) it reduces the short-term risk of ice blockages at the Jenpeg powerhouse, and 2) it increases the long-term winter conveyance capacity of the outlet channels.

The objective of this research is to enhance the predictive capability of the program through the development of a tool that can be used to provide a quantifiable estimate of frazil, skim, and border ice production on the short term. The model should be applicable within the requirements of the Program and be able to assess the system's response to a wide range of hydraulic conditions within specific modelling constraints. Secondly, this research should work to further validate the use of two-dimensional numerical modelling for use in regional scale river ice studies. In this regard, the dynamic nature of the hydraulic and ice regimes experienced in this study area provide a very comprehensive test of the capability of the CRISSP-2D model.

## 8.2 Conclusions

Calibration of the CRISSP-2D numerical model used in this study is performed by isolating and testing each of its individual components, namely the hydrodynamic module, the thermal ice module, and the ice dynamics module. Each is subsequently validated across a range of dynamic flow conditions and ice regimes. The results of this analysis produces very encouraging results and helped identify the model's strengths and weaknesses.

The hydrodynamic module is shown to provide a very accurate simulation of the hydraulic conditions. Comparing the simulation results at each of the gauge locations in the study area shows a very good estimate of water elevation across all flow conditions. The modelled water surface elevation is within  $\pm 0.2$  meters at all gauges with a confidence of 98.5%. The largest error is equivalent to  $\pm 0.5$  meters at the furthest upstream gauge, with proportionally decreasing errors as you progress downstream.

Flow distribution between connecting channels is less accurate, particularly between the Ominawin Bypass Channel and the Lower Ominawin Channel. Flow through the bypass is underestimated by roughly 28%, having instead been routed through the lower reach of the Ominawin Channel. This in turn works to exaggerate the relatively low flow through this channel by 230%. The error is attributed to dated and sparse bathymetric information available for this region. A significant effort was required to produce a best estimate of the underlying bathymetry, but it is clear that further work is needed.

Proceeding to the thermal ice simulation, the model is capable of producing very good results in relation to the timing and extent of the border ice cover. The model uses a heavily empirical approach to simulate the dynamics of border ice growth, which could be expanded to include approximations for the rate of thermal growth and frazil accretion. Likewise, the spatial distinction between skim

and frazil ice generation is accurately reproduced in the model across a wide range of flow and meteorological conditions.

The model does suffer from limitations to the mass exchange parameters governing the vertical transport of ice between the surface and subsurface layers. Skim ice production tends to be overestimated, particularly during the latter parts of the freeze-up period. This is attributed to a lack of re-entrainment of surface skim ice parcels as they passed through regions of high turbulence. Re-entrainment is defined globally in the model, thereby eliminating any way of capturing any locally isolated influence on this process. Frazil ice generation is also overestimated, which is similarly attributed to a limitation where frazil rise velocity or deposition parameters could not be reduced in regions of high turbulence.

The calibrated model is validated using six independent freeze-up periods and is capable of predicting both the onset and type of ice regime observed. In addition, the location of the ice front correlates well to modelled ice thicknesses of 0.10 meters for skim ice and 0.30 to 0.45 meters for frazil ice fronts. This is limited to the early stages of freeze-up only, and should not be applied beyond the initial front formation for those reasons previously identified.

The model performs poorly during warm ( $> 0^{\circ}\text{C}$ ) or semi-warm conditions (between  $0^{\circ}\text{C}$  and  $-5^{\circ}\text{C}$ ). Decay of the ice front is generally under predicted

during times of positive air temperature. Similarly, ice generation is generally exaggerated when air temperatures were only slightly below the freezing point. Both of these errors are associated with the estimation of the heat flux at the water surface.

With regards to freeze-up forecasting, the modelling process is hindered by computational requirements whereby the fully dynamic simulation could not be completed in the time allotted by the Ice Stabilization Program. In its current capacity, however, the model is fully capable of predicting two of the most important aspects of freeze-up: timing the onset of first ice and defining the ice regime that is to be expected. It is capable of immediate implementation within the Ice Stabilization Program, and may be used to augment operator experience or analyze any uncertainty in operating decisions. Future enhancement efforts are recommended and will serve to increase the modelling capability and improve on the overall accuracy and credibility of model output.

The findings of this study serve, in part, to validate the use of two-dimensional numerical modelling in simulating river ice freeze-up regimes. The dynamic nature of the hydraulics in this study area covers a wide range of hydrologic features that could not reasonably be captured by a one-dimensional model. These include islands, lakes and bays, and flow splits or merges. A two-dimensional representation allows for direct consideration of each feature and explicitly includes its influence on the overall ice regime.

Furthermore, it is necessary for the purposes of this study to have a means of capturing the mixed ice regime specific to unique reaches within the domain. The presence of secondary bridges, preferential paths, and other local phenomena has a large influence on the overall ice regime at any given time. A two-dimensional model is proven successful in capturing most of these events and producing accurate results. The presence of local bridging during thermal regimes is not fully captured; however, this is a limitation inherent to any river ice model given the random nature of this event.

### 8.3 Future Work and Recommendations

The work performed throughout this study identifies numerous opportunities for enhancements to both the specific implementation of CRISSP-2D in relation to the Ice Stabilization Program, and the overall modelling capability. The enhancements specific to this implementation are summarized as follows:

- 1) There is a need for more detailed bathymetric data, particularly in the region of the Lower Ominawin Channel, Kiskittogisu Bay, and the Metchanais Channel.
- 2) The bathymetric data should be updated across the entire study domain to better capture the current morphology, specifically that of Manitou and Saskatchewan Rapids.
- 3) The finite element mesh should be refined to accept this increased level of detail.

- 4) The flow estimation through the Jenpeg powerhouse and spillway requires analysis to confirm the 10% underestimation of flows.
- 5) Flow measurements across the entire operational range are necessary to directly estimate the upstream flow distribution between Playgreen and Kiskittogisu Lake.
- 6) Satellite imagery during the freeze-up period should be tested as a calibration or comparative reference on which to assess model output.

The enhancements specific to the CRISSP-2D model are summarized as follows:

- 1) Improve the border ice simulation routine to include frazil accretion, and shift the estimation of border ice growth towards a physically-based relationship.
- 2) Provide a means of defining reach specific parameters controlling re-entrainment of surface parcels, deposition of suspended parcels at the surface, and frazil rise velocity.
- 3) Calculate frazil rise velocity based on particle and flow characteristics.
- 4) Improve the thermodynamic heat transfer estimation to better model freeze-thaw mechanics.

The model is capable of immediate implementation within the Ice Stabilization Program. It is designed to augment operator experience, first hand observations, and forecasting in defining the operational strategy during freeze-up. The initial implementation effort should commence will in advance of the Ice Stabilization Program to ensure that staff is properly trained in setting up, executing, and

interpreting runs. Subsequent implementations should follow a structured approach based on the following recommendations.

The Program should be implemented well in advance of ice formation (2 weeks minimum). The model may be applied on a daily or weekly basis to simulate water cooling and predict the first occurrence of ice. This will ensure that the dispatch of staff on-site is neither premature nor late. Upon arrival, staff should establish necessary data feeds and take first-hand measurements to ensure accuracy in the forcing data.

The model should be applied on a daily basis to predict overnight ice formation when the water temperature nears the freezing point ( $\sim 2$  to  $3^{\circ}\text{C}$ ). This process should follow the rolling window sequence where the model is set-up and run each morning, and results are analysed in the afternoon. Together with first hand observations, experience, and forecasts, a decision can be made with regards to the overnight operating strategy. Commencing prior to or at the start of ice formation, the model should be applied in a full predictive manner to assess the impact of different operating strategies on the ice regime. Several alternative strategies can be assessed concurrently to determine, for example, the benefit (or lack thereof) of a flow cutback. The results of this analysis may form one part of the nightly operating decision.

Following the conclusion of the primary ice program, the model may be applied to monitor ice thickening or the overall regime. Potential also exists to perform specific studies in relation to freeze-up or, given further model development, break-up.

---

## REFERENCES

---

Anderson, E. (1954). Energy-budget studies. In United States Geological Survey, *Water-loss investigations: Lake Hefner studies* (pp. 71-119). Washington: United States Department of the Interior.

Andrishak, R., & Hicks, F. (2008). Simulating the effects of climate change on the ice regime of the Peace River. *Canadian Journal of Civil Engineering* , 35, 461-472.

Ashton, G. D. (1986). *River Lake Ice Engineering*. Littleton: Water Resources Publications, LLC.

Blackburn, J., & Steffler, P. (2002). *River2D: two-dimensional depth averaged model of river hydrodynamics and fish habitat*. Edmonton: University of Alberta.

Bolsenga, S. (1977). Preliminary observations on the daily variation of ice albedo. *Journal of Glaciology* , 18 (80), 517-521.

Bolsenga, S. (1969). Total albedo of Great Lakes ice. *Water Resources Research* , 5 (5), 1132-1133.

---

## REFERENCES

---

Bowen, I. (1926). The ratio of heat losses by conduction and by evaporation from any water surface. *Physical Review* , 27, 779-787.

Brady, D. K., Graves, W. L., & Geyer, J. C. (1969). *Surface heat exchange at power plant cooling lakes*. New York: Electrical Institute Publications.

Brunt, D. (1932). Notes on radiation in the atmosphere. *Quarterly Journal of the Royal Meteorological Society of London* , 58 (247), 389-420.

Burt, W. V. (1954). Albedo over wind-roughened water. *Journal of Meteorology* , 11, 283-290.

Carroll, J., & Fitch, B. (1981). Effects of solar elevation and cloudiness on snow albedo at the South Pole . *Journal of Geophysical Research* , 86, 5271-5276.

Carson, R. (1972). *Summary of completed and outstanding work*. Winnipeg: Manitoba Hydro.

Carson, R., & Groeneveld, J. (1997). Evolution of the ICESIM model. *The 9th Workshop on River Ice* (pp. 289-302). Fredericton: CRIPE - Committee on River Ice Processes and the Environment.

Chow, V. (1959). *Open-channel hydraulics*. New York: McGraw-Hill Book Co.

Clark, S. P. (2006). *An experimental study of the formation and evolution of frazil ice*. Winnipeg: University of Manitoba.

Cogley, J. (1979). The albedo of water as a function of latitude. *Americal Meteorological Society* , 775-781.

---

## REFERENCES

---

Coley, R. W. (1971). *Progress report - Lake Winnipeg Regulation - Nelson River backwater studies*. Winnipeg: Manitoba Hydro.

Cooper, P. (1969). The absorption of solar radiation in solar stills. *Solar Energy* , 12 (3), 33-346.

Curi, F., Carson, R., & Gee, R. (2011). Numerical simulation and field test of river ice conditions in the Yukon River. *16th Workshop on the Hydraulics of Ice Covered Rivers* (pp. 56-67). Winnipeg: Committee on River Ice Processes and the Environment.

Daly, S. F., & Ettema, R. (2006). Frazil ice blockage of water intakes in the Great Lakes. *Journal of Hydraulic Engineering* , 132 (8), 814-824.

Denis, L. G., & Challies, J. B. (1916). *Water-Powers of Manitoba, Saskatchewan, and Alberta*. Toronto, Ontario, Canada: Warwick Bro's & Rutter.

Denis, L. G., & White, A. V. (1911). *Water-Powers of Canada*. Ottawa, Ontario, Canada: The Mortimer Co. Ltd.

Dingman, S., Weeks, W., & Yen, Y. (1968). Effects of thermal pollution on river ice conditions. *Water Resources Research* , 4 (4), 349-362.

Duffie, J. A., & Beckman, W. A. (1980). *Solar Engineering or Thermal Processes*. New York: Wiley.

Frohlich, C., & Brusa, R. W. (1981). Solar radiation and its variation in time. *Solar Physics* , 74, 209-215.

---

## REFERENCES

---

Gardner, A. S., & Sharp, M. J. (2010). A review of snow and ice albedo and the development of a new physically based broadband albedo parameterization . *Journal of Geophysical Research* , 115, F01009.

Geiger, R., Aron, R. H., & Todhunter, P. (2003). *The climate near the ground*. Lanham: Rowman & Littlefield Publishers, Inc.

Giddings, J., & LaChapelle, E. (1961). Diffusion theory applied to radiant energy distribution and albedo of snow. *Journal of Geophysical Research* , 66, 181-189.

Gilfilian, R., Kline, W., Osterkamp, T., & Benson, C. (1972). Ice formation in a small Alaskan stream. *International Symposium on the Role of Snow and Ice in Hydrology* (pp. 505-513). Banff: International Association of Hydrological Sciences.

Glover, J., & McCulloch, J. S. (1958). The empirical relationship between solar radiation and hours of sunshine. *Quarterly Journal of the Royal Meteorological Society of London* , 84 (360), 172-175.

Hanley, T., & Michel, B. (1977). Laboratory formation of border ice and frazil slush. *Canadian Journal of Civil Engineering* , 4 (2), 153-160.

Henneman, H. E., & Stefan, H. G. (1999). Albedo models for snow ice on a freshwater lake. *Cold Regions Science and Technology* , 29, 31-48.

Heron, R., & Woo, M.-k. (1994). Decay of a High Arctic lake-ice cover: observations and modelling. *Journal of Glaciology* , 40 (135), 283-292.

---

## REFERENCES

---

Holder, G., & Saade, R. G. (1991). Design of heat balance, ice generation, and cover modules. *6th Workshop on the Hydraulics of Ice Covered Rivers* (pp. 35-52). Ottawa: Committee on River Ice Processes and the Environment.

Iqbal, M. (1983). *An Introduction to Solar Radiation*. Don Mills: Academic Press Canada.

Judge, D., Lavender, S., Carson, R., & Ismail, S. (1997). Headpond ice jams - where will they occur? *The 9th Workshop on River Ice* (pp. 73-87). Fredericton: CRIPE - Committee on River Ice Processes and the Environment.

Klein, W. H. (1948). Calculation of solar radiation and the solar heat load on man. *Journal of Meteorology* , 5 (4), 121-130.

Lindenschmidt, K.-E., van der Sanden, J., Demski, A. D., & Geldsetzer, T. (2011). Characterising river ice along the Lower Red River using RADARSAT-2 imagery . *16th Workshop on River Ice* (pp. 198-213). Winnipeg: Committee on River Ice Processes and the Environment.

Liu, L., & Shen, H. (2005). *CRISSP2D version 1.0 programmer's manual*. Potsdam: Clarkson University.

Lunde, P. J. (1980). *Solar Thermal Engineering*. New York: Wiley.

Malenchak, J. (2012). *Numerical modeling of river ice processes on the Lower Nelson River*. Winnipeg: University of Manitoba.

---

## REFERENCES

---

Malenchak, J., Doering, J., & Shen, H. T. (2011). Modeling of Anchor Ice and Aufeis Formation at Sundance Rapids. *16th Workshop on River Ice* (pp. 161-178). Winnipeg: CGU HS Committee on River Ice Processes and the Environment.

Manitoba Hydro. (n.d.). *Churchill River Diversion*. Retrieved 10 24, 2011, from Manitoba Hydro Electric Energy and natural Gas: [http://www.hydro.mb.ca/corporate/water\\_regimes/churchill\\_river\\_diversion.shtml](http://www.hydro.mb.ca/corporate/water_regimes/churchill_river_diversion.shtml)

Manitoba Hydro. (2010). *Report on Jenpeg Generating Station Spillway Rating Curve Review and Revision*. Winnipeg: Manitoba Hydro.

Martinson, K., Sydor, M., Marcotte, N., & Beltaos, S. (1993). RIVICE model update. *Proceedings of the Workshop on Environmental Aspects of River Ice* (pp. 127-144). Saskatoon: National Hydrology Research Institute.

Matousek, V. (1992). Frazil and skim ice formation on rivers. *Ice Symposium* (pp. 1-22). Banff: International Association for Hydro-Environment Engineering and Research.

Matousek, V. (1984b). Regularity of the freezing-up of the water surface and heat exchange between water body and water surface. *Ice Symposium* (pp. 187-201). Hamburg: International Association of Hydro-Environment Engineering and Research.

---

## REFERENCES

---

Matousek, V. (1984a). Types of ice run and conditions for their formation. *Ice Symposium* (pp. 315-327). Hamburg: The International Association for Hydro-Environment Engineering and Research.

Meinander, O., Kontu, A., Lakkala, K., Heikkila, A., Ylianttila, L., & Toikka, M. (2008). Diurnal variations in the UV albedo of arctic snow. *Atmospheric Chemistry and Physics* , 8, 6551-6563.

Michel, B. (1967). From the nucleation of ice crystals in clouds to the formation of frazil ice in rivers. *International Conference on Low Temperature Science* (pp. 119-136). Sapporo: Hokkaido University.

Michel, B., Mascotte, N., Fonseca, F., & Rivard, G. (1982). Formation of border ice in the Ste. Anne River. *2nd Workshop on the Hydraulics of Ice Covered Rivers* (pp. 38-61). Edmonton: Committee on River Ice Processes and the Environment.

Miles, T. M. (1993). *A study of border ice growth on the Burntwood River*. Winnipeg: University of Manitoba.

Morse, B., & Richard, M. (2009). A field study of suspended frazil ice particles. *Cold Regions Science and Technology* , 55, 86-102.

Newbury, R. (1968). *The Nelson River: A Study of Subarctic River Processes*. Baltimore: The Johns Hopkins University.

---

## REFERENCES

---

Osterkamp, T. (1977). Frazil-ice nucleation by mass-exchange processes at the air-water interface. *Journal of Glaciology* , 19 (81), 619-625.

Osterkamp, T., & Gilfilian, R. (1975). Nucleation characteristics of stream water and frazil ice nucleation. *Water Resources Research* , 11 (6), 926-928.

Osterkamp, T., Ohtake, T., & Warntment, D. (1974). Detection of airborne ice crystals near a supercooled stream. *Journal of the Atmospheric Sciences* , 1464-1465.

Perovich, D., Maykut, G., & Grenfell, T. (1986). Optical properties of ice and snow in the polar regions. I: Observations. *SPIE Ocean Optics Proceedings* (pp. 232-241). Orlando: Society of Photo-Optical Instrumentation Engineers.

Phelps, D. J. (1973). *Lake Winnipeg regulation, control, and generating station - Lower West Channel backwater studies*. Winnipeg: Manitoba Hydro.

Prowse, T. D. (1995). Chapter 2. River ice processes. In S. Beltaos, *River Ice Jams* (pp. 29-70). Highlands Ranch: Water Resources Publications.

Rimsha, V., & Donchenko, R. (1957). The estimation of heat loss from free water surfaces in wintertime. *Trudy Leningrad Gosud. Hidrol. Institute* , 65, 58-83.

Robert, S. (1979). *Contributions to the study of nucleation of frazil*. Quebec City: Laval University.

---

## REFERENCES

---

Santeford, H. S. (1990). Formation and growth of river ice. In W. L. Ryan, & R. D. Crissman, *Cold Regions Hydrology and Hydraulics* (pp. 469-483). New York: American Society of Civil Engineers.

Satterlund, D. R. (1979). An improved equation for estimating long-wave radiation from the atmosphere. *Water Resources Research* , 15 (6), 1649-1650.

Shen, H. T., Wang, D. S., & Lal, A. W. (1995). Numerical simulation of river ice processes. *Journal of Cold Regions Engineering* , 9 (3), 107-118.

Steffler, P., & Blackburn, J. (2002). *River2D: Introduction to depth averaged modelling and user's manual*. Edmonton: University of Alberta.

Theriault, I., Saucet, J.-P., & Taha, W. (2010). Validation of the Mike-Ice model simulating river flows in presence of ice and forecast of changes to the ice regime of the Romaine river due to hydroelectric project. *The 20th IAHR Symposium on Ice*. Lahti: The International Association for Hydro-Environment Engineering and Research.

Tsang, G. (1982). *Frazil and anchor ice: a monograph*. Ottawa: NRC Subcommittee on Hydraulics of Ice Covered Rivers.

Tuthill, A. (1999). *Special Report 99-8: Flow Control to Manage River Ice*. Hanover: Cold Regions Research and Engineering Laboratory.

Wiscombe, W. J., & Warren, S. G. (1981). A model for the spectral albedo of snow. I: Pure snow. *Journal of the Atmospheric Sciences* , 37, 2712-2733.

---

## REFERENCES

---

Wojtowicz, A. M. (2010). *2-D modeling of freeze-up processes on the Athabasca River downstream of Fort McMurray, Alberta*. Edmonton: University of Alberta.

World Meteorological Organization. (1988). *General meteorological standards and recommended practices*. Geneva: World Meteorological Organization.

Wunderlich, W. (1972). *Heat and mass transfer between a water surface and the atmosphere*. Norris: Tennessee Valley Authority Engineering Laboratory.

Zbigniewicz, H. S. (1997). Lake Winnipeg Regulation Ice Stabilization Program. *The 9th Workshop on River Ice* (pp. 43-53). Fredericton: Canadian Committee on River Ice Processes and the Environment.

---

## **APPENDIX A:**

### Hydrodynamic Validation Results

---

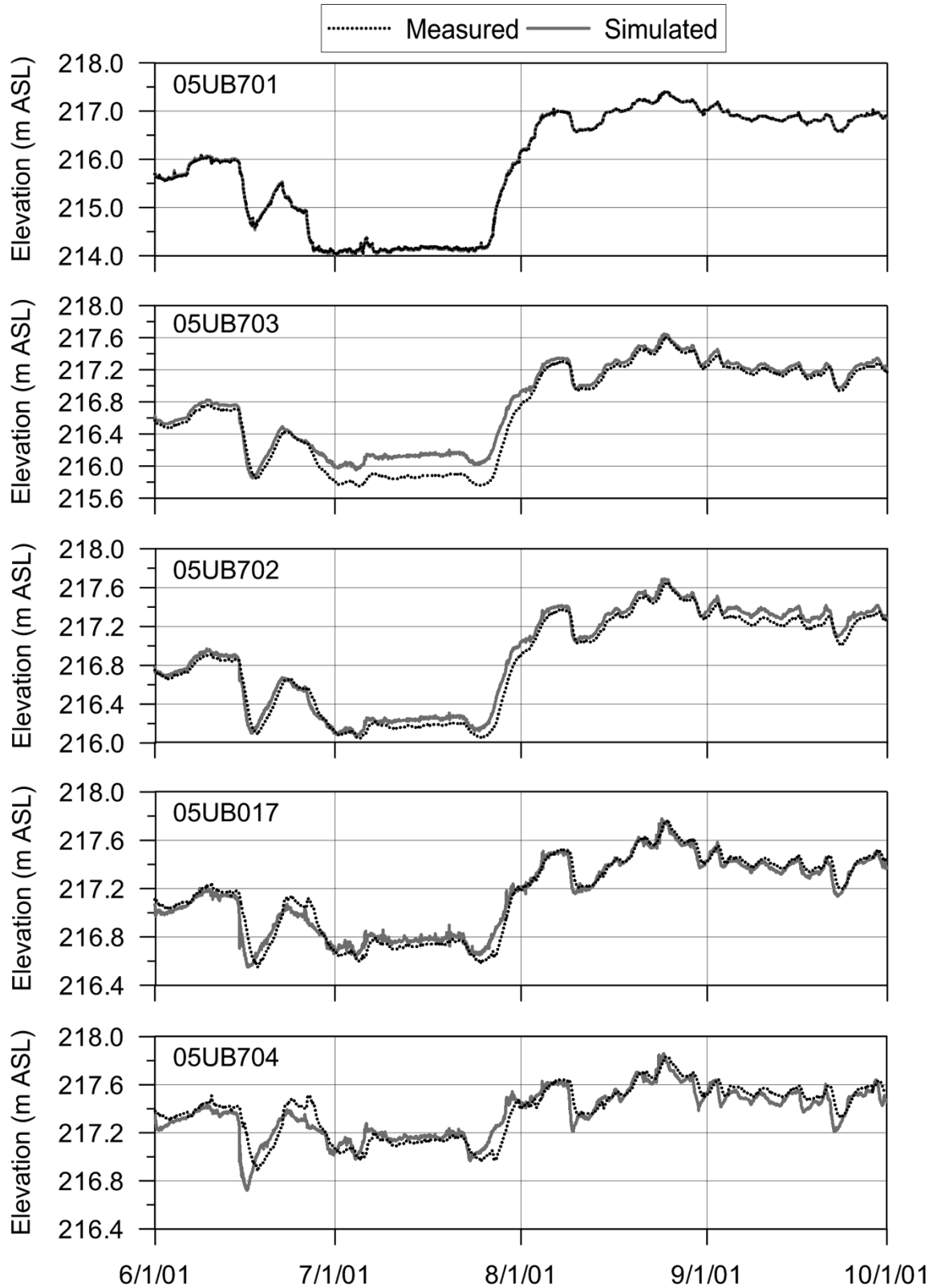


Figure A.1. Hydrodynamic validation, 2001

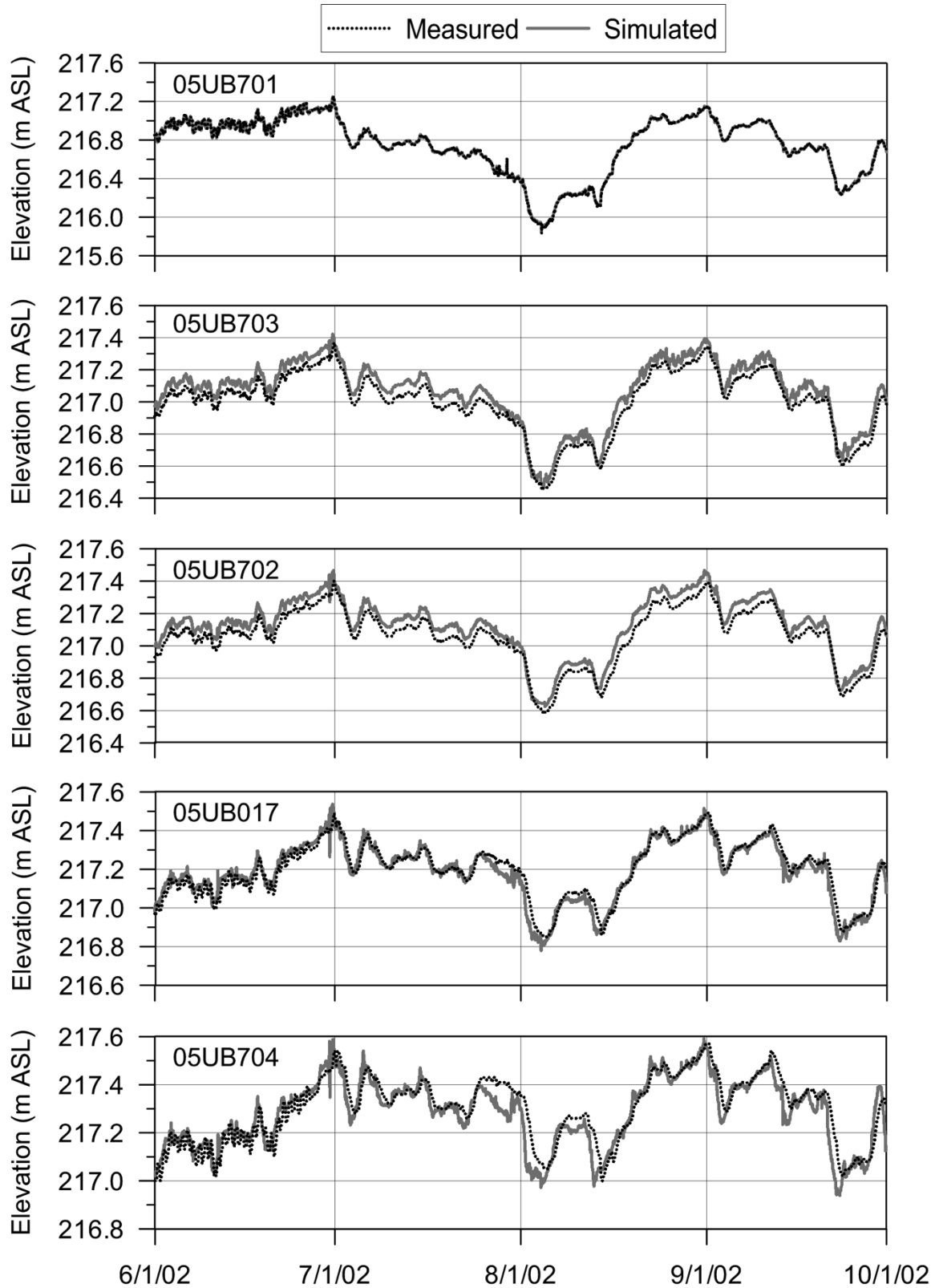


Figure A.2. Hydrodynamic validation, 2002

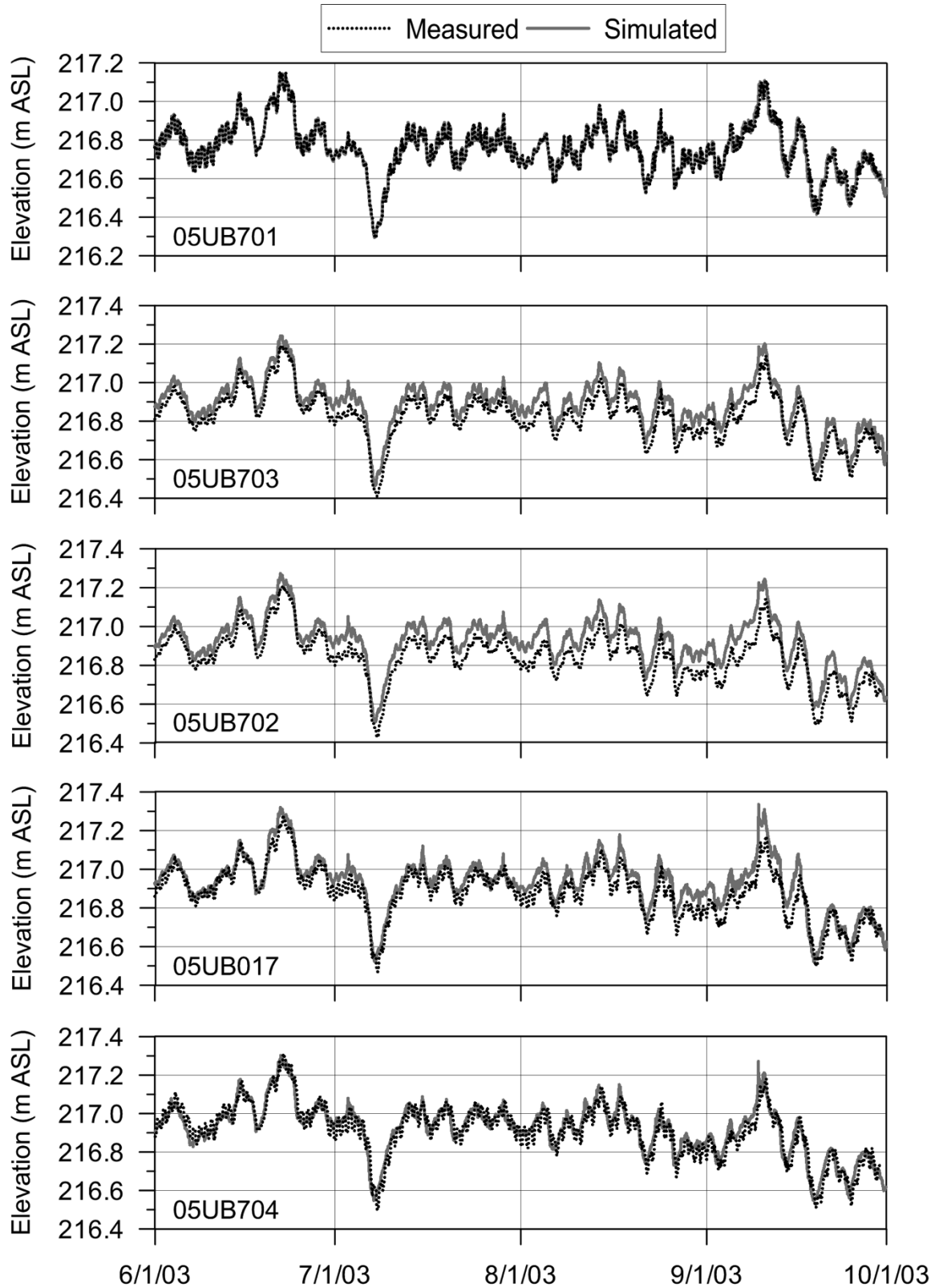


Figure A.3. Hydrodynamic validation, 2003

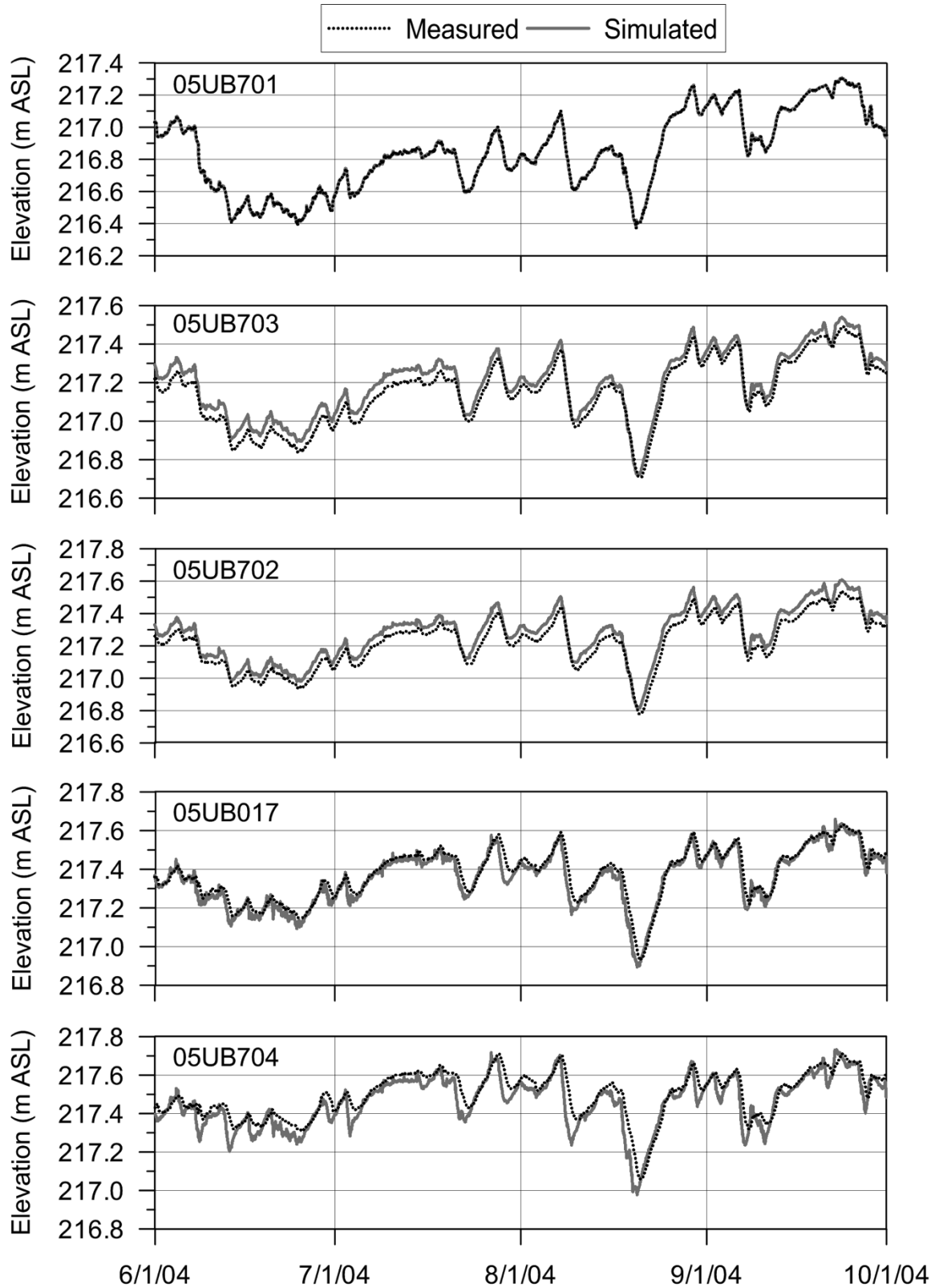


Figure A.4. Hydrodynamic validation, 2004

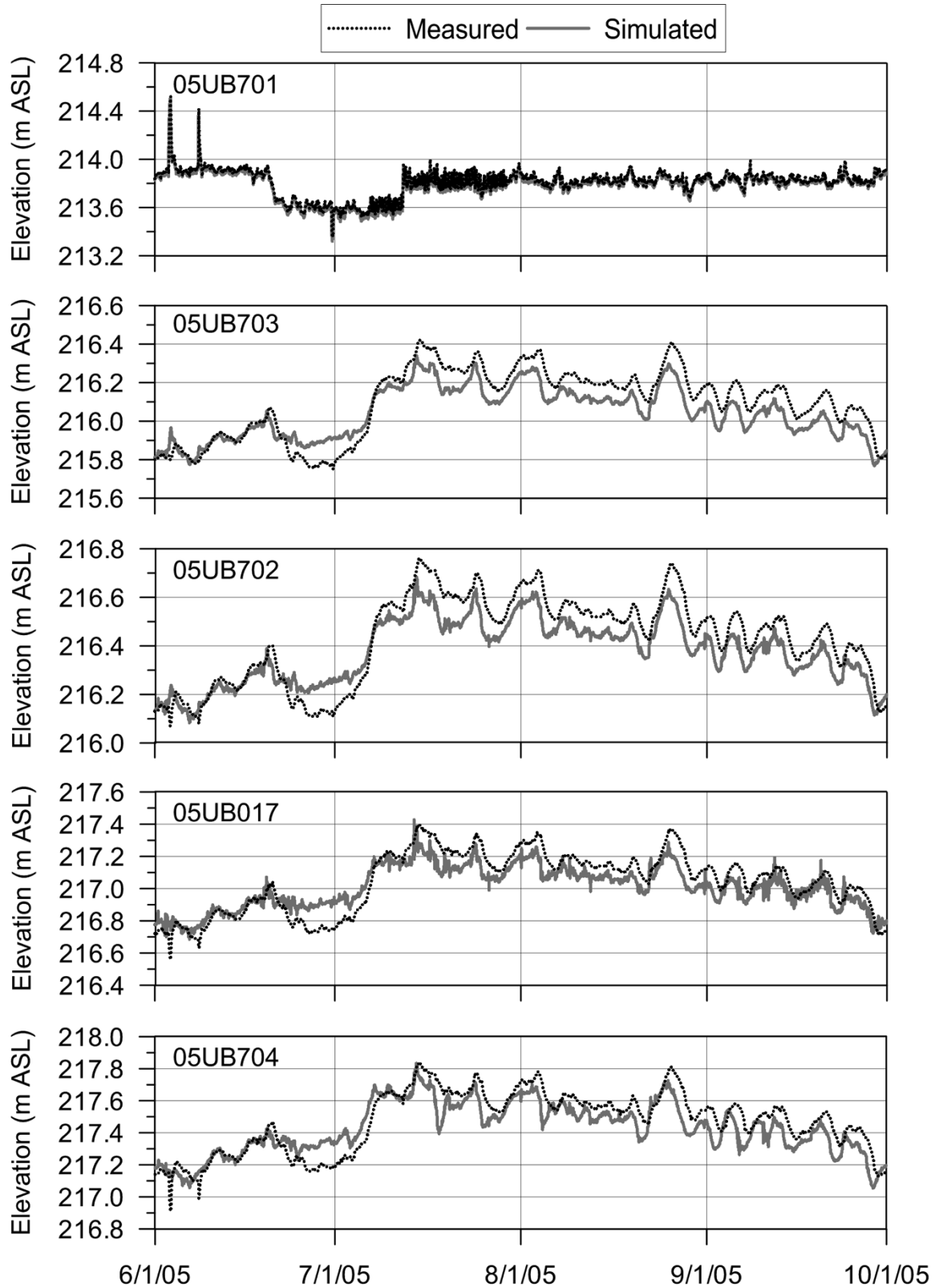


Figure A.5. Hydrodynamic validation, 2005

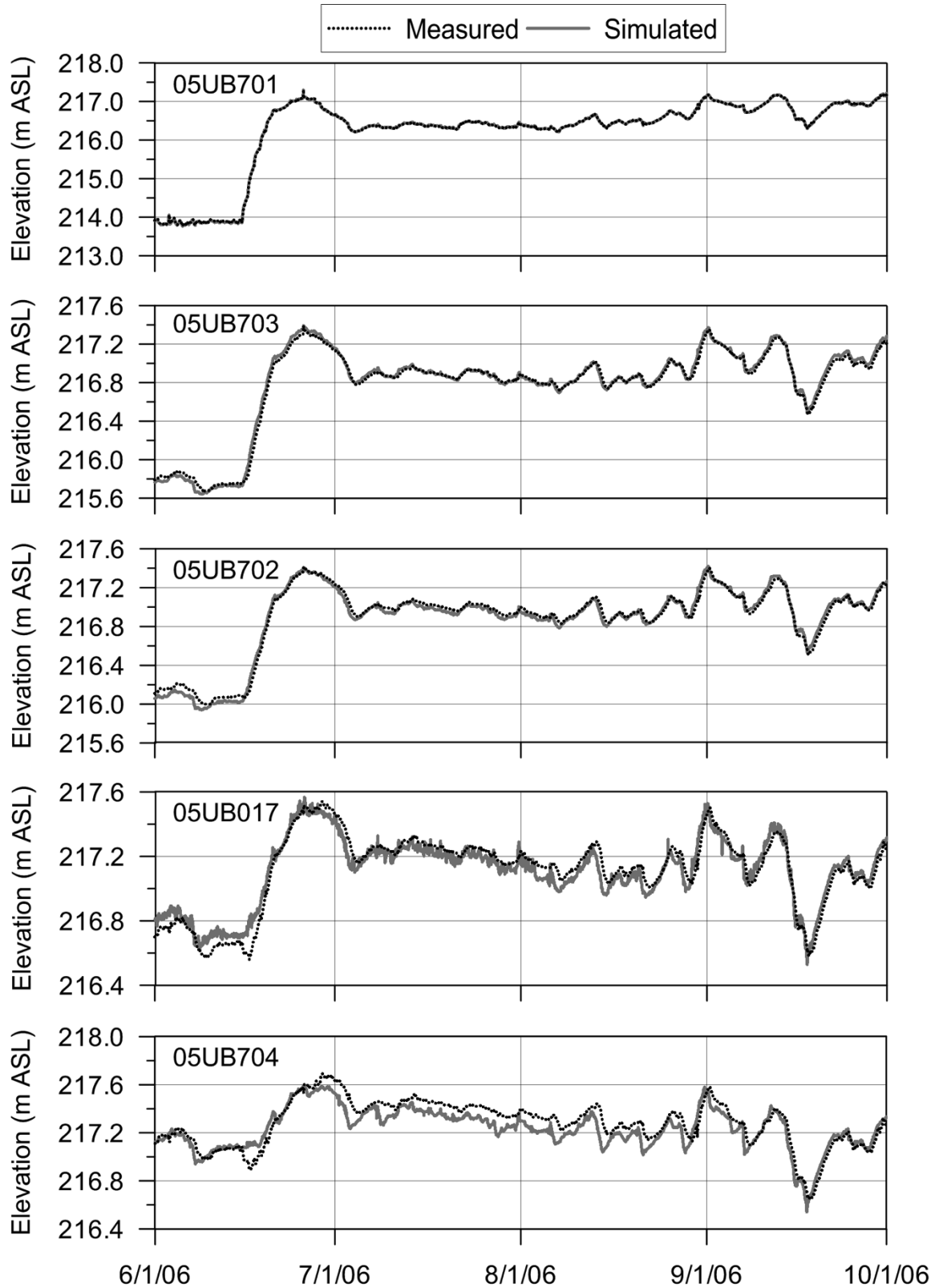


Figure A.6. Hydrodynamic validation, 2006

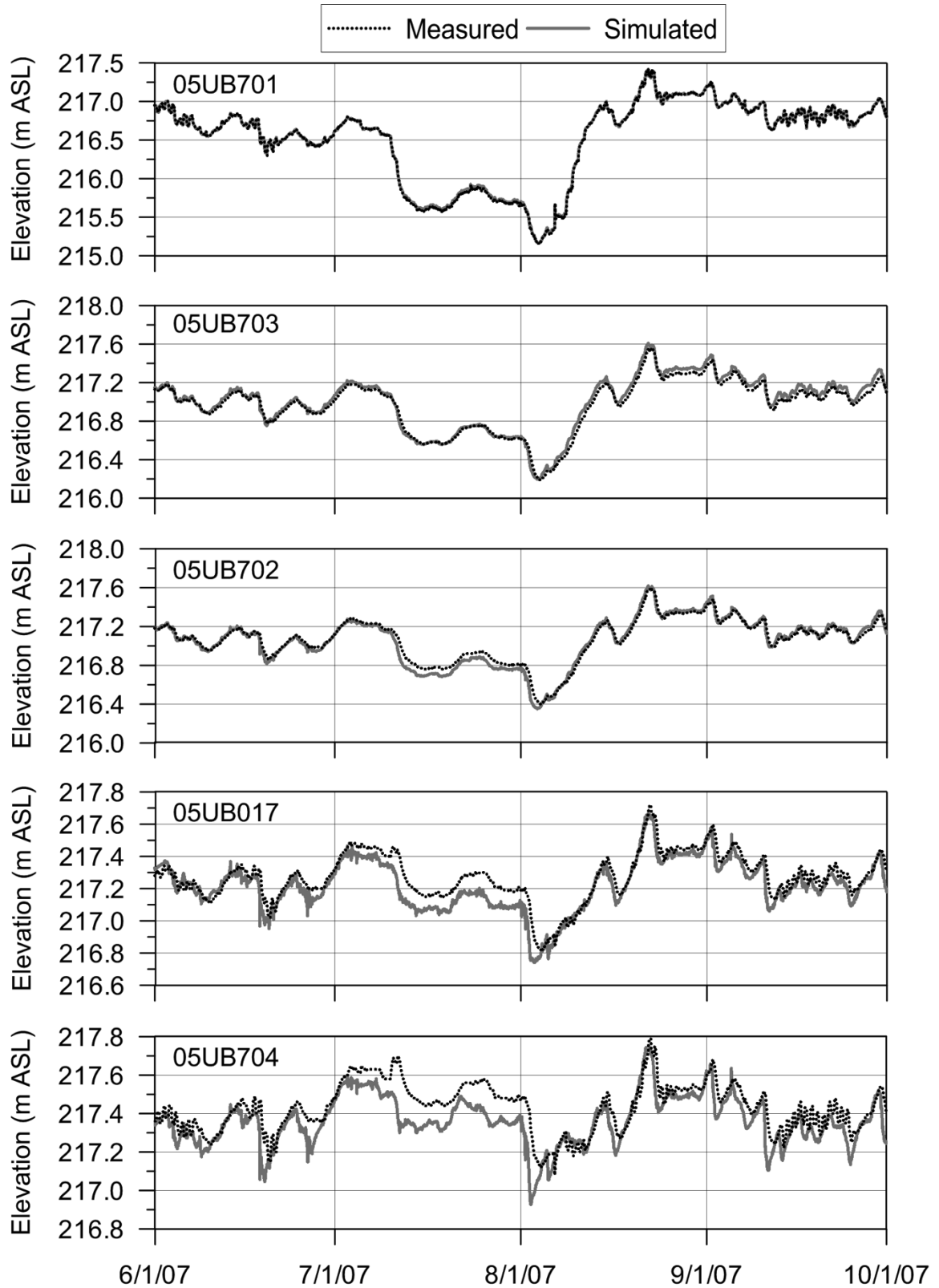


Figure A.7. Hydrodynamic validation, 2007

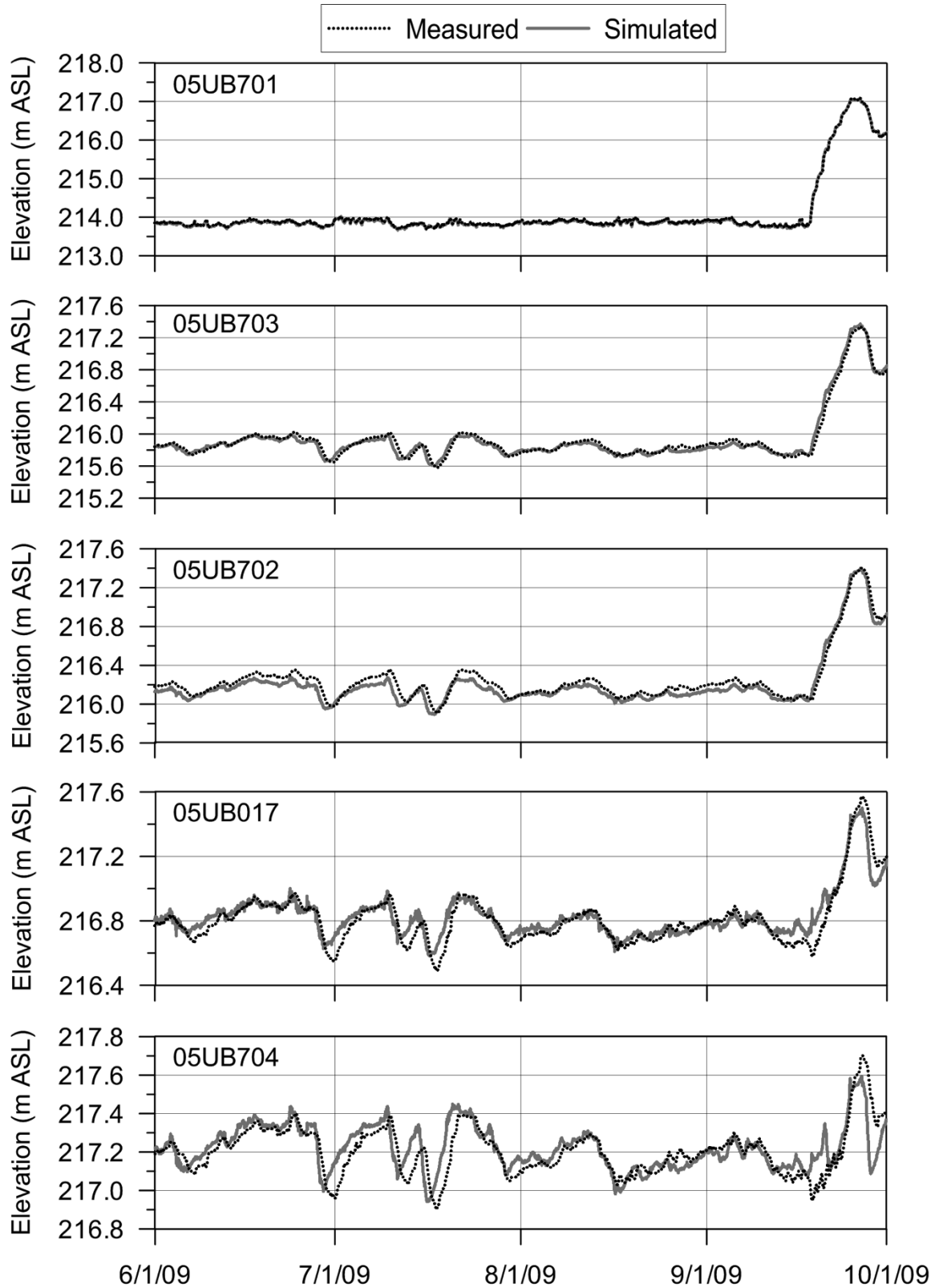


Figure A.8. Hydrodynamic validation, 2009

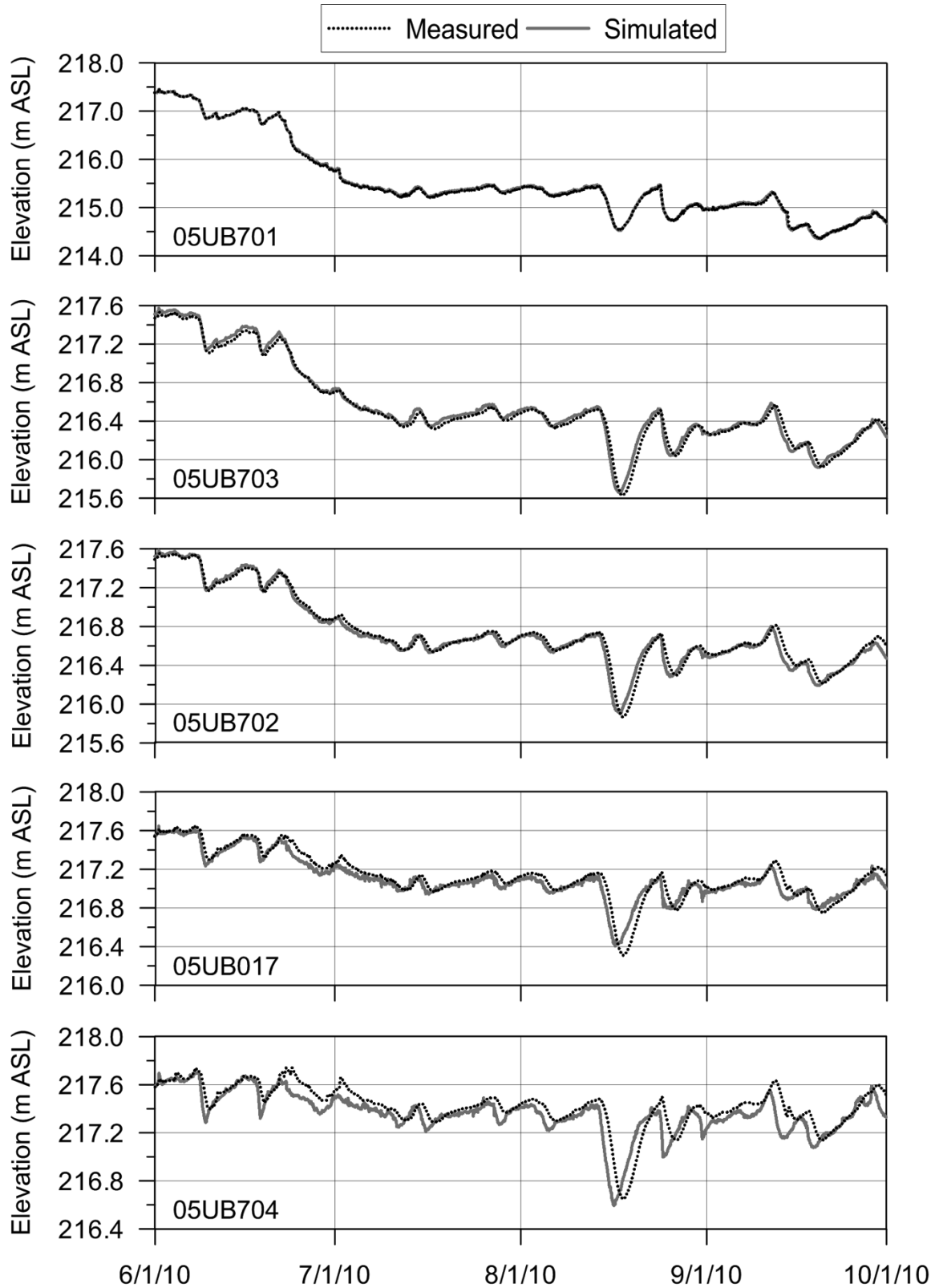


Figure A.9. Hydrodynamic validation, 2010

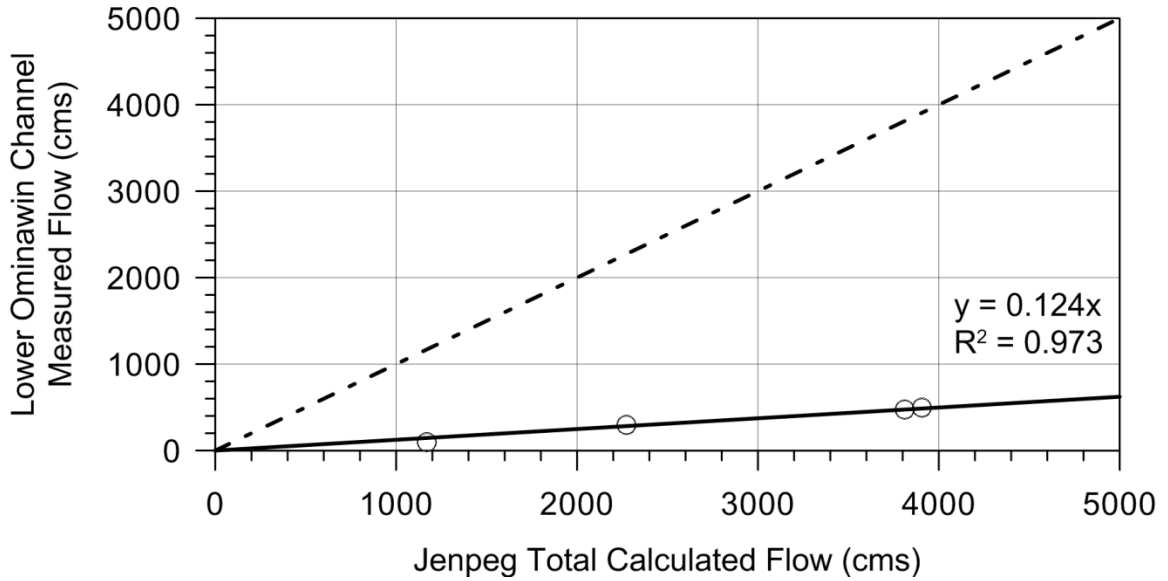


Figure A.10. Lower Ominawin Channel flow distribution

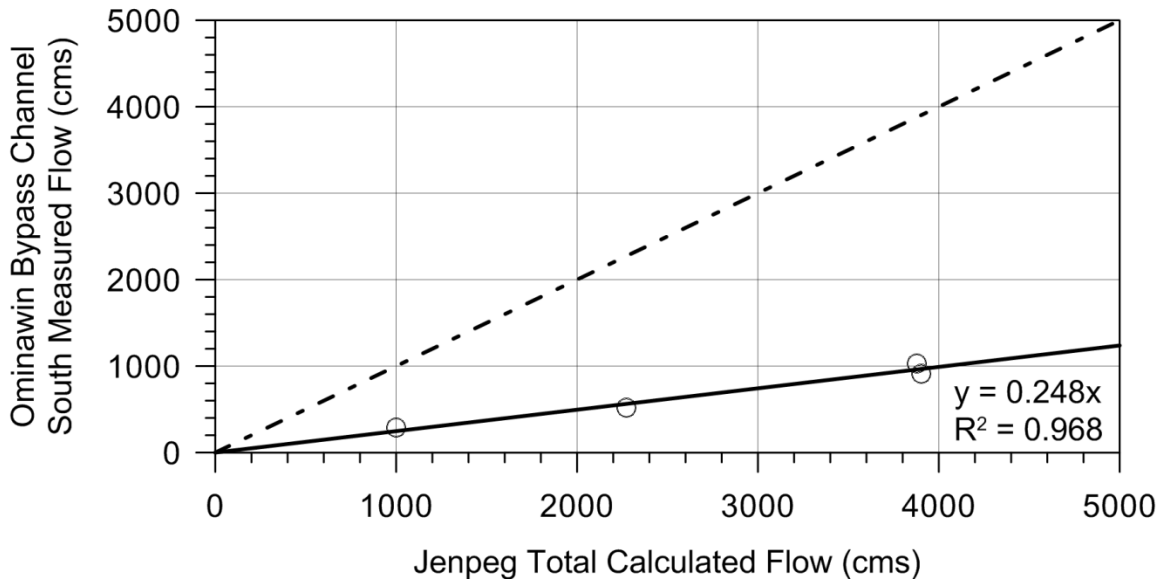


Figure A.11. Ominawin Bypass Channel South flow distribution

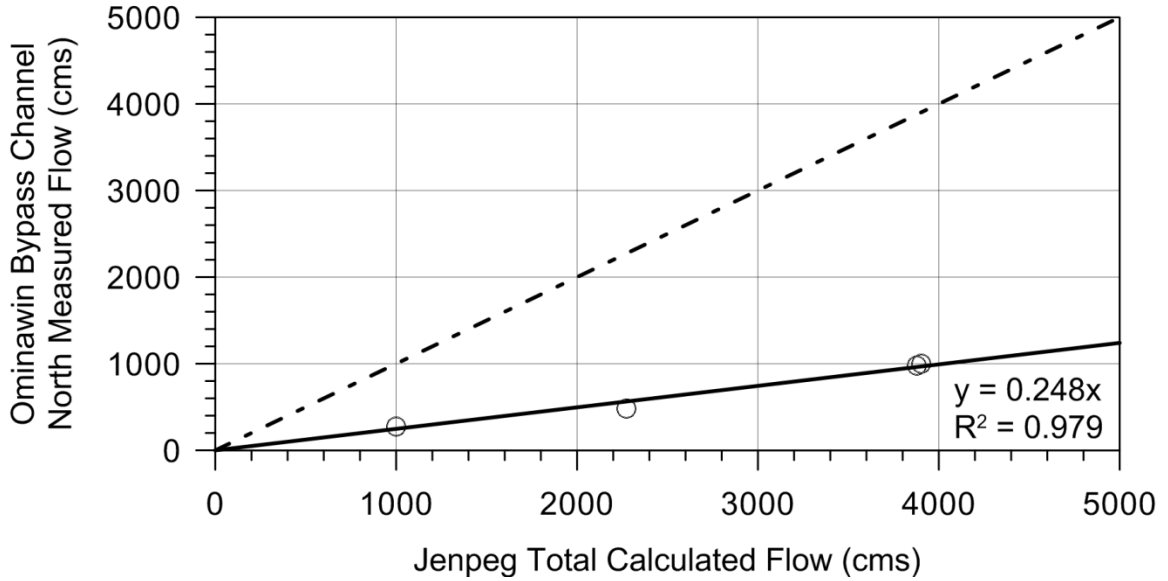


Figure A.12. Ominawin Bypass Channel North flow distribution

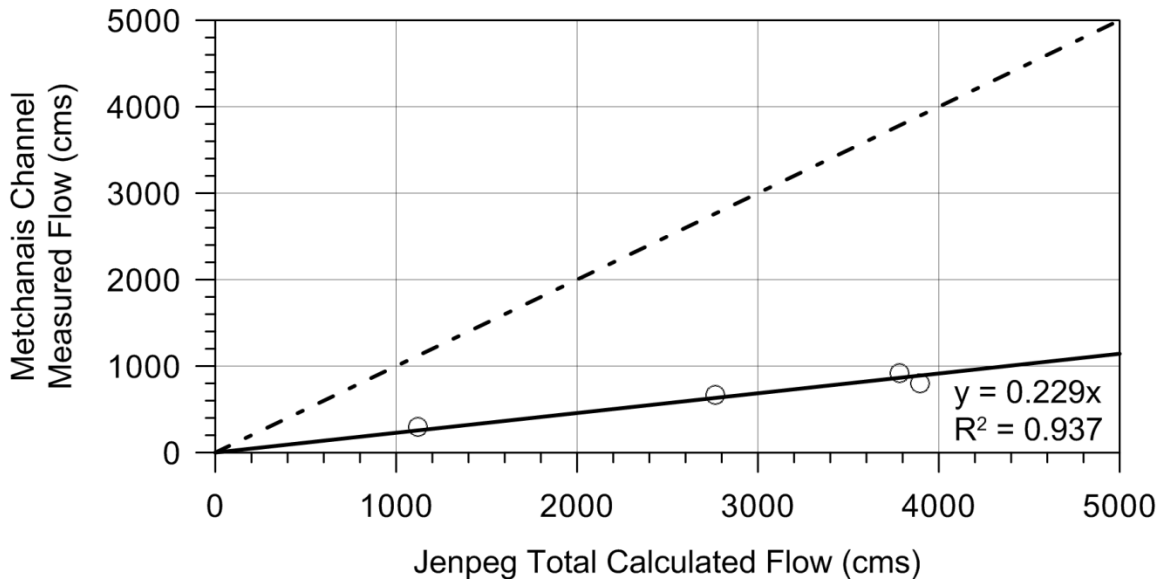


Figure A.13. Metchanais Channel flow distribution

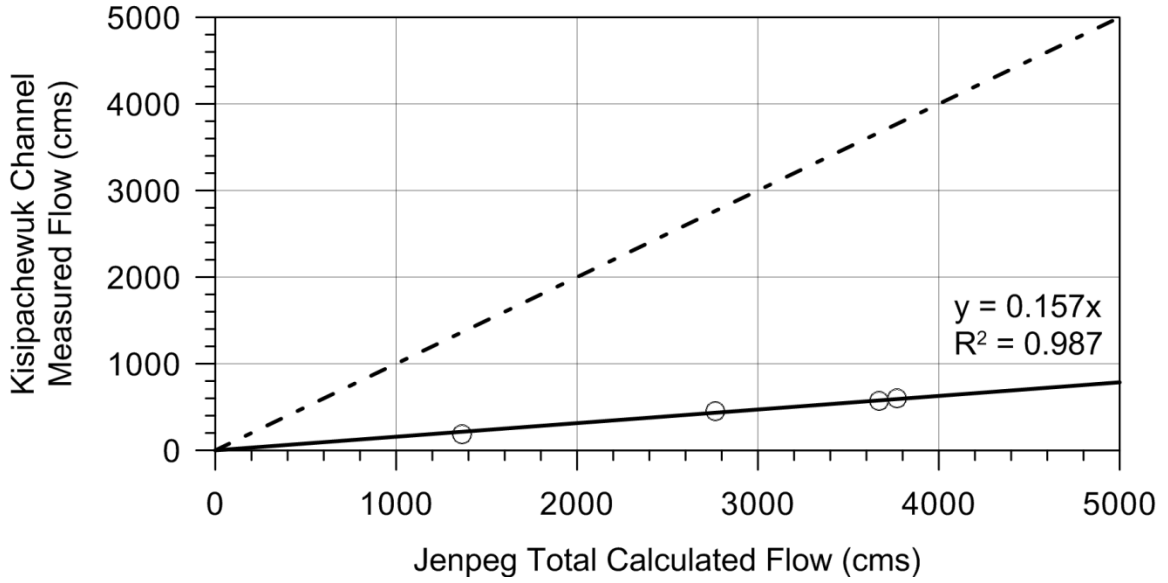


Figure A.14. Kisipachewuk Channel flow distribution

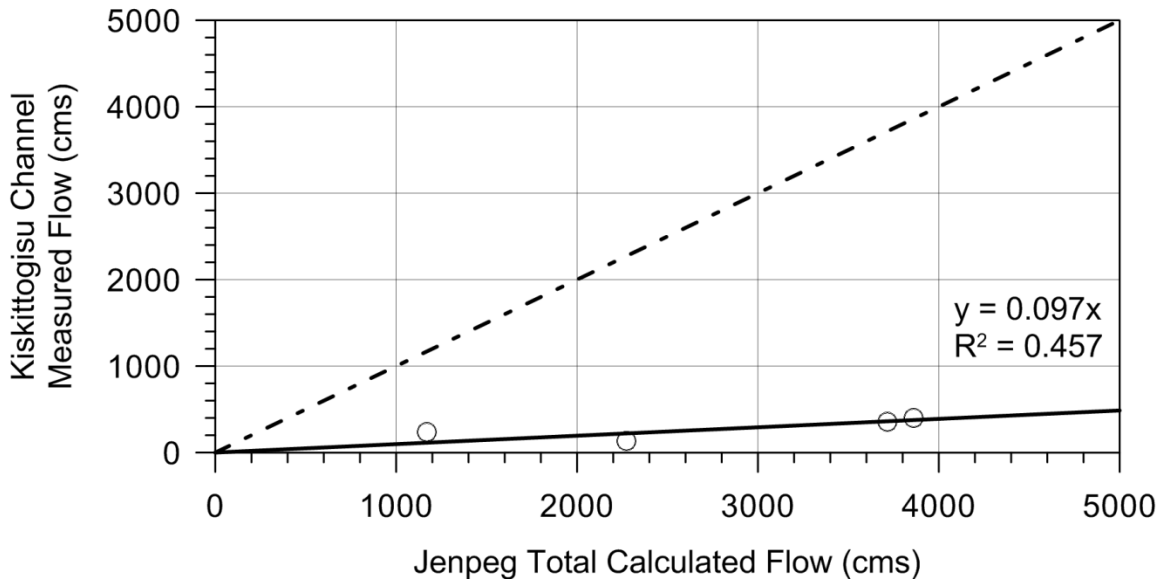


Figure A.15. Kiskittogisu Channel flow distribution

---

## **APPENDIX B:**

### Linear Heat Transfer Results

---

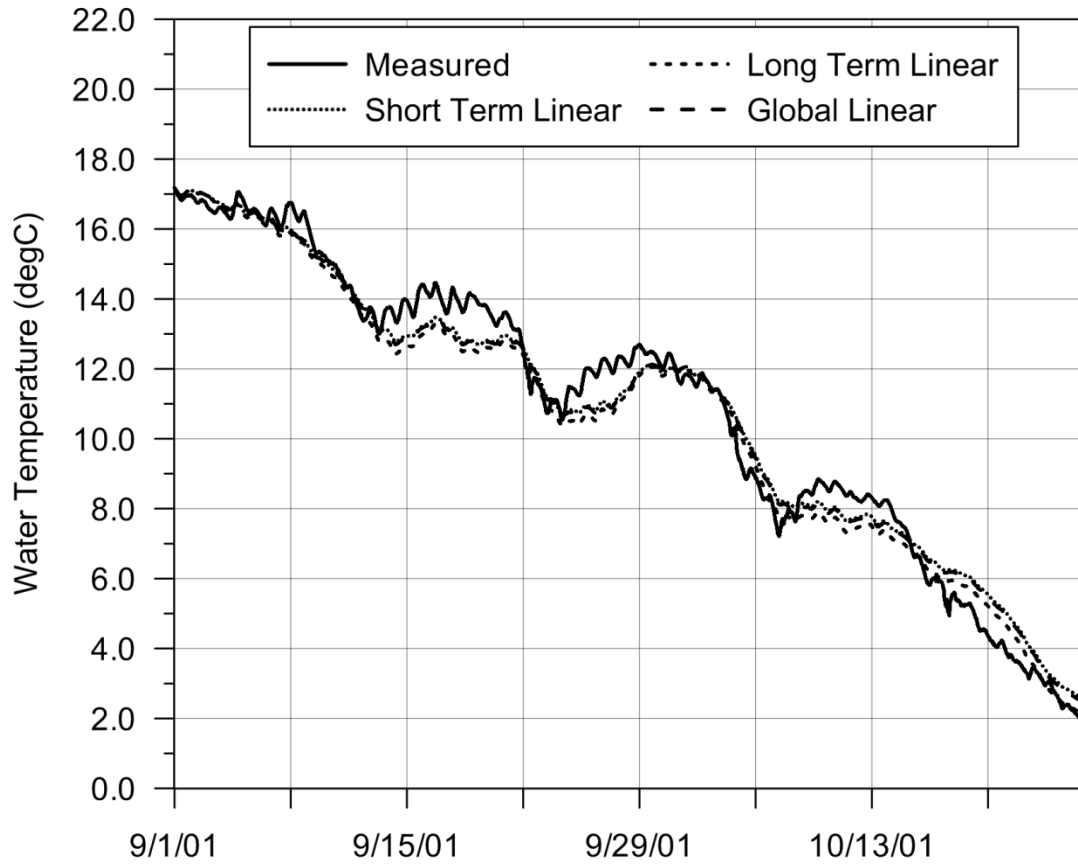


Figure B.1. Linear heat transfer calibration, 2001

Table B.1. Linear heat transfer calibration statistics, 2001

Method	Bulk Heat Transfer Coefficient [W/m <sup>2</sup> °C]	Slope	R <sup>2</sup>
Short-term Linear Average	21.90	0.984	0.977
Long-term Linear Average	24.46	0.967	0.980
Global Linear	22.38	0.980	0.978

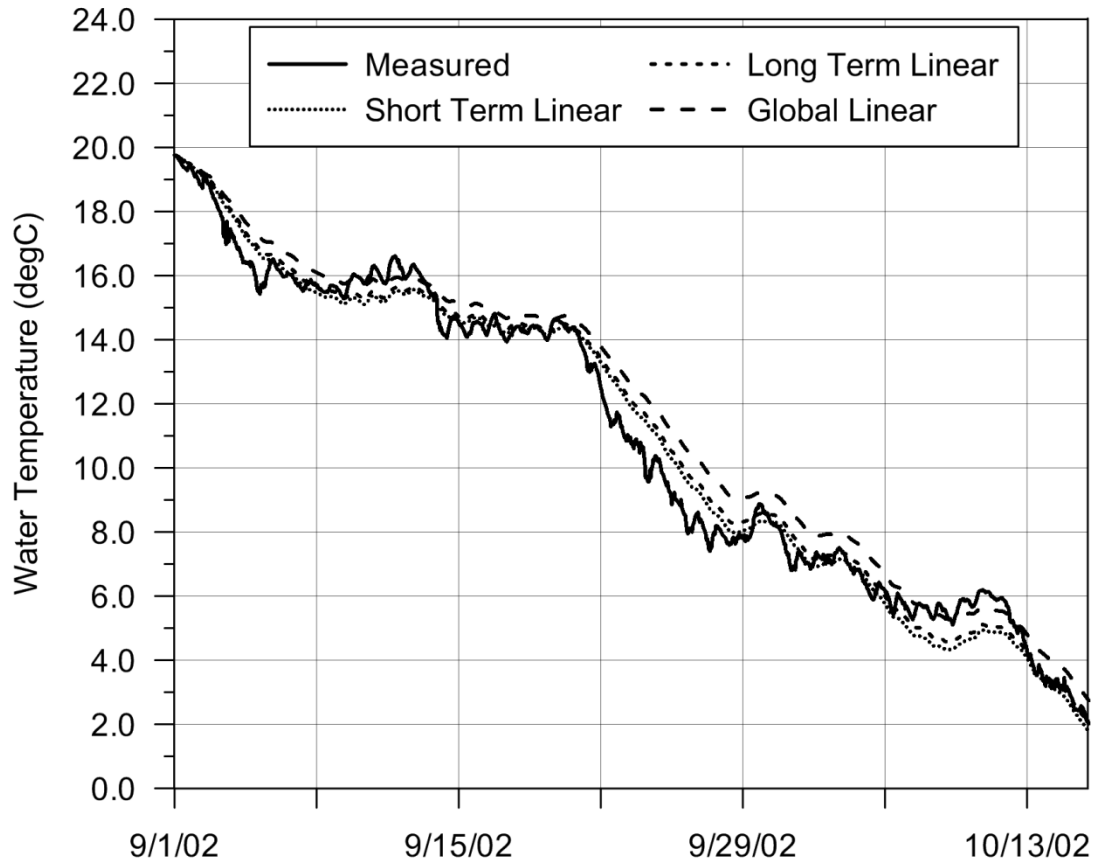


Figure B.2. Linear heat transfer calibration, 2002

Table B.2. Linear heat transfer calibration statistics, 2002

Method	Bulk Heat Transfer Coefficient [W/m <sup>2</sup> °C]	Slope	R <sup>2</sup>
Short-term Linear Average	28.03	1.004	0.983
Long-term Linear Average	26.35	1.016	0.983
Global Linear	22.38	1.048	0.975

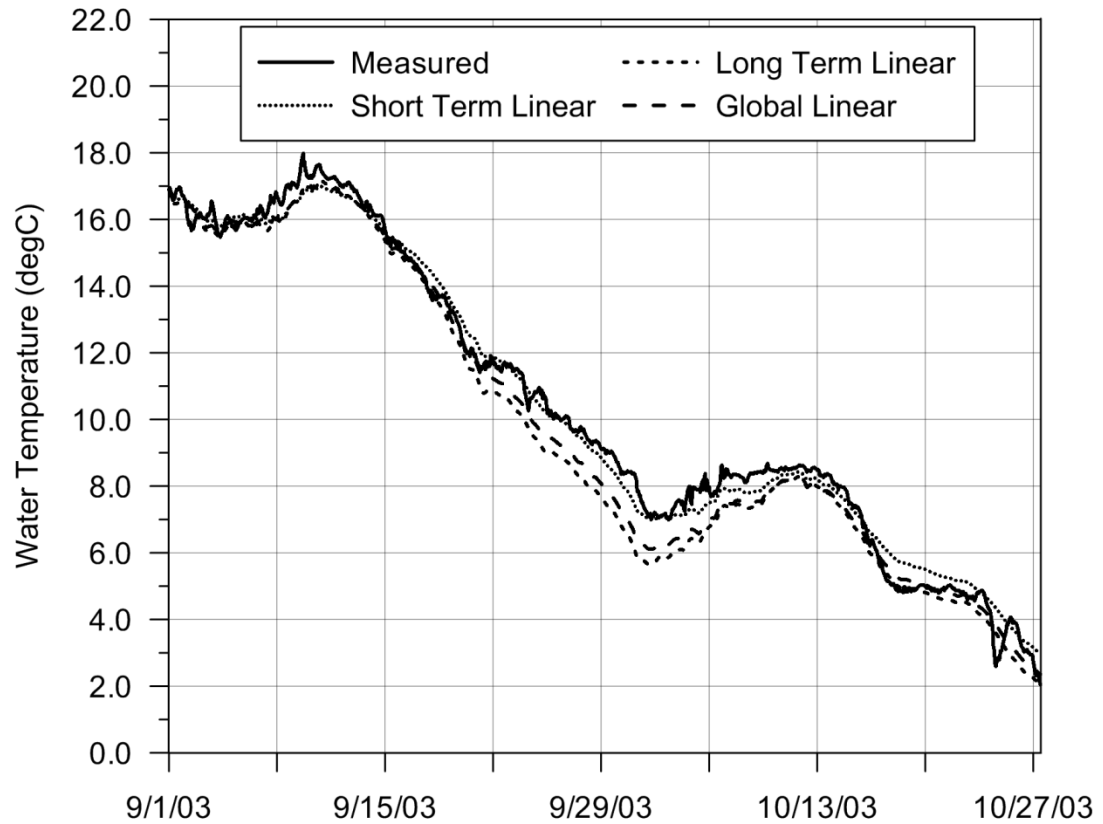


Figure B.3. Linear heat transfer calibration, 2003

Table B.3. Linear heat transfer calibration statistics, 2003

Method	Bulk Heat Transfer Coefficient [W/m <sup>2</sup> °C]	Slope	R <sup>2</sup>
Short-term Linear Average	18.50	0.993	0.991
Long-term Linear Average	24.83	0.952	0.981
Global Linear	22.38	0.966	0.987

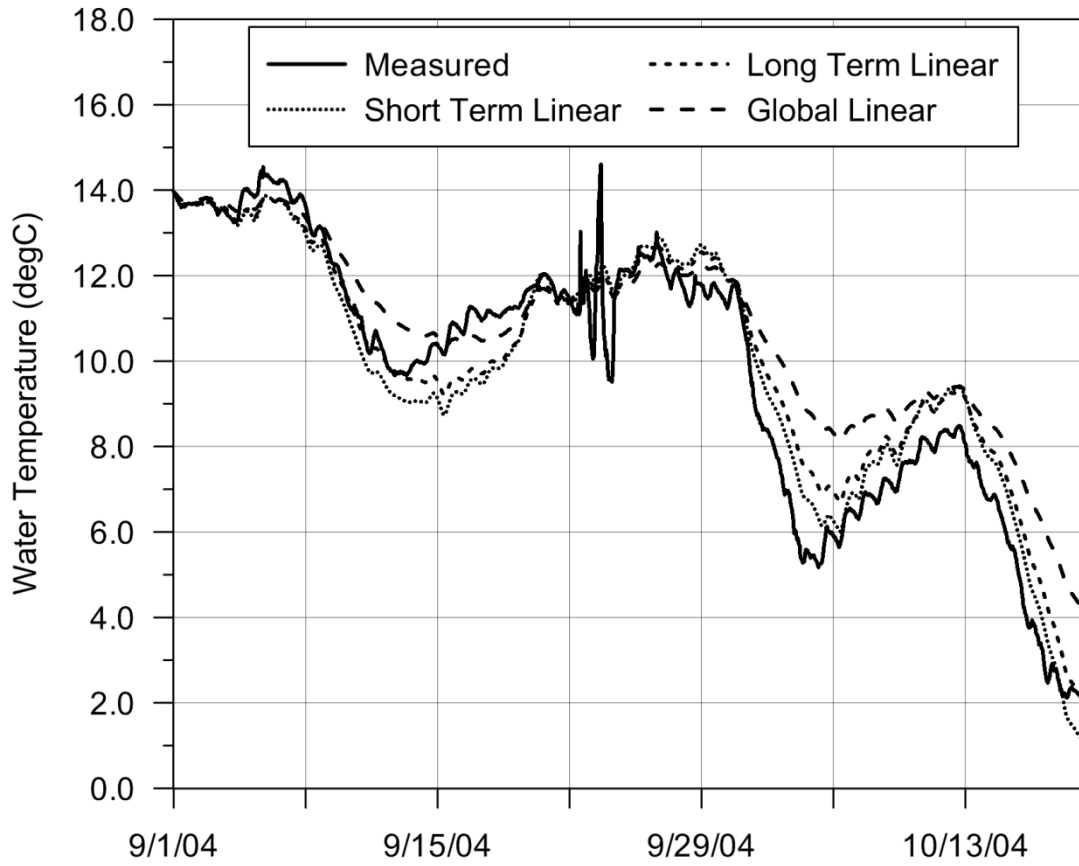


Figure B.4. Linear heat transfer calibration, 2004

Table B.4: Linear heat transfer calibration statistics, 2004

Method	Bulk Heat Transfer Coefficient [W/m <sup>2</sup> °C]	Slope	R <sup>2</sup>
Short-term Linear Average	43.47	0.999	0.918
Long-term Linear Average	35.45	1.012	0.886
Global Linear	22.38	1.047	0.633

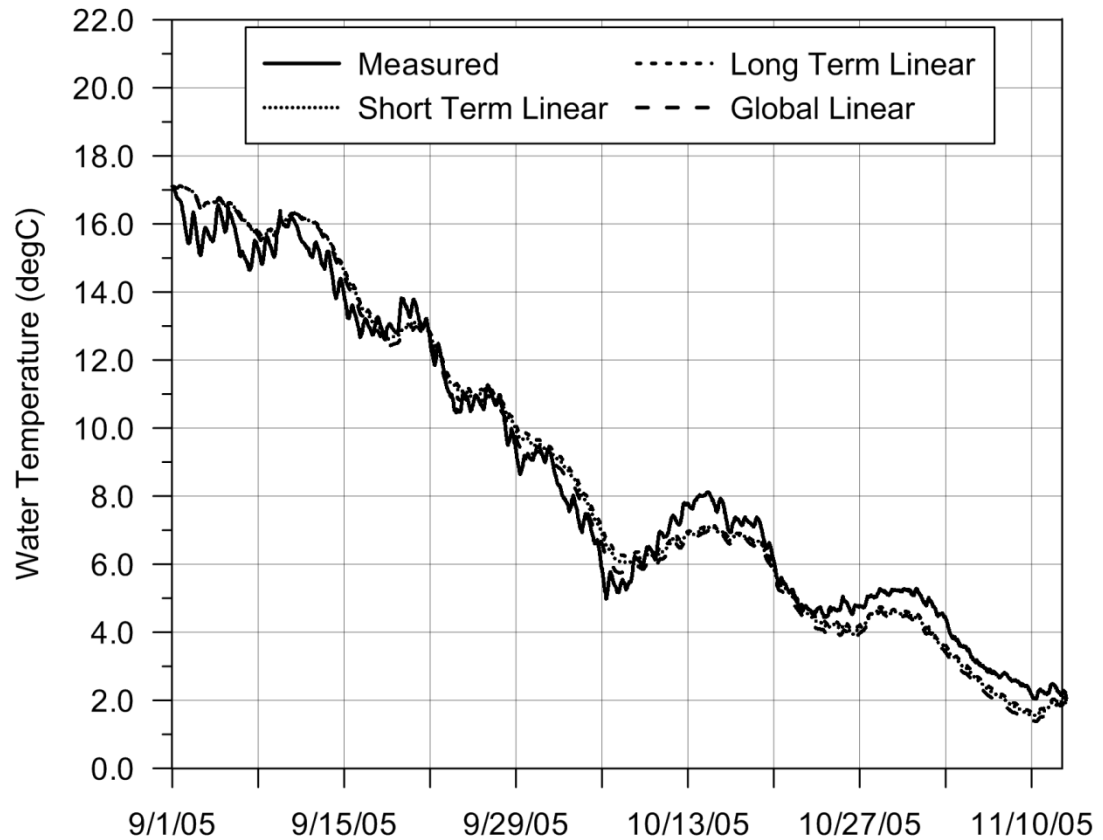


Figure B.5. Linear heat transfer calibration, 2005

Table B.5. Linear heat transfer calibration statistics, 2005

Method	Bulk Heat Transfer Coefficient [W/m <sup>2</sup> °C]	Slope	R <sup>2</sup>
Short-term Linear Average	20.59	1.016	0.985
Long-term Linear Average	19.69	1.023	0.985
Global Linear	22.38	1.003	0.983

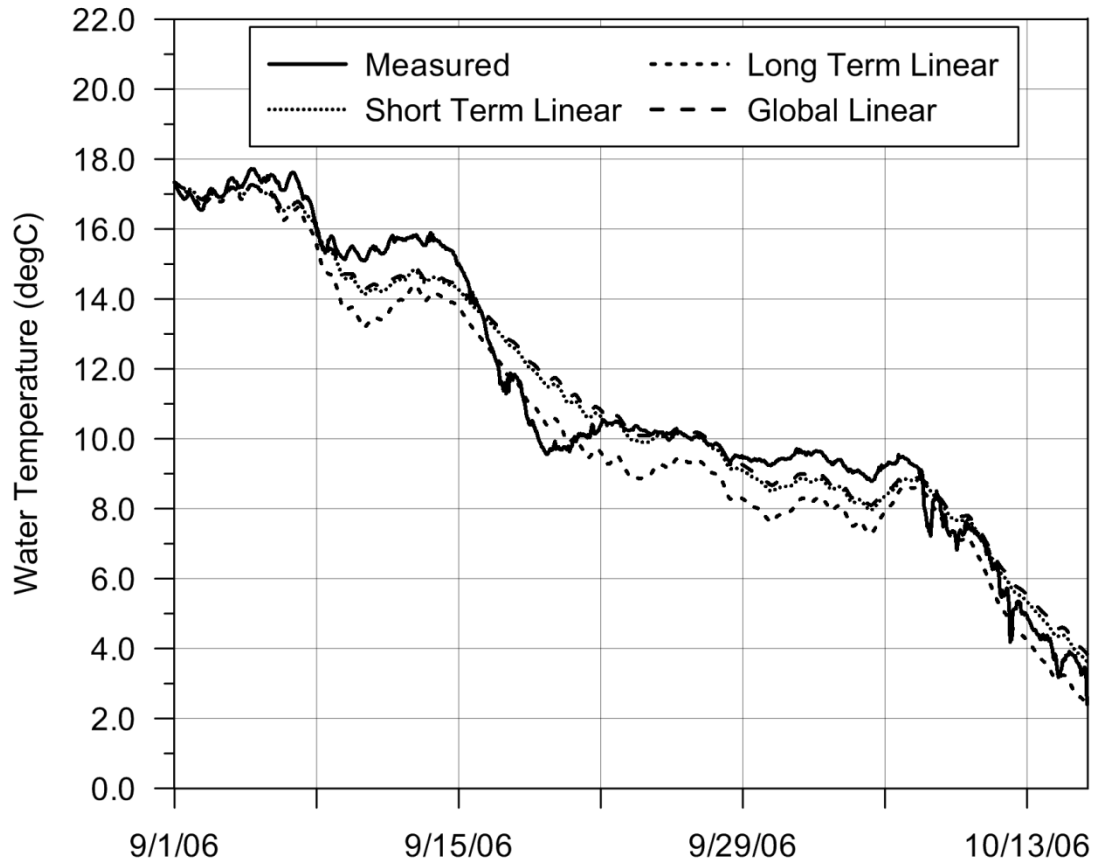


Figure B.6. Linear heat transfer calibration, 2006

Table B.6. Linear heat transfer calibration statistics, 2006

Method	Bulk Heat Transfer Coefficient [W/m <sup>2</sup> °C]	Slope	R <sup>2</sup>
Short-term Linear Average	23.71	0.982	0.965
Long-term Linear Average	33.50	0.935	0.970
Global Linear	22.38	0.991	0.960

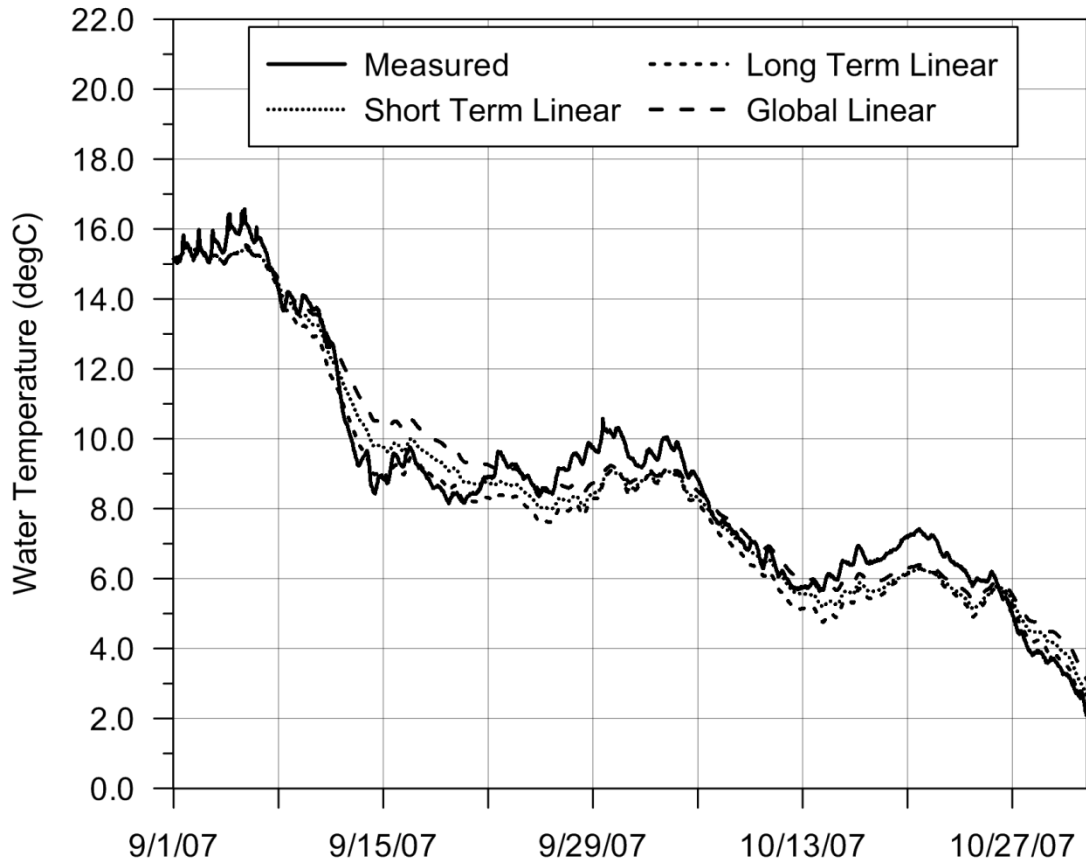


Figure B.7. Linear heat transfer calibration, 2007

Table B.7. Linear heat transfer calibration statistics, 2007

Method	Bulk Heat Transfer Coefficient [W/m <sup>2</sup> °C]	Slope	R <sup>2</sup>
Short-term Linear Average	27.37	0.972	0.965
Long-term Linear Average	33.63	0.947	0.974
Global Linear	22.38	0.999	0.948

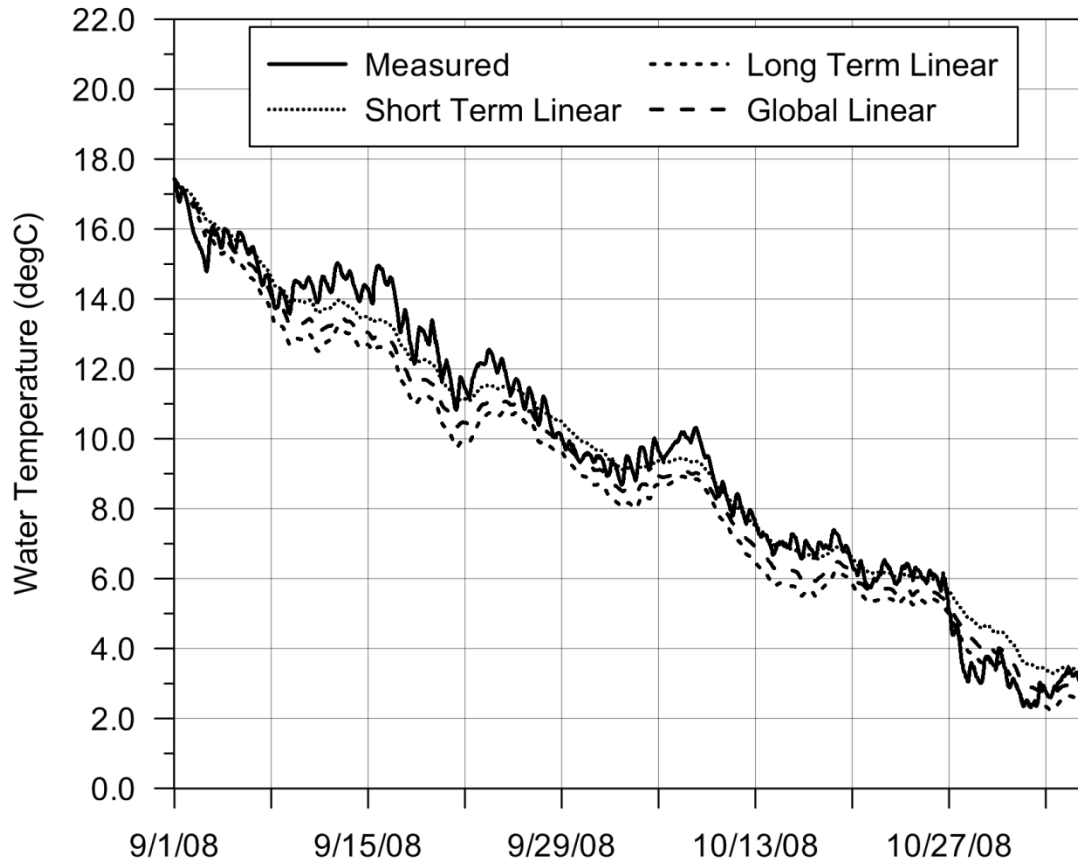


Figure B.8. Linear heat transfer calibration, 2008

Table B.8. Linear heat transfer calibration statistics, 2008

Method	Bulk Heat Transfer Coefficient [W/m <sup>2</sup> °C]	Slope	R <sup>2</sup>
Short-term Linear Average	17.86	0.988	0.976
Long-term Linear Average	27.01	0.914	0.977
Global Linear	22.38	0.946	0.979

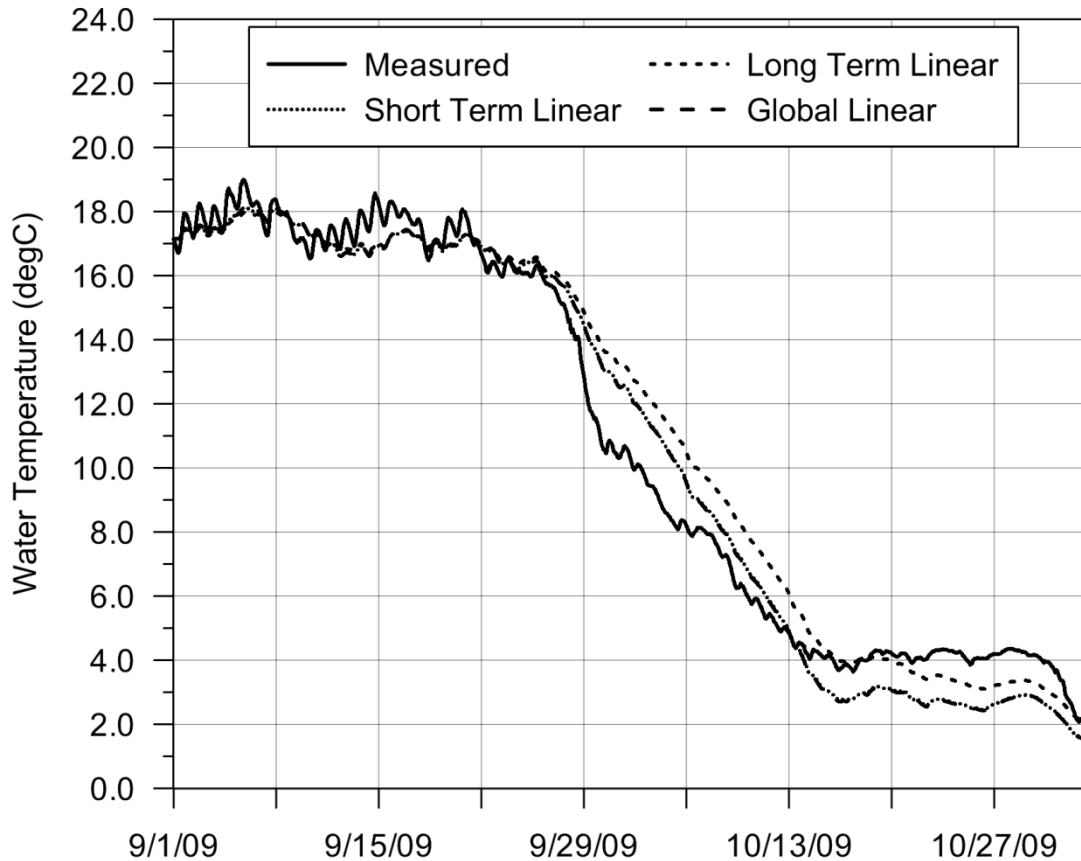


Figure B.9. Linear heat transfer calibration, 2009

Table B.9. Linear heat transfer calibration statistics, 2009

Method	Bulk Heat Transfer Coefficient [W/m <sup>2</sup> °C]	Slope	R <sup>2</sup>
Short-term Linear Average	22.18	1.000	0.971
Long-term Linear Average	18.21	1.019	0.960
Global Linear	22.38	1.000	0.971

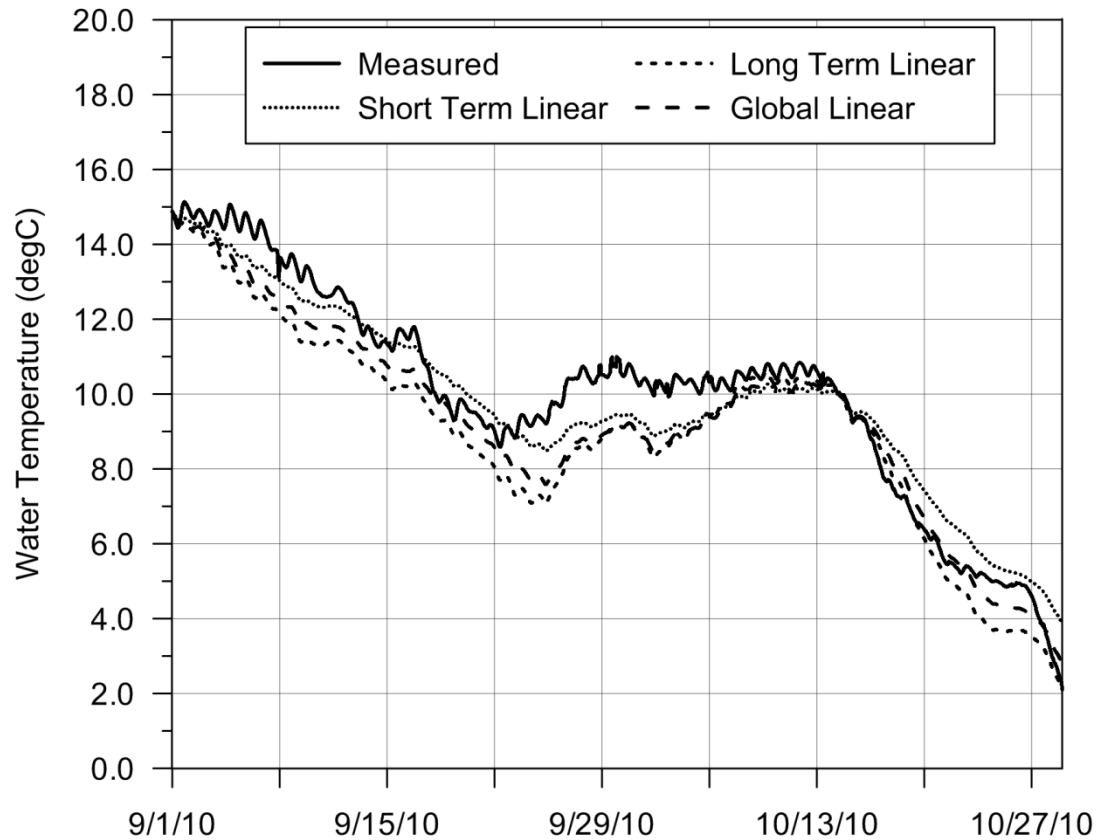


Figure B.10. Linear heat transfer calibration, 2010

Table B.10. Linear heat transfer calibration statistics, 2010

Method	Bulk Heat Transfer Coefficient [W/m <sup>2</sup> °C]	Slope	R <sup>2</sup>
Short-term Linear Average	16.26	0.969	0.919
Long-term Linear Average	27.80	0.907	0.945
Global Linear	22.38	0.929	0.950